Universidade de Aveiro
2021

SANDRA PEREIRA MAGINA

# NOVAS FORMULAÇÕES POLIMÉRICAS A PARTIR DE LENHOSSULFONATOS

# NEW POLYMERIC FORMULATIONS BASED ON LIGNOSULPHONATES

**Universidade de Aveiro**
**2021**

**SANDRA PEREIRA MAGINA**

# NOVAS FORMULAÇÕES POLIMÉRICAS A PARTIR DE LENHOSSULFONATOS

# NEW POLYMERIC FORMULATIONS BASED ON LIGNOSULPHONATES

Tese apresentada à Universidade de Aveiro para cumprimento dos requisitos necessários à obtenção do grau de Doutor em Engenharia Química, realizada sob a orientação científica do Doutor Dmitry Victorovitch Evtyugin, Professor Associado com Agregação do Departamento de Química da Universidade de Aveiro, e da Doutora Ana Margarida Madeira Viegas de Barros-Timmons, Professora Auxiliar do Departamento de Química da Universidade de Aveiro.

Apoio financeiro da FCT e do FSE (BD/121275/2016) no âmbito do III Quadro Comunitário de Apoio.

À minha família, em especial ao meu marido Paulo e à minha filha Joana

**o júri**

Presidente

Prof. Doutor Fernando Joaquim Fernandes Tavares Rocha
professor catedrático da Universidade de Aveiro

Prof. Doutora Ana Paula Coelho Duarte
professora catedrática da Universidade da Beira Interior

Prof. Doutor Mikhail Yurievitch Balakshin
equiparado a professor associado da Universidade de Aalto

Prof. Doutora Luísa Maria Hora de Carvalho
professora coordenadora do Instituto Politécnico de Viseu

Prof. Doutora Paula Cristina de Oliveira Rodrigues Pinto
investigadora do Raiz - Instituto de Investigação da Floresta e do Papel

Prof. Doutor Dmitry Victorovitch Evtyugin
professor associado com agregação da Universidade de Aveiro

**agradecimentos**

Em primeiro lugar, gostaria de agradecer aos meus orientadores, o Professor Doutor Dmitry Evtyugin e a Professora Doutora Ana Barros-Timmons, pela orientação científica, apoio e disponibilidade constantes ao longo de todo este percurso.

À CAIMA Indústria de Celulose S.A. pelo fornecimento dos licores sulfito.

À Sika Portugal – Produtos Construção e Indústria S.A, em especial ao Ricardo Mendonça, pela preparação das pastas de cimento e execução dos testes de espalhamento.

À Novozymes pelo fornecimento da lacase.

À Professora Doutora Luísa Carvalho e à Doutora Margarida Almeida pela realização dos testes de determinação da força de adesão dos adesivos por ABES.

Ao Professor Doutor Luís Cadillon e à Doutora Sílvia Soreto pela determinação das propriedades elétricas das membranas poliméricas.

À Doutora Alisa Rudnitskaya pelo apoio na preparação dos sensores potenciométricos e avaliação do seu desempenho na deteção de metais de transição em solução.

À Engenheira Ana Caço pela realização dos ensaios de análises térmicas e, em especial, pelo carinho, apoio e incentivo.

Quero agradecer à Marina Matos, à Inês Mendes, à Belinda Soares e ao Nuno Gama pela amizade, carinho e incentivo.

Quero também agradecer aos meus colegas de laboratório bem como aos outros docentes pelo apoio que me prestaram quando precisei.

Gostaria de agradecer aos meus Pais pelo apoio incondicional ao longo da minha vida.

Finalmente, um agradecimento muito especial ao meu marido Paulo e à minha filha Joana pelo amor, compreensão, incentivo e apoio diários.

**palavras-chave**

Licores sulfito; lenhossulfonatos; dispersantes; betão; compósitos condutores; poliuretanos; adesivos.

**resumo**

Os lenhossulfonatos (LS) são subprodutos sulfonados derivados da lenhina presentes nos licores sulfito (SSL) do cozimento sulfito ácido. Os SSL são principalmente queimados para a recuperação da base inorgânica e produção de energia e são considerados recursos naturais subaproveitados. A possibilidade de aumentar os lucros da empresa com a valorização dos LS, através da produção de produtos de valor acrescentado para diferentes aplicações de mercado, é altamente motivadora e um desafio no âmbito dos conceitos de biorrefinaria e economia circular.

O processo de cozimento sulfito ácido com base de magnésio adotado na CAIMA Indústria de Celulose S.A. mudou significativamente nos últimos anos. Anteriormente, destinava-se à produção de pasta celulósica para a produção de papel a partir de madeira de eucalipto, mas hoje em dia a CAIMA produz pasta solúvel a partir de madeira de *Eucalyptus globulus* em condições mais severas. Considerando que a alteração do processo sulfito pode ter causado mudanças inevitáveis na composição final do SSL, a primeira tarefa desta tese consistiu numa análise química sistemática para avaliar as características químicas de SSL, seguido pelo isolamento das frações ricas em LS a partir de SSL, obtendo-se LS purificado. A composição química do SSL mostrou que condições de cozimento mais severas levam a um aumento de compostos voláteis, como o ácido acético, metanol e furfural, enquanto que a quantidade de açúcares solúveis e LS aumentou de forma menos significativa. Por sua vez, a estrutura química do LS mostrou que condições de cozimento mais severas levam ao aumento do peso molecular, grau de condensação e grau de sulfonação. As seguintes tarefas da tese visam o desenvolvimento de novas formulações baseadas em LS.

A segunda tarefa focou a modificação química dos LS para melhorar o seu desempenho como dispersantes em formulações de betão. A primeira abordagem consistiu num tratamento oxidativo dos LS catalisado por uma lacase visando o aumento do seu peso molecular ($M_w$) e a quantidade de grupos oxidados. A oxidação catalisada por lacase nas condições otimizadas (40 ºC, pH 4,5, concentração de enzima de 83–500 $U \cdot g^{-1}$ durante 90 min) permitiu obter um aumento de $M_w$ até 11 vezes superior e quase duplicou a quantidade de grupos carbonilos e carboxilos sem usar quaisquer mediadores. Os LS modificados mantiveram a sua solubilidade em água e o seu potencial zeta foi semelhante ao do LS inicial. A caracterização do LS modificado por UV-Vis, FTIR-ATR e espectroscopia de RMN $^{13}C$ quantitativo foi realizada e os grupos sulfónicos e fenólicos foram determinados por titulação condutimétrica. Concluiu-se que a polimerização dos LS ocorreu principalmente através da formação de novas ligações éter-arilo (dois terços da modificação) e ligações bifenilo (o terço restante).

**resumo (*continuação*)**

De seguida, outras estratégias de modificação química foram estudadas, incluindo a (i) modificação dos LS catalisada por polioxometalatos e a modificação dos LS catalisada por lacase mediada por polioxometalatos, (ii) glioxalação, (iii) técnicas de polimerização radicalar com desativação reversível (RDRP), tais como transferência reversível de cadeia por adição-fragmentação (RAFT), e (iv) síntese de dispersantes poliméricos a partir de LS não iónicos usando dois derivados diferentes oligoméricos epoxidados de poli (etileno glicol) (PEG) e poli (propileno glicol) (PPG). Os LS modificados foram usados para preparar pastas de cimento, cuja fluidez/trabalhabilidade foi avaliada e comparada com superplastificantes de fonte petrolífera, como policondensado de formaldeído e naftaleno sulfonado (NSF) e copolímero éter policarboxilato (PCE). Os resultados revelaram que os produtos mais promissores são LS modificados com PPG devido ao enxerto de cadeias de PPG nos grupos hidroxilo fenólicos nos LS. Estes produtos apresentaram a melhor eficiência dispersante, provavelmente relacionada à repulsão eletrostática (causada pelos grupos ionizáveis, tais como grupos sulfónicos nos LS), e simultaneamente com o impedimento estérico (devido às cadeias PPG enxertadas).

A terceira tarefa consistiu na preparação de poliuretanos (PU) a partir de LS dopados com nanotubos de carbono (MWCNTs) na gama de concentrações 0,1–1,4% m/m, produzindo um copolímero condutor compósito, que foi utilizado na produção de sensores químicos potenciométricos no estado sólido. Os PUs a partir de LS dopados com 1,0% m/m MWCNTs exibiram a condutividade elétrica mais relevante e adequada para a aplicação em sensores. O sensor potenciométrico a partir de LS exibiu uma resposta quase Nernstiana ou supernernstiana a uma ampla gama de metais de transição, incluindo Cu(II), Zn(II), Cd(II), Cr(III), Cr(VI), Hg(II) e Ag(I) a pH 7 e Cr(VI) a pH 2. Igualmente, exibiu uma resposta redox ao par redox Fe(II)/(III) a pH 2. Ao contrário de outros sensores potenciométricos a partir de materiais compósitos semelhantes a partir de outras lenhinas, esta membrana polimérica flexível a partir de LS não sofreu complexação irreversível com Hg(II). Adicionalmente, foi registada uma resposta fraca em relação aos líquidos iónicos, $[C_2mim]Cl$ e ChCl. Ao contrário dos compósitos a partir de LS contendo MWCNTs, aqueles dopados com óxido de grafeno (GO), GO reduzido (rGO) e grafite (Gr) não revelaram a mesma condutividade elétrica, mesmo com cargas até 10% m/m. Este fato está associado, pelo menos parcialmente, com as diferentes capacidades de dispersão da carga dentro da matriz polimérica.

Por fim, a quarta tarefa consistiu em avaliar a viabilidade em usar LS não modificado como poliol na formulação de adesivos de poliuretano (PU). O LS purificado foi dissolvido em água para simular a sua concentração no licor sulfito (SSL) e, de seguida, reagiu com difenilmetano-4,4'-diisocianato polimérico (pMDI) na presença ou ausência de poli(etileno glicol) com $M_w$ 200 ($PEG_{200}$) como segmento de reticulação flexível. Os adesivos de PU a partir de LS resultantes foram caracterizados por espectroscopia de infravermelho e técnicas de análise térmica. A força de adesão dos novos adesivos foi avaliada usando *Automated Bonding Evaluation System* (ABES) tendo sido usadas tiras de madeira como material de teste. Os resultados mostraram que a adição de $PEG_{200}$ contribuiu positivamente tanto para a homogeneização da mistura de reação e melhor reticulação da rede polimérica, como para as interações de interface e resistência adesiva. Este último foi comparável à resistência adesiva registada para uma cola branca comercial com valores de tensão de corte de quase 3 MPa. A formulação de adesivo de PU otimizada a partir de LS foi avaliada quanto à cinética de cura usando os métodos de Kissinger e Ozawa por calorimetria diferencial de varrimento não isotérmica. Concluiu-se que o processo de cura segue uma tendência semelhante à observada com outras formulações de PU e que a energia de ativação está na gama de 60–70 $kJ \cdot mol^{-1}$ dependendo do método aplicado.

**keywords**

Sulphite spent liquors; lignosulphonates; dispersants; concrete; conductive composites; polyurethanes; adhesives.

**abstract**

Lignosulphonates (LS) are sulphonated lignin-derived by-products present in sulphite spent liquors (SSL) from acidic sulphite pulping. SSL are mostly burned for inorganic base and energy recovery and considered as underutilized natural resources. The possibility of increasing the company profits with the valorization of LS, through the production of value-added products for different market applications, is highly motivating and is a challenge towards the biorefinery and circular economy concepts.

The magnesium-based acidic sulphite cooking process adopted at CAIMA Indústria de Celulose S.A. changed significantly in the last years. Formerly, it aimed at the production of paper-grade cellulosic pulp from eucalypt wood, but nowadays CAIMA produces dissolving pulp from *Eucalyptus globulus* wood under harsher conditions. Considering that the re-profiling of the sulphite process may have caused inevitable changes in the composition of the final SSL, the first task of this thesis consisted in a systematic chemical analysis to assess the structural features of sulphite spent liquors (SSL) followed by the isolation of LS-rich fractions from SSL yielding purified LS. The chemical composition of SSL showed that more severe pulping conditions led to an increase of volatile compounds, such as acetic acid, methanol and furfural, whilst the amount of dissolved sugars and LS increased less significantly. In turn, the chemical structure of LS, showed that harsher pulping conditions lead to the increase of the molecular weight, degree of condensation and sulphonation degree. The following tasks of the thesis aimed at the development of new formulations based on LS.

The second task focused on the chemical modification of LS to improve their performance as plasticizing dispersants in concrete formulations. The first approach consisted on a laccase-catalyzed oxidative treatment of LS targeting the increase of their molecular weight ($M_w$) and the amount of oxidized groups. The laccase assisted oxidation under optimized conditions (40 ºC, pH 4.5, enzyme loads of 83–500 $U \cdot g^{-1}$ for 90 min) allowed a $M_w$ increase up to 11-fold and almost doubled the amount of carbonyl and carboxyl groups without using any mediators. Modified LS maintained their solubility in water and their zeta-potential was closed to that of initial LS. Characterization of modified LS by UV-Vis, FTIR-ATR, and quantitative $^{13}C$ NMR spectroscopy was performed and the sulphonic and phenolic groups were assessed by conductometric titration. It was concluded that LS polymerization occurred mostly via the formation of new aryl ether bonds (two thirds of the modification) and biphenyl bonds (the remaining third). Thereafter, other chemical modification strategies were examined including the (i) polyoxometalate-catalysed modification and

**abstract (*continuation*)**

polyoxometalate-mediated laccase modification of LS, (ii) glyoxalation, (iii) reversible deactivation radical polymerization techniques (RDRP), such as reversible addition-fragmentation chain transfer (RAFT), and (iv) synthesis of LS-based non-ionic polymeric dispersants using two different epoxidized oligomer derivatives of poly(ethylene glycol) (PEG) and poly(propylene glycol) (PPG). The modified LS were used to prepare cement pastes, which fluidity/workability was evaluated and compared with commercial petroleum-based superplasticizers, such as naphthalene sulfonate formaldehyde polycondensate (NSF) and copolymer polycarboxylate ethers (PCE). Results revealed that the most promising products are PPG-modified LS due to the grafting of PPG chains in the phenolic hydroxyl groups in LS. The enhanced dispersant efficiency of the ensuing products is probably related to electrostatic repulsion (caused by the ionizable groups such as sulfonic groups from LS) along with steric hindrance (due to the grafted PPG chains).

The third task consisted in preparing LS-based polyurethanes (PUs) doped with multiwalled carbon nanotubes (MWCNTs) within the range of 0.1–1.4 % w/w, yielding a unique conducting copolymer composite, which was employed as a sensitive material for all-solid-state potentiometric chemical sensors. LS-based PUs doped with 1.0 % w/w MWCNTs exhibited relevant electrical conductivity suitable for sensor applications. The LS-based potentiometric sensor displayed a near-Nernstian or super-Nernstian response to a wide range of transition metals, including Cu(II), Zn(II), Cd(II), Cr(III), Cr(VI), Hg(II), and Ag(I) at pH 7 and Cr(VI) at pH 2. It also exhibited a redox response to the Fe(II)/(III) redox pair at pH 2. Unlike other lignin-based potentiometric sensors in similar composite materials, this LS-based flexible polymeric membrane did not show irreversible complexation with Hg(II). Only a weak response toward ionic liquids, [$C_2$mim]Cl and ChCl, was registered. Contrary to LS-based composites comprising MWCNTs, those doped with graphene oxide (GO), reduced GO (rGO), and graphite (Gr) did not reveal the same electrical conductivity, even with loads up to 10 % (w/w), in the polymer composite. This fact is associated, at least partially, with the different filler dispersion abilities within the polymeric matrix.

Finally, the fourth task consisted in assessing the feasibility of using LS unmodified polyol in the formulation of polyurethane (PU) adhesives. Purified LS was dissolved in water to simulate its concentration in sulphite spent liquor and then reacted with 4,4'-diphenylmethane diisocyanate (pMDI) in the presence or absence of poly(ethylene glycol) with $M_w$ 200 ($PEG_{200}$) as soft crosslinking segment. The ensuing LS-based PU adhesives were characterized by infrared spectroscopy and thermal analysis techniques. The adhesion strength of new adhesives was assessed using Automated Bonding Evaluation System (ABES) employing wood strips as a testing material. The results showed that the addition of $PEG_{200}$ contributed positively both to the homogenization of the reaction mixture and better crosslinking of the polymeric network, as well as to the interface interactions and adhesive strength. The latter was comparable to the adhesive strength recorded for a commercial white glue with shear stress values of almost 3 MPa. The optimized LS-based PU adhesive formulation was examined for the curing kinetics using the Kissinger and Ozawa methods by non-isothermal differential scanning calorimetry. It was concluded that the curing process follows a similar trend to that observed with other PU formulations and that the activation energy is within the range of 60-70 $kJ \cdot mol^{-1}$ depending on the applied method.

## Content

**List of abbreviations and symbols**

| | |
|---|---|
| $^{1}$H NMR | proton nuclear magnetic resonance |
| $^{13}$C NMR | carbon-13 nuclear magnetic resonance |
| 1D | one-dimensional |
| 2D | two-dimensional |
| 3D | three-dimensional |
| ABES | automated bonding evaluation system |
| ABTS | 2,2′-azino-bis(3-ethylbenzthiazoline-6-sulfonic acid) |
| ATRP | atom transfer radical polymerization |
| BPA | bisphenol A |
| BiBB | 2-bromoisobutyryl bromide |
| CNT | carbon nanotube |
| CP | conducting polymer |
| CPM | conducting polymeric membranes |
| $D_2O$ | deuterated oxide |
| DAEO | dodecyloxy-poly(ethylene glycol) glycidyl ether |
| DCM | dichloromethane |
| DDMAT | 2-(dodecylthiocarbonothioylthio)-2-methylpropionic acid |
| DGEBA | diglycidyl ether bisphenol A |
| DMA | dynamic mechanical analysis |
| DMC | dimethyl carbonate |
| DP | degree of polymerisation |
| DSC | differential scanning calorimetry |
| $E_a$ | activation energy |
| EBriB | ethyl 2-bromoisobutyrate |
| EC | ethylene carbonate |
| ECH | epichlorohydrin |
| EPEG | ethoxy (2-hydroxy) propoxy-poly(ethylene glycol) glycidyl ether |
| FTIR-ATR | attenuated total reflectance Fourier transform infrared spectroscopy |
| FOH | furfuryl alcohol |
| GC | glycerol carbonate |
| GC-FID | gas chromatography – flame ionization detector |
| GO | graphene oxide |
| GPC | gel permeation chromatography |
| Gr | graphite |
| HBT | 1-hydroxy-benzotriazole |
| HMDA | 1,6-hexamethylenediamine |
| HMDI | hexamethylene diisocyanate |

| | |
|---|---|
| HPLC | high performance liquid chromatography |
| HSQC | heteronuclear single quantum coherence |
| $H_{(t)}$ | enthalpy of the reaction up to time *t* |
| $H_T$ | total enthalpy of the reaction |
| KL | kraft lignin |
| LB | Langmuir–Blodgett |
| LBL | layer-by-layer |
| LCA | life cycle assessment |
| LCC | complex lignin-carbohydrate |
| LS | lignosulphonates from spent sulphite liquor |
| $LS_{lyo}$ | lyophilized sulphite spent liquor |
| LSF | purified lignosulphonates from thin spent sulphite liquor |
| LSG | purified lignosulphonates from thick spent sulphite liquor |
| MDI | 4,4'-diphenylmethane diisocyanate |
| MDF | middle density fibre board |
| MF | melamine-formaldehyde |
| MLS | maleated lignosulphonate |
| $\bar{M}_n$ | number average molecular weight |
| MOFs | metal-organic frameworks |
| MUF | melamine-urea-formaldehyde |
| MWCNT | multiwalled carbon nanotube |
| $\bar{M}_w$ | weight average molecular weight |
| MWCO | molecular weight cut off |
| NCO | isocyanate group |
| NIPU | non-isocyanate polyurethane |
| NSF | naphthalene sulfonate formaldehyde polycondensate |
| NMR | nuclear magnetic resonance |
| o.d. | oven-dried |
| $OCH_3$ | methoxyl group |
| OH | hydroxyl group |
| $OH_{phen}$ | phenolic hydroxyl group |
| OL | organosolv lignin |
| PANI | polyaniline |
| PC | propylene carbonate |
| PCE | polycarboxylate ether |
| PCL | poly(ε-caprolactone) |
| PCLLA | poly(ε-caprolactone-*co*-lactide |
| PDI | polydispersity index |
| PEDOT | poly(3,4-ethylenedioxythiophene) |
| PEG | poly(ethylene glycol) |

| | |
|---|---|
| $PEG_{200}$ | poly(ethylene glycol) with molecular weight 200 |
| PEGDE | poly(ethylene glycol) diglycidyl ether |
| PF | phenol-formaldehyde |
| PHU | poly(hydroxyurethane) |
| PLLA | poly(L-lactic acid) |
| PMAA | poly(methacrylic acid) |
| PMDETA | *N*,*N*,*N*′,*N*″,*N*″-pentamethyldiethylenetriamine |
| pMDI | polymeric 4,4’-diphenylmethane diisocyanate |
| PO | propylene oxide |
| POM | polyoxometalate |
| PPG | poly(propylene glycol) |
| PPGDE | poly(propylene glycol) diglycidyl ether |
| PU | polyurethane |
| PUF | polyurethane foam |
| RAFT | reversible addition-fragmentation chain transfer |
| rGO | reduced graphene oxide |
| RI | refractive index |
| ROP | ring opening polymerization |
| SEC | size exclusion chromatography |
| SSL | (thin) spent sulphite liquor |
| $T$ | temperature |
| TDI | toluene-2,4-diisocyanate |
| TEMPO | 2,2,6,6-tetramethyl-1-piperidinyloxy |
| TFA | trifluoroacetic acid |
| $T_g$ | glass transition temperature |
| TGA | thermogravimetric analysis |
| THSL | thick spent sulphite liquor |
| $T_p$ | peak temperature |
| UF | urea-formaldehyde |
| VA | vanillin alcohol |
| XOS | xylo-oligosaccharides |
| α | degree of cure or conversion |
| β | heating rate |
| ε | absorption coefficient |
| δ | chemical shift (in ppm) |
| $k$ | reaction rate coefficient or rate of constant |
| $\sigma_{AC}$ | alternating current electrical conductivity |
| $\sigma_{DC}$ | direct current electrical conductivity |

## List of Figures

## List of Tables

# 1. Introduction

## 1.1. BACKGROUND

In the 20th century, most of the energy supply and chemicals production derived from fossil fuel-based resources, such as crude oil. However, the continued depletion of finite fossil resources and their adverse environmental impacts have highlighted the necessity to reduce the dependence on this type of resources. Due to the increasing threat of global warming and also considering the impact of the public view, governments began to look seriously for alternative and more sustainable resources as feedstock replacements, namely biomass. The biorefinery and circular economy concepts are becoming imperative in the industrial sector, especially in the pulp and paper industry. Thus, in order to improve the economic sustainability of pulp mills, the valorisation of the ensuing by-products has been directed towards new added-value products to expand their economic profits. In particular, industrial (technical) lignin has attracted worldwide attention as it is an abundant biodegradable renewable resource for the production of biofuels, and a platform to prepare new chemicals, and value-added products such as polymers.

In 2019, the worldwide production of wood pulps exceeded 190 million tons (this information being solely based on kraft and sulphite pulps) (Figure 1a). The world dominant process to produce chemical wood pulp is the kraft pulping method while the sulphite process, which affords lignosulphonates (LS) as by-products, only represents *ca*. 2% of the world chemical pulp production as illustrated in Figure 1b [1]. Yet, the global lignin market is mostly composed of lignosulphonates (*ca*. 88 %, LS), followed by kraft lignin (*ca*. 9 %, KL) and organosolv lignin (*ca*. 2 %, OL), which is gaining popularity due to the production of second generation biofuels (bioethanol production) and high-quality lignin [2,3]. Therefore, the main economically viable source of lignin is the sulphite process, which has been attracting significant attention in the context of the biorefinery concept. The sulphite chemical pulp is marketed as a raw material (*e.g*., dissolving pulp) and sulphite spent liquors (SSL) are processed to produce fuels (such as bioethanol), additives (proteins, xylitol, etc.) and/or lignin-based chemicals.

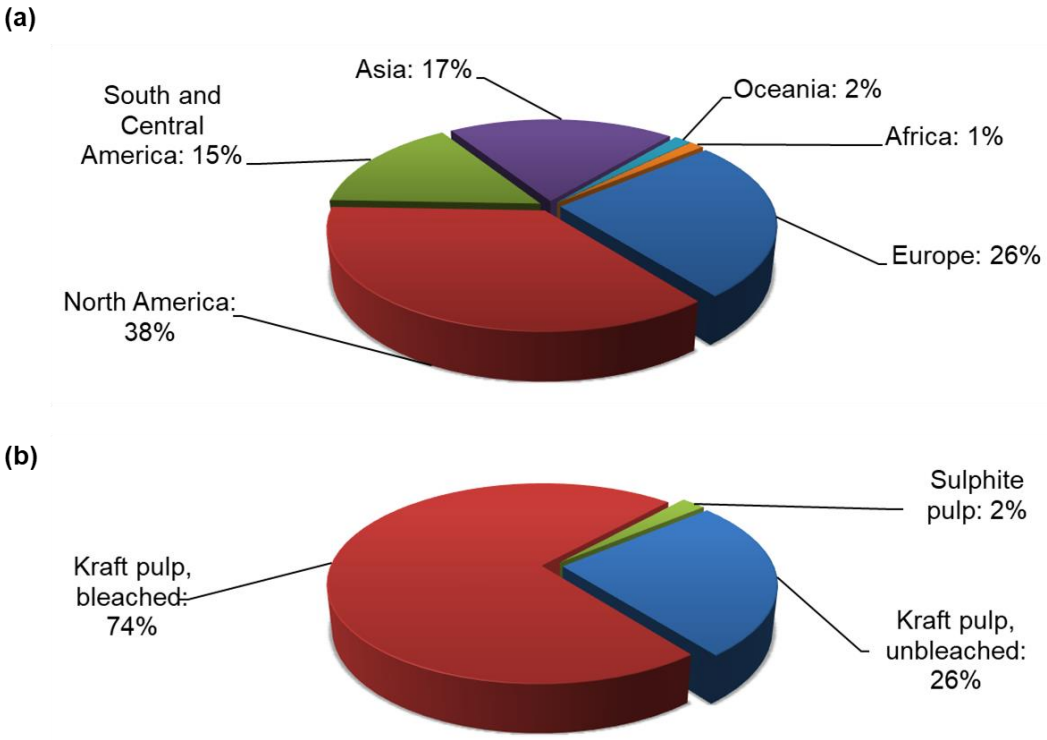


**Figure 1.** World production of wood pulp in 2019 in different world regions (a) and by different production methods (b) [1]**.**

Nowadays, *Eucalyptus globulus* is the major wood source to produce hardwood bleached kraft pulp in Europe, including Portugal and Spain. There is only one Portuguese company, CAIMA Indústria de Celulose SA, that produces dissolving pulp from *Eucalyptus globulus* through the magnesium-based acidic sulphite cooking process generating LS-rich sulphite spent liquors (SSL). In 2019, the volume of dissolving pulp production by Caima reached 107 thousand tons [1] and, nowadays, the company has the capacity to produce around 125 thousand tons of dissolving pulp per year [4]. Changing the pulping process from the production of paper-grade to the production of dissolving pulp might have caused inevitable changes in the composition of the final sulphite spent liquor affecting its potentialities for subsequent processing to meet biorefinery requirements. Hence, this thesis aims at addressing this issue as it is briefly described in section1.2.

## 1.2. OBJECTIVES AND OUTLINE OF THE THESIS

Lignosulphonates (LS) from the sulphite pulping industry can find a wide variety of applications (as binders, dispersants and other minor applications), most of them depending on their good water-solubility, which is the reason for the world lignin market being largely restricted to LS. The possibility of increasing the company profits with the valorization of their by-products, such as LS, through the production of value-added products for different market applications is highly motivating. Furthermore, LS from eucalypt (hardwood) wood are the least studied in polymeric applications compared to LS from softwood and kraft pulping. Therefore, this Ph.D. project targets opportunities for the valorization of eucalypt LS towards new added-value products to expand the economic profits of the pulp industry within the scope of biorefinery and circular economy concepts. The main objectives of this study were as follows:

1. The comprehensive characterization of the structural features of lignosulphonates (LS) from the magnesium-based acid sulphite pulping of *Eucalyptus globulus* wood for the production of dissolving pulp.

2. The targeted modification of LS to enhance their plasticising effect in additives to improve the workability of concrete formulations.

3. The synthesis and characterization of new LS-based polyurethane conductive polymeric membranes (CPM) and evaluation of their potential in conducting devices and sensor applications.

4. The development of LS-based formaldehyde-free adhesives for potential application in biocomposites.

This thesis is divided in eight chapters, the first one (**CHAPTER 1**) includes the background and the objectives of this Ph.D. thesis herein presented.

**CHAPTER 2** provides an overview of the literature focused on lignin and LS structure and lignin-based materials with particular attention to employing LS as a macromonomer for the production of polymeric materials. The referred materials are directed to the applications of interest to this Ph.D. project and include plasticizers/dispersants for concrete applications, lignin-based conducting composites and adhesives for biocomposites.

**CHAPTER 3** consists in the experimental section where all materials and experiments performed are thoroughly described including all details necessary for possible reproduction.

**CHAPTER 4** presents the complete characterization of sulphite spent liquors provided by CAIMA company as well as the purification of LS from these liquors and their thorough structural characterization. These results are essential to assess the viability of using eucalypt LS in the synthesis of polymeric formulations for specific applications.

**CHAPTER 5** describes and discusses the synthesis of LS-based dispersants for concrete applications. Different approaches were investigated including (*i*) laccase oxidative polymerization of LS, (*ii*) polyoxometalate-mediated laccase modification of LS, (*iii*) glyoxalation of LS, (*iv*) reversible deactivation radical polymerization techniques (RDRP), such as reversible addition-fragmentation chain transfer (RAFT), and (*v*) the synthesis of LS-based non-ionic polymeric dispersants using two different epoxidized oligomer derivatives of poly(ethylene glycol) (PEG) and poly(propylene glycol) (PPG). The most promising LS-based products were characterized and were used to prepare cement pastes, which fluidity/workability was evaluated.

**CHAPTER 6** is devoted to the synthesis of flexible conducting membranes for sensing applications. Specifically, LS-based polyurethanes (PUs) doped with multiwalled carbon nanotubes (MWCNTs) were prepared and employed as a sensitive material for all-solid-state potentiometric chemical sensors for the detection a wide range of transition metals. Other carbon fillers, such as graphene oxide, reduced graphene oxide and graphite, were also studied for the same goal.

**CHAPTER 7** is dedicated to the synthesis of LS-based polyurethanes (PU) adhesives using commercial 4,4'-diphenylmethane diisocyanate (pMDI) with or without polyethylene glycol with $M_w$ 200 ($PEG_{200}$) as soft crosslinking segment. LS-based PU adhesives were characterized and their adhesion strength was assessed. Furthermore, the kinetics of the curing process of the most promising LS-based PU adhesive formulation was studied by non-isothermal differential scanning calorimetry.

Finally, in **CHAPTER 8** the main conclusions of the work are presented including some perspectives for future work.

# 2. State of the art

Lignocellulosic biomass (wood and non-wood) is the most abundant renewable resource in the world. The properties of biomass are unique to the plant and are dependent on plant species, source and growth conditions. Wood is mainly composed of holocellulose comprising cellulose (30–50 %) and hemicelluloses (20–35 %), both accounting for approximately two thirds of the wood material, lignin (*ca.* 15–30 %) and in a minor extent other components such as extractives, minerals and proteins [5,6]. Worldwide, eucalypts are among the most important short-rotation hardwoods planted for the pulp and paper industry [7]. Different species are grown in different countries and, in Portugal and Spain, *Eucalyptus globulus* is the major wood source used for the production of bleached kraft pulp and dissolving pulp. Only one Portuguese company produces dissolving pulp using the magnesium-based acidic sulphite pulping of eucalypt wood. Due to the economic and commercial importance of the *Eucalyptus globulus* species, the evaluation of its chemical composition has been the focus of several studies over the years and is summarized in Table 1.

**Table 1.** Chemical composition of *Eucalyptus globulus* wood (% w/w o.d. wood) [5,7–10].

| **Wood component** | ***Eucalyptus globulus*** |
|---|---|
| Ash | 0.3–0.6 |
| Extractives | |
| Dichloromethane | 0.3–0.4 |
| Toluene-ethanol | 1.7 |
| Ethanol | 0.9–2.3 |
| Methanol-water | 2.4 |
| Water | 1.3–3.4 |
| Total lignin | 22.1–26.1 |
| Klason lignin | 19.5–21.9 |
| Soluble lignin | 1.6–4.9 |
| Holocellulose | 64.1–72.0 |
| Cellulose | 48.3–54.0 |
| Glucan | 49.8 |
| Xylans | 14.4 |
| Pentosans | 14.1–18.9 |
| Hemicelluloses | 18.7 |
| 1% NaOH solubles | 8.2–17.4 |

## 2.1. THE STRUCTURE OF LIGNIN

Lignin is the second most abundant renewable natural polymer from biomass after cellulose and is the most abundant aromatic-based renewable source with the advantage that it does not compete with food stocks. Lignin is generated in huge amounts worldwide from forestry and agricultural activities. As a matter of fact, the amount of lignin in forest biomass is massive. Considering that it has been estimated that there are approximately 3 trillion trees on Earth [11], the global amount of lignin can be assessed at around 100 000 million tonnes (if assuming an average lignin content of 25 %) [12]. The worldwide production of lignin is approximately 100 million tons per year and was valued at 732.7 million USD in 2015. This is expected to reach 913.1 million USD by 2025 with a compound annual growth rate (CAGR) of 2.2 % [2] and reach 1.12 billion USD by 2027 [13]. The most important source of lignin feedstock is the pulping and paper industry, mainly the kraft pulping process, generating annually around 50–70 million tons of lignin dissolved from wood. However, only 1–2 % of the total amount of lignin is recovered to produce specialty chemicals such as dispersants, adhesives, surfactants and other value-added products, since most of these applications depend on the good water-solubility of lignin. The majority of the lignin is burned as low-value fuel to generate electricity and heat [2,14]. Lignin can also be extracted from herbaceous crops, such as corn stover, wheat, rice, flax and others [15,16]; however, considering the focus of this thesis, lignin from herbaceous sources will not be discussed.

Lignin is responsible for water repellence and structural integrity in plants. This results from the fact that it consists in an amorphous polymer, which has an irregular hyperbranched or crosslinked aromatic structure, depending on both botanical origin of plant material and the extraction process used for lignin isolation [17,18]. Lignin is formed through the polymerization of the three main phenylpropanolic monomers, the so-called monolignols. Monolignols differ in structure, in particular in the degree of methoxylation, depending on plant type and include *p*-coumaryl alcohol (H unit), coniferyl alcohol (G unit) and synapyl alcohol (S unit) (Figure 2a). Lignification differs considerably from simple dimerization of the monolignols. Lignification occurs via radical coupling reaction involving the $\beta$-carbon, the phenolic hydroxyl (OH) and the aromatic C5 (only in G or H units); hence, originating carbon−carbon and ether bonds forming the ensuing three-dimensional macromolecular structure [19,20]. As a result, lignin comprises different types of inter-unit linkages (Figure

2b) and several chemical functional groups including hydroxyl, methoxyl, carbonyl and carboxyl groups, as depicted in Figure 2c.

In growing plants, lignin forms chemical linkages with polysaccharide constituents, such as hemicelluloses (xylan and glucomannan) and, possibly, to a minor extent with cellulose, which are designated as lignin-carbohydrate complexes (LCC) [5,21,22]. Three main types of LCC bonds have been suggested in the literature, namely benzyl esters, benzyl ethers, and phenyl glycosides [5,21]. Furthermore, the presence of phenolic and aliphatic OH moieties promotes inter- and intramolecular associations through hydrogen bonding enhancing lignin's cohesive energy [23]. Therefore, lignin exhibits relatively high glass transition temperatures ($T_g$) ranging between 70 and 170 ºC [24–27], which is higher for softwood lignins than for hardwood lignins [23]. The glass transition, $T_g$, is the temperature assigned to a region above which amorphous materials are fluid or rubbery and below which they are immobile and rigid [28]. Depending on the source and the method to produce the technical lignins, lignins may also comprise other reactive moieties such as carbonyl, carboxyl and sulphonic groups [24–27].

Lignin from angiosperms (hardwood) exhibits striking structural differences from gymnosperms (softwood) due to their different content of methoxyl groups (Figure 2a). Lignin in hardwood is mainly composed of both G and S units with traces of H units and is usually referred as "guaiacyl-syringyl lignin", while lignin from softwood is mainly built up of G units with minor amounts of H units and is usually referred as "guaiacyl lignin" [18–20]. In general, the lignin content in wood is in the range 20–40 %, whereas in herbaceous plants it is less than 20 % as shown in Table 2.

Due to the complex and heterogeneous molecular architecture of lignin and its derivatives, their complete chemical and structural characterization is a difficult task. Therefore, various techniques must be used, including several wet chemistry procedures (*e.g.* chemical oxidation to determine monomeric proportions of S, G and H sub-units; specific methodologies to determine the diverse functional groups, among others), size exclusion chromatography (SEC) for weight molecular distribution and polydispersity assessment, nuclear magnetic resonance spectroscopy (NMR such as $^{1}$H NMR, $^{31}$P NMR,

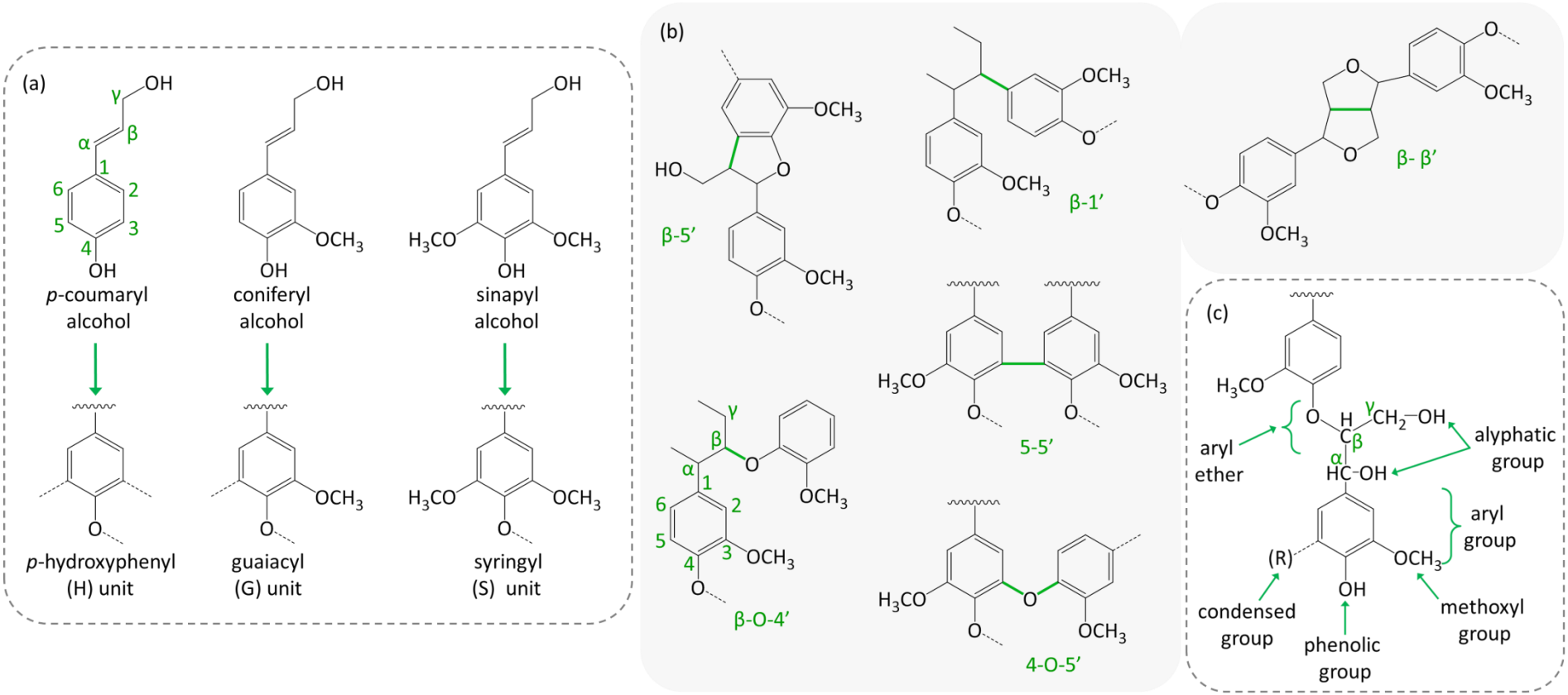


**Figure 2.** Chemical structure of (a) the three main monolignols and the corresponding building blocks in lignin, (b) some inter-unit linkage types and (c) functional groups in lignin [20,29].

quantitative $^{13}C$ NMR, and two-dimensional NMR) for structure elucidation including the content of inter-molecular linkages, functional groups, as well as other techniques [18,20,24,25,30–37].

**Table 2.** Lignin content (%) in some woody and herbaceous plants.

| **Species** | **Common name** | **Klason Lignin** | **Acid-soluble lignin** | **References** |
|---|---|---|---|---|
| Softwood | | | | |
| *Abies balsamea* | Balsam fir | 29.1 | *n.f.* | [5] |
| *Juniperus communis* | Common juniper | 30.1–32.1 | 0.7 | [5,38] |
| *Picea abies* | Norway spruce | 26.7–29.0 | 0.5 | [5,21,38,39] |
| *Picea orientalis* | Oriental spruce | 26.1–27.5 | 0.3 | [40,41] |
| *Pinus radiate* | Monterey pine | 26.4 | 0.6 | [42] |
| *Pinus sylvestris* | Scots pine | 27.5–27.7 | *n.f.* | [5,41] |
| *Pseudotsuga menziesii* | Douglas fir | 27–29.3 | *n.f.* | [5,43] |
| Hardwood | | | | |
| *Acacia mangium* | Brown salwood | 27.1 | 0.5 | [8,44] |
| *Acer rubrum* | Red maple | 25.4–27.4 | 3.8 | [5,39] |
| *Acer saccharum* | Sugar maple | 21.5–25.2 | 3.6 | [5,43,45] |
| *Betula alleghaniensis* | Yellow birch | 18.6 | 4.6 | [45] |
| *Betula papyrifera* | Paper/white birch | 18–22.6 | 3.9 | [5,39,43] |
| *Eucalyptus camaldulensis* | River red gum | 21.8–31.3 | 2.3 | [5,7] |
| *Eucalyptus globulus* | Blue gum | 20.5–21.9 | 1.6–5.0 | [5,7–9] |
| *Eucalyptus grandis* | Rose eucalypt | 25.1–25.7 | 1.0–2.7 | [7,8] |
| *Eucalyptus maculate* | Spotted gum | 18.5 | 3.1 | [7] |
| *Eucalyptus resinífera* | Red mahogany | 28.1 | 2.8 | [7] |
| Herbaceous plants | | | | |
| *Cannabis sativa* | Hemp | 4.6 | 1.5 | [46] |
| *Corchorus capsularis* | Jute | 13.3 | 2.8 | [46] |
| *Hibiscus cannabinus* | Kenaf | 12.2 | 3.0 | [46] |
| *Linun usitatissiumum* | Flax | 2.9 | 1.6 | [46] |
| *Tritium aestivum* | Wheat straw | 16 | 2.4 | [22] |

*n.f.* – data not found.

Currently, technical lignins are mostly obtained as side products of the three dominant chemical pulping processes, namely kraft, sulphite (both types of lignins contain a certain amount of sulphur groups) and soda (which is sulphur-free) (Figure 3). Technical lignin can also be produced in minor amounts from organosolv pulping (which is sulphur-free) (Figure

3). Therefore, depending on the main reactions during the selected delignification process (and naturally depending on the type of source), the structure of lignin in the plant/wood cell wall is modified, resulting in an entirely different technical lignin with unique chemical and structural features [24,25,27,31,47,48].

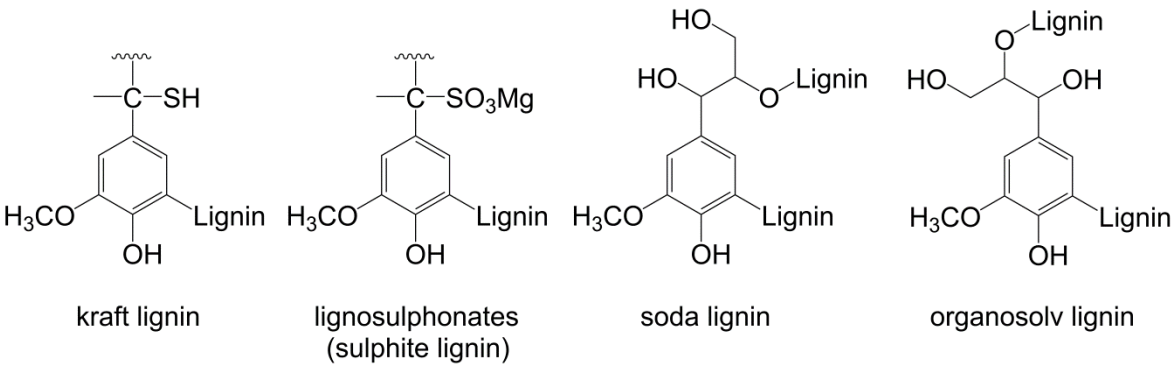


**Figure 3.** Schematic representation of the chemical structure of the repeating unit of technical lignins.

### 2.1.1. Sulphite pulping

The sulphite pulping process is used for the production of paper- or dissolving-grade pulps. Evtuguin [49] reviewed the fundamental principles of sulphite pulping and discussed the chemical composition and valorisation of spent sulphite liquors. A simplified scheme of the sulphite pulping process is depicted in Figure 4. Briefly, sulphite pulping is carried out in a digester filled with wood chips and cooking acid. Afterwards, the brown stock is washed and the pulp is separated from the spent sulphite liquor (SSL) and directed to the bleaching plant. The SSL is then concentrated by evaporation to produce 56–68 % (w/w) thick SSL (THSL). Part of THSL is burned along with other fuels, such as raw biomass, to produce energy and to regenerate the pulping base and $SO_2$ while the remaining fraction is processed into commercial products, as illustrated in Figure 4.

The sulphite processes are usually classified according to the pH range of the resultant pulping liquor, as shown in Table 3. Therefore, during sulphite pulping of wood, sulphur dioxide ($SO_2$) is used as the reagent and is present in aqueous solution in the form of hydrosulphite ($HSO_3^-$) or sulphite ($SO_3^{2-}$), depending on the medium pH. Consequently, at pH < 1 nearly all $SO_2$ is present in solution as undissociated $H_2SO_3$, at pH 4–5 as

hydrosulphite and at pH > 8 as sulphite [49]. The dissolution of $SO_2$ in aqueous solution decreases when the temperature increases preventing the effective delignification of wood when only $SO_2$ is used.

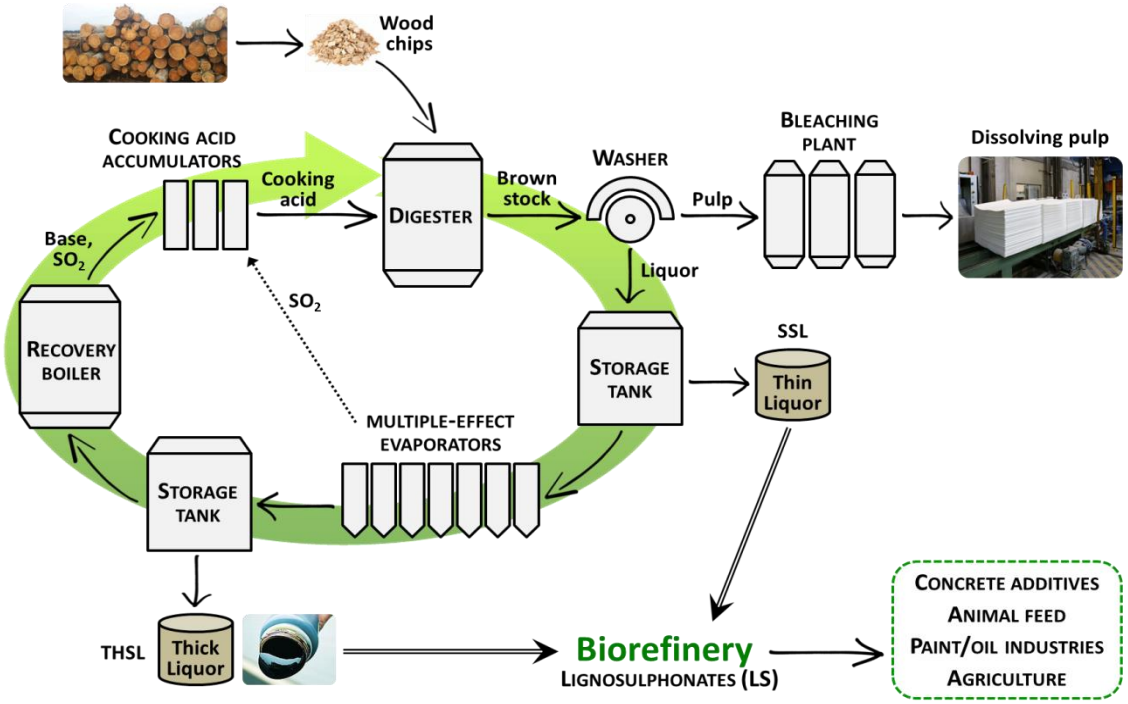


**Figure 4.** Scheme of the sulphite pulping and spent liquors recovery (adapted from [49]).

**Table 3.** Sulphite pulping processes classification [49].

| Method | pH range | Base alternative | Active reagents | T (ºC) |
|---|---|---|---|---|
| Acid sulphite | 1–2 | $Na^+$, $Ca^{2+}$, $Mg^{2+}$, $NH^{4+}$ | $H^+$, $HSO_3^-$ | 130–140 |
| Bisulphite | 3–5 | $Na^+$, $Mg^{2+}$, $NH^{4+}$ | ($H^+$), $HSO_3^-$ | 150–170 |
| Neutral sulphite | 6–9 | $Na^+$, $NH^{4+}$ | $HSO_3^-$, $SO_3^{2-}$ | 160–180 |
| Alkaline sulphite | 10–13 | $Na^+$ | $SO_3^{2-}$ | 160–180 |

Cooking bases, such as metal oxides of Na, Ca, Mg, and $NH_3$, are added to increase the retention of $SO_2$ in aqueous solution while a certain quantity of $SO_2$ is in the form of hydrosulphite or sulphite, depending on the type and amount of base involved. Nowadays, the most common regenerable base used in the sulphite process for the production of chemical pulps is magnesium [50]. Magnesium hydrosulphite solutions are stable at pH up to *ca*. 5 so both the acid sulphite pulping process at pH < 2 (comprising $SO_2/HSO_3^-$) and the

bisulphite pulping process at pH 3–5 (comprising $HSO_3^-$) can be carried out using this base [49,50].

Notice should be made that the sulphite pulping process is sensitive to the type of wood species used, especially the acid sulphite process. Some woods contain a significant amount of extractives, such as resins and polyphenols, which prevent effective delignification due to the occurrence of condensation reactions with lignin. For this reason, coniferous woods, such as spruce and hemlock, and hardwoods, namely beech, birch and some eucalyptus species, with a minimum content of extractives are favoured as raw material for acid sulphite pulping [50]. The chemical composition of hardwood LS is rather different from that of softwood LS [24,51]; LS from eucalypt wood is of lower molecular weight, less condensed and less structurally branched than LS from softwoods.

Basically, wood pulping consists in the degradation of lignin and subsequent dissolution in the cooking liquor allowing the release of the wood fibres. During the acid sulphite cooking process, delignification occurs through two types of reactions, sulphonation and hydrolysis. The sulphonation reaction allows the incorporation of sulphonic groups in the lignin macromolecular structure (Figure 5), especially in the α-position of the side chain of the phenylpropane unit (though in the γ-position it is also possible), while the hydrolysis reaction breaks the ether bonds between the phenylpropane units in lignin and polysaccharides (LCC) [49,50,52–55]. Lignin degradation (and sulphonation) under acidic conditions is also accompanied by condensation reactions, which lead to the formation of new alkyl-aryl linkages hence, increasing lignin molecular weight as depicted in Figure 6 [49,54,55].

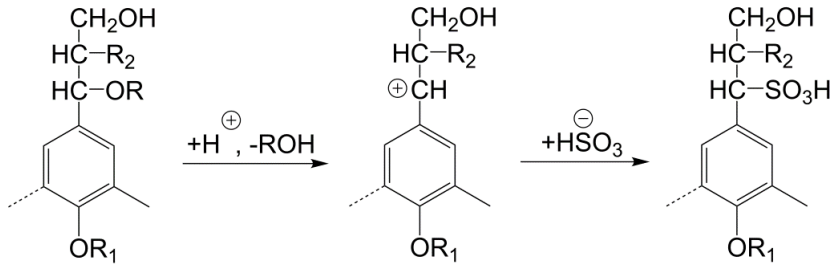


R = H, alkyl, aryl
$R_1$ = H, neighbouring lignin unit
$R_2$ = neighbouring lignin unit

**Figure 5.** General scheme of the sulphonation reactions of lignin units during acidic sulphite pulping [52,53].

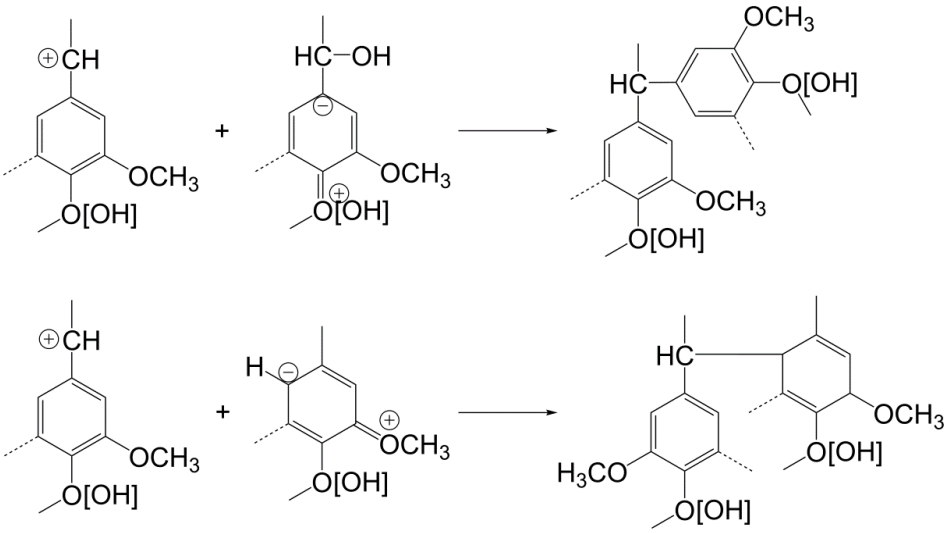


**Figure 6.** Acid-promoted condensation reactions of phenolic and non-phenolic units [49,54].

The high degree of lignin sulphonation (> 0.3 per phenylpropane unit) is only possible under acidic conditions [49] and may vary from 0.3 to 0.8 per phenyl propane unit [51,56]. The extensively sulphonated lignin is called lignosulphonate (LS) and is hydrophilic exhibiting enhanced water solubility. As mentioned above, lignin sulphonation is strongly affected by the acidity of the cooking liquor being more relevant when the pH value decreases. The best conditions for the hydrolysis and lignin sulphonation are provided during the acid sulphite cooking yielding pulps with low content of residual lignin. However, the excessive acidity of the cooking liquor leads to the hydrolytic degradation of polysaccharides and to the decrease in pulp yield and mechanical strength. Another problem associated with the acid sulphite process is that the impregnation of wood chips under acidic conditions is

very limited, making it difficult to diffuse the chemical reactants in the wood [49,50,52,53,55]. SSL from acid sulphite pulping of hardwoods, such as eucalypt, is mainly composed of water-soluble lignosulphonates (LS), xylo-oligosaccharides (XOS) and contains high amounts of pentose sugars and extractives of polyphenolic origin, which limits its refining by bioprocessing [51,57–59]. Fairly efficient refining of LS can be done by dialysis/ultrafiltration [51,60], fractionation on ion-exchange resins [61], and other separation processes, although membrane technology, such as ultrafiltration, has been recognized as a viable commercial process for recovering LS from SSL [14,47].

### 2.1.2. Lignosulphonates (LS) from sulphite spent liquors (SSL)

Worldwide, approximately 1 million tons of LS are produced annually [62], most of it isolated from SSL. Therefore, LS is the most abundant type of lignin available in the market in a large scale representing *ca*. 88% of the global lignin market [2,27,49,63]. LS market is dominated by key companies with strong global presence including Borregaard LignoTech (Norway), which is the largest producer of LS worldwide with more than 500 thousand tons (on dry basis), followed by Tembec (Rayonier Advanced Materials, Canada), and others such as Nippon Paper Industries Co. (Japan), Burgo Group (Italy), Domsjö Fabriker AB (Sweden), Xinyingda Chemicals Co. (Wuhan, China) and Xingzhenghe Chemical Co. (Shenyang, China) [27,63,64]. In 2018, LS market was valued at 760 million USD and it increased up to 790.6 million USD in 2019. Growth in the construction sector due to infrastructure development and population increase, rising demand from the animal feed business, increase in oil well exploration, and infrastructure development are some factors that are expected to boost the progress of the global LS market. Considering these factors, it is expected that LS market will spread above 1.03 billion USD by 2027, growing at a CAGR of 3.4 % from 2020 to 2027 [64,65].

The sulfonic acid groups in LS are mainly responsible for some of the unique physicochemical properties including the molecular conformation of LS in solution. Myrvold [66,67] suggested that the LS molecule is a randomly branched polyelectrolyte that coils in solution to form a ball-shaped like molecule with most of the sulphonated groups on its surface, as depicted in Figure 7. Supported by experimental data, Myrvold described how branched polyelectrolytes are similar to microgels, except when it comes to polyelectrolyte

expansion, confirming that LS is not a microgel. Moreover, the author proposed that the longest chain in the LS molecule is the backbone, to which side chains are covalently attached, and this backbone is less sulphonated than the side chains thus, it is more hydrophobic [66].

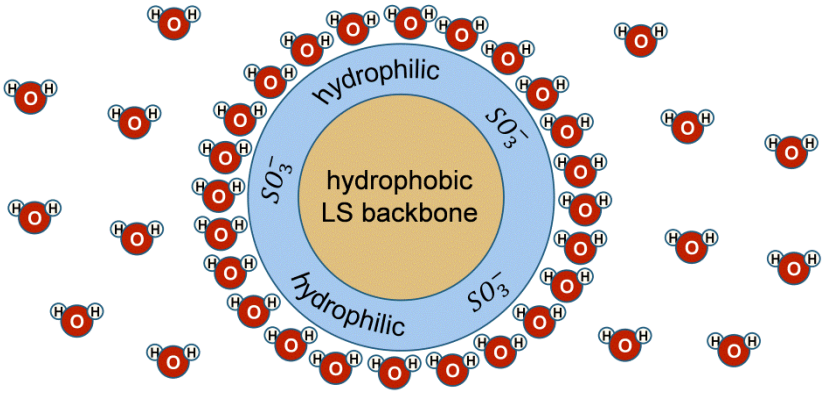


**Figure 7.** Schematic representation of the molecular conformation of LS in solution according to Myrvold [66,67].

Another important feature of LS in solution is that LS molecules interact with themselves forming intermolecular aggregates, depending on the LS concentration and temperature [68,69]. It should also be noted that disaggregation of these LS aggregates is a very slow process that can last for several weeks but can be speeded up by increasing the pH and/or the temperature of the LS solution [68]. Ruwoldt summarized the physicochemical properties of lignosulphonates regarding their composition and structure in order to understand and outline the behaviour and properties of LS in aqueous solutions, at surfaces and interfaces [70]. In aqueous solution, the conformation of LS, the colloidal state, and adsorption at surfaces or interfaces can be affected by a variety of parameters, such as pH, the concentration of other electrolytes, temperature as well as the presence of organic solvents. Additionally, the monolignol composition, the molecular weight distribution, and chemical modification may also affect the physicochemical behaviour of LS. LS structure comprises ionizable functional groups (mainly sulfonic acid groups, but also carboxylic acid groups) as well as hydrophobic groups (including aromatic, residual aliphatic units and also some oxygen containing groups). The balance of hydrophilic (ionizable) and hydrophobic

moieties rules the behaviour of LS in solution and can ultimately be used for fine-tuning LS to specific applications [2,31,71–81].

As illustrated in Figure 8, alongside energy recovery, LS can find a wide variety of applications such as binders (adhesive properties), dispersants and emulsifiers (surface-stabilizing properties) and sequestrants (chelation properties). LS have also been marketed for animal feed additives industries as well as for other minor applications such as components of coal briquettes, components of linoleum paste, dispersant for dyes and pigments, dispersant in oil-drilling mud, metal sequestrant for water treatment for boilers and cooling systems, flocculants, among others. In particular, sodium LS are the most commercialized LS mainly used as economical plasticizers in concrete admixtures and pellet binder in animal feed. Calcium LS are favoured for animal feeds and oil well additives. Magnesium LS are mostly employed in animal feed applications owing to their antimicrobial and preservative properties as well as substitutes for conventional chloride materials in dust control applications [47,48,65]; the other portion of SSL corresponding to XOS can be used to produce bioethanol [49,82,83]. LS are also prospective raw materials for the production of aromatic aldehydes and flavours [84,85], fine chemicals for pharmaceutics [86], flocculants, adsorbents and dispersants in different (waste) water systems [80], precursors for textile dyes [87] and synthetic polymers [88,89], including formaldehyde-based adhesives [89,90], and conducting composites [91], though these applications have not reached large scale production. Most of these applications depend on the good water-solubility of these technical lignins, which is the reason for world lignin market being largely restricted to LS [2]. The valorisation of LS represents an important profit for pulp companies and is an opportunity towards biorefinery and circular economy concepts yet, its applicability is still quite a challenge.

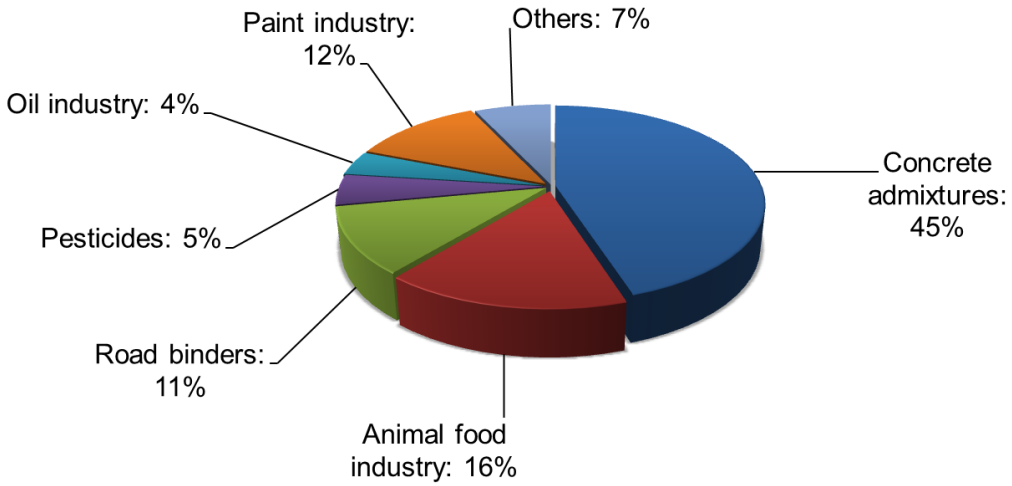


**Figure 8.** Lignosulphonates consumption in different applications [62].

### 2.2. LIGNIN-BASED MATERIALS

Since the 60's, various patents [48] related to the use and/or modification of lignin including LS for a wide diversity of applications were submitted and since then many others emerged. In fact, the huge number of patents related to lignin reflects the commercial relevance of lignin-based research and development designed for its use in high-value products [48]. Lignin-containing formulations can be used in a wide range of applications such as dispersant and concrete additives, batteries and energy storage, flocculants, metal adsorbents, dust suppressants, biomedical applications, composites, adhesive binders, resins, food packaging, foams, sensor applications [2,31,71,72,74–81,92]. Therefore, numerous polymers have been synthesized using lignin including LS (as such or after chemical modification) as an additive, a blend component and/or a macromonomer. Technical lignins can be used without chemical modification being directly incorporated into a polymeric matrix, which, in terms of industrial applications, is particularly attractive due to the possibility of reducing production costs and obtaining bio-based products. However, only relatively small amounts of lignin (up to 20–30 %) can be incorporated due to the poor mechanical properties of the ensuing composites [26,93]. In many cases, the reactivity of lignin is lacking due to a reduced amount of reactive sites and limited accessibility, the latter being caused by steric hindrance. Hence, it is essential to improve the chemical and structural characteristics of lignin. The conversion of lignins into functional bio-based materials can

be achieved through two major routes: *(i)* lignin depolymerization into monomeric fragments with reduced molecular weights and high functionality, which in turn can be polymerised into new materials (which will be only briefly discussed in Section 2.2.1), and *(ii)* chemical modifications of the macromolecular structure of lignin to afford functional polymers without completely losing their primary structure hence, retaining their polymeric properties (which will be discussed in Section 2.2.2 with focus on LS modification).

### 2.2.1. Polymers from lignin-derived chemicals

Fragmentation or depolymerization of lignin is an important method that yields valuable chemical products such as oligomeric products (with high functionality and low molecular weights) and small molecules such as phenols and aromatic aldehydes, as for instance vanillin. Lignin depolymerization is carried out by thermochemical procedures in the presence or absence of some solvents, chemical additives and catalysts; the two main procedures being hydrogenolysis and oxidation [74,83–86,94–96]. Hydrogenolysis consists of a pyrolysis (thermolysis) procedure performed in the presence of hydrogen in the temperature range 300–600 ºC during which the molecular structure of lignin is broken down into smaller units yielding liquid fuel and chemicals such as phenols [74,94,95]. Oxidation, also known as oxidative cracking, involves the cleavage of the lignin rings, aryl ether bonds, or other linkages within the lignin, generating products with increased complexity and functionalization (compared to those obtained by the hydrogenolysis process) such as phenolic aldehydes (*e.g.* vanillin) and carboxylic acids [74,83–86].

The production of chemicals through the depolymerization of lignin implies high production costs compared to analogous petroleum-derived chemicals generally resulting in low conversion yields. Therefore, vanillin is currently the only commercial monomer produced from LS at industrial scale exclusively from the biorefinery facility of Borregaard [47,74,84,94,97], which represents 15 % of the total vanillin production [47,97]. Vanillin is one of the most important commercial flavours that can also be used for the synthesis of several second-generation fine chemicals and several pharmaceutical products [86]. Since vanillin can be produced from a sustainable lignin-to-vanillin process, it is considered by some researchers as an important renewable building block for the preparation of renewable polymers [98]. So, vanillin and its derivatives can be used in the synthesis of biobased

monomers that in turn can be applied in the preparation of epoxy polymers, polyesters, and polyurethanes, and other polymers [74,98–103]. Nonetheless, the possibility of using lignin as a raw material for the synthesis of new products without any additional degradation/depolymerization procedure would be energetically positive. Therefore, some research efforts have focused on the conversion of technical lignins into functional materials without completely losing their primary structure hence, retaining their polymeric features [104]. Aiming at producing materials from technical lignins, especially LS, while preserving their polymeric structure, the next sections will focus on this route and discuss the major conversion procedures according to particular applications highlighting those of interest to this project.

### 2.2.2. Materials from lignin macromonomer

As aforementioned, lignin (and in particular LS) can be used as a macromonomer bearing multiple reactive sites, *i.e.*, as a multifunctional monomer it can react to generate a branched copolymer or a crosslinked polymer network depending on the ratio of lignin reactive sites to monomer. Additionally, lignin can undergo chemical modifications mostly via its phenolic and aliphatic hydroxy groups to generate functional polymers [75,104,105].

#### *2.2.2.1. Plasticizers for concrete formulations*

Concrete consists of a composite material made by mixing cement, aggregates (coarse and fine) and water, with or without the incorporation of admixtures [106], which is mainly used in building construction. Admixtures are chemicals added at low concentrations (not more than 5 % by mass of the cement content of the concrete) to concrete either before or during the mixing process affecting the consistence of the concrete mix [107]. Their main purpose is to improve the concrete properties such as workability, mechanical performance and durability. There are many types of chemical admixtures including (but not only) water reducing admixtures (also known as plasticizers, which reduce the quantity of mixing water required to produce concrete of a given consistency) and high-range water reducing admixtures (also known as superplasticizers), the latter being much more efficient than the former. The efficiency of these admixtures is assessed by the reduction of the water content

in the concrete mix, which should be higher than 5 wt. % for plasticizers and higher than 12 wt. % for superplasticizers [107,108]. Currently, there are different types of superplasticizers including naphthalene sulfonate formaldehyde polycondensate (NSF) and a last-generation and more commonly employed copolymer poly(carboxylate ether) (PCE) (Figure 9a and Figure 9b). NSF is mostly a linear anionic polymer whereas PCE consists of an anionic backbone comprising carboxylic groups and side chains of polyethers covalently attached to the backbone, exhibiting a comb-like architecture (Figure 9c) [107,109]. Studies indicate that NSF disperses cement particles and reduces attractive inter-particle forces, such as van der Waals forces, via electrostatic repulsion, whereas PCE acts via both electrostatic repulsion and steric hindrance between nonadsorbing side chains [110,111]. The most efficient superplasticizers are PCEs comprising carboxylate and oligo(ethylene oxide) side chains which confer steric hindrance [107,112,113].

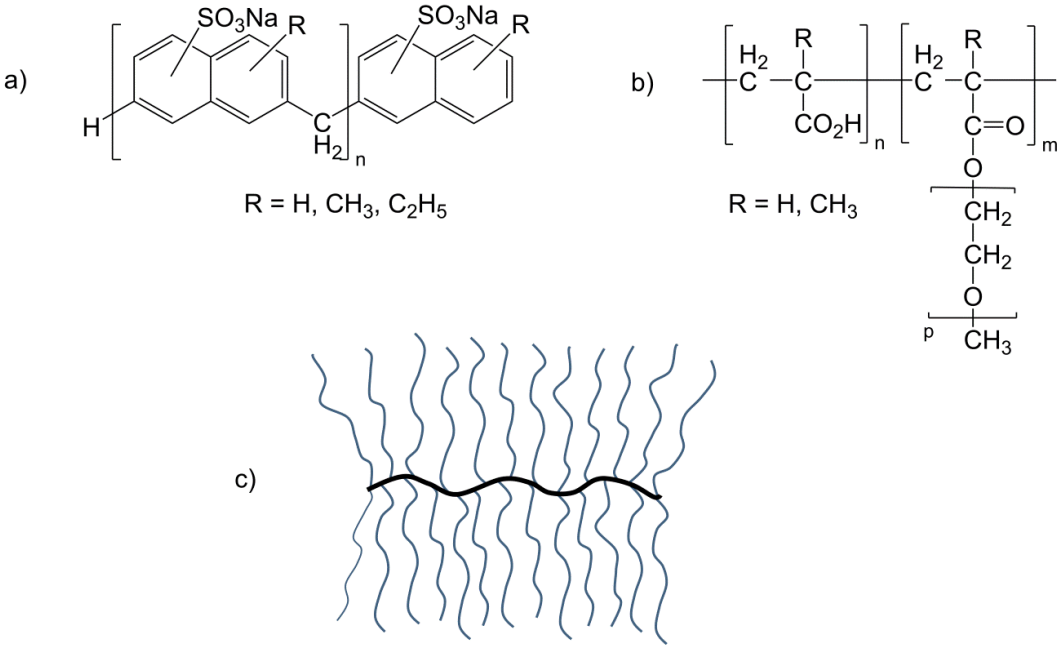


**Figure 9.** Chemical structures of superplasticizers: (a) NSF and (b) example of a PCE; molecular architecture of a comb-like PCE superplasticizer (c).

LS are natural polymeric surfactants that contain both hydrophobic groups (such as aromatic and aliphatic groups) and hydrophilic groups (such as sulfonic, carboxyl and phenolic hydroxyl groups). Therefore, LS can be widely used as concrete water reducers [114,115], coal water slurry dispersants [116,117], oil-well dispersants [118] and pesticide

dispersing agents [119]. In fact, LS were first introduced as plasticizers and water-reducing admixtures to concrete in the 1930s [120] and now 60 to 90 % of LS in different countries are used for this purpose resulting in a concrete with good workability, lower water/cement ratio and higher compressive strength. However, the plasticizing and water-reducing effects of LS are limited. Indeed, even though LS is the most used material for the formulation of water-reducing admixtures, it is barely used in the design of high-performance concrete [109,121–124]. In this field of application, LS compete with petroleum-based polymeric formulations such as PCEs. PCEs are much more efficient than LS giving rise to a concrete with superior fluidity or more noticeable water-reduction; however, PCEs are more expensive than LS by a factor up to 10. Due to their poor efficiency, LS are usually used combined with PCEs in concrete formulations. Yet, some strategies can be used to improve LS performance namely: *(i)* refining to remove low molecular lignin fractions, concomitant sugars and extractives [121], *(ii)* oxidative polymerization in order to increase their molecular weight whilst preserving their solubility in water [125–127] or *(iii)* introducing carboxylic/carbonyl groups by oxidation [128].

The increase of the molecular weight of LS can be achieved by oxidative polymerization using laccases (EC 1.10.3.2) [129], which are multi-copper oxidoreductase enzymes widely distributed in the nature such as in plants, fungi, bacteria and also insects. Laccases catalyse the one-electron oxidation of diverse substrates, namely, phenolics, aromatic amines, ascorbate and metal cyanides [130,131]. This class of enzymes is regarded as multi-purpose "eco-friendly" biocatalysts with potential applications in different industrial fields such as the food industry for food additive and beverage processing [132,133], the textile industry for denim finishing and cotton bleaching [133,134], and the pulp and paper industry for the delignification of wood fibres [135,136]. However, when used alone, laccases promote lignin polymerization with minor structural changes. In fact, laccases oxidize the phenolic components of lignin, leading to aliphatic or aromatic C–C bond cleavage and depolymerization [137]. Yet, spontaneous polymerization of the quinonoid radical intermediates usually occurs rather than depolymerization, thus polymerization through laccase treatment prevails, as depicted in Figure 10 [138]. Hence, the oxidation of free phenolic end-groups to phenoxy radicals leads to a significant decrease of the phenolic content and an increase of LS molecular weight by 5 to 25-fold [125,139]. It is important to note that the oxygen supply plays an essential role in the polymerization process [139,140].

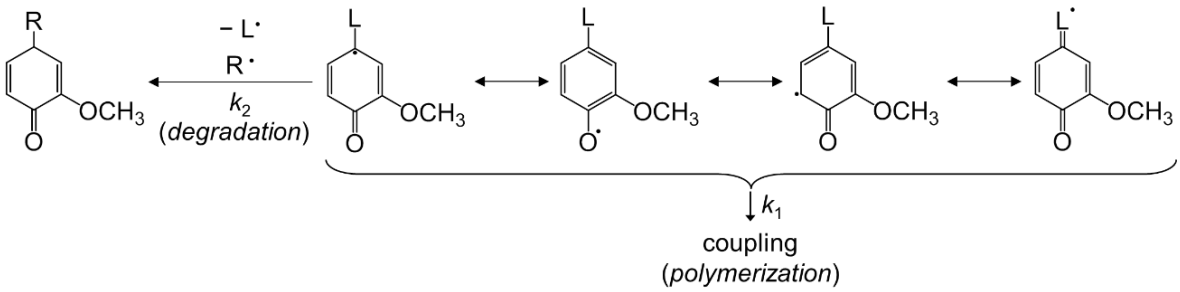


**Figure 10.** Schematic representation of the reactions that lignin units can undergo in the presence of laccase, where lignin polymerization prevails over lignin degradation ($k_1 > k_2$), R- oxygen-centred active specie and L is the propane chain derived moiety.

In the presence of mediators, laccases are capable of oxidizing not only phenolic units but also non-phenolic units in lignin [141,142] hence, special attention in the choice of mediator should be taken based on their efficiency as well as on their reactivity towards phenolic subunits in lignin [138,139]. In fact, oxidation of nonphenolic lignin moieties in the presence of mediators, such as synthetic mediators 2,2′-azino-bis(3-ethylbenzthiazoline-6-sulfonic acid) (ABTS), 1-hydroxy-benzotriazole (HBT) and 2,2,6,6-tetramethyl-1-piperidinyloxy (TEMPO) or natural mediators (e.g. vanillin, syringaldehyde and 2,6-dimethoxyphenol) may hinder polymerization and induce delignification instead [139,142–145]. Also, polyoxometalates (POMs) can be used as laccase mediators in lignin degradation being of particular interest for oxygen pulp bleaching [146–149]. The use of eco-friendly natural-occurring mediators, such as those mentioned above, could contribute to the industrial implementation of laccases and be an alternative to synthetic mediators, which are expensive and could exhibit toxicity [143]. Also, by controlling the reaction conditions, the use of mediators could contribute to enhance the laccase polymerization of lignin.

Though most of the studies propose the enhancement of the dispersant properties of lignin through an enzymatic modification treatment, other routes have also been tested. For instance, the oxidation of LS with peroxyacetic acid followed by sulphomethylation gives rise to LS with increased molecular weight and content in sulphonic groups, thus improving the water reducing properties of the modified LS in the concrete paste compared to unmodified LS [150].

Another approach reported to improve the dispersant properties of lignin is the preparation of lignin-based non-ionic polymeric dispersants (amphiphiles) from organosolv and kraft (softwood and hardwood) lignins and LS [151–153]. Lignins were reacted with different commercial epoxylated poly(ethylene glycol) (PEG) derivatives namely poly(ethylene glycol) diglycidyl ether (PEGDE), its monoglycidyl ether (EPEG), and dodecyloxypoly(ethylene glycol) glycidyl ether (DAEO) in alkaline medium. The goal was to graft a hydrophilic polymer (PEG derivative) onto the hydrophobic lignin core to increase its surfactant properties. The most promising results were obtained using the PEGDE- and EPEG-derived amphiphiles from softwood lignin, which displayed enhanced dispersants properties compared with the other lignin-based analogues. The best dispersibility results were obtained from DAEO-derivatized LS, probably due to the presence of DAEO segments, which contribute to the formation of a stable dispersion of cement particles in water [153]. Moreover, softwood lignin-based amphiphiles displayed higher cement dispersibility than hardwood kraft-based analogues and even LS. Comparing these results, the authors attributed the differences to the fact that softwood lignins are mainly build-up by G units where phenolic OH groups are more accessible than those from hardwood lignins, which contain high content of S units with higher steric hinderance. Therefore, it is possible that the modification of hardwood KL was not as efficient as the modification of softwood lignin. However, the authors [151] were not able to show evidence of this possibility neither did they discuss how nor why such amphiphiles show admirable cement dispersibility compared to LS. Furthermore, the chemical modification of lignins with PEG segments in alkaline medium has also been reported to yield epoxidized/PEGylated lignins with potential application as thickener in bio-lubricant formulation [154] and bio-based surfactants [155]. Yet, the discussion on the dispersion mechanisms involved are also limited.

More recently, the grafting of softwood LS and KL with poly(3-sulfopropyl methacrylate) (PSPMA) and poly(methacrylic acid) (PMAA) anionic grafts via ATRP at pH 11 was reported (Figure 12) [156]. The workability of cement pastes prepared using these hybrid polymers as plasticizers was assessed by the mini-slump testing method[1]. The results were compared with those obtained with PEGylated lignin analogues and a commercial PCE superplasticizer. Slump values significantly increased for both cases when using the PMAA-

1. Test method used to determine the consistency of the cement paste. The result is the slump value, which is the change in height of the cement paste slump (recorded along with the spread).

grafted lignins compared to the other dispersants meaning that significant reductions in the cement water content were achieved. In particular, the highest slump value was reached with PMAA-grafted LS approaching the performance of commercial PCE and suggesting that the chemical nature of the grafted chains has a strong effect on the dispersant properties of the ensuing material. Adsorption, zeta potential, and intrinsic viscosity were measured for the graft lignin analogues in order to examine the correlation between lignin and the chemical nature of the grafted chains in the cement dispersion mechanisms. Yet, no straightforward conclusions could be drawn due to the complexity of the systems.

#### *2.2.2.2. Adhesives for biocomposites*

Wood-based composites cover a variety of products, from fibreboards and particleboards to laminated beams and plywood, and are used for numerous non-structural and structural applications such as panels for interior, furniture, support structures in buildings, and others. Elements used in the production of wood-based composites include fibres, particles, flakes, veneers, laminates, or lumber [157,158]. In most conventional wood-based composites, adhesive bonding is achieved by non-renewable petroleum-derived thermosetting synthetic resins including phenol-formaldehyde (PF), urea-formaldehyde (UF), melamine-formaldehyde (MF), and polymeric 4,4-diphenylmethane diisocyanate (pMDI). Certain chemicals are also added to plasticize adhesive polymers, enhance tackiness, improve heat resistance, or lower costs [158–160]. The use of bio-based adhesives in wood and fibre composites has attracted scientific and economic interests for several decades, not only due to the decline of the petrochemical supplies but also due to the public awareness related to the environment and its protection as well as governmental regulations [160–164]. Extensive research has been carried out in order to use technical lignins, including KL, OL as well as LS, as adhesives or as a partial replacement in adhesives formulations, and as raw material for synthetic resins [47,75,164–167]. Yet, the next examples will mostly focus on the use of LS in adhesive formulations, which are the focus of this thesis.

***Phenolic resins***. Wood-based panels containing thermosetting adhesives, such as phenol formaldehyde (PF) resins, may release phenol and formaldehyde, which are classified as toxic chemicals and have negative health effects on humans [162,163]. Therefore, numerous works have focused on finding methods to reduce and if possible, eliminate the release of

free phenol and/or formaldehyde from wood-based panels. Lignins are phenolic-like polymers and theoretically could be used alone as a binder for the production of composite wood panels. However, there are essentially two drawbacks in using lignin alone as binders. First, the chemical and structural features of lignins is vary variable depending on the source and production method. Second, lignins exhibit reduced reactivity as wood binders toward formaldehyde (due to its high molecular weight and steric hinderance) compared to conventional resin systems such as PF resins requiring longer press curing times [161,168,169]. Henceforth, in order to achieve efficient crosslinking by condensation reactions in lignin, during the composite board pressing process, high heating temperatures and long pressing times are necessary leading to several problems such as corrosion due to the acidity, high energy costs, among others. Yet, lignins, including LS, can be used as such or chemically modified as partial replacement (below 50 wt. %) of phenol in the synthesis of lignin-based PF resins without detrimental effects on the mechanical properties of the final wood panels [170,171].

Usually, chemical modification of lignins to improve their reactivity is necessary and include hydroxymethylation (also known as methylolation), demethylation, phenolation, sulphonation, hydrolytic depolymerization, and reductive depolymerization [75,165,169,172]. Due to the complex mixture from which lignins are obtained, purification prior to chemical modification into adhesives and other polymeric formulations is a critical step since undesirable side-products can be formed and interfere with the expected properties and applications [83,89–91,173].

Several works investigated the hydroxymethylation of different technical lignins, such as LS, KL and OL from hardwood, softwood and even from non-wood sources (namely sugarcane bagasse and wheat straw) [174–178]. All hydroxymethylation reactions were carried out in alkaline medium, different initial formaldehyde/lignin weight ratios, temperatures and even pH were tested (some taking into account the undesirable Cannizzaro reaction). Detailed physicochemical characterization of the ensuing modified/activated lignins have established that all lignins can be used as partial replacement of phenol in phenolic resin though LS-based resins were the most promising candidates for paper impregnation applications due to their water solubility [174–177]. Furthermore, by replacing 35 wt. % of phenol by hydroxymethylolated LS, the ensuing lignin-PF resin displayed

analogous features to that of the commercial PF resol resin fulfilling the prerequisite specifications for its utilization in the plywood production [178].

Other chemical modifications were also applied to improve the reactivity of LS namely alkaline hydrolysis [90] and phenolation [179]; both methodologies increase the number of active sites, such as phenolic OH moieties and aromatic protons yielding LS products with enhanced reactivity towards formaldehyde. While during the hydrolysis reaction (in alkaline or acidic medium), reactive degradation products are formed [90], in the phenolation reaction, lignin is treated with phenol under acidic conditions, leading to the condensation of phenol with lignin side chains [179].

Since formaldehyde is toxic, carcinogenic and suspected to be mutagenic [180,181], its substitution by a potentially sustainable and less toxic alternative could consequently eliminate possible formaldehyde emissions during the production and the use of phenolic resins. To overcome this problem, glyoxal, which is the simplest dialdehyde (typically supplied as an aqueous 40 wt. % solution) and displays low toxicity and low volatility [182], has been considered a promising alternative to formaldehyde in PF resins [183–191]. The reaction of lignin with glyoxal, also known as glyoxalation of lignin, is an alternative to the conventional methylolation. El Mansouri and co-workers [183,184] were the first to report the use of glyoxal instead of formaldehyde for the synthesis of lignin-based wood adhesives. During glyoxalation, similar reactions occur as during methylolation, though other reactions also occur, such as lignin depolymerization and repolymerization as well as condensation reactions between lignin and glyoxal [192,193]. Glyoxalated lignins, including LS, can give rise to safer adhesives (compared to formaldehyde-based ones) displaying satisfactory properties according to relevant international standard specifications and yield panels with press times comparable to those built-up of formaldehyde-based commercial adhesives [183–185,189].

***Polyurethanes***. Polyurethanes (PUs) are versatile designer polymers that display varied properties being adjustable to a wide range of applications namely foams, elastomers, paints and coatings, adhesives, and even in medical applications [194–197]. Typically, PUs are prepared through the addition of isocyanates (comprising more than one reactive isocyanate group per molecule) and polyols (containing two or more reactive OH groups per molecule)

yielding polyurethane linkages in the polymer backbone [194–197]. Alternatively, PUs may also be obtained by reacting diisocyanates with diamines. Since diisocyanates have raised severe health hazard concerns [198,199], the synthesis of non-isocyanate PUs (NIPUs) has recently gained an increasing interest in chemical industry, the most promising method being the synthesis of poly(hydroxyurethane)s (PHUs) based on the reaction between multicyclic carbonates and aliphatic amines [200–203]. Yet, this route still needs major developments before reaching industrial scale.

Technical lignins, including LS, can function as macropolyols in PU synthesis due to the high amount of phenolic and aliphatic hydroxyl moieties in their structure [78,204–208]. The direct exploitation of technical lignins, as polyols or blending with industrial polyols, is energetically and environmentally advantageous [74] and the ensuing biomass-based PUs are more biodegradable than those derived from petroleum-based polyols [209]. Hence, lignins can be used as such or after chemical modification to get a more reactive lignin, via hydroxyalkylation, esterification, etherification reactions, and depolymerization processes, alone or in combination with other polyols [204–208,210–212]. Both aliphatic and phenolic OH groups in lignin are reactive so lignins with high OH content, for instance, OLs, can be used as macromonomers without further chemical modification [211,212]. Additionally, considering that the aromatic structure of technical lignins is extremely dependent on the plant source from which it is extracted, the final properties of the lignin-based PUs depend highly on the lignin's plant source [213]. The low reactivity of the lignin macromonomer towards isocyanate groups is usually related to the fact that only a certain portion of the total OH groups can directly react (probably due to steric hindrance from the highly branched three-dimensional structure of lignin) yielding products without desirable performance [213–215]. Therefore, the content of the unmodified lignin in the ensuing PU is generally below 15–30 wt. % in order to reach an acceptable performance [206]. Although chemical modification of lignins improves the reactivity of lignin, this type of pre-treatments may increase the cost as well as the environmental impact of the ensuing PUs, and thus reduce their competitive advantage over conventional PU systems based on petroleum-derived polyols [216].

The use of other polyols as soft segments, such as PEG and poly(propylene glycol) (PPG) [207,217–219], or even bio-based polyols, such as castor oil [218,220–223], crude glycerol [220] and poly(ε-caprolactone) (PCL) [224] in lignin-based PU synthesis can counterbalance

the stiff character of the lignin macromolecules yielding grafted and cross-linked PUs with the possibility of controlling the flexibility and/or rigidity. For instance, Zhang and co-workers [223] prepared a series of castor oil-based waterborne PU composites with different amounts of LS, which was used as functional filler. The results showed that the increase of LS content up to 10 wt. % yielded composite films with increased mechanical strength but lower elongation at break compared to PU films without LS probably due to increasing physical crosslinking together with the rigid characteristic of LS. De Oliveira and co-workers [208] also used castor oil in LS-based PU formulations to adjust their final properties.

As already mentioned, the reactivity of technical lignins towards isocyanate can be enhanced by chemical modification, which may also increase lignin's solubility in polyol systems, decrease brittleness of lignin-based PU materials, and improve lignin's processability [74,76]. Lignin hydroxyalkylation, in particular oxypropylation in alkaline medium, has been widely studied to improve the reactivity of lignins to produce homogeneous PU networks [97,207–209,212,225–230]. The oxypropylated lignin corresponds to a branched copolymer with lignin as the core unit and flexible grafted propylene oxide (PO) chains. These PO chains counterbalance the lignin stiffness significantly lowering the $T_g$ (*ca*. 50–100 ºC) of the ensuing oxypropylated lignin [212,226], their length depending mostly on the stoichiometry and the amount of catalyst used [228,231]. De Oliveira and co-workers [208] investigated the impact of using LS, oxypropylated LS and the addition of castor oil (aforementioned in this section) in PU formulations. Results indicated that the final properties of the LS-based PUs could be adjusted by using oxypropylated LS or by combining castor oil with LS (unmodified LS or oxypropylated LS), which enables the production of materials with tuneable properties.

PO is a commodity chemical used as a starting material for a broad range of products; however, its handling involves huge risks due to its high vapour pressure, flammability, toxicity, and carcinogenicity [232]. On this point, five-membered cyclic organic carbonates, such as propylene carbonate (PC) and ethylene carbonate (EC), are considered attractive and promising alternatives to PO due to their biodegradability, high solvency, high boiling and flash points, low evaporation rates, low (eco)toxicity, and they are available in large amounts and at low prices [233,234]. They are used as solvents in nearly every field of chemistry as well as environmentally friendly building blocks in synthesis. Mimini and co-workers [235] successfully modified LS with bio-based glycerol carbonate and the ensuing LS-based

product was reacted with 1,6-hexamethylenediamine (HMDA), instead of a isocyanate, to form a NIPU material. Furthermore, in this study, vanillin alcohol (VA) was employed as a simple lignin model compound and was reacted with glycerol carbonate for mechanistic studies. Chemical and structural characterization (using FTIR, 1D- and 2D NMR) of the resulting VA-based product proved that the etherification occurred only at the benzylic position and that the phenolic OH group was only acetylated [235].

Hemmilä and co-workers [236] synthesised LS-based adhesives and evaluated the effect on using two different crosslinkers, bio-based furfuryl alcohol (FOH) and synthetic pMDI. All adhesives were prepared with unmodified LS and used for gluing 2-layered veneer samples and particleboards. LS-pMDI-based adhesive cured at the lowest temperature (107 ºC from DSC analysis) along with the formation of urethane linkages between LS and pMDI (confirmed by FTIR analysis). The mechanical properties of the particleboards produced using LS-FOH-based adhesive (internal bond of 0.17 $N \cdot mm^{-2}$) were inferior to those produced using LS-pMDI-based adhesive (internal bond: 0.62 $N \cdot mm^{-2}$). A similar trend was observed with the thickness swelling test. Although particleboard properties were worse for the LS-FOH-based samples, the tensile shear strengths of both LS-based adhesive types were at the same level as the melamine-urea-formaldehyde reference. It was suggested that the lower performance of LS-FOH-based adhesive could probably be due to the shorter pre-polymerization time and low FOH and total glue amount.

The production of lignin-based PUs membranes through the co-polymerization of different technical lignins, namely KL, LS and OL, with TDI-terminated poly(propylene glycol) has been reported [91,237–239]. The main goal for the preparation of this materials was to use them as support for ion-selective membranes potentiometric chemical sensors. To enhance the electrical conductivity of the lignin-based PU membranes, conductive carbon fillers, such as carbon nanotubes (CNTs) were added as fillers to yield a conducting PU based composite. The use of lignins in the preparation of composites will be discussed ahead in Section 2.2.2.3.

Besides using LS in PU films and adhesive formulations, some research works have also reported the preparation of LS-based PU foams (PUFs). Wysocka and co-workers [240] used LS and hydrolysed LS as the polyol components in PU foam formulations. Surprisingly, although hydrolysis is known to increase lignin's reactivity (as aforementioned), in this study

the use of unmodified LS yielded PUFs with improved thermal and mechanical properties compared to those from hydrolysed LS-based PUFs. However, the authors did not provide further explanation for this occurrence. Muller and co-workers [241,242] reported the preparation of bio-based polyols from the liquefaction of KL, OL and LS in crude glycerol, which were employed to prepare rigid PUFs. The bio-based contents of the PUFs were 44 wt. % for KL-, 55 wt. % for OL- and 32 wt. % for LS-based polyol. The mechanical and thermal properties of the bio-based PUFs were comparable to those from commercial products but were different depending on the type of technical lignin with KL clearly yielding foams with superior qualities. Based on Hatakeyama's work [243], Lu and co-workers [244,245] investigated LS as partial substitute of diethylene glycol (DEG) and the resulting polyol was copolymerized with isocyanate to produce LS-based rigid PUFs. LS increased the thermal stability of LS-based PUFs and the best thermal stability was obtained for PUFs containing 15 wt. % of LS (based on DEG). Furthermore, it was also shown that LS could improve the flame retardancy of the ensuing PUFs. Though these examples are not directly related to adhesives, the fact that PU properties are easily tuneable makes this class of materials too important to not be referred.

***Polyesters***. Polyesters are polymeric materials comprising ester linkages widely used in our daily life ranging from bottles for carbonated soft drinks and water, to fibres for shirts, among others. Polyesters can be produced by three main different methods, namely, ring opening reactions with cyclic esters, condensation polymerization using carboxylic acid chloride, and dehydration polymerization with dicarboxylic acids [74,104]. Wang and co-workers [246,247] investigated the modification of LS with maleic anhydride in alkaline medium, which yielded esterified, *i.e.*, maleated LS (MLS) with increased content of carboxyl groups and double bonds. MLS was then blended with PCL via melt blending to obtain MLS/PCL composites, whose thermal stability and mechanical properties were compared with those of unmodified LS/PCL composites. The tensile strength and Young's modulus values of the MLS/PCL composites increased significantly (1.7- and 1.1-fold, respectively) compared to those of the LS/PCL composites when the content reached 50 %, probably due to the stronger adhesion between MLS particles and PCL phase. On the contrary, the elongation at break of both types of composites decreased drastically due to the brittleness of LS and the thermal stability of the MLS/PCL composites was worse than that

of the LS/PCL composites. Xu and co-workers [248] modified LS with methacrylic anhydride and evaluated the possibility of using the ensuing methacrylated LS to enhance the adhesion within flax fibre reinforced soybean-derived polyester thermosets. When soaking the flax fibres in 5 wt. % methacrylated LS solution, both tensile and flexural properties of the fibre composites improved significantly (from 2.6 to 6.7 GPa and from 36 MPa to 76.8 MPa, respectively).

***Epoxy resins***. Epoxy resins are a relevant class of high-performance thermosetting polymers that are widely used as composite matrices, protective coatings, adhesives, sealants, among other applications [249]. Epoxy resins are low molecular weight pre-polymers (monomers and/or oligomers) containing at least two reactive epoxy groups that, in the presence of curing agents and under optimal curing and processing conditions, form a stable highly crosslinked 3D network macromolecule [249–251]. One of the most common types of epoxy resin is made of diglycidyl ether bisphenol A (DGEBA), which accounts for around 90 % of the world production of epoxy resins and is produced from the reaction between bisphenol A (BPA) and epichlorohydrin (ECH) [249,252]. Due to harmful effects to human health and the environment caused by exposure to BPA [253,254], serious efforts have been made to reduce the consumption of (or even replace) DGEBA and BPA. Therefore, much research has focused on the production of epoxy resins using natural resources, such as vegetable oils, tannins, lignin and others. The incorporation methods of lignin in the production of epoxy resins can be classified into three categories: *(i)* physical blending of lignin and epoxy resin, *(ii)* pre-modification of lignin before epoxidation, and *(iii)* direct epoxidation of lignin [251,255]. While simply blending lignin can only allow the substitution of a small percentage (<20–30 wt. %) of epoxy resins, the other two approaches make it possible to achieve a high substitution proportion up to complete substitution of petroleum-based materials by lignin [251,255]. Ismail and co-workers [256] developed adhesives through the esterification of succinic anhydride, ethylene glycol and LS to prepare a prepolymer to which glycerol diglycidyl or ethylene glycol diglycidyl ether were subsequently added to crosslink the structure. Yamini and co-workers [257,258] adopted a three-step modification strategy, which included methylolation, followed by epoxidation and finally by carbonation (*i.e.*, $CO_2$ fixation), to convert LS into a final product as a cyclocarbonated LS, a reactive filler for epoxy matrix composites. The ensuing LS-based

reactive product was then blended with DGEBA epoxy resin followed by amine-curing (using diethylenetriamine) to produce biocomposites. Comparing with the neat DGEBA network, by increasing the content of cyclocarbonated LS up to 30 wt. % in the biocomposite, tensile strength decreased, flexural modulus was well-preserved, and the Young's and storage modulus were greatly improved, probably due to the stiffening effect of the modified LS particles as well as the formation of urethane bonds (from the opening of the cyclocarbonated ring) and intermolecular interactions such as hydrogen bonding. Yet, the most promising biocomposites contained 20 wt. % of cyclocarbonated LS displaying the following properties: decomposition temperature (at a 5 % weight loss) 321 °C, storage modulus 2.84 GPa, Young's modulus 2.07 GPa, elongation at break 39.1%, flexural modulus 2.56 GPa, and flexural strength 49.7 MPa. Though no application was tested, the possibility of tuning these products' characteristics could allow their use as adhesives.

#### *2.2.2.3. Other lignin-based polymers*

Reversible deactivation radical polymerization techniques (RDRP) commonly referred to as controlled polymerization methods have been employed as versatile procedures to produce well-defined polymers with controlled molecular weight, narrow molecular weight distribution and site-specific functionality. These processes enable control of polymer compositions, architectures, and functionalities, hence allowing the development of novel materials with tailored physical and chemical properties, as is the case of atom transfer radical polymerization (ATRP) [259,260] and reversible addition-fragmentation chain transfer (RAFT) [261]. Graft copolymers usually consist of a backbone polymer as the main chain and randomly distributed side chains with a different composition (or more than one) connected to the backbone via covalent bonds. Consequently, the graft copolymers display tuneable properties defined by the functional groups on the grafted polymers, length of the graft, and grafting density.

The graft copolymerization of lignin combines the advantages of the physical and chemical properties of both lignin and synthetic polymers leading to the successful synthesis of lignin-based polymers. In this case, lignin acts as the backbone polymer (or core unit). Numerous polymerizations methodologies have been employed including ATRP, RAFT, ring-opening polymerization (ROP), and radical polymerization. There are mostly two

different grafting strategies: the "*grafting from*" and the "*grafting to*", as illustrated in Figure 11. In the "*grafting from*" process, polymers are grown from the lignin. Hydroxyl functional groups in lignin work as initiating sites in ROP methods, while, in the case of ATRP and RAFT procedures, lignin is first modified (mostly from the OH groups on lignin) giving rise to a lignin macroinitiator in the case of ATRP and lignin macro transfer agent in the case of RAFT. In the "*grafting to*" procedure, polymers (the side chains) are previously and separately synthesized followed by functionalization at one end, and only then are covalently grafted to the lignin through its functional groups. [102,262].

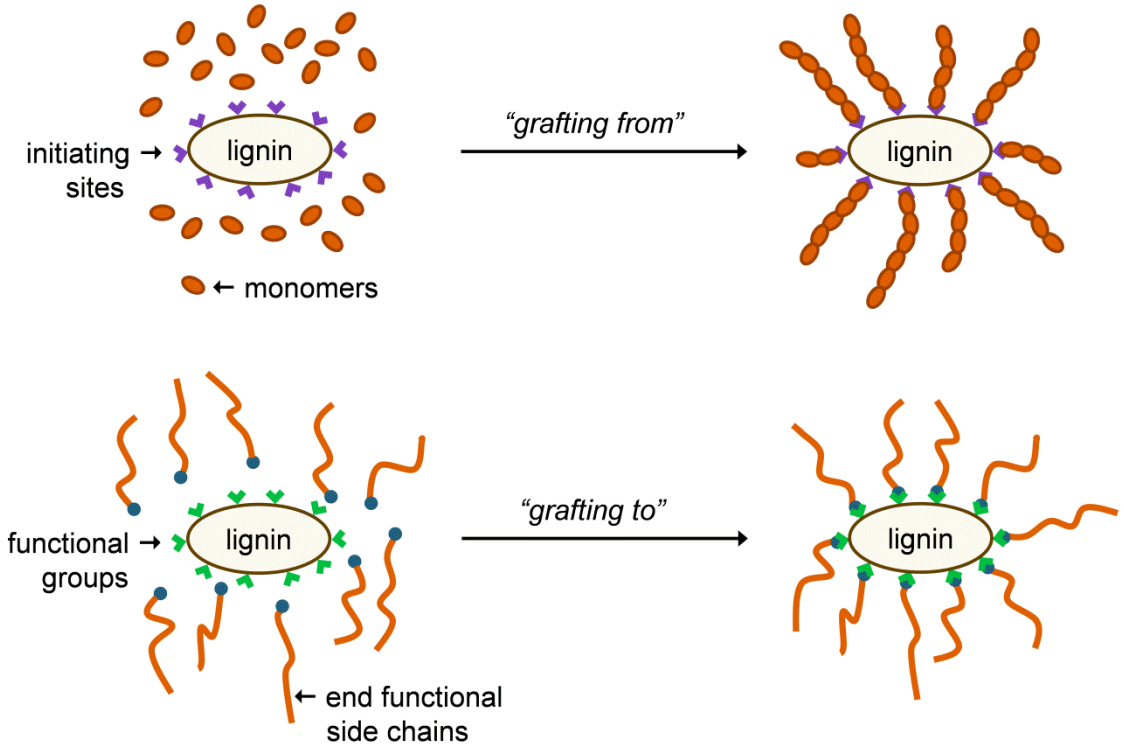


**Figure 11.** Synthesis of lignin-based copolymers via "grafting from" (top figure) and "grafting onto" (bottom figure) methods (adapted from [102,105,262]).

Recently, the controlled graft copolymerization of lignin to produce novel value-added lignin-based polymeric materials has been thoroughly reviewed [102,262]. ATRP is the most common controlled radical polymerization process for the graft polymerization of lignin. This is mostly due to its simplicity and broad applicability, and the possibility to synthesize macromolecules with controlled molecular weight, topology, composition and functionality, therefore opening up routes to new materials for a wide range of applications [259,260]. The

ensuing lignin-based polymeric materials comprise strong and stable covalent bonds between lignin and synthetic polymers. These hybrid materials exhibit enhanced properties such as better miscibility, compatibility, and reproducibility compared with lignin-polymer blend products (without covalent bonds). However, even though numerous reports have emerged describing remarkable achievements in this field and various companies have already introduced products based on controlled/living radical polymerization into many high value markets [263], much work regarding this type of approach is still required especially with LS since no relevant bibliography was found.

#### *2.2.2.4. Lignin-based conducting composites*

A composite material can be defined as a material structure that combines at least two macroscopically identifiable materials working together to achieve optimum (or notably enhanced) material characteristics [264]. Composite materials are present in our daily life in a wide variety of products that are used in construction, military and medical applications, oil and gas, transportation, sports, aerospace, and many more.

Conducting polymeric composites (CPCs) are an important class of organic multifunctional materials, which exhibit unique physical and electrical properties. The possibility of fine-tuning their optical and conducting properties makes them promising candidates for a wide range of applications including the fields of energy, electronics, catalysis, electromagnetic interference shielding, biomedicine and sensors [265,266]. In general, CPCs are made of a polymeric backbone comprising highly π-conjugated $sp^2$ hybridized chains, which are responsible for the occurrence of charge delocalization within their structure. These polymers usually exhibit low conductivity (~$10^{-10}$–$10^{-5}$ $S \cdot cm^{-1}$) in their pure state, nonetheless this property can be significantly enhanced to ~1–$10^4$ $S \cdot cm^{-1}$ by suitable doping with other species such as metal or metal oxide nanoparticles, metal-organic frameworks (MOFs), carbon-based nanomaterials, and others [265–267]. Carbon-based materials, such as CNTs, graphene, carbon dots, and porous carbon, have attracted scientific interest worldwide since these nanofillers exhibit enhanced conductivity, high chemical stability, mechanical strength, and large surface area. Therefore, numerous studies have been focused on the preparation of CPCs using these carbon-based materials as nanofillers in order to improve their electrical and mechanical properties but also allowing the production

of small, light-weight and cost-effective composites for a variety of application fields including electronics, energy, automotive and aerospace industries and sensors [265,267–269].

Considering its special structural features, lignin is a potential material towards the production of intrinsically conducting polymers-based composites. In fact, new lignin-based bulk-sensing polymeric membranes have been developed through covalent immobilization of the lignin inside a polymer matrix. In particular, the production of lignin-based PUs membranes as mentioned above has been reported [91,237–239]. The lignin-based PUs were doped with MWCNTs to increase their electrical conductivity and produce CPCs with prospective application as ion-selective membranes for potentiometric chemical sensors [237,239]. In fact, the lignin-based PUs exhibited relatively low $T_g$ combined with sufficiently high electrical conductivity and so were used in the fabrication of self-plasticizing sensing materials. The ensuing lignin-based sensors displayed a very low or no sensitivity to all alkali, alkali-earth and most transition metal cations ions. At the same time, the sensor properties were strongly dependent of the lignin origin. Indeed, some concomitants of poly-phenolic origin in KL changed radically the sensitivity and selectivity to Cu(II) [239]. Potentiometric sensors highly sensitive to Cr (VI) at pH 2 were obtained with LS and in less extent with OL [237].

Chen and co-workers [270] developed a humidity sensor based on a multi-layered thin-film comprising LS (as moisture sensing) and reduced graphene oxide (rGO) (as resistant transduction layer). The rGO/LS thin-film sensor exhibits a maximum response nearly four orders of magnitude higher than that of pure rGO thin-film and is flexible, low cost, simple designed, portable and suitable for large-scale manufacturing

Besides sensing applications, CPCs are also relevant for energy storage, such as solar cells [271,272]. Over the last few years, research related to the exploitation of lignin towards the development of energy storage devices based on lignin or lignin blends with organic and inorganic compounds has significantly increased [12,273,274]. Nevertheless, despite of the potential of lignin as a green multipurpose raw material for the energy storage field has been established, most of the studies focus on the development of carbonization-based lignin conversion into versatile carbon products [12,273,274]. Therefore, much research on supercapacitors, batteries, and solar and fuel cells based on lignin-based CPCs is still needed.

## 2.3. FINAL REMARKS

The rising awareness of climate change and scarcity of fossil resources has drawn attention to the relevance of the biorefinery concept worldwide and as a result of this to the potential of renewable materials. Yet, it is imperative to monitor, evaluate and forecast the use of bio-based materials such as lignin in order to ensure that the bioeconomy sector operates within safe ecological limits. Overall, technical lignins can be functionalized and directed to various applications as dispersants, adhesives, plastics, resins, conducting polymeric composites, among many others. In particular, the examples aforementioned confirmed that LS, which is much less studied than other lignins, such as KL and OL, can be used in other applications than concrete formulations, namely for adhesives (most examples focused on phenolic resins and polyurethanes) and for sensing applications. Since most of the current industrial applications depend on the good water-solubility of technical lignins, world lignin market is largely restricted to LS, therefore their marketing and consequent profit is guaranteed. On the contrary, the massive abundance of KL, which is not soluble in water, makes this type of lignin the main focus of a vast number of research works targeting the synthesis of KL-derivatives for a wide range of applications. However, the production costs of lignin-based materials depend not only on the type of lignin used (and its pre-treatment/purification) but also on the functionalization method towards the application. Moreover, the quality of the lignin-based materials must be the same, or higher than the commercial products. This requirement, in particular, is quite difficult due to the lack of a unique and well-defined lignin structure with specific features and functionalities. Hence, it is a challenge to produce value-added lignin-based products with consistent properties. Even though in the last years many research studies were carried out, further investigation is still needed thus, efforts must concentrate on the materials quality (of the lignin and end-products) and production costs before lignin-based materials can replace commercial products. Towards that end, critical considerations must be addressed: *(i)* the chemical and structural features of technical lignins must be fully evaluated, and *(ii)* the synthesis route chosen for the development of new products should be highly selective and cost efficient leading to lignin-based materials that could compete with the analogous commercial products in terms of chemical, physical and mechanical properties. As a consequence, a question arises: “Do alternative lignin-based products offer in reality genuine environmental and cost benefits compared to their fossil corresponding products?” For this

purpose, analytical tools such as life cycle assessment (LCA) should be used to evaluate the potential environmental impacts of this bioeconomy sector [275,276]. Indeed, very recently, LCA studies have been conducted investigating the use of lignin for the production of chemicals and products, namely regarding the sustainable production of lignin-based resins/adhesives for wood composites [277–280], vanillin [281], adipic acid [282], catechol [283], PU foams [284], among others. However, assessing the environmental impacts of lignin and lignin-based products with LCA can be very challenging since multiple life cycle modelling choices have to be defined. More recently, Moretti and co-workers [285] published a critical review based on forty-two peer-reviewed LCAs regarding lignin and derived products. The authors reviewed choices made to conduct each LCA study such as (but not only) the product system investigated, the modelling approach and the type of data used, the methods to deal with co-products (*i.e.*, the multifunctionality of lignin), the environmental impact, etc. These studies demonstrated that LCA is an efficient tool to optimize the studied lignin-based process and improve its sustainability. Some studies identified the key parameters to achieve this goal. The main impact categories considered in most studies is climate change and the comparison between lignin-based products and their fossil-based counterparts. Furthermore, most of the LCA studies showed that lignin-based processes demonstrate better environmental performance compared to the conventional fossil-based process. Moreover, one of the findings of the review is that the impact of lignin and lignin-based products depends significantly on the type of energy source that is used to replace the burning of lignin in biorefineries and paper mills [285].

Yet, despite of all these promising reports, it is still necessary to assess other crucial factors such as feasible production processes and life cycle costs. For instance, Lettner and co-workers [286] studied specific barriers and incentives regarding technological, economic and environmental aspects of two lignin-based products: the use of KL in PF resins for wood-based panels and the use of KL in PU resins for PU foams. These authors identified multiple barriers related with uncertainties concerning techno-commercial interactions that may hinder long-term industrial planning, such as consistency and (in)constant quality of the lignin that may affect its reactivity (and so the final product quality) and the varying price and costs of lignin (depending on the type of lignin, pre-treatment may vary thus counting up additional costs).

# 3. Experimental section

### 3.1. MATERIALS

Industrial thin and thick (after multi-effect evaporation stage) sulphite spent liquor (SSL and THSL, respectively) from the magnesium-based acidic sulphite pulping of *Eucalyptus globulus* for the production of dissolving pulp were supplied by Caima - Indústria de Celulose S.A. (Constância, Portugal) – Figure 4. Lignosulphonates from SSL and THSL, hereafter designated as LSF and LSG, respectively, were purified by dialysis against distilled water for 24 hours (with water exchange intervals of 3 hours, except overnight) using a partially benzoylated cellulose membrane of 2000 NMWCO (Sigma-Aldrich, Madrid, Spain), followed by freeze-drying (Figure 12) [24]. SSL, THSL and purified LS (LSF and LSG) were analysed in terms of their basic chemical composition and structural information of the main components according to previously developed methodologies [24,51].

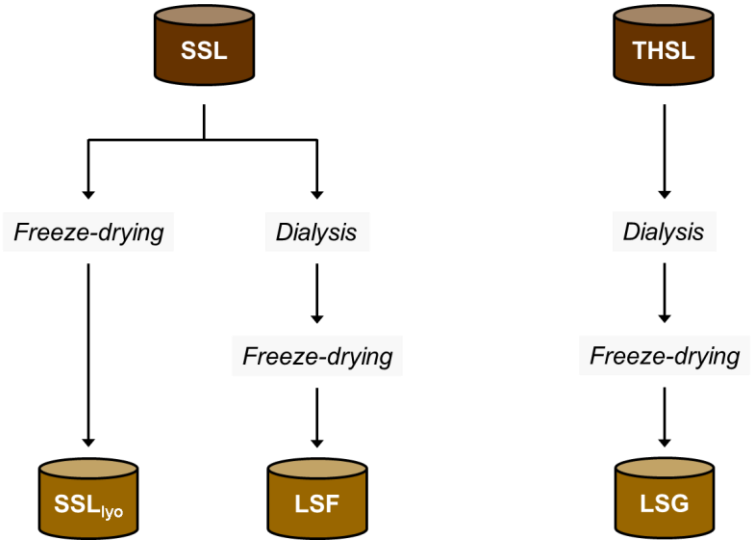


**Figure 12.** Scheme representative of the preparation methodology of the lignosulphonates-rich fractions LSG and LSF (including the lyophilized SSL denoted as $SSL_{lyo}$), obtained from thick (THSL) and thin (SSL) liquors, respectively.

Laccase Novozym® 51003 (from *Aspergillus oryzea*) was kindly supplied by Novozymes (Bagsvaerd, Denmark) and was used in all experiments without further purification.

2-(dodecylthiocarbonothioylthio)-2-methylpropionic acid (DDMAT), poly(ethylene glycol) diglycidylether (PEGDE, $\overline{M}_n$ ~500 g·mol$^{-1}$), poly(propylene glycol) diglycidyl ether (PPGDE, $\overline{M}_n$ ~380 g·mol$^{-1}$), poly(propylene glycol)-toluene diisocyanate copolymer

(PPGDI, $\bar{M}_n$ ~2300 g·mol$^{-1}$, DP ~34, isocyanate content ~3.6 wt. %), and dibutyltin dilaurate (DBTDL), were purchased from Sigma-Aldrich (Madrid, Spain) and used without any further purification. Glyoxal solution (40 wt. % in $H_2O$) and PEG with average $M_w$ 200 ($PEG_{200}$) were supplied by Acros (Lisbon, Portugal). All solvents and other reagents, namely, 2-Amino-2-(hydroxymethyl)-1,3-propanediol (Tris), potassium dichromate, chromium(III) chloride hexahydrate, zinc(II) chloride, lead(II) nitrate, ammonia, sodium nitrate, cadmium(II) nitrate, copper(II) chloride, silver(I) nitrate, mercury(II) chloride, potassium ferricyanide(III) and potassium ferrocyanide(II) were of analytical grade and were purchased from either Acros (Lisbon, Portugal) or Sigma-Aldrich (Madrid, Spain). All solvents for SEC analysis were HPLC grade.

A 0.1 M aqueous solution of $[SiW_{11}Mn^{III}(H_2O)O_{39}]^{5-}$ (hereafter designated as $SiW_{11}Mn$) was prepared from its potassium salt, which was previously synthesized according to published methodology [287].

Two superplasticizers, NFS and PCE, were kindly supplied by Sika company (Ovar, Portugal). Portland cement type II A-L 42.5R [288,289] from Cimpor company (Souzelas, Portugal) was used to prepare the cement pastes at Sika company.

Multi-wall carbon nanotubes (MWCNTs) Nanocyl-3150 (purity > 95 %, length 1–5 μm and diameter 5–19 nm) were supplied from Nanocyl, S.A. (Sambreville, Belgium). Graphene oxide (GO, apparent density 0.2–0.4 g·cm$^{-3}$) and reduced graphene oxide (rGO, apparent density 0.06-0.09 g·cm$^{-3}$, electrical conductivity ≈ 667 S·m$^{-1}$) were supplied by Graphenea (San Sebastián, Spain). Graphite (Gr) was supplied by Graphite Technologies Lda (Oliveira de Azeméis, Portugal).

Polyaniline (PANI)-modified screen-printed electrodes (SPE) with carbon working and auxiliary electrodes and silver reference electrode were supplied by Metrohm DropSens (Oviedo, Spain). All solutions for the potentiometric measurements were prepared using ultrapure water (18 mΩ·cm$^{-1}$).

Oligomeric isocyanate 4,4'-methylene diphenyl diisocyanate (pMDI) (Voranate M229) with 31.1% of NCO, a functionality of 2.7, a viscosity of 190 mPa·s (at 25 °C) and an isocyanate equivalent of 135 (values provided by the supplier) was kindly supplied by Dow Chemicals (Estarreja, Portugal). Commercial polyvinyl acetate (PVA) glue (white glue) was purchased in the local market.

For each analysis, three to five repeated measurements were performed and the results correspond to the mean value ± the standard deviation.

## 3.2. METHODS

### 3.2.1. Chacterization of SSL and purified LS (Chapter 4)

***Ash content.***

Ash content in SSL and purified LS was determined gravimetrically by calcination at 525 ± 25 ºC according to Tappi standard T 211 om-12.

***Neutral sugars analysis.***

Sugars analysis as alditol acetate derivatives was carried out using gas chromatography with flame-ionization detection (GC-FID) after Saeman hydrolysis [290]. The methodology was as follow: acid hydrolysis of polysaccharides present in the lignosulphonates samples was carried out by treatment of 50 mg of lignosulphonates (in the case of liquors around 300 mg of SSL or 100 mg for THSL) with 4.8 mL of 6 % $H_2SO_4$ for 2,5 hours at 100 ºC. Afterwards, the hydrolyzate was cooled and 200 µL of 2-deoxyglucose as internal standard (10 $mg \cdot mL^{-1}$ solution) was added. Then 1 mL of the mixture was neutralized with 200 µL of 25 % $NH_3$ solution followed by the reduction of the monosaccharides to alditols by adding 100 µL of 3 M $NH_3$ solution containing 150 $mg \cdot mL^{-1}$ of $NaBH_4$. After 1 hour at 30 ºC, 50 µL of acetic acid was added twice. Next, the alditols were acetylated by adding to 300 µL of the above solution 450 µL of 1-methylimidazole and 3 mL of acetic anhydride. The solution was maintained at 30 ºC for 30 minutes. The alditol acetates were extracted with dichloromethane and the organic phase was washed with distilled water. The solvent was evaporated under nitrogen flowing atmosphere. Any remaining of water residue was eliminated by coevaporation with acetone. Standard solutions were also prepared for the identification and elaboration of calibration curves for the quantification of each sample sugar. Alditol acetates were quantitated using a Focus GC-FID (Thermo Scientific, Waltham, MA, USA) using Chrom-Card software to ensure complete control of the instrument operation and data acquisition under the following conditions: inlet temperature

225 ºC with a split flow of 30 $mL \cdot min^{-1}$; oven temperature 220 ºC with a run time of 28 minutes and carrier flow of 3 $mL \cdot min^{-1}$; detector temperature 250 ºC.

***Content of sugars, acids, methanol and furfural in SSL.***

Furfural, sugars (glucose and xylose), acids (formic and acetic acids) and methanol present in the industrial SSL were quantified by high performance liquid chromatography (HPLC). Standard solutions were also prepared for the identification and elaboration of calibration curves for the quantification of each component. Prior the HPLC analysis, the SSL diluted solutions were filtered using syringe filters with polyethersulfone membrane (0.45 μm porosity and 25 mm diameter). The HPLC analysis was carried out using an Accela HPLC system (Thermo Scientific, Waltham, MA, USA) equipped with an Accela 600 pump, Accela PDA and RI detectors, and a 8 μm Thermo Scientific HyperRez XP Organic Acids column 100×7.7 mm. ChromQuest software was used to ensure complete control of the instrument operation and data acquisition. The isocratic method consisted on using 0.001 M $H_2SO_4$ as the eluent at a 300 $\mu L \cdot min^{-1}$ flow rate, with a run duration of 70 min, keeping the column at 40 ºC.

***Thermogravimetric analysis (TGA).***

TGA of the samples was carried out using a Setsys Evolution 1750 TGA-DSC (Setaram, Caluire, France) thermogravimetric analyser equipped with a DSC plate rod accessory and the thermal analysis software Setsoft 2000. Samples were analysed from room temperature up to 800 ºC at a heating rate of 10 $C \cdot min^{-1}$ in nitrogen or oxygen gas at flow rate of 200 $mL \cdot min^{-1}$ using an alumina crucible. A blank experiment (with empty crucible) was carried out under the same conditions for each type of experiments (under $N_2$ or $O_2$) prior the experiments with samples, in order to subtract the buoyancy effect. Temperature and heat flow calibrations were carried out using the melting points of four standards (In, Pb, Al, and Au) at three different heating rates (5, 10, and 15 $ºC \cdot min^{-1}$).

***Fourier-transform infrared (FTIR) spectroscopy.***

FTIR spectra of LS and LS-based products were recorded using a FTIR System Spectrum BX (PerkinElmer, Massachusetts, USA), coupled with a universal ATR sampling accessory, in absorbance mode from 4000 to 500 $cm^{-1}$ with a 4 $cm^{-1}$ resolution. Samples were analysed as powders, 128 scans were averaged, and all spectra were baseline corrected and normalized (using the min-max normalization technique [291]) for further analysis.

***UV-Vis spectroscopy.***

The quantification of LS comprised in SSL was carried out using a Evolution 200 UV-Vis Spectrophotometer (Thermo Scientific, Massachusetts, USA) at 273 nm, using experimentally determined absorption coefficient (ε).

***Molecular weight determination.***

Size exclusion chromatography (SEC) analysis was carried out using two PL aquagel-OH MIXED 8 μm 300×7.5 mm columns protected by a PL aquagel-OH Guard 8 μm pre-column on a PL-GPC 110 system (Polymer Laboratories, Shropshire, UK) equipped with a RI detector. The columns, injection system and detector were maintained at 36 ºC during the analysis. LS were dissolved in 0.1 M $NaNO_3$ aqueous solution to a concentration of about 10 $mg \cdot mL^{-1}$ (1% w/v). The eluent (0.1 M aqueous solution of $NaNO_3$) was pumped at a flow rate of 0.9 $mL \cdot min^{-1}$. The calibration was performed using pullulan standards (Polymer Laboratories, Shropshire, UK) covering the molecular weight range of 738–48000 Da.

***Nuclear magnetic resonance (NMR) spectroscopy.***

Quantitative $^{13}C$ NMR and $^{1}H$ NMR spectra were recorded using a ASCEND$^{TM}$ 500 spectrometer (Bruker, Wissembourg, France) operating at 500.16 MHz for proton and at 125.77 MHz for carbon. The $^{1}H$ NMR and $^{13}C$ NMR spectra of LS and modified LS were registered in $D_2O$ at 295 K using typical sample concentrations of 2.5 % for proton and of 25 % for carbon spectra. Sodium 3-(trimethylsilyl) propionate-d4 was used as internal standard ($\delta = 0.00$) in proton spectra. The relaxation delay was 14 s and about 200–300 scans

were collected (90º pulse). The quantitative carbon NMR spectra were acquired using a 90º pulse, 12 s relaxation delay and 18000–20000 scans were collected. The internal standard used was acetone (δ = 30.89).

The phase-sensitive $^{1}$H-detected heteronuclear single quantum coherence (HSQC) spectra were recorded using a ASCEND$^{TM}$ 500 spectrometer (Bruker, Wissembourg, France) operating at 295 K. HSQC spectra of LS and modified LS were acquired in $D_2O$ over an F1 spectral weight of 12,000 Hz and an F2 width of 2000 Hz with a 2048×1024 matrix and 128 transients per increment. The delay between scans was 2 s and the delay for polarization transfer was optimized for $^{1}J_{C\text{-}H}$ = 150 Hz.

***Sulfonic ($SO_3H$) and phenolic ($OH_{phen}$) groups content in LS.***

The sulphonic and phenolic hydroxyl groups content in LS was determined by conductometric titration [33]. The procedure was as follow: About 50 mg of LS were dissolved in 20 mL of distilled water, then 500 mg of Dowex® 50WX2 (50–100 mesh) ion-exchange resin were added. After 24 hours, the resin was separated in a glass filter and thoroughly washed with distilled water. The filtrate and wash waters were quantitatively transferred into a erlenmeyer flask and conductometrically titrated with 0.1 N LiOH until 3 mL of titrant were used, then titrated with 0.1 N HCl again until 3 mL were used. The content of $SO_3H$-groups is giben by Equation 1:

$$[SO_3H] = (100 \times a \times f)/A \quad (1)$$

whereas the content of $OH_{phen}$-groups is given by Equation 2:

$$[OH_{phen}] = (100 \times b \times f)/A \quad (2)$$

where *a* and *b* are the titrant volumes in mL (0.1 N LiOH and 0.1 N HCl, equivalent to the content of $SO_3H$- and $OH_{phen}$-groups, respectively); *f* is the titer of LiOH and HCl; and *A* is the LS sample weight in mg. Both concentrations are given in meq/g.

***Dynamic light scattering (DLS).***

Zeta potential was measured using a Zeta sizer Nano Series analyser (Malvern Instruments, Worcestershire, UK).

### 3.2.2. LS-based dispersants for concrete formulations (Chapter 5)

***Evaluation of the laccase activity***.

Laccase activity was determined at 30 ºC by oxidation of 2,2'-azino-bis-(3-ethyl benzthiazoline-6-sulphonate) (ABTS) in sodium acetate buffer, pH 5.0 [141]. Oxidation of ABTS was followed by absorbance increase at 420 nm ($\varepsilon_{420}$ = $3.6\times10^4$ $cm^{-1}$). Enzyme activity was expressed in laccase activity units (U, $\mu$mol·$min^{-1}$).

***Laccase-oxidative polymerization of LS***.

The enzymatic treatment consisted in adding laccase (loadings ranging from 42 to 500 U·$g^{-1}$ of LS) to 10 mL of a 100 g·$L^{-1}$ LS solution (pH adjusted to 4.3) in a 25 mL jacketed glass reactor equipped with a magnetic stirrer and a heating circulating water bath. The reactions were carried out at 40 ºC with continuous pure oxygen bubbling for 90–120 minutes. Samples were withdrawn from the reaction vessel at 10, 20, 30, 60 and 90 minutes of reaction time. The water-soluble modified LS samples were analysed by SEC and UV-Vis spectroscopy and then were freeze-dried for further characterization by ATR-FTIR spectroscopy, quantitative $^{13}$C NMR and $^{1}$H-$^{13}$C HSQC NMR (*see section 3.2.1*).

***Synthesis of aqueous solutions of molybdovanadophosphate POMs***

Molybdovanadophosphate POM solutions were synthesized using stoichiometric amounts of $MoO_3$, $V_2O_5$, $NaH_2PO_4.H_2O$ and anhydrous $Na_2CO_3$ [292]. The synthesis of a 0.1 M $[PMo_{10}V_2O_{40}]^{5-}$ solution (hereafter designated as $PMo_{10}V_2$) was carried out as follow: 14.4 g (0.1 mol) of $MoO_3$, 1.82 g (0.01 mol) of $V_2O_5$ and 1.38 g (0.01 mol) of $NaH_2PO_4.H_2O$ were suspended in 35 mL of distilled water in a 250 mL Erlenmeyer flask with a magnetic stirring bar, at room temperature. Then, 5.3 g (0.05 mol) of anhydrous $Na_2CO_3$ was slowly added in small portions to the stirred mixture, causing $CO_2$ liberation. A condenser was

placed on top of the Erlenmeyer and the mixture was refluxed for 3 h until a deep red translucent solution was obtained. Then the solution was allowed to cool down to room temperature. At this point, 50 ml of a 2 M $H_2SO_4$ solution was added. The final solution was transferred to a glass flask, flushed with $N_2$ (g) and kept in the dark.

A similar procedure was carried out for the synthesis of 0.1 M $[PMo_{11}VO_{40}]^{4-}$ solution (hereafter designated as $PMo_{11}V$), but in this case, different amounts of $MoO_3$ (15.84 g, 0.11 mol) and $V_2O_5$ (0.91 g, 0.005 mol) were used. Both POM solutions were used as such without further purification.

***POM-mediated laccase-oxidative modification of LS***.

The laccase oxidative treatment of LSF was performed according to previous methodology [293] with the introduction of a certain amount of a selected POM. The procedure consisted in adding 200 μL of a 0.1 M aqueous solution of $[SiW_{11}Mn^{III}(H_2O)O_{39}]^{5-}$ to 10 mL of a 100 $g \cdot L^{-1}$ LSF solution (pH adjusted to 4.3) in a 25 mL jacketed glass reactor equipped with a magnetic stirring bar and a heating circulating water bath, which temperature was set at 40 °C. Then laccase (85 $U \cdot g^{-1}$ LS) was added to the solution. The reaction was carried out at 40 °C with continuous pure oxygen bubbling for 60 min. At the end of the reaction, the water-soluble modified LS solution was cooled down using an ice bath and finally stored in the refrigerator (4–6 °C). The same procedure was carried out using the 0.1 M $[PMo_{10}V_2O_{40}]^{5-}$ and $[PMo_{11}VO_{40}]^{4-}$ solutions. The sample was analysed by SEC and UV-Vis spectroscopy and then a small amount was freeze-dried for further characterization by ATR-FTIR spectroscopy (see section 3.2.1).

***Synthesis of LS-based amphiphiles***.

The procedure consisted in dissolving 12 g of LSG in 20 mL of distilled water in a 50 mL two-neck round bottom glass flask equipped with a condenser and a magnetic stirring bar. The LSG solution (pH ~4.6) was heated up to 100 °C and then 17 mL of PEGDE was added corresponding to a OH ratio of LS toward PEGDE of 1:2. The reaction was carried out at 100 °C for 2 h under nitrogen atmosphere, without the addition of any catalyst. Upon this, the reaction mixture was cooled down to room temperature and finally stored in the

refrigerator. A similar procedure using the same conditions and reagents proportions was carried out but, in this case, 13 mL of PPGDE was added instead of PEGDE.

For SEC analysis and cement paste preparation, samples were kept in the refrigerator (4–6 °C) and then used as such without further treatment/purification step. For chemical characterization, such as FTIR and NMR analyses, samples were purified by dialysis against distilled water for 8 h at room temperature using a partially benzoylated cellulose membrane of 2000 NMWCO (Sigma-Aldrich, Madrid, Spain), freeze-dried and then kept in a desiccator. (see section 3.2.1).

***Characterization of cement pastes - Flow table test***.

The workability/fluidity of a cement paste is assessed by the flow table test according to a standard procedure EN 12350-5:2009 [294] with some adjustments. The cement paste was prepared as follow: 400 g of water was added to 1 kg of cement, followed by the addition of 10 g of an admixture solution containing 40 wt. % solids content. Various samples were tested as admixture in the cement formulation, such as unmodified LS, THSL, different modified LS samples and two commercial superplasticizers, one PCE and one NSF. The selected products are listed in Table 4 including corresponding description and reference name. The cement paste components were mixed using a laboratory cement paste mixer for 4 min. During this time period, the mixing was stopped and the sides of the mixing bowl were scrapped for 20 to 30 seconds. Finally, a cement paste slurry was obtained. The paste was filtered to break up lumps that may be present and then poured into the truncated flow cone mould on a glass plate/table. Once the cone was lifted, the cement paste collapsed and spread, as seen in Figure 13. The paste was allowed to flow on the plate for 30 seconds. The maximum diameter of the spread was measured; three values were registered and the average value was reported as the fluidity of the cement paste. This first average value was registered at 8 min with the initial time (t = 0 min) corresponding to the be-ginning of the preparation of the cement paste. The cement paste was collected and kept for further fluidity procedures, one at 30 min and another final one at 60 min.

**Table 4.** Selected LS-based products and commercial petroleum-based dispersants to be tested in cement pastes.

| Material* | Description |
|---|---|
| THSL | Unmodified thick sulphite spent liquor |
| LS | Unmodified purified LS from SSL/THSL |
| LSF-laccase | Laccase-modified LSF without mediator[a] |
| LSF-POM-laccase | POM-mediated laccase-modified LSF[b] |
| LSG-PPGDE (1:2) | PPG-modified LSG (LS:PPGDE = 1:2) |
| LSG-PEGDE (1:2) | PEG-modified LSG (LS:PEGDE = 1:2) |
| PCE | Commercial petroleum-based superplasticizer |
| NSF | Commercial petroleum-based superplasticizer |

*a* – Laccase load of 500 $U \cdot g^{-1}$ LS from previous work [293]
*b* – Laccase load of 85 $U \cdot g^{-1}$ LS, POM used $SiW_{11}Mn$.

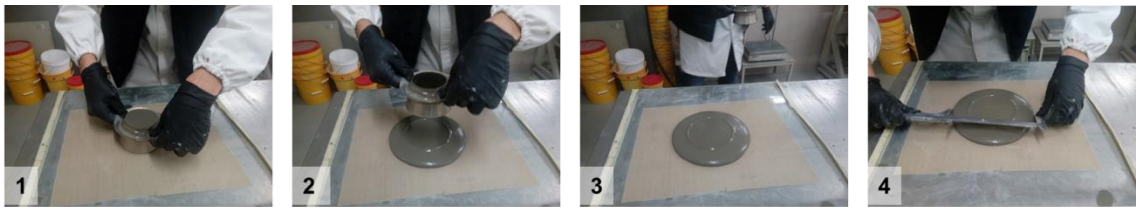


**Figure 13.** Flow table test: spreading of cement paste.

### 3.2.3. LS-based conducting membranes for sensor applications (Chapter 6)

***Synthesis of LS-based composite polyurethanes membranes***.

The polycondensation reaction of LS (purified from thick SSL) with isocyanate was carried out according to the literature [91,211,237–239] with only slight adjustments. For all syntheses, the amounts of LS and PPGDI were chosen in order to obtain a NCO/OH ratio of 1.5. LS was previously ground alone using an agate mortar and pestle and then mixed with MWCNTs (without grinding). Hence, LS powder (500 mg), or a mixture of LS powder with a certain proportion of MWCNT (0.1, 0.2, 0.5, 0.8, 1.0 and 1.4 % w/w in relation to the total mass of the overall mixture, *i.e.*, LS and PPGDI), was placed in a 25 mL jacketed glass reactor equipped with an overhead mechanical stirrer and a heating circulating water bath. Then, PPGDI (4 mL) was added and the mixture was stirred for 45 minutes at 60 ºC in order to obtain a homogeneous viscous solution. Then, liquid catalyst dibutyltin dilaurate (*ca*. 2% w/w in relation to the PPGDI) was added. The homogeneous mixture was stirred for a further 5–7 minutes until it started to thicken. At this point, the mixture was removed from the

reactor and poured into a flat PTFE mould. The reaction was carried out under nitrogen atmosphere. Obtained LS-based PU films were used for polymer characterization. Similar reactions were carried out using other carbon-based filler materials such as graphene oxide (GO), reduced graphene oxide (rGO) and graphite (Gr). Sensors were prepared by placing a thin layer of polymer on the working electrode of SPE. At least three parallel sensors of the same composition were prepared. Polymeric films were cured during 4 hours at 60 °C while sensors were cured for 4 days at room temperature in a desiccator.

FTIR-ATR, TGA (under $N_2$) analyses were carried according to procedures described in section 3.2.1.

***Measurement of films thickness***.

A hand-held digital micrometre (Mitutoyo Corporation) with an accuracy of 10 μm was used to measure the thickness of the LS-PU films. The thickness was measured at randomly selected locations on each film (n = 4/5) and the mean values were recorded.

***Dynamic Mechanical Analysis (DMA)***.

DMA analysis of the LS-based PU composites undoped and doped with carbon-based fillers (MWCNT, GO, rGO and Gr) was carried out using a Tritec 2000 DMA (Triton Technology, Leicestershire, United Kingdom). In the case of LS-based PU membranes, a rectangular piece with 30×5 $mm^2$ was mounted in tension geometry and then submitted to a temperature scan using a constant heating rate of 2 ºC·$min^{-1}$ from -100 º up to 60 ºC (before starting the run, an initial static force was applied (1 N) to guarantee that the sample remains under a net tensile force). The displacement was 0.010 mm and the frequency of deformation (oscillating frequency) was alternated between 1 and 10 Hz (due to the frequency dependence of data). The glass transition temperature, $T_g$, was determined from the maximum value of the peak in tan δ. (It is worth noting that when comparing the tan δ peak for a $\beta$ transition at 1 and 10 Hz, differences of more than 10 ºC between peaks are expected, while for an $\alpha$ transition, *i.e.* $T_g$, smaller differences around 3–7 ºC between peaks are normal [295,296]).

***Scanning Electron Microscopy (SEM)***.

SEM images of LS grinded powder, LS powder mixed with carbon filler and LS-based PUs membrane composites were recorded using a Hitachi S-4100 microscope (Tokyo, Japan). The powdered samples were placed on the carbon tape surface and the excess was blown. The membranes were cut (with dimensions *ca*. 2×4 mm) and glued with carbon glue on top of the holder in order to visualize their cross section. All samples were gold-coated prior SEM analysis during which an acceleration voltage of 5 kV was applied.

***Dielectric measurements***.

DC electrical conductivity was measured at temperatures between –110 and 100 °C using a 617 Keithley electrometer (Keithley Instruments GmbH, Munich, Germany). Electrical contacts were made by painting polymer films on both sides with silver paste, simulating a parallel plate capacitor with a surface area of about 1 $cm^2$ and 1 mm distance between electrodes.

Dielectric measurements for frequencies between 100 Hz and 1 MHz were carried out using an Agilent 4294A Precision Impedance Analyzer (Agilent, California, USA) at temperatures between –82 and 108 °C under helium atmosphere. Electrical contacts were made by placing the polymer films between two electrodes, simulating a parallel plate capacitor with a surface area of about 1 $cm^2$ and distance between electrodes 1 mm.

***Potentiometric measurements***.

Potentiometric chemical sensors were prepared by depositing a thin layer of LS-based PU doped with 1% w/w MWCNTs (before curing) on the surface of PANI-SPE. Then the polymer was cured at room temperature in a desiccator for 4 days before usage.

Electrochemical measurements were carried out in the following galvanic cell:

Ag | AgCl, KClsat | sample | PANI polymer membrane | carbon

The electromotive force values, Emf, were measured vs. Ag/AgCl reference electrode with a precision of 0.1 mV using a custom-made multichannel voltmeter with high input impedance connected to the PC for data acquisition and processing. Calibration

measurements were made in the solutions of zinc nitrate, cadmium nitrate, lead nitrate, copper(II) chloride, mercury(II) chloride, silver nitrate, chromium(III) chloride, potassium dichromate, potassium ferrocyanide and potassium ferricyanide in the concentration range $1.0\times10^{-7}$–$1.0\times10^{-2}$ M. Tris buffer solution with a concentration of 1 mM and pH 7 adjusted by addition of hydrochloric acid was used as supporting electrolyte. Redox response was studied in the solutions of two redox pairs, Cr(III)/Cr(VI) and $Fe(CN)_6^{3-/4-}$ at pH 2 on the background of 0.01 M HCl and at pH 7 on the background of 1 mM Tris buffer solution. Total concentration was 1 mM for both pairs with the ratio of oxidized to reduced form varying from 0.01 to 100. Parameters of Nernst equation, *i.e*

., slope of the electrode function and standard potential were calculated using linear regression and averaged over replicated calibration runs for each ion.

The sensor selectivity was estimated using the matched potential method (MPM) at pH 7 on the background of Tris buffer solution. At least 3 replicated measurements were run for each ion.

### 3.2.4. LS-based polyurethane adhesives (Chapter 7)

***LS-based adhesive synthesis***

For all formulations, purified LS powder (500 mg) was first dissolved in water (400 μL) or a mixture of water with $PEG_{200}$ (0, 50, 100 and 150 μL) to form the base solution. The volume of water used was initially optimized to ensure full solubilization of LS and ease of agitation. The mixture was kept under constant magnetic stirring for 5 min and then 50 μL of DBTDL was added as the catalyst. Finally, 900 or 1000 mg of crosslinker pMDI was introduced in the reaction mixture and the reaction proceeded for a certain time period ranging from 30 s to 5 min depending on the application. For all formulations, the quantities of LS, water and DBTDL were kept constant (500 mg, 400 μL and 50 μL, respectively) while only the contents of $PEG_{200}$ and pMDI were varied, according to the formulations presented in Table 5. The molar ratio NCO/OH was calculated based on the contribution of the total amount of OH groups in LS [297] and OH groups in $PEG_{200}$. In the ABES testing, a 5 min stirring time was chosen.

For the ABES testing, a 5 min stirring time was chosen. For the study of the curing process (DMA and DSC), the stirring time was 30 s. For the FTIR and TGA analyses (see section 3.2.1), a 5 min stirring was performed and then the adhesive was left curing for 48 h at room temperature.

**Table 5.** Formulations of the LS-based PU adhesives prepared.

| Formulation | LS (mg) | $H_2O$ (µL) | $PEG_{200}$ (µL) | DBTDL (µL) | MDI (mg) | NCO/OH molar ratio* |
|---|---|---|---|---|---|---|
| 1 | 500 | 400 | 0 | 50 | 900 | 3.2:1 |
| 2 | 500 | 400 | 50 | 50 | 900 | 2.6:1 |
| 3 | 500 | 400 | 100 | 50 | 900 | 2.2:1 |
| 4 | 500 | 400 | 150 | 50 | 900 | 1.9:1 |
| 5 | 500 | 400 | 0 | 50 | 1000 | 3.6:1 |
| 6 | 500 | 400 | 50 | 50 | 1000 | 2.9:1 |
| 7 | 500 | 400 | 100 | 50 | 1000 | 2.4:1 |
| 8 | 500 | 400 | 150 | 50 | 1000 | 2.1:1 |

* Without water

***Dynamic Mechanical Analysis (DMA)***.

Dynamic mechanical analysis (DMA) of the polymer films was carried out using a Tritec 2000 DMA instrument (Triton Technology, Leicestershire, UK). The LS-based PU formulation before curing was studied as such using a stainless-steel material pocket accessory [298] in single cantilever bending mode. A first temperature scan for the LS-based formulation curing process was carried out from room temperature up to 180 °C at a heating rate of 5 °C·min$^{-1}$, with a displacement of 0.020 mm and at a frequency of deformation (oscillating frequency) of 1 Hz. Next, the same material pocket containing the cured LS-based PU was used to perform a second temperature scan in order to determine its $T_g$. This second DMA run was carried out from –20 °C up to 200 °C (before degradation) at a heating rate of 2 °C·min$^{-1}$, with a displacement of 0.020 mm and at a frequency of 1 Hz.

***Differential scanning calorimetry (DSC)***

DSC analysis was carried out in a Power Compensation Diamond DSC (PerkinElmer, Waltham, MA, USA) previously calibrated using the melting points of indium and lead as

standards for temperature calibration and the heat of fusion of indium as standard for heat calibration [299,300]. The LS-based PU formulation samples (around 5–10 mg) were encapsulated in hermetically sealed stainless-steel pans that can with-stand a maximum internal pressure of 24 bar. Dynamic (non-isothermal) DSC runs were performed in the temperature range from –10 to 150 °C, at different heating rates, namely 5, 10, 15 and 20 °C·min$^{-1}$.

***Evaluation of adhesive strength by auto-mated bonding evaluation system (ABES)***

The strength development of LS-based adhesives was assessed using the automated bonding evaluation system (ABES, Corvallis, Oregon, USA). Tests with ABES apparatus were carried out using beech (Fagus sylvatica) veneer strips (with a dimension of 117 mm × 20 mm and thickness of 0.5 mm). For each test, a new LS-based adhesive sample formulation was prepared. After adding pMDI (according to the synthesis method), the formulation was mixed using a magnetic stirring for 5 min. Afterwards, 10 mg of pre-cured adhesive was applied and evenly distributed on the standard configuration of the beech veneer (over 5 mm of the edge of the beech veneer strips to cover the bonding area of 100 mm$^2$), according to Figure 14. Then, a wood strip without adhesive was overlapped over the one with adhesive making sure the two strips were aligned giving an overlapping area of 100 mm$^2$ (20 x 5 mm). This strip was glued to another strip in the same configuration and a 500 g load (49 kPa) was placed on top of the jointed wood strips. The structure was kept in this form for 24 h at room temperature for adhesive curing and the strips to be glued.

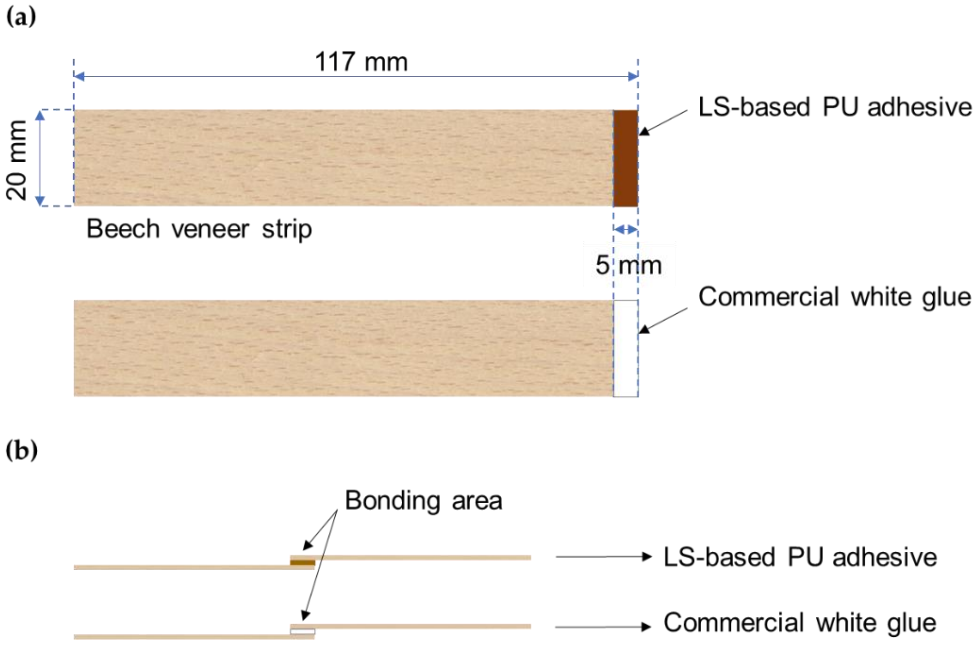


**Figure 14.** Scheme representing (a) the beech veneer strips and the area where the adhesives are applied and (b) the final set of two beech strips bonded with selected adhesive.

# 4. Characterization of SSL and LS

Part of this chapter was presented as a poster at the *15th European Workshop on Lignocellulosics and Pulp (EWLP2018)* in Aveiro (Portugal), 26-29th June, 2018:

Sandra Magina, Ana Barros-Timmons, Dmitry V. Evtuguin. Changes in potentialities of acidic sulphite pulping spent liquors while re-profiling mill from paper-grade to dissolving pulps. *Proceedings of the 15th European Workshop on Lignocellulosics and Pulp (EWLP2018) – Posters Presentations*, Aveiro, Portugal, 26–29 June, **2018**; pp. 303–306.

## 4.1. ABSTRACT

The magnesium-based acidic sulphite cooking process adopted at CAIMA significantly changed in the last years. Formerly the cooking process ran at 130 ºC and moderate acidity (pH *ca* 1.5) aiming the production of paper-grade cellulosic pulp from *Eucalyptus globulus* wood. Nowadays, CAIMA produces dissolving pulp from *Eucalyptus globulus* wood through an acidic sulphite process carried out at 145 ºC and at a final pH below 1.0. Considering that the re-profiling of the sulphite process may have caused inevitable changes in the composition of the final SSL, a systematic chemical analysis is necessary and was carried out. In that sense thin (SSL) and thick (THSL) sulphite spent liquors from the dissolving pulp production were analysed as well as the purified lignosulphonates (LS) from both liquors, namely LSF from SSL and LSG from THSL. The main results were compared with those obtained for SSL and LS from the production of paper-grade pulp.

## 4.2. INTRODUCTION

The global lignin market is mostly composed of lignosulphonates (*ca*. 88%) [2], typically obtained from the sulphite process, which has been attracting significant attention in the context of biorefinery. While the chemical pulp is marketed as a raw material (*e.g*. dissolving pulp), sulphite spent liquor (SSL) side product can be processed to produce fuels (*e.g*. bioethanol), food additives (proteins, xylitol, etc.), bioplastics (*e.g*. polyhydroxyalkanoates) and a set of lignin-based chemicals [49]. After the sulphite pulping batch, the brown stock is washed and the pulp is separated from SSL, which is then concentrated by evaporation to produce 56-68% (w/w) thick SSL (THSL). A fraction of THSL is burned to produce energy and to regenerate the pulping base and $SO_2$ while the other fraction is processed into commercial products. SSL obtained from sulphite pulping of hardwoods are different than those from softwood sulphite pulping [24,51] and are mainly composed of water-soluble lignosulphonates (LS) and xylo-oligosaccharides (XOS). While a certain LS proportion is valorized into concrete additives, animal feed, paint and oil industries, and agriculture; the other portion corresponding to dissolved sugars and XOS could be used to produce bioethanol [58].

There is only one Portuguese company that produces dissolving pulp from *Eucalyptus globulus* through the magnesium-based acidic sulphite cooking process. During acid sulphite pulping, delignification occurs through two types of reactions, sulphonation and hydrolysis (as described in section 2.1.1). The sulphite pulping process adopted at CAIMA – Indústria de Celulose significantly changed in the last years by re-profiling the production of paper-grade to dissolving pulp. While formerly the cooking process ran at 130 ºC and moderate acidity (pH *ca*. 1.5), nowadays the process is carried out at 145 ºC and at a final pH below 1.0. This fact may cause inevitable changes in the composition of the final sulphite spent liquor affecting its potentialities in subsequent processing for the biorefinery requirements. Therefore, the main objective of this work was to carry out a comparative analysis of SSL and THL from the magnesium-based acid sulphite cooking of eucalypt wood when changing the production profile from paper-grade pulp to dissolving pulp, including a comparison between the chemical and structural features of purified LS ensued from the two different cooking processes.

## 4.3. RESULTS AND DISCUSSION

LSF and LSG were analysed on ash content, neutral sugars composition, and functional groups ($SO_3H$ and $OH_{phen}$-groups). The main structural features were evaluated by 1D/2D liquid-state NMR spectroscopy and FTIR-ATR. Thermal stability was assessed by TGA under inert ($N_2$) and oxidative ($O_2$) atmosphere and the molecular weight by SEC.

### 4.3.1. Chemical composition of SSL

The analysis of SSL and THSL showed that the pH of liquors decreased 0.5 (SSL) to 1 % (THSL) and the dry solids increased 1 to 2 % in SSL compared to previous analyses [51], as a result of the pulping process modifications (Table 6). Overall, both liquors are composed of three major groups of nonvolatile components, namely, ash, lignosulphonates, and sugars. The amount of ashes decreased in liquors compared to former data [51] while the differences in other components were not as significant. The changing of pulping conditions led to an increase in volatile compounds such as acetic and formic acids, methanol and furfural in the

liquor whilst the amount of LS increase in THSL was moderate. A relevant amount of acetic acid still remained in THSL after the SSL evaporation.

**Table 6.** Chemical composition of *Eucalyptus globulus* thin (SSL) and thick (THSL) liquors (% w/w liquor).

| | SSL | THSL |
|---|---|---|
| pH | 2.6 ± 0.0 | 2.8 ± 0.0 |
| Density ($gcm^{-3}$) | 1.06 ± 0.00 | 1.38 ± 0.02 |
| Dry solids | 13.1 ± 0.2 | 61.2 ± 0.3 |
| Ash | 1.9 ± 0.0 | 7.3 ± 0.3 |
| Lignosulphonates | 8.2 ± 0.2 | 32.6 ± 0.2 |
| Glucose | 0.4 ± 0.0 | 2.0 ± 0.3 |
| Xylose | 2.4 ± 0.2 | 10.6 ± 0.5 |
| Methanol | 0.2 ± 0.0 | 0.85 ± 0.37 |
| Furfural | 0.01 ± 0.00 | 0.04 ± 0.01 |
| Formic acid | 0.02 ± 0.00 | 0.09 ± 0.01 |
| Acetic acid | 1.1 ± 0.1 | 0.50 ± 0.02 |

### 4.3.2. Chemical and structural analysis of purified LS

Comparing LSF with original SSL freeze-dried ($SL_{lyo}$) in terms of neutral sugars content (Table 7), it is obvious that the dialysis purification of LS using 2000 Da MWCO membrane was not efficient to remove all carbohydrates present in SSL, since a remnant amount of *ca*. 6 % w/w is still present in LSF. This occurrence was previously elucidated [51] and has been related to the presence of xylo-oligosaccharides (XOS) that exhibit similar LS molecular weight. Unsurprisingly, contents on neutral sugars, sulphonic and phenolic hydroxyl groups in LSG are lower than in LSF. The evaporation of SSL at the pulp mill to obtain THSL is carried out in a multiple-effect evaporation system composed of 7 evaporators running under vacuum with the evaporation temperature ranging from 130 ºC in the first effect to 60 ºC in the last effect. Therefore, the evaporation conditions contribute to the occurrence of condensation reactions and further degradation of functional groups and carbohydrates.

**Table 7.**Chemical composition of purified lignosulphonates LSF and LSG (% m/m).

| | **LSF** | **LSG** | **$SL_{lyo}$** |
|---|---|---|---|
| **Ash** | 11.6 ± 0.5 | 12.1 ± 0.4 | 12.8 ± 0.4 |
| **Neutral sugars** | 6.1 ± 0.2 | 5.1 ± 0.2 | 14.9 ± 0.5 |
| *Arabinose* | *0.1 ± 0.0* | *0.1 ± 0.0* | *0.3 ± 0.0* |
| *Xylose* | *3.9 ± 0.2* | *3.2 ± 0.1* | *10.6 ± 0.2* |
| *Mannose* | *0.4 ± 0.0* | *0.3 ± 0.0* | *0.7 ± 0.0* |
| *Galactose* | *0.4 ± 0.1* | *0.4 ± 0.0* | *1.0 ± 0.1* |
| *Glucose* | *1.2 ± 0.2* | *1.0 ± 0.1* | *2.2 ± 0.1* |
| C | 43.5 ± 0.3 | 43.3 ± 0.4 | 36.2 ± 0.5 |
| H | 5.3 ± 0.1 | 5.9 ± 0.1 | 5.4 ± 0.1 |
| S | 9.6 ± 0.1 | 5.9 ± 0.2 | 8.2 ± 0.0 |
| $SO_3H$ groups | 21.1 ± 0.7 | 17.1 ± 0.9 | 21.5 ± 1.2 |
| $OH_{phen}$-groups | 3.0 ± 0.4 | 2.4 ± 0.4 | 2.5 ± 0.4 |

The molecular weight of $SL_{lyo}$ and purified LSF and LSG was assessed by SEC and the ensuing curves are presented in Figure 15. The molecular weight distribution of all LS was bimodal. The curve related to $SL_{lyo}$ displays two peaks: one around elution time 18.0–19.8 min, which corresponds to a low molecular weight fraction containing sugars, oligosaccharides, and low molecular weight compounds, while the other peak around elution time 16.0–17.9 min corresponds to the fraction of LS with higher molecular weight. The curves corresponding to LSF and LSG revealed the decrease of the RI signal intensity at elution time around 18.0–19.8 min due to the removal of part of low molecular weight fractions from SSL during dialysis, which was more considerable in the case of LSG. As a matter of fact, in the case of $SL_{lyo}$, the LS fraction represents 42.5 % of the total, while for LSF it is 57.4 % and for LSG 60.1 %. Based on the calibration curve, the weight average molecular weight (Mw) of LS at elution interval 18.0–19.8 min was calculated being 2890 Da for $SL_{lyo}$ (PDI = 1.49), 3650 Da for LSF (PDI = 1.63) and 4130 Da for LSG (PDI = 1.77).

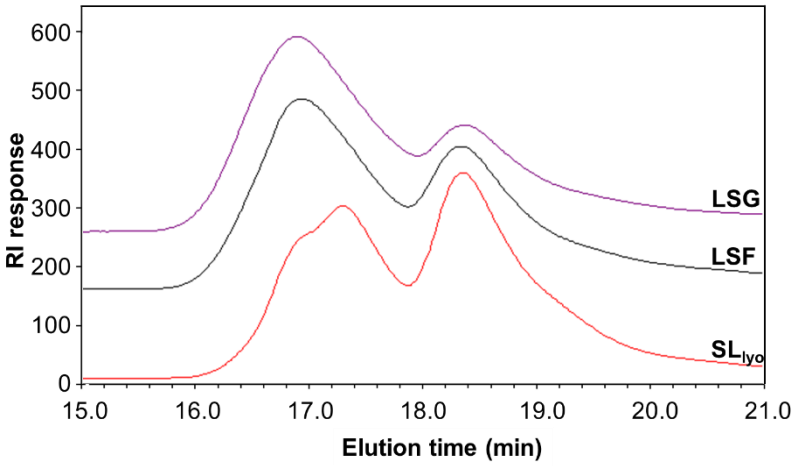


**Figure 15.** SEC curves of lyophilized spent sulphite liquor ($SL_{lyo}$) and LSF and LSG.

The FTIR-ATR spectra of LSF and LSG are very similar (Figure 16 and Table 8). Both LS exhibit a broad band at *ca*. 3000–3600 $cm^{-1}$, attributed to stretching of hydroxyl groups in phenolic and aliphatic structures, and two bands centred around 2940 and 2848 $cm^{-1}$, mainly derived from C-H stretching in aromatic methoxyl groups and in methyl and methylene groups of side chains [301–303]. The bands at 1604, 1510 and 1426 $cm^{-1}$ are assigned to aromatic skeleton vibrations, while the band at 1460 $cm^{-1}$ is associated to the C–H deformation in methoxyl groups combined with aromatic ring vibration [302–304]. These bands between *ca*. 1420 and 1600 $cm^{-1}$ are characteristic for all lignins [304], though change in the intensity of the bands may be observed and related to the amounts of $OCH_3$ groups present. Spectra of sulphonic acids are characterised by bands near 1350 and 900 $cm^{-1}$, while spectra of the corresponding salts are characterised by a group of strong bands between 1120 and 1230 $cm^{-1}$ [305,306], as seen in Figure 16. Below 1400 $cm^{-1}$, the assignment of the bands becomes much more difficult since the same band can be assigned different vibrations. Hence, the bands around 1330 and 1210 $cm^{-1}$ can be assigned to C-O vibrations associated to the aromatic ring as well as to sulphonic groups, namely the symmetric and asymmetric stretching of the S=O group [51,303–307], while the bands around 1154 and 1112 $cm^{-1}$ can be assigned to aromatic C-H in-plane deformation, C-O-C groups and also to sulphonic groups [303,304,306]. The strong band at 1034 $cm^{-1}$ can be attributed to aromatic C-H in-plane deformation related with C-O, C-C stretching and C-OH stretching, sulphonic groups and alkyl-aryl ether linkages such as β-O-4 interunit bonds and methoxyl groups [51,303,304,307]. Finally, the bands at 914 and 818 $cm^{-1}$ are assigned to aromatic C-H

deformation out-of-plane [303,304], while the bands at 650 and 630 $cm^{-1}$ are assigned to sulphonic groups in particular to the S-O stretching and C-S stretching vibrations, respectively [51,302,308].

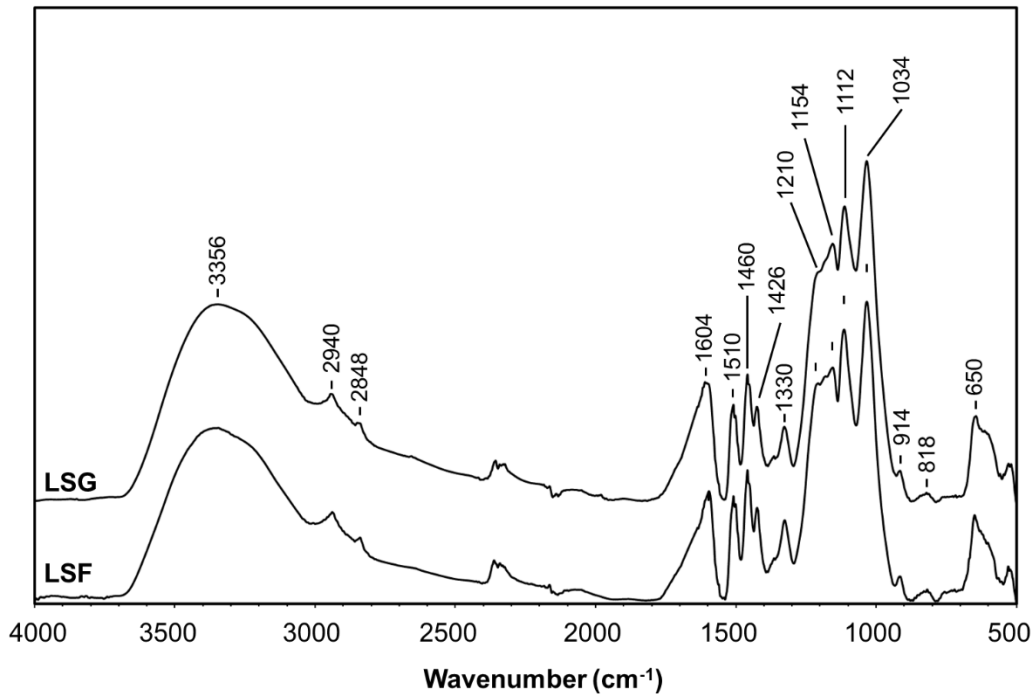


**Figure 16.** FTIR-ATR spectra of *Eucalyptus globulus* purified LSF and LSG.

The signals in $^{13}C$ and $^{1}H$ NMR spectra of both LSF and LSG were assigned based on the interpretation of NMR database of *Eucalyptus globulus* lignin [309,310] and lignosulphonates [24,310], as well as sulphonated lignin model compounds [52,53,311] and are presented in Figure 17 and Table 9.

The chemical shifts depicted in Table 9 corresponding to various structures (Figure 18) were similar to those reported for lignosulphonates [24,310] and for model compounds (considering the differences in solvents used and temperature of spectra acquisition) [311].

**Table 8.** Assignment of bands in FTIR-ATR spectra of purified LSF and LSG [51,301–308].

| LSF ($cm^{-1}$) | LSG ($cm^{-1}$) | Assignment |
|---|---|---|
| 3356 | 3356 | O-H stretching, H-bonded |
| 2938 | 2940 | C-H stretching in methyl, methylene and O-$CH_3$ groups |
| 2838 | 2848 | C-H stretching in O-$CH_3$ groups |
| 1600 | 1604 | Aryl ring stretching, symmetric |
| 1508 | 1510 | Aryl ring stretching, asymmetric |
| 1458 | 1460 | C-H bending in O-$CH_3$ groups, asymmetric |
| 1426 | 1426 | Aromatic skeletal vibration combined with C-H bending in O-$CH_3$ groups, asymmetric in-plane |
| 1326 | 1330 | $C_{aryl}$-O vibrations, $SO_3H$ groups (S=O stretching vibration) |
| 1210 | 1210 | $C_{aryl}$-O vibrations, C-C, C-O, C=O stretching, metallic salt of $SO_3H$ groups (S=O stretching vibration) |
| 1154 | 1154 | Aromatic C-H in-plane deformation, $SO_3H$ groups |
| 1114 | 1112 | Aromatic C-H in-plane deformation, C-O-C groups, metallic salt of $SO_3H$ groups |
| 1030 | 1030 | Aromatic C-H in-plane deformation related with C-O, C-C stretching and C-OH stretching, $SO_3H$ groups, $C_{alkyl}$-O ether vibrations (O-$CH_3$ and β–O-4) |
| 912 | 914 | C-H deformation out-of-plane, aromatic ring |
| 816 | 818 | C-H deformation out-of-plane, aromatic ring |
| 650 | 650 | $SO_3H$ groups (S-O stretching vibration) |
| 630 | 630 | $SO_3H$ groups (C-S stretching vibration) |

Structural assignments were confirmed by proton-carbon HSQC correlation 2D NMR spectra (Figure 19) according to the literature [24,310]. Generally, the most abundant structures are structure **A**, *β-O*-4 linkages, xylo-oligosaccharides and glucuronic acid (GlcA), while the other structures occur in smaller amounts being difficult to identify them in the HSQC spectra. Signals from xylo-oligosaccharides (XOS) and gluco-oligosaccharides (GOS) were identified being clear the highest abundance of XOS. This observation is in agreement with the chemical analysis of LSF and LSG that still contain 5–6 % of carbohydrates after SSL dialysis (Table 7) suggesting that part of XOS and GOS are chemically linked to lignin structures [24]. An unknown small signal at 6.5/112 ppm appears in both spectra. Therefore, further structural analysis is recommended, such as homonuclear correlation spectroscopy (COSY) or total correlation spectroscopy (TOCSY), in order to identify this signal and confirm some structures.

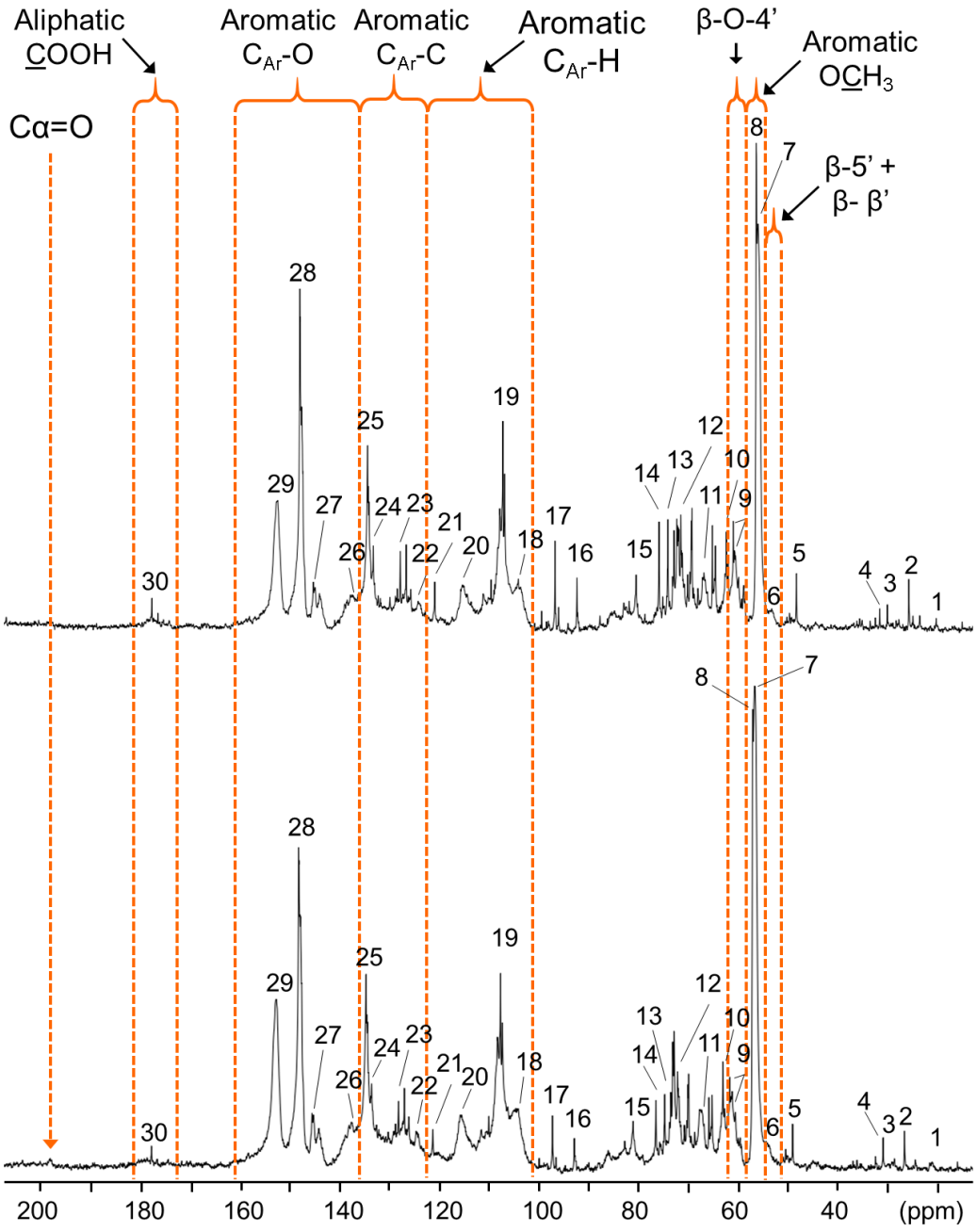


**Figure 17.** Quantitative $^{13}C$ NMR spectrum of LSF (top figure) and LSG (bottom figure) in $D_2O$ at 295 K.

The analysis of the main lignin structures in LSF and LSG is summarized in Table 10. The calculations were carried out per one hundred aromatic rings according to previously established methodology [24,309,310]. The aromatic region equivalent to six carbon atoms was integrated at 100–160 ppm. Lignosulphonate structures are mainly constituted by syringyl units since syringyl:guaiacyl ratio is 80:20 and 78:22 for LSF and LSG,

respectively. The abundance of lignin structures linked by *β-O*-4 bonds was calculated based on signals integrals at 60.0–62.0 ppm and only for the purified LSF.

**Table 9.** Assignment of carbon signals in $^{13}C$ NMR spectra of lignosulphonates.

| Signal | δC (ppm) | Assignment |
|---|---|---|
| 1 | 21.3 | $CH_3$ in acetyl groups |
| 2 | 26.6 | C*β* in **I** structures |
| 3 | 30.8 | acetone |
| 4 | 32.4 | C*β* in **D** structures |
| 5 | 49.1 | C*γ* in **D** structures |
| 6 | 54.0 | C*β* in **B** structures |
| 7 | 56.8 | Carbon in $OCH_3$ bonded to aromatic ring |
| 8 | 57.1 | C*α* in **F** structures |
| 9 | 60.6/61.1 | C*α* in **A** structures |
| 10 | 63.1 | C*γ* in **B** structures and C5 in xylan (int. units) |
| 11 | 67.4 | C*α* in **A**, **B** and **J** structures (*overlapped*) |
| 12 | 72.1 | C2,5 in glucan (int. units) |
| 13 | 74.6 | C2,3 in xylan (int. units) |
| 14 | 76.6 | C4 (int. units) and C3 (red. units) in xylan |
| 15 | 81.1 | C*β* in **A** structures |
| 16 | 92.9 | C1 in xylose reducing unit (*α*-isomer) |
| 17 | 97.3 | C1 in xylose reducing unit (*β*-isomer) |
| 18 | 104.7 | C2,6 in S units without sulphonic group at C*α* |
| 19 | 107.7 | C2,6 in S units with sulphonic group at C*α* |
| 20 | 115.5 | C2,5 in G units with sulphonic group at C*α* |
| 21 | 121.3 | C*γ* in **C** structures |
| 22 | 124.4 | C6 in G units with sulphonic group at C*α* |
| 23 | 128.3 | C1 in **C** structures |
| 24 | 133.7 | C*β* in **C** structures |
| 25 | 134.8 | C1 in **A**, **B**, **D**, **E**, **F**, and **I** structures |
| 26 | 137.7 | C4 in non-phenolic 4-*O*-5 and in **E** structures |
| 27 | 145.2 | C4 in phenolic G structures |
| 28 | 148.1 | C4 in phenolic S and C3,4 in non-phenolic G structures; C3,5 in phenolic S structures |
| 29 | 152.8 | C3,5 in non-phenolic S structures |
| 30 | 177.9 | COOH in COOH-$CH_2$-CH($SO_3H$)-Ar |

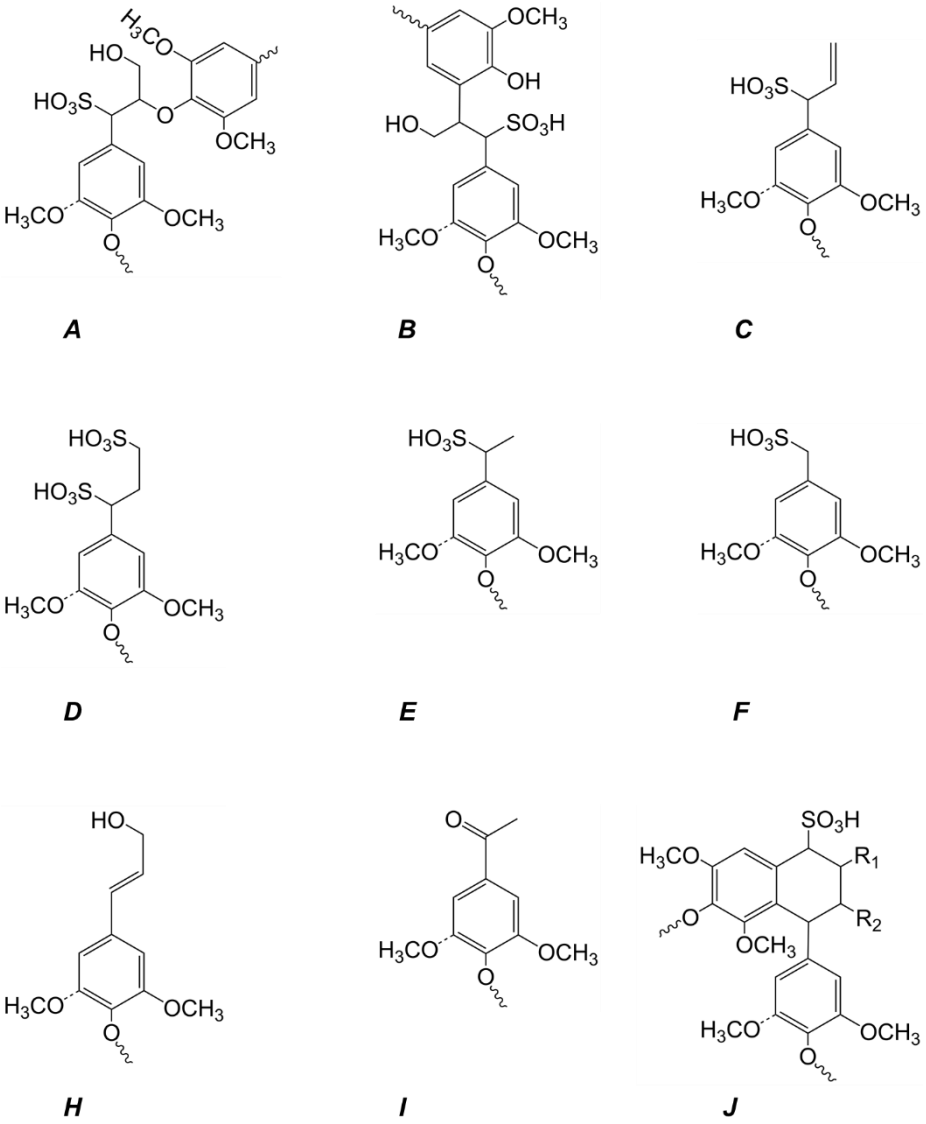


**Figure 18.** Lignosulphonate structures.

The results were similar to previous work [24] and revealed a reduced number of β-aryl ether structures in LSF (36 per 100 C6) comparing with wood lignin [309,310] due to strong depolymerisation of eucalypt wood lignin during acidic sulphite pulping (*via* partial cleavage of *β-O*-4 structures) [53,310]. The abundance of aromatic quaternary oxygenated (Ar-O), nonoxygenated (Ar-C) and tertiary (Ar-H) carbons were determined based on the integration of corresponding characteristic spectra intervals at 140–160, 122–140, and 100–122 ppm, respectively (Table 10). Abundances for both LS are similar except for quaternary non-oxygenated carbons (Ar-C), which are in higher amount in LSG than in LSF, suggesting that during evaporation of SSL condensation reactions occur.

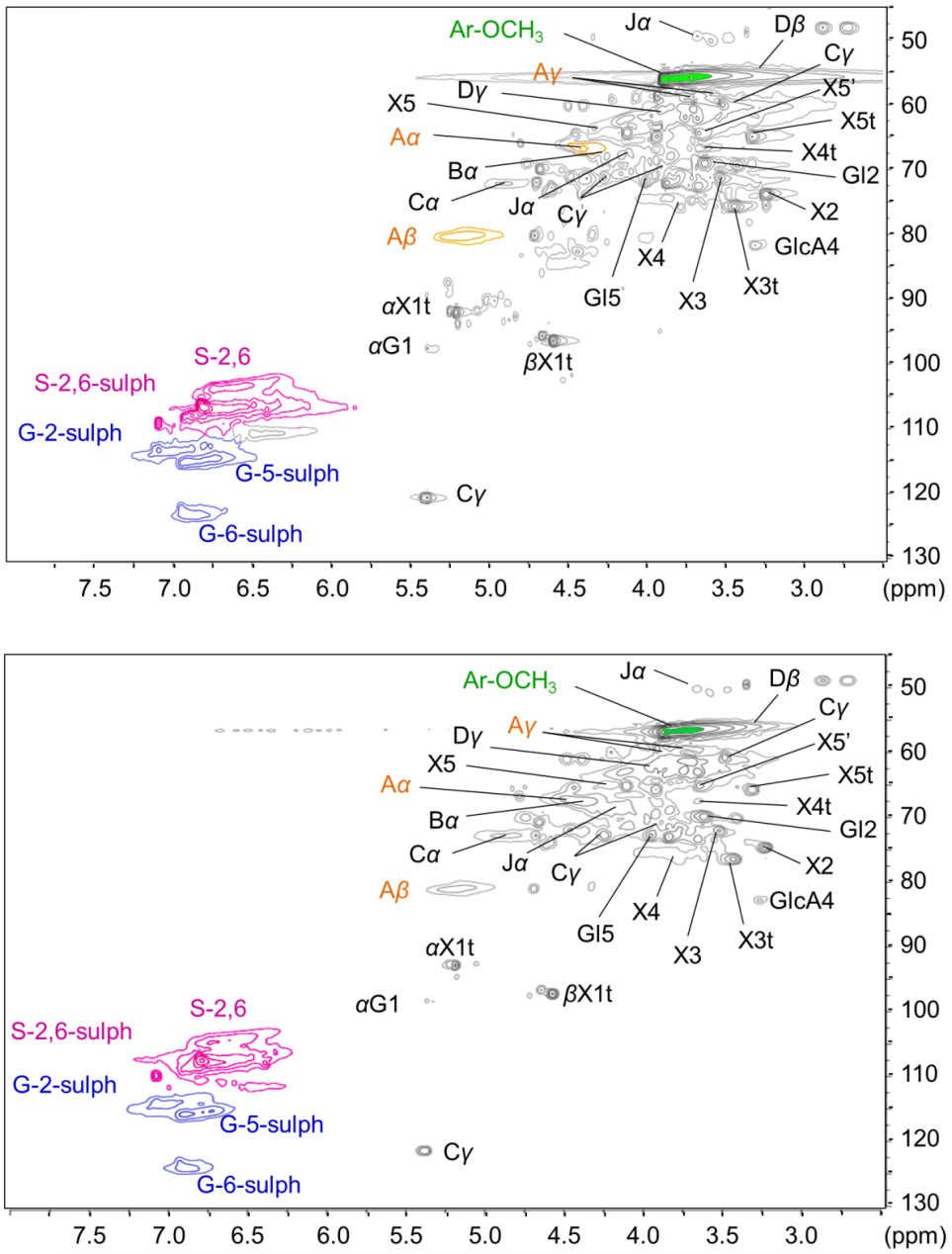


**Figure 19.** HSQC spectra of LSF (top figure) and LSG (bottom figure) in $D_2O$.

Based on the assignments and abundance calculations, it is clear that LSF and LSG present similar structures than lignosulphonates previously characterised [24,51]. Although the acidic sulphite process at CAIMA changed in the last years, formerly the cooking process ran at 130 ºC and pH 1.5 (liquid-to-wood ratio of 3.5–4.0) and nowadays the process is carried out at 145 ºC and pH 1.0 (liquid-to-ratio of 3.5–4.0), it seems that it does not affect the main structural features of the lignosulphonates.

**Table 10.** Structural analysis of lignosulphonate (LS) by quantitative $^{13}C$ NMR (per 100 phenylpropane units $C_6C_3$).

| Structural elements | LSF | LSG |
|---|---|---|
| β-O-4 structures | 36 | 34 |
| β-5 structures | 7 | 4 |
| $OCH_3$ | 151 | 152 |
| Ar-H | 196 | 200 |
| Ar-C | 180 | 190 |
| Ar-O | 222 | 224 |
| S:G ratio | 80:20 | 78:22 |

It is well established that the thermal degradation of lignin covers a wide temperature range (160–900 ºC) and is strongly dependent on the lignin nature, heating rate and degradation atmosphere [312–314]. Due to its complex composition and structure, which include aromatic rings with various branches and oxygen functional groups (phenolic hydroxyl, carbonyl groups and benzylic hydroxyl), lignin exhibits different thermal stabilities [312,314]. The cleavage of the functional groups originates low molecular weight products and at higher temperatures rearrangement of the backbone occurs giving rise to a high content of char (30–50 wt. %) and to the release of volatile products [312,314].

Correspondingly, both lignosulphonates LSF and LSG undergo similar thermal decomposition process exhibiting four degradation stages (Figure 20). Like lignins, cleavage of functional groups plays an important role (release of low molecular mass products and formation of char) and, due to the presence of sulphonated groups, release of sulphur dioxide during heating is also expected [312]. Under inert gas flow, LSF and LSG exhibit similar TGA and DSC profiles giving rise to a high content of residue, 38.6 and 41.1 %, respectively. However, under oxidative gas flow, TGA and DSC profiles for LSF and LSG are different, especially during the fourth stage in the temperature range 500–680 ºC, giving rise to a residue content rounding 9.2–9.8 %. The first stage, from room temperature up to 150 ºC, was similar for both lignosulphonates under inert and oxidative gas flow and is related to the release of strongly absorbed water (endothermic peak).

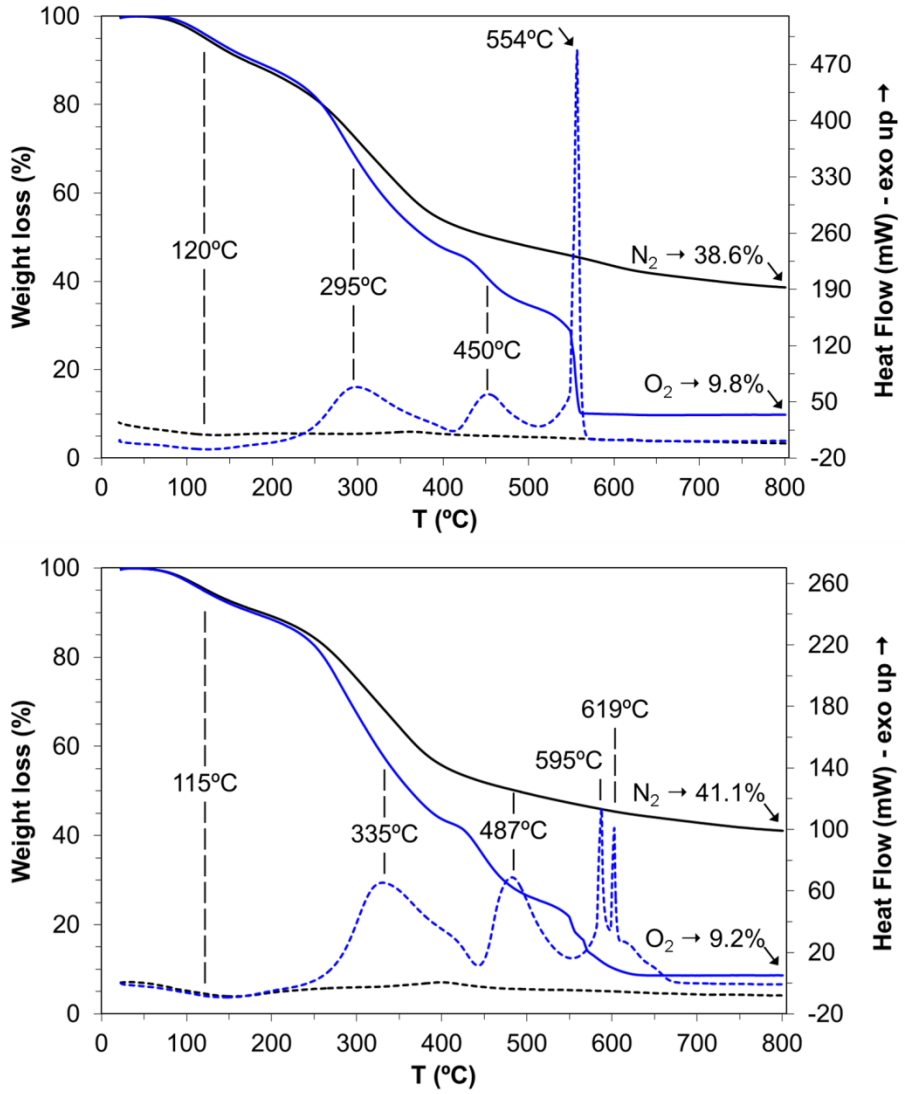


**Figure 20.** TGA thermograms and DSC profiles for LSF (top figure) and LSG (bottom figure) under $N_2$ (●) and $O_2$ (●) gas flow (▬ ▬ TGA; ▪▪▪ ▪▪▪ DSC).

The last three stages are directly related to the decomposition of LS corresponding to exothermic peaks in the respective DSC profiles. For both LS, the second stage started around 180–200 ºC and is characterised by release of sulphonic groups and $SO_2$, lignin degradation via side chain reactions (dehydration, decarboxylation, etc.) with a maximum weight loss rate at 280 ºC and 320 ºC for LSF and LSG, respectively (derivative of the TG profile not shown). In the same way, for both LS, the third stage of decomposition started around 380 ºC and is characterised by a maximum weight loss rate at 450 ºC and 445 ºC for LSF and LSG, respectively (DTG profile not shown). In this last degradation stage, the

degradation of LSF was more abrupt than for LSG, which last stage is bimodal. In both cases, char formation occur via rearrangement reactions in the range between 440–600 ºC.

### 4.4. CONCLUSIONS

The chemical composition of thin (SSL) and thick (THSL) sulphite spent liquors resulted in features like those of SSL/THSL formerly studied. Among major groups of liquor components, volatile compounds showed the highest relative increase, whereas the sugars and LS fractions revealed a minor relative increment. Although the acidic sulphite process at CAIMA changed in the last years, it seems that it does not affect the main chemical and structural features of the ensuing lignosulphonates. After dialysis, purified LS still contain 5–6 wt. % carbohydrates. Some reservations concerning the identification of some structural features require further analysis. The minor changes in LS structures are associated with higher condensation degree and subsequent increase of the molecular weight and simultaneous increment of bonded sulphonic groups. No significant differences in the abundance of the $\beta$-O-4 bonds have been detected. Hence, considering the applications of LS, the changes detected in its composition and structure due to the cooking modification may be potentially advantageous to produce modified plasticizers and/or water-reduction agents for concrete formulations, formaldehyde-based or formaldehyde-free adhesives for biocomposites, and conducting composites.

# 5. LS-based dispersants for concrete formulations

The first part of this chapter was presented as an oral presentation at the *20th International Symposium on Wood, Fiber and Pulping Chemistry (ISWFPC2019)* in Tokyo (Japan), 9-11th September, 2019, and published as:

Sandra Magina, Ana Barros-Timmons, Dmitry V. Evtuguin. Laccase-catalyzed oxidative modification of lignosulfonates from acidic sulfite pulping of eucalyptus wood. *Holzforschung*, **2020**, *74*(6), 589-596. DOI: 10.1515/hf-2019-0272

The second part was published as:

Sandra Magina, Ana Barros-Timmons, Dmitry V. Evtuguin. Synthesis of Lignosulfonate-Based Dispersants for Application in Concrete Formulations. *Materials*, **2021**, *14*(23), 7388. DOI: 10.3390/ma14237388

## 5.1. ABSTRACT

Lignosulphonates (LS) are products from sulphite pulping process that could be applied as renewable environmentally-friendly polymeric surfactants. Being widely used as plasticizers and water-reducing admixtures in concrete formulations LS compete in the market with petroleum-based superplasticizers, such as naphthalene sulfonate formaldehyde polycondensate (NSF) and copolymer polycarboxylate ethers (PCE). In this work, different chemical modification strategies were used to improve LS performance as dispersants for concrete formulations. One strategy consisted in increasing the molecular weight of LS through different approaches, such as laccase and polyoxometalate-mediated polymerization, glyoxalation and reversible addition-fragmentation chain transfer (RAFT) polymerization. The other strategy consisted in preparing LS-based non-ionic polymeric dispersants using two different epoxidized oligomer derivatives of poly(ethylene glycol) (PEG) and poly(propylene glycol) (PPG). Modified LS were used to prepare cement pastes, which were examined for their fluidity. Results revealed that the most promising products are PPG-modified LS due to the introduction of PPG chains by reaction with phenolic moieties in LS. The enhanced dispersant efficiency of the ensuing products is probably related not only to electrostatic repulsion caused by the sulphonic ionizable groups in LS, but also to steric hindrance phenomena due to the grafted bulky PPG chains.

## 5.2. INTRODUCTION

Lignosulphonates (LS) are sulfonated technical lignins present in spent liquor (SSL) from the sulphite pulping. Worldwide, approximately 1 million tons of LS are produced annually [62], which makes LS the most abundant type of lignin available in the market in a large scale representing *ca*. 88% of the global lignin market [2,27,49,63]. Considering the potential applications of LS, beside burning for energy recovery, it is marketed for specialty applications, such as dispersants for concrete formulations, animal feed, paint and oil industries, agriculture, among others [2,27,49,82]. Most of these applications are due to the good water solubility of LS, which is the reason for the restriction of the world market to these technical lignins [2].

LS are natural polymeric surfactants that contain both hydrophobic (aromatic rings and aliphatic chains) and hydrophilic (sulfonic, carboxyl and phenolic hydroxyl groups) moieties. Therefore, LS are widely used as concrete water reducers [114,115], coal water slurry dispersants [116,117], oil-well dispersants [118] and pesticide dispersing agents [119]. LS were first introduced as plasticizers and water-reducing admixtures to concrete in the 1930s [315] and nowadays 60 to 90 % of LS are used for this purpose. Concrete consists of a composite material made by mixing cement, aggregates and water, with or without the incorporation of admixtures [106], which are chemicals used to improve the concrete properties such as workability, mechanical performance and durability [107]. Chemical admixtures include, but are not limited to superplasticizers, the effectiveness of which is assessed by the possibility of reducing the water content in the concrete mixture. Therefore, when using plasticizers, a water content reduction of more than 5% by weight is expected, while superplasticizers provide a water content reduction of greater than 12% by weight [107,108]. LS are the most widely used concrete plasticizers, whose plasticizing and water reduction efficiency, however, is limited compared to synthetic superplasticizers [109,122–124]. Indeed, LS compete with petroleum-based polymeric superplasticizers, namely naphthalene sulfonate formaldehyde polycondensate (NSF) and a last-generation recently employed copolymer polycarboxylate ethers (PCE) (Figure 9) [107,109]. PCEs are much more efficient than LS giving rise to a concrete with superior fluidity or more noticeable water-reduction. However, PCEs are often 10 folds more expensive than LS, since the formers are synthetic petroleum-based products and LS are by-products from the sulphite pulp industry. Therefore, the common industrial practice is to mix both LS and PCEs in concrete admixture systems to improve their working and cost efficiency. Research results indicate that NSF disperses cement particles and reduces attractive inter-particle forces, such as van der Waals forces, by electrostatic repulsion, whereas PCE acts through both electrostatic repulsion and steric hindrance of nonadsorbing side chains [110,111]. On the contrary, LS dispersant and adsorption mechanism is based only on electrostatic repulsion forces, is pH dependent and influenced by the formation of aggregates [316]. Due to the presence of sulphonic groups in LS structure (likewise in NSF), LS can bind to the positively charged cement particles, causing them to be electrostatically repelled, recharging their surface, which prevents the fresh cement mixture from agglomerating, *i.e.*, prevent flocculation of cement particles, thus increasing its fluidity [317].

Some strategies can be used to improve LS performance, including increasing their molecular weight whilst preserving their solubility in water using an enzymatic modification treatment [125,126,293]. Enzymatic modification of lignin is considered as a convenient method due to its high specificity, mild reaction conditions, lack of undesired by-products and being environmentally friendly. Two different enzymes are commonly in use, peroxidases and laccases, though laccases are easier to apply in an industrial process than peroxidases because of the widest range of operating conditions and the nature of the oxidant (oxygen *vs* hydrogen peroxide). Thus, laccases require molecular oxygen, which has higher stability, lower price, and does not decompose spontaneously into radicals (no inactivation of the enzyme) as hydrogen peroxide [125]. Laccases mainly oxidize the phenolic lignin units [137]; however, they are able to oxidize the non-phenolic lignin units in the presence of certain redox mediators [141,142]. Among a variety of mediators, polyoxometalates (POMs), such as $K_5[SiW_{11}VO_{40}]$ and $H_5[PMo_{10}V_2O_{40}]$, have shown to be suitable mediators in laccase-mediator systems for oxidative polymerization purposes displaying synergistic behaviour when applied in the presence of laccase [318]. Since the adsorption of chemical admixtures on cement particles is related to the charge types and the charge density [319], another strategy to improve LS performance is the introduction of carboxylic groups, for instance, by oxidation via ozonolysis [128]. Another approach reported to improve the dispersant properties of lignin is the preparation of lignin-based non-ionic polymeric dispersants (amphiphilic derivatives) from organosolv and kraft (softwood and hardwood) lignins and LS [151–153]. Lignins were reacted with different commercial epoxidized oligomer derivatives and the most promising results were obtained using poly(ethylene glycol) diglycidyl ether (PEGDE) and poly(ethylene glycol) monoglycidyl ether (EPEG) with softwood lignin. The ensuing amphiphilic derivatives containing both hydrophilic and lipophilic moieties displayed enhanced dispersant properties compared with hardwood lignin-based counterparts. Moreover, the softwood lignin-based amphiphilic derivatives displayed even higher cement dispersibility than LS since only half of the amount of softwood lignin-based dispersants was necessary to achieve the same cement dispersibility compared to the use of unmodified LS. The chemical modification of lignins with PEG segments has also been reported to yield PEGylated lignins with potential application as thickener in bio-lubricant formulation [154] and bio-based surfactants [155]. Yet, the discussion on the dispersion mechanisms involved is quite limited.

An alternative pathway to modify lignin that has been reported consists in the reaction of lignin with glyoxal in an alkaline medium, resulting in the corresponding ethylol derivative suitable for adhesive applications. Besides glyoxalation, side lignin reactions take place leading to its depolymerization and repolymerization via condensation reactions yielding adducts with interesting structural properties [191–193].

In the last two decades, reversible deactivation radical polymerization techniques (RDRP), such as atom transfer radical polymerization (ATRP) [259,260] and reversible addition-fragmentation chain transfer (RAFT) [261], have been employed to produce regular polymers including the modification of lignocellulosic natural polymers. Regarding lignin modification, the grafting of softwood LS and KL with poly(3-sulfopropyl methacrylate) (PSPMA) and poly(methacrylic acid) (PMAA) anionic grafts via ATRP at pH 11 was reported [156]. compared with PEGylated lignin analogues and the commercial PCE superplasticizer. The best results approaching the performance of commercial PCE were achieved when using PMAA-grafted LS. It was suggested that the chemical nature of the grafted chains has a strong effect on the dispersant properties of the ensuing material. Adsorption, zeta potential, and intrinsic viscosity were measured for the grafted lignin analogues in order to examine the correlation between lignin and the chemical nature of the grafted chains in the cement dispersion mechanisms. Yet, no straightforward conclusions could be drawn due to the complexity of the system.

The purpose of this study was to enhance the dispersant properties of LS for further application in concrete formulations using different strategies. The first approach consisted on LS polymerization via laccase-oxidative polymerization without any mediators [293], followed by a second approach, which consisted on the POM-mediated laccase oxidation of LS (to complement the first strategy). In the third approach, the LS modification was carried out using RAFT polymerization with 2-(dodecylthiocarbonothioylthio)-2-methylpropionic acid (DDMAT) as the RAFT agent. Then, a fourth approach consisting on LS glyoxalation was examined. Finally, the modification of LS using two different epoxidized oligomer derivatives, poly(ethylene glycol) and poly(propylene glycol) diglycidyl ethers, PEGDE and PPGDE, respectively, was performed. In order to assess the dispersant performance of the samples, the fluidity/workability of cement pastes prepared with the different modified LS was determined and compared with the results obtained for cement pastes prepared with

unmodified LS and two different commercial petroleum-based superplasticizers, PCE and NSF.

### 5.3. LS MODIFICATION VIA LACCASE POLYMERIZATION

Laccase-catalyzed oxidative polymerization of purified eucalyptus LS from SSL was carried out under previously pre-selected conditions (temperature, exposure time, pH, different enzymatic loads) without using any mediators [320]. The optimal oxidation temperature used and the reaction time were 40 ºC and 90 min, respectively. Although the optimum reaction temperature applied in this study is in agreement with that reported previously by Areskogh and co-workers [125], the optimum recommended pH of laccase nearly 7 was not used in the present work because the natural pH of purified LS solution was nearly 3.5 and the pH increase to 7 by NaOH addition led to partial release of sulphonic groups. Consequently, the pH of the reactions with laccase was kept close to 4.5 according to the pH range 4–8 recommended by the laccase producer.

The results of enzymatic oxidation revealed the possibility of an 11-fold increase of the initial eucalyptus LS' $M_w$, *i.e.*, from 3240 Da up to 36800 Da, without using any external mediators (Figure 21). These results are in agreement with those obtained in a previous work by Areskogh with co-workers [125], who demonstrated that laccase polymerization of commercial lignosulphonates without using mediators led to a significant $M_w$ increase including the reduction of phenolic hydroxyls along with only minor structural changes. In addition, Leonowicz and co-workers [127] using lignin models provided evidence of the possible different oxidation routes involved in the reaction with laccase at low (*ca*. 3.5) and nearly neutral pH.

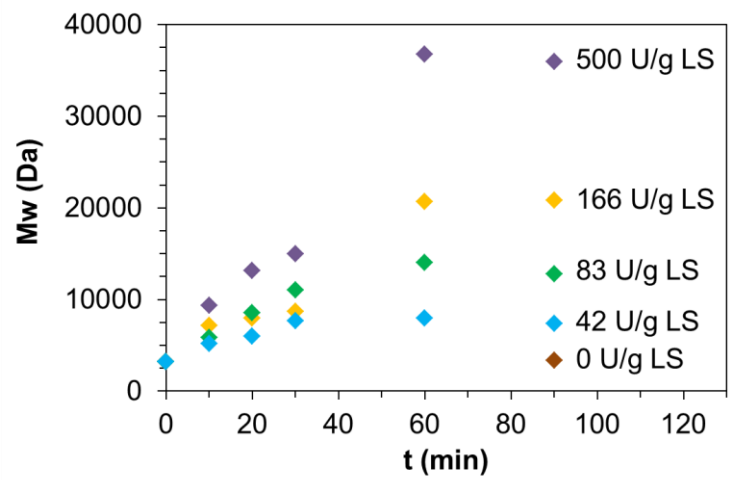


**Figure 21.** Changes in $M_W$ of LS modified by laccase oxidation at 40 ºC. Laccase loads varied within the range of 42-500 $U \cdot g^{-1}$ of LS.

In order to assess the eventual structural changes of LS in reaction with laccase the ATR-FTIR and UV-Vis spectroscopy analyses have been carried out to compare LS before and after laccase treatment. The modified LS were soluble in water and exhibited structural changes compared to the initial LS as revealed by UV-Vis analysis (Figure 22). The UV-Vis spectra showed a new band with a maximum at around 360 nm attributed to an increased amount of conjugated phenolic structures with α-carbonyl groups or double bonds [33,321].

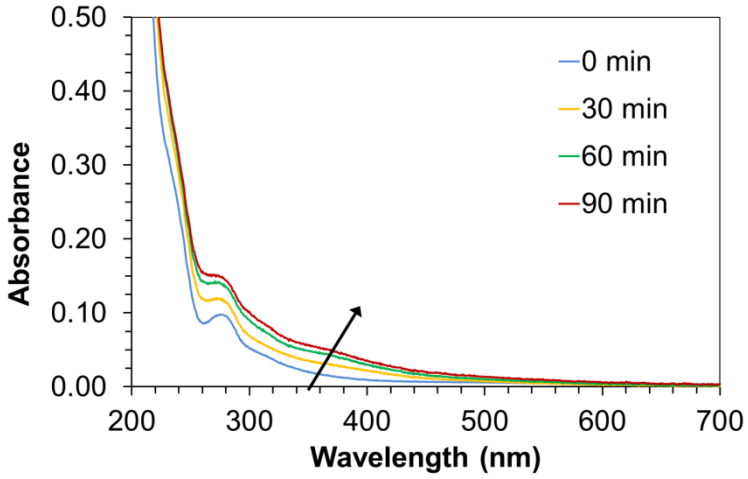


**Figure 22.** UV-Vis spectra of initial and modified LS for 30, 60 and 90 min (laccase load of 166 $U \cdot g^{-1}$ of LS).

The intensity of this band increased in time indicating the increased abundance of this type of structures compared to unmodified LS. Areskogh and co-workers [322] studied the reaction mechanism of laccase oxidation without mediators for several phenolic end-group lignin models. They considered the oxidation of benzylic carbon to corresponding keto group in the side chain as a non-productive reaction pathway with no possibility to obtain oxidation coupling products, *i.e.*, dead-end reactions hindering further lignin polymerization. In fact, the LS solution became much darker than before laccase modification, thus showing the extensive formation of chromophore groups.

FTIR-ATR spectra of the initial and modified LS (laccase load of 500 $U \cdot g^{-1}$ of LS) are depicted in Figure 23, where the main spectra differences are highlighted. The splitting of the band at 1592 $cm^{-1}$ (associated with the aromatic skeleton vibrations in the original LS) into a doublet at 1660 $cm^{-1}$ confirms the presence of conjugated structures with aromatic double bonds, along with the reduction of the number of phenolic hydroxyls and methoxyl groups content (absorption bands at 1220 and 1114 $cm^{-1}$) [303,308].

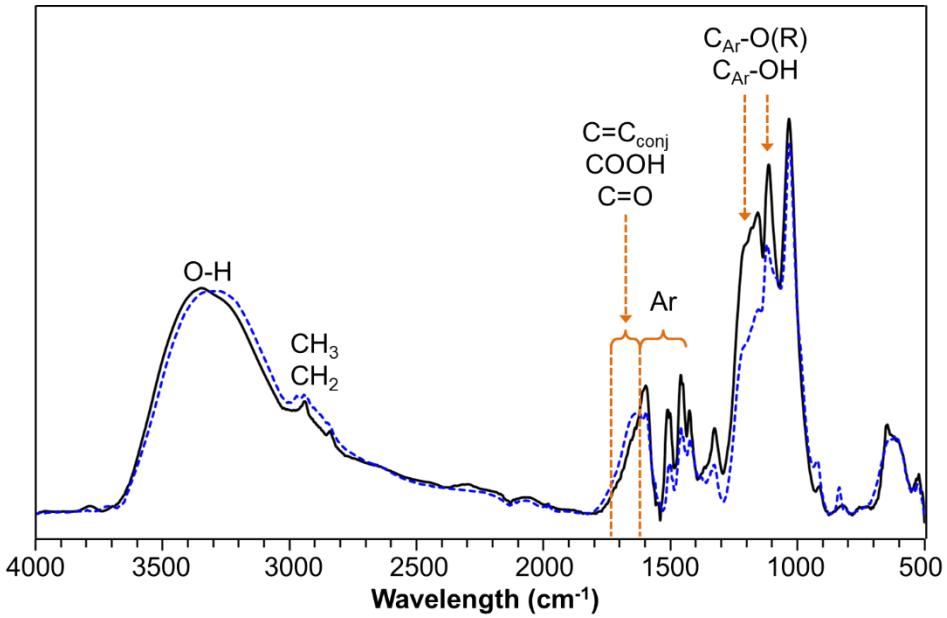


**Figure 23.** FTIR-ATR spectra of LS (solid line) and modified LS (dashed blue line) (laccase load of 500 $U \cdot g^{-1}$).

Further chemical and structural analyses of the modified LS were carried out using quantitative $^{13}C$ NMR supported by $^{1}H$-$^{13}C$ NMR (HSQC) spectra. Since $^{13}C$ NMR spectra

of LS modified using high loads of laccase (250 and 500 U·g$^{-1}$ of LS) revealed pronounced amounts of concomitants from laccase sample overlapping with the lignin signals, so only the spectra of LS modified with a laccase load of 83 U·g$^{-1}$ of LS are presented. The signals in $^{13}$C NMR spectra of both initial and modified LS (Figure 24) were assigned based on the NMR database of *Eucalyptus globulus* lignin [309,310] and corresponding LS [24,310] as well as sulphonated lignin model compounds [52,53,311].

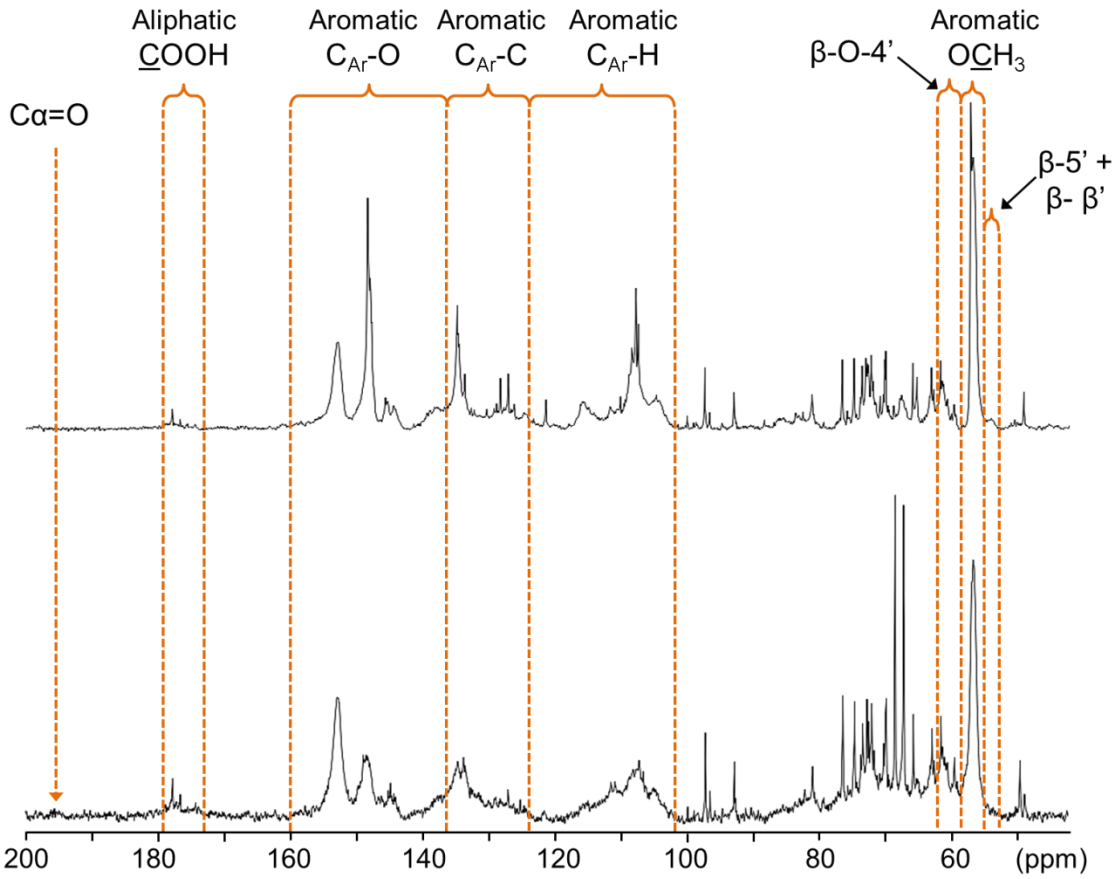


**Figure 24.** Quantitative $^{13}$C NMR spectra ($D_2O$, 295 K) of LS (top figure) and modified LS (bottom figure) in laccase-catalyzed oxidation at 40ºC and laccase load of 83 U/g.

Structural assignments were confirmed by HSQC spectra (Figure 25) according to the previously inferred assignments [24,310]. However, after purification, lignosulphonates still contained xylo-oligosaccharides [51,297] and, in the case of modified LS, laccase concomitants that hindered the full spectra assignments.

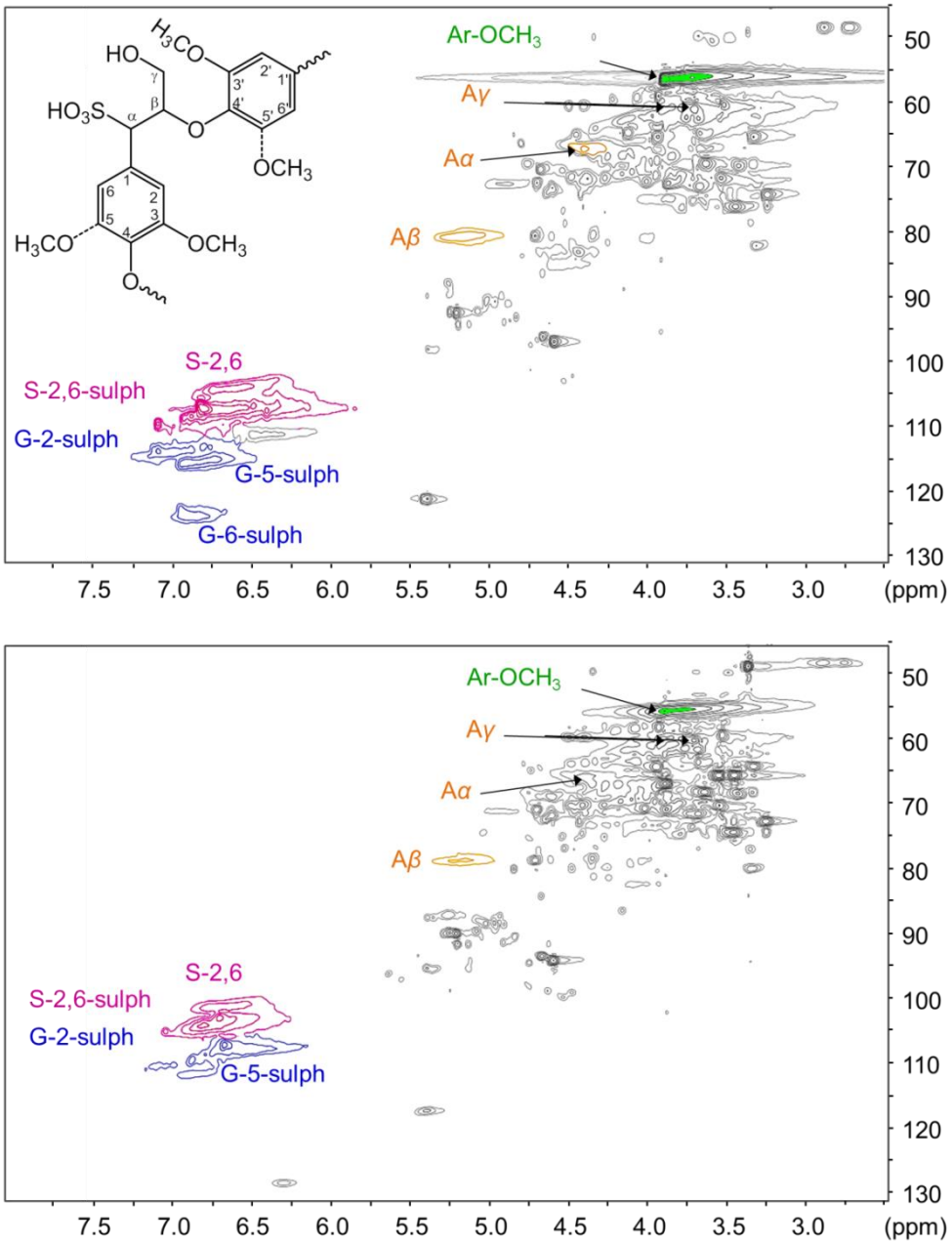


**Figure 25.** HSQC NMR spectra ($D_2O$, 295 K) of LS (top figure) and modified LS (bottom figure) in laccase-catalyzed oxidation at 40 ºC and laccase load of 83 $U \cdot g^{-1}$.

The comparison of $^{13}C$ NMR spectra of initial and modified LS (Figure 24) evidenced the abrupt reduction in intensity of the peak centred at *ca.* 148.6 ppm in modified LS assigned to the C4 in etherified guaiacyl (G) units and C3/C5 in phenolic syringyl (S) structures. Simultaneously, the resonance intensity of the peak centred at *ca.* 152.8 ppm assigned to the

C3/C5 in etherified S units increased substantially. These features indicated clearly the formation of new aryl ether bonds upon LS oxidative modification with laccase.

The quantification of the main lignin structures in LS is summarized in Table 11. The calculations were carried out per aromatic ring (C6) according to previously established methodology [24,309]. The aromatic region equivalent to six carbon atoms was integrated at 102–160 ppm and the calculations of structural elements were carried out per aromatic ring ($n_x = I_x/(I_{102\text{-}160}/6)$). The tertiary carbons in aromatic ring were integrated at 102–124 ppm, quaternary at 124-136 ppm and oxygenated at 136–160 ppm (Figure 24). The ratio S:G was calculated based on the amount of tertiary carbons in corresponding units (in the S at 102–110 ppm and in the G at 110–124 ppm) [309]. The abundance of lignin structures linked by *β*-O-4′ bonds was calculated based on signal integrals at 59.0–61.0 ppm (Cγ resonance in *β*-O-4′ structures). Similarly, the abundance of phenyl coumaran (β-5′) and pino/syringaresinol (*β*-*β*′) structures was assessed based on C*β* resonances in corresponding structures (Figure 24).

**Table 11.** Structural elements of initial and modified by laccase oxidation lignosulphonates (LS) as assessed by quantitative $^{13}$C NMR (per 100 phenyl propane units).*

| Structural elements | LS | Modified LS |
|---|---|---|
| *β*-O-4’ structures | 41 | 38 |
| *β*-5’ + *β*-*β*’ structures | 5 | 5 |
| COOH | 10 | 17 |
| Ar-COOH | 2 | 3 |
| $C_\alpha$=O | 2 | 5 |
| $OCH_3$ | 158 | 139 |
| Ar-H | 198 | 174 |
| Ar-C | 148 | 155 |
| Ar-O | 254 | 271 |
| S:G ratio | 79:21 | 70:30 |

*LS modified with laccase load of 83 U·g$^{-1}$

The results from the quantitative $^{13}$C NMR spectra (Table 11) did not show significant changes in the main lignin structures (*β*-O-4′, *β*-5′ and *β*-*β*′), but confirmed the decrease in the tertiary carbons and the simultaneous increase in quaternary and oxygenated carbons of the aromatic ring in the laccase modified LS. This means the formation of new Ar-C and Ar-O linkages upon oxidative modification of LS mediated by laccase. More specifically,

looking at the balance between Ar-H, Ar-C and Ar-O in initial and modified LS, it could be concluded that nearly one-third of newly formed substitutions in the aromatic ring belong to Ar-C and two-thirds to Ar-O-C type structures. This feature is apparently due to the coupling of Ar-O and Ar or Alk radicals giving rise to one-electron oxidized phenolic lignin structures (Figure 26). Accordingly, the most probable structures formed are those of aryl ether and biphenyl types. The first ones are confirmed by the sharp increase of the resonance centred at 133.8 ppm of modified LS assigned to C5 in 4-O-5´ structures and the second ones by the increase of signal intensity at *ca.* 127 ppm assigned to C5 in 5-5´structures [323]. In addition to 5-5' bonds, the other biphenyl linkages could probably also be formed, but these were not clearly detected. Some decrease of the amount of methoxy groups after laccase treatment could be tentatively explained by the reduction of the S/G ratio from 79:21 in initial LS to 70:30 in the modified LS (Table 11). This may be due to the fact that some part of low molecular weight S structures were degraded during the catalytic oxidation or was eventually involved in radical substitution reactions at C3 with the elimination of methoxy group.

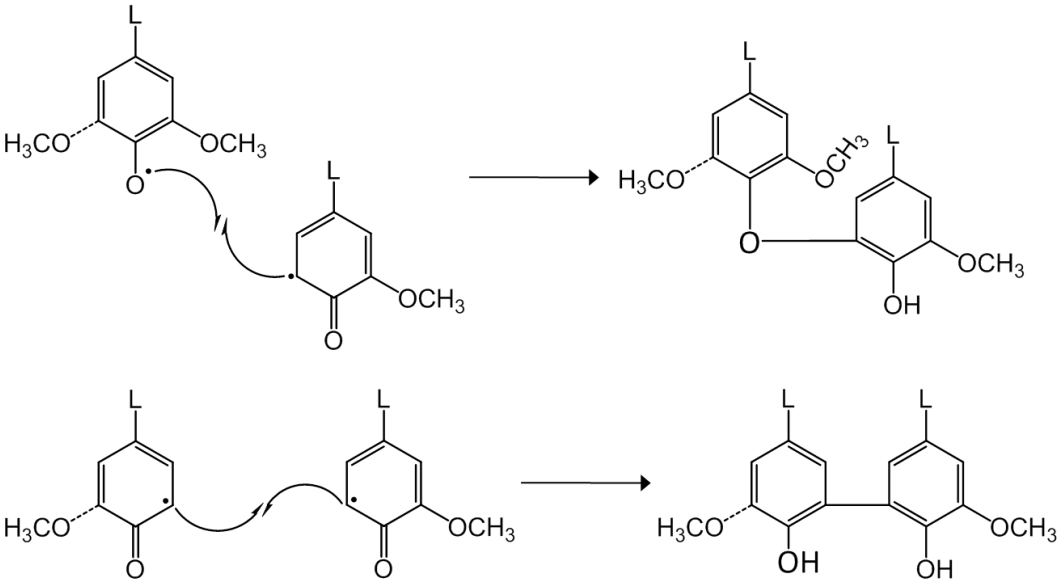


**Figure 26.** Schematic representation of oxidative lignin polymerization catalyzed by laccase. Radical coupling leads to formation of new aryl ether (top figure) and biphenyl structures (bottom figure).

No significant changes in the amounts of sulphonic groups of LS after the oxidative modification catalysed by laccase was registered (Table 12). This was probably the reason why the zeta-potential of modified lignins were also comparable to that of unreacted LS.

**Table 12.** Contents of sulphonic and phenolic groups and zeta-potential values of initial and modified by laccase oxidation lignosulphonates (LS).

| Sample* | $SO_3H$ (% w/w) | $OH_{phen}$ (% w/w) | Zeta Potential (mV) |
|---|---|---|---|
| LS | 21.1 (±0.6) | 3.0 (±0.4) | –25.6 (±0.9) |
| Modified LS (83) | - | - | –24.9 (±0.9) |
| Modified LS (250) | 21.4 (±1.6) | 2.6 (±0.4) | –24.0 (±0.5) |
| Modified LS (500) | 21.2 (±0.9) | 2.5 (±0.3) | –23.4 (±0.7) |

* Laccase loads (83, 250 and 500 $U \cdot g^{-1}$) in the catalyzed oxidation of LS are depicted in parenthesis.

Some decrease in the amount of phenolic groups after the biocatalytic oxidation of LS could be explained by coupling reactions of phenolic LS units leading to the increasing of its molecular weight (Figure 22). Regarding the oxidized groups, such as carbonyl and carboxyl, these were increased noticeably after the enzymatic treatment (Table 11). Thus, the content of α-carbonyl groups increased more than twice and the amount of aromatic carboxyl 1.5 times after the enzymatic treatment of LS even at the lowest laccase load (83 $U \cdot g^{-1}$) (Table 11). However, the total amounts of carbonyl and carboxyl groups still remained moderate. The more significant oxidation of benzylic carbons was hindered by the presence of sulphonic groups in the α-position of LS [324]. The increase of the amounts of α-carbonyl groups is one of the reasons for the increment of UV spectra absorbency (Figure 22) in the range of 300–350 nm [33].

The modified LS showed also an increased amount of aliphatic carboxylic groups integrated in the $^{13}C$ NMR spectra at 173–179 ppm (Table 11). These groups apparently belong to concomitant extractives and bound carboxylic acids that were not removed during the dialysis. Hence, it can be proposed that these COOH-containing molecules belong to the contaminants in the commercial laccase used for the lignin modification. At least these resonances increased proportionally to the amount of laccase applied in the biocatalytic oxidation.

The ensuing modified LS (solution with *ca.* 100 $g \cdot L^{-1}$ of LS) were concentrated by evaporation at 80 ºC under vacuum to obtain a final product mimicking the thick liquor containing a solids content of 40 % w/w, as required for concrete additives. Surprisingly, the LS concentration led to *ca*. 3-fold decrease in $M_w$ of the modified LS (from nearly 30 kDa to nearly 10 kDa). This outcome indicates that at least part of the newly formed linkages is relatively labile under acidic conditions and moderate temperature (pH 3.5–4, 80 ºC). This

is certainly not a case of aryl ether and biphenyl structures that are stable under these conditions. Most likely some kind of semi-acetal type linkages could be formed between lignin functionalities and carbohydrate complex both in the composition of LS and in laccase formulation. Hence, the mechanisms involved in lignin polymerization under oxidative modification catalyzed by laccase still need further studies.

## 5.4. LS MODIFICATION VIA OTHER STRATEGIES

### 5.4.1. POM-mediated oxidative polymerization of LS

Polyoxometalates (POMs) can be inorganic mediators in lignin oxidation by laccase, when one-electron oxidized lignin molecules are polymerized by radical coupling and the reduced POMs in turn are reoxidised by laccase under aerobic conditions [318]. In this study, $SiW_{11}Mn$, $PMo_{11}V$ and $PMo_{10}V_2$, were used for the oxidative polymerization of LS in order to increase its $M_w$. POM-mediated oxidative polymerization by laccase was compared to LS oxidation with POM or laccase alone for comparative purpose (Table 13).

**Table 13.** Molecular weight of LSF modified by laccase with and without POM (40 °C).

| Sample | Material | $M_w$ (Da) 0 min | $M_w$ (Da) 60 min |
|---|---|---|---|
| **1** | LSF | 3240 | – |
| **2** | LSF–laccase * | – | 11015 |
| **3** | LSF–$SiW_{11}Mn$ | – | 4500 |
| **4** | LSF–$SiW_{11}Mn$–laccase * | – | 4820 |
| **5** | LSF–$PMo_{11}V$ | – | 3430 |
| **6** | LSF–$PMo_{11}V$–laccase * | – | 2880 |
| **7** | LSF–$PMo_{10}V_2$ | – | 3300 |

* – Laccase loads of 85 $U.g^{-1}$ LS.

As expected from previous studies [125,293], the enzymatic oxidation of LSF without mediator yielded a modified LS (run 2, Table 13) with significantly increased $M_w$. Indeed, the $M_w$ increased from 3240 Da to 11015 Da after a 60 min reaction time without using any external mediators and enzyme load of 85 $U \cdot g^{-1}$ LS. However, when POMs were used as mediators for laccase oxidation of LS, reactions were not as successful as when using only

laccase, in terms of increase of $M_w$. When $SiW_{11}Mn$ was used as a mediator, only a slight increase of *M*w was observed (run 4, Table 13), from 3240 up to 4820 DA, probably due to the sinergetic effect reported by Kim and co-workers [318] leading to oxidative polymerization of LS, but not as effective as when using laccase alone. In contrast, $PMo_{11}V$ was used as a mediator and $M_w$ decreased (run 6, Table 13) compared to the initial $M_w$ value of unmodified LS (sample 1, Table 13) thus contributing to the LS oxidative depolymerization that prevailed over polymerization [146,149,325]. For this reason, the system LSF–$PMo_{10}V_2$–laccase was not examined. Finally, when each POM was used alone without laccase, only a slight increase of $M_w$ was observed when using $SiW_{11}Mn$ (run 3, Table 13) while both $PMo_{11}V$ and $PMo_{10}V_2$ practically did not alter the $M_w$ of LS (runs 5 and 7, respectively) suggesting that the LS structure was not affected by these two POMs and probably no significant chemical/structural modification of LS took place.

In order to assess the eventual structural changes of LS after modification by POM and POM-mediated laccase oxidative treatment, ATR-FTIR and UV-Vis spectroscopy analyses were carried out to compare LS structure before and after modification with $SiW_{11}Mn$. FTIR-ATR spectra of the initial and modified LS are depicted in Figure 27. The spectra are quite similar except for the weak band at 1648 $cm^{-1}$ in the spectrum of $SiW_{11}Mn$-mediated laccase-modified LS (LSF–$SiW_{11}Mn$–laccase, Figure 27c) related to the presence of conjugated structures with aromatic double bonds along with an apparent slight reduction of phenolic hydroxyl and methoxyl group content (absorption bands at 1204 and 1110 $cm^{-1}$, respectively) [303,308]. Similar features were already observed in our previous work [293], where laccase was used without any mediator. The similarities between LS and $SiW_{11}Mn$-modified LS (LSF–$SiW_{11}Mn$) spectra suggest that the POM used in the reaction, $SiW_{11}Mn$, did not change significantly the chemical structure of LS, probably due to the lack of reactivity.

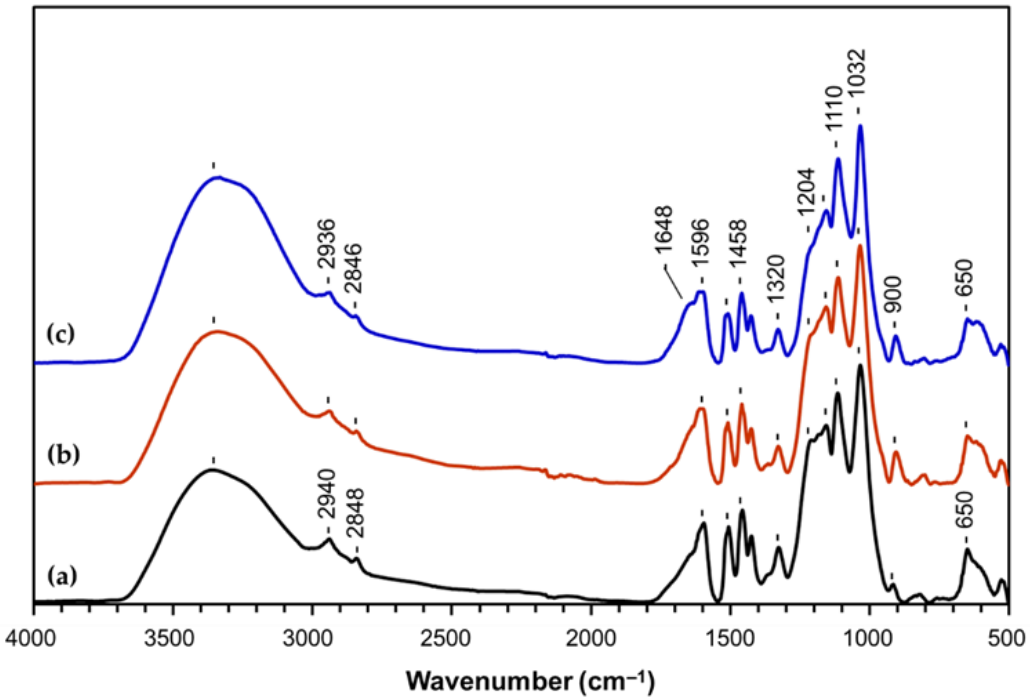


**Figure 27.** FTIR-ATR spectra of (a) LSF, (b) $SiW_{11}Mn$-modified LS (LSF–$SiW_{11}Mn$), and (c) $SiW_{11}Mn$-mediated laccase-modified LS (LSF–$SiW_{11}Mn$–laccase).

The UV-Vis analysis (Figure 28) corroborated the FTIR results. A similar laccase oxidative treatment of LS in the absence of any mediator was carried out for comparison. It is clear that when using only POMs (Figure 28a), the band with a maximum at around 360 nm, attributed to an increased amount of conjugated phenolic structures with α-carbonyl groups or double bonds [33,321], was not observed. Additionally, only a slight increment (almost negligible) of the band around 360 nm was detected (Figure 28b) for the samples obtained from the POM-mediated laccased oxidative polymerization of LS. This clearly corroborates the FTIR analysis: *i.e.*, POMs do not alter the chemical structure of LS and when used as mediators, only impart slight changes to the molecular weight.

Overall, the results obtained showed that, in this case, and considering the reaction conditions, the chosen POMs did not significantly affect the chemical structure of LS even when used as mediators for laccase oxidative modification. Therefore, different approaches were considered to prepare LS-based materials with enhanced dispersant characteristics while preserving the primary structure of LS.

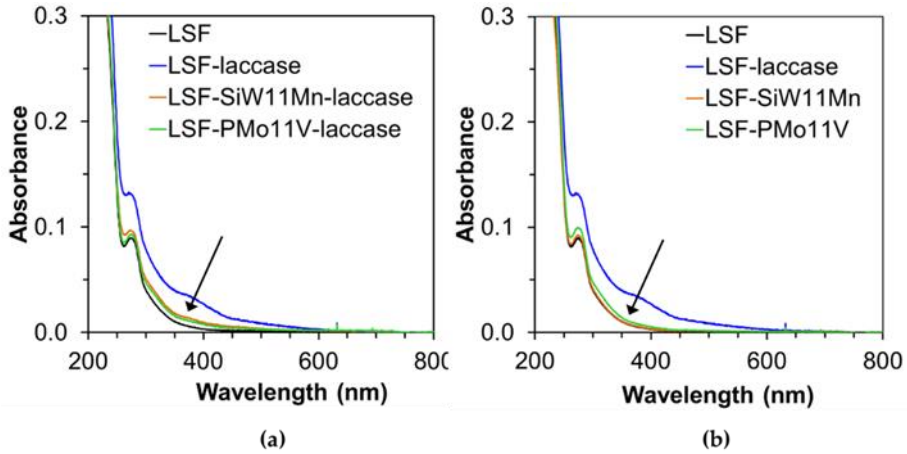


**Figure 28.** UV-Vis analysis of (a) POM-mediated laccase-modified LS (LS-POM-laccase), and (b) POM-modified LS (LSF-POM-laccase), where POM is $SiW_{11}Mn$ or $PMo_{11}V$. Comparison with unmodified LS and laccase oxidative polymerized LS (LSF-laccase). In laccase treatments, laccase load was 85 $U \cdot g^{-1}$ LS.

***RAFT polymerization of LS***. The first alternative method studied was the "grafting-from" approach via RAFT using DDMAT as the RAFT agent. DDMAT, which is a carboxyl-terminated thiocarbonate, has a very high chain-transfer efficiency allowing control over the radical polymerization [326]. Attempts to solubilize DDMAT in water at low pH (around 4) and LS in organic solvents, such as tetrahydrofuran (THF) and pyridine [327–329] were unsuccessful. Additionally, other attempts were explored, such as preparing solvent mixtures by dissolving LS in water and DDMAT in other solvents namely THF and dimethyl sulfoxide among others. However, the results were unsatisfactory.

***Glyoxalation of LS***. In another approach, the glyoxalation of LS in alkaline medium was carried out [191], during which hydroxyl groups in ethylol moieties are expected to be introduced in the LS structure. In addition, the eventual depolymerization/repolymerization of lignin via crosslinking yielding adducts with increased $M_w$ was expected [191–193]. Unfortunately, the high pH (> 12) necessary to carry out the glyoxalation reaction probably led to changes in the LS structure with the apparent loss of water solubility. As the pH of the LS solution was increased from initial 4.3 up to 12, by adding NaOH solution, LS started to precipitate hindering further reaction with water soluble glyoxal. The precipitation of LS was observed most probably due to the partial desulphonation of LS under these conditions and/or by known reaction of sulfonic groups with aldehyde moieties with the formation of the corresponding semi-acetal adducts favouring the gel formation.

Finally, a third approach was considered, which involved the modification of LS using PEG and PPG derivatives, such as PEG and PPG diglycidyl ethers, PEGDE and PPGDE, respectively, which will be discussed next in detail.

### 5.4.2. Modification of LS with PEGDE and PPGDE

Grafting PEG moieties onto lignin occurs via nucleophilic substitution through phenolic hydroxide groups usually under moderately alkaline pH conditions (pH > 11) [155]. Previous studies [151,154] reported the successful modification of lignin with epoxidized PEGs in alkaline medium via epoxy ring-opening reaction. However, in the present study, alkaline pH could not be considered since it compromises the water-solubility of our acidic LS due to its partial desulfonization. Nevertheless, the first syntheses were carried out in alkaline medium (with the addition of NaOH until pH ~13). However, due to the apparent precipitation of the LS from the solution, this procedure was discontinued. Instead, experiments were then carried out in water at an initial pH of 2.5 (LS solution) before adding PEGDE or PPGDE. The purified LSG was used in these experiments simulating the industrial thick liquor usually used for the concrete additives.

FTIR spectroscopy was used to confirm the structural changes resulted after LS modification. Figure 29 shows the spectra of LS, LS modified with PEGDE (LS-PEG) and LS modified with PPGDE (LS-PPG). The grafting modification of LS can be confirmed through the presence of a characteristic absorption band at 1250–1210 $cm^{-1}$ assigned to the stretching vibration of C–O–C in the PEGDE structure [330]. Furthermore, the significant decrease in the relative intensity of the OH band around 3350 $cm^{-1}$ in the spectra of LS-PEG and LS-PPG indicates part of LS hydroxyl groups was consumed during the epoxidation reaction, which was more pronounced in the case of LS-PPG (Figure 1). The characteristic aromatic bands of LS at 1604, 1510, and 1420 $cm^{-1}$ [302–304,308] decreased considerably in LS-PEG and LS-PPG because the final product includes not only LS but also PEG or PPG moieties.

Additional structural analysis of purified LS, PEG-modified LS (LS-PEG) and PPG-modified LS (LS-PPG) was conducted using quantitative $^{13}C$ NMR and the spectra are presented in Figure 30. Comparing the spectra of LS-PPG and LS-PEG with LS, it is clear that the main differences before and after LS modification occur in the range between 43

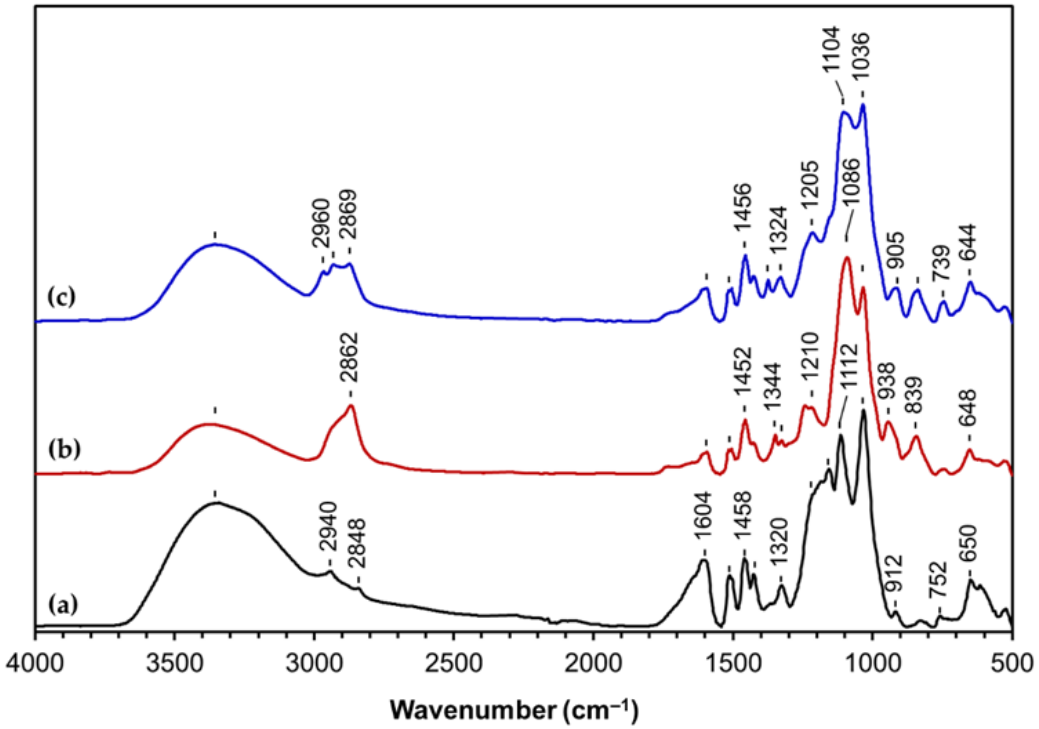


**Figure 29.** Normalized FTIR-ATR spectra of (a) LS, (b) LS epoxidized with PPGDE (LS-PPG), and (c) LS epoxidized with PEGDE (LS-PEG).

and 80 ppm where signals from LS and the PPG/PEG moieties overlap. The expected chemical shifts for the majority of the carbons are quite similar. Therefore, it was not possible to differentiate and identify most of them. Yet, using the ChemNMR $^{13}$C Prediction tool from ChemDraw Professional software, a few signals from PPG and PEG moieties in each product were identified. Considering the spectrum of PPG-modified LS (Figure 30c and Table 14), the signal at 78.4 ppm is related to the carbon linked to the methyl group (blue carbon in the structure) distributed along the PPG chain. In turn, the signal at 62.7 ppm is related to the carbon linked to the OH group included in the terminal group of the PPG chain (green carbon). The signal at 15.2 ppm is assigned to the carbon from the methyl groups in the PPG chain (orange carbon). Analysing the spectrum of PEG-epoxidized LS (Figure 30b), the signal at 78.1 ppm is assigned to the carbon linked to the oxygen in the PEG chain (blue carbon). In the same way as in the previous spectrum, the signal at 62.7 ppm corresponds to the terminal carbon in the PEG chain (green carbon). Due to the overlapping of signals from LS and PEG/PPG and the fact that most of the carbons in the PEG and PPG are expected to induce identical chemical shifts in the range 72-78 ppm, it was not possible to determine the content of PPG/PEG grafted to the LS structure. Yet, upon

the analysis of signals 1, 2, 3 and 4 in all spectra, a subtle difference is observed specially in the intensity of dual signal 4 and unresolved signal 3, which decreased in the spectrum of PPG-modified LS and were assigned to C4 in phenolic guaiacyl (G) and syringyl (S) structures, respectively [24,52,53,311,331,332]. On the contrary, the intensity of signals 1 and 2, which assignments are described in Table 14, did not change so much upon LS modification. The remarked difference in signal intensity, showing in the decrease of intensity of signals 3 and 4 in the spectrum of PPG-modified LS confirmed that PPG-grafting occurred at least via reaction of phenolic hydroxyl groups in G/S structures with epoxy moieties of PPGDE, as illustrated in Figure 30c.

Based on the $^{13}C$ NMR spectra analysis, the content of phenolic OH groups in G structures (signal 4 in Figure 30) and of the methyl groups in the PPG chain were determined and the calculations were carried out per one hundred aromatic rings (100 C6) according to previously established methodology [24,309,310]. The content of phenolic OH groups in G structures present in LS is quite similar to the one in PEG-modified LS, 26 and 28 per 100 C6, respectively. These results suggest that phenolic OH groups did not react or at most reacted in small extent with PEGDE, which is in agreement with the FITR analysis (Figure 30c). Since phenolic OH groups in syringyl (S) structures are expected to be less reactive than in G structures due to steric hindrance, it is possible that the reaction of LS with PEGDE resulted only in a negligible modification of LS with no relevant changes in LS structure. Moreover, the molecular weight of PEG-modified LS was similar to the one of unmodified LSG (*ca*. 3500 Da). This indicates that the resonances from the PEG moieties in the spectrum (Figure 30b) probably derive from PEGDE homopolymer formed during the reaction and that were not removed during the purification by dialysis. Therefore, the product analysed by FTIR and $^{13}C$ NMR could actually be a mixture mainly composed of LS and PEG homopolymer. On the contrary, the content of phenolic OH groups in G structures present in PPG-modified LS is 15 per 100 C6 against 26 per 100 C6 in LS clearly confirmed that some of these groups reacted with PPG derivative (PPGDE). This is in agreement with FTIR analysis (Figure 29b) where a reduction of the intensity of the band assigned to hydroxyl groups was observed. However, due to the overlapping the various resonances (Table 14), the accurate calculation of reacted phenolic groups in S structures (signal 3, Figure 30) was impossible. Additionally, the content of methyl groups in the PPG chain is 280 per 100 C6. Even if PPGDE homopolymer was produced during the reaction and was retained in the

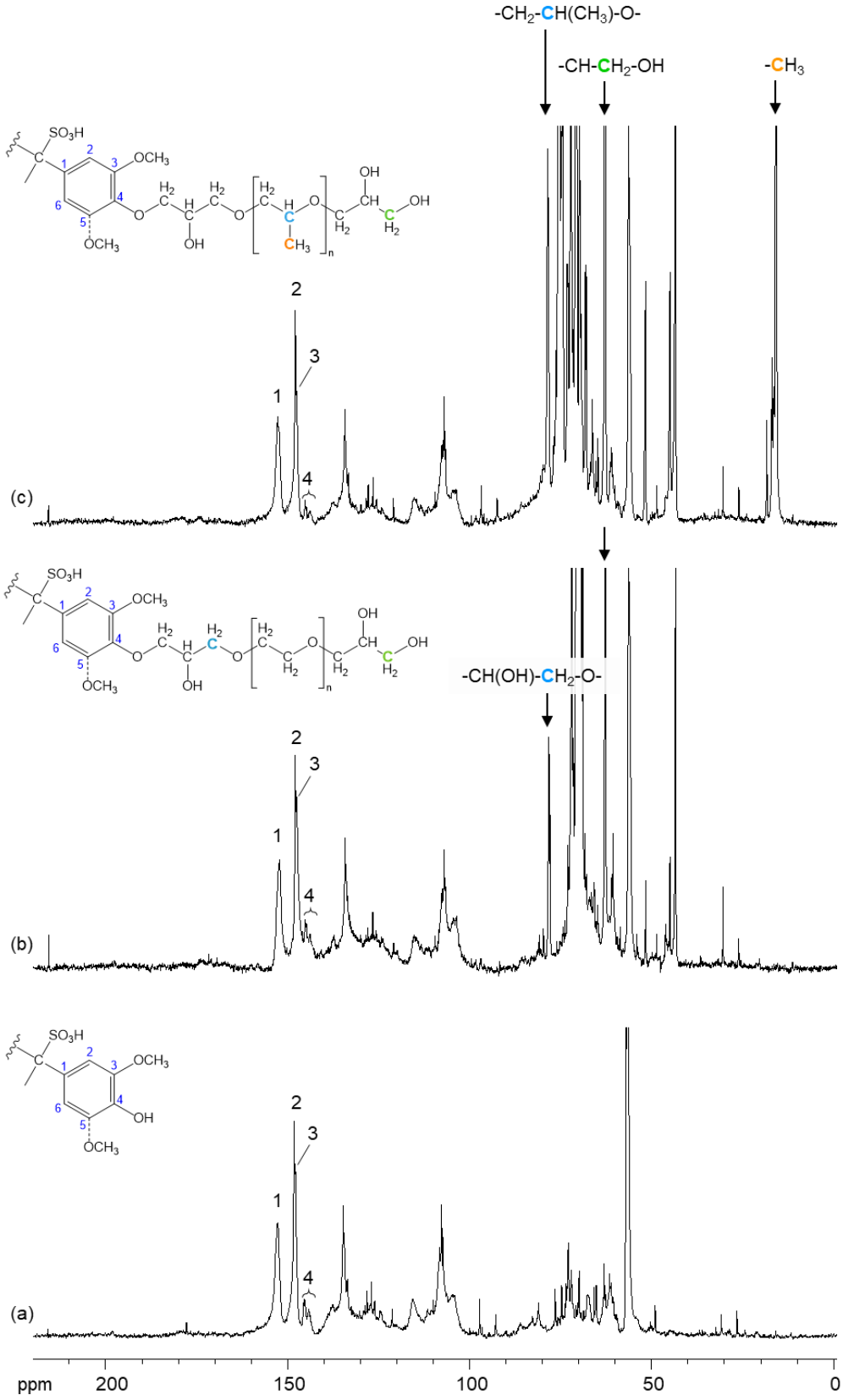


**Figure 30.** Quantitative $^{13}C$ NMR spectrum of LS (a), PEG-modified LS (b) and PPG-modified LS (c) in $D_2O$ at 295K.

**Table 14.** Assignment of carbon signals in $^{13}C$ NMR spectra of LS and modified LS [24,52,53,309–311].

| Signal | δC (ppm) | Assignment |
|---|---|---|
| *LS, PEG-modified LS and PPG-modified LS (all spectra)* | | |
| 1 | 152.8 | C3,5 in etherified S structures |
| 2 | 148.1 | C3 and C4 in etherified G, C4 in etherified S structures |
| 3 | 148.0 | C3,5 and C4 in phenolic S structures |
| 4 | 145–146 | C4 in phenolic G structures and tannins |
| *PEG-modified LS* | | |
| - | 78.4 | -$CH_2$-**C**$H_2$-O- |
| - | 62.7 | -CH(OH)-**C**$H_2$-OH |
| *PPG-modified LS* | | |
| - | 78.4 | -$CH_2$-**C**H($CH_3$)-O- |
| - | 62.7 | -CH(OH)-**C**$H_2$-OH |
| - | 15.2 | -**C**$H_3$ |

purified fraction of PPG-modified LS product after dialysis, results clearly corroborate that modification of LS with PPG derivative occurred.

Regarding the possible reactions of aliphatic hydroxyls of LS, these were discarded due to the very small amount of secondary hydroxyls in LS [52,53], and the practically unchanged intensity of resonance centred at *ca*. 61.0 ppm ($C_\gamma H_2OH$ in *β*-O-4′ structures) in the quantitative carbon spectra before and after the reaction with PEGDE/PPGDE.

Considering this situation, the structures of some possible ensuing products derived from the reaction between phenolic groups and PPGDE are depicted in Figure 31, including the structure of PPGDE homopolymer (Figure 31c). It is possible that PEGDE did not react with LS due to its higher $\overline{M}_n$ (500 g·mol$^{-1}$) compared to PPGDE ($\overline{M}_n$ ~380 g·mol$^{-1}$), which may hinder its mobility. Considering this possibility along with the aformentioned steric hindrance of LS aromatic structure, it is possible that epoxide groups in one PEGDE molecule reacted preferably with epoxide groups of another molecule or with water, thus favouring the formation of PEG homopolymer (Figure 31c). In fact, PEGDE has been considered more reactive in homopolymer formation than PPGDE [151–153]. In turn, the most probable scenario of LS reaction with PPGDE could be the acid-catalysed etherification but without crosslinking adjacent molecules (Figure 31a), because the molecular weight of obtained derivatives was increased insignificanly (*ca*. 3800 Da).

LS are anionic surface-active polymers due to their sulfonic and carboxylic groups. Therefore, LS zeta potential values are highly negative (Table 15). Laccase-oxidation of LSF resulted in modified LS with increased $M_w$, (Figure 21) but the content of oxidised functional groups did not change significantly since the zeta potential values remained similar to that of unmodified LSF. In the case of modified LSG, LSG-PEG and LS-PPG, the reaction did not cause much $M_w$ increase of the modified LS and the content of functional groups apparently did not change since the zeta potential values are similar to patent LS. Of particular relevance is the fact that the zeta potentials values of LS and modified LS are quite similar to that of NSF, which was expected since NSF also comprise sulfonic groups (Figure 9). The zeta potential of PCE, however, is -4.7 mV probably due to its lower fraction of ionizable groups per molecule and the larger diffusional path in the electric double layer.

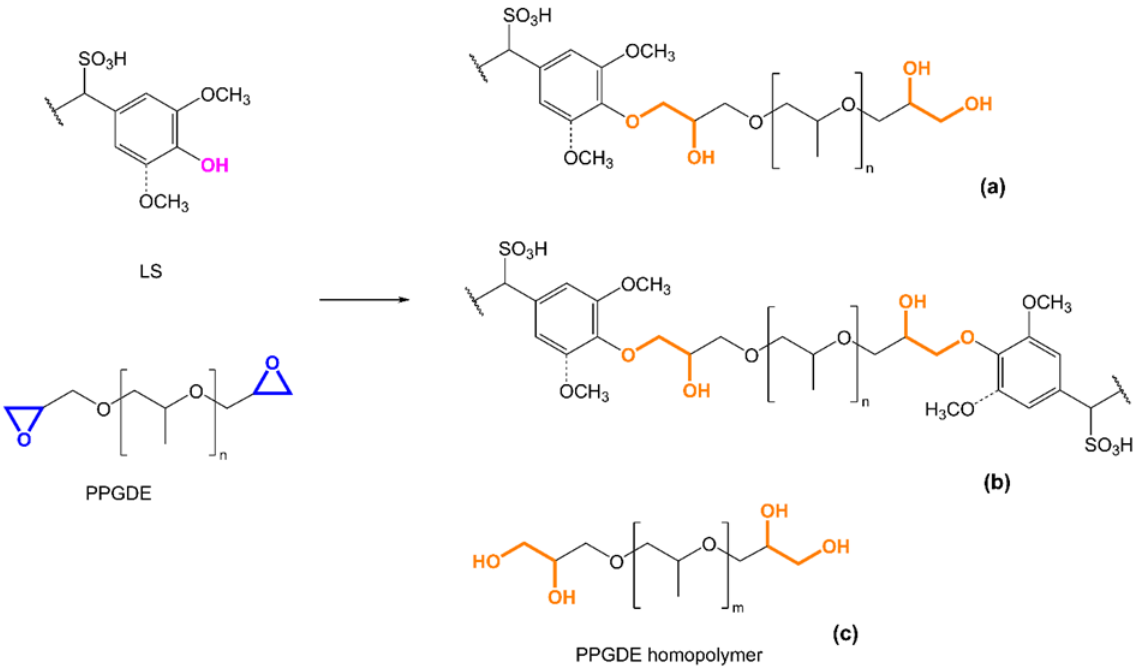


**Figure 31.** Reaction scheme of LS modification with PPGDE including some possible ensuing products.

**Table 15.** Zeta potential values of unmodified LS and modified LS by laccase oxidation and epoxidation with PEGDE and PPGDE.

| Material | C (g/L) | pH | Zeta potential (mV) | Reference |
|---|---|---|---|---|
| LSF | 0.51 | 4.4 | -25.6 (± 0.9) | [293] |
| LSF-laccase (83) * | 0.51 | 4.3 | -24.9 (± 0.9) | [293] |
| LSF-laccase (250) * | 0.51 | 4.5 | -24.0 (± 0.5) | [293] |
| LSF-laccase (500*) * | 0.51 | 4.6 | -23.4 (± 0.7) | [293] |
| LSG | 0.51 | 4.6 | -20.9 (± 1.1) | – |
| LSG-PPGDE | 0.57 | 6.3 | -21.1 (± 0.8) | – |
| LSG-PEGDE | 0.61 | 6.3 | -19.9 (± 0.9) | – |
| NSF | 1% v/v | 7.0 | -29.3 (± 3.4) | – |
| PCE | 1% v/v | 5.3 | -4.7 (± 1.6) | – |

*Laccase loads of 83, 250 and 500 U $g^{-1}$ of LS

### 5.4.3. Flow table test of cement pastes

To assess the performance of modified LS regarding the dispersant characteristics for concrete formulation, the workability/fluidity of cement pastes used in concrete formulations with different admixtures/dispersants (according to Table 4) was studied. The same cement paste formulation was used differing only on the dispersant employed. The flow table test was used for this purpose and the results are depicted in Figure 32. Results obtained from the different modified LS products were compared with those from unmodified LS/SSL (used as reference and as the minimum value) and with results obtained using two distinct commercial superplasticizers, NSF and PCE.

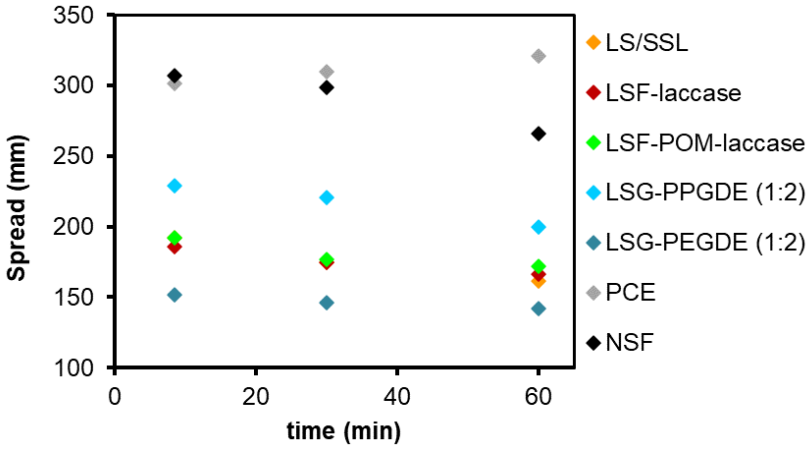


**Figure 32.** Spread values determined by the flow test table (the relative errors did not exceed 5%).

The results show clearly that the different unmodified LS/SSL, modified LS and superplasticizers, display different dispersant characteristics. Both PCE and NSF yielded the highest cement paste spreading reaching about 300 mm, clearly indicating its superplasticizer ability. Comparing both commercial superplasticizers, the best results were revealed by PCE, especially after 60 min run. This shows that PCE has a retarding effect on the cement paste hardening, allowing higher working time compared to NSF. As already mentioned, the high dispersant efficiency of PCEs is related to both electrostatic repulsion and steric hindrance between their nonionic side chains (Figure 9) [110,111,331], which stretch out into the solution and act as a steric barrier keeping the cement particles at a distance [331,332]. As a consequence, polymeric superplasticizers adsorb on the surface of the cement particle assuming a favourite conformation. This favourite conformation is distorted when a polymer-coated particle approaches another polymer-coated particle. Subsequently, when polymer layers start to overlap, a repulsive steric force emerges [333]. Electrostatic repulsion is related to the surface charge, which arises from the dissociation of surface groups and/or specific adsorption of ions or ionic polymers in water, as well as to the amount of the surface ionizable groups [333].

Noteworthy is the fact that cement pastes prepared with unmodified LS/SSL, laccase-LS and POM-laccase modified LS products displayed similar fluidity results and much smaller than those obtained using the commercial superplasticizers (around 190 mm at 8 min and around 169 mm at 60 min). This indicates that laccase oxidative modification of LS with or without any mediator, did not affect the dispersant properties of the product. In fact, this is in agreement with the fact that the use of POM for the modification of LS or as mediator in the laccase modification of LS did not change significantly the structure of LS (Figure 27 and Figure 28). Therefore, a spreading behaviour similar to the one obtained using unmodified LS/SSL would be expected.

Gelardi and co-workers [109] have reported that LS comprising a degree of sulfonation up to 0.5–0.7 per phenyl propane unit exhibited optimized water solubility and plasticizing effect as is the case of eucalypt LS used in this study, which contains 0.57 sulphonic groups per phenyl propane unit [297]. the results obtained in the present work show that LS dispersant properties are far from comparing to those of commercial superplasticizers. This is due to the fact that LS dispersant and adsorption mechanism is affected by electrostatic repulsion forces, is pH dependent and influenced by the formation of aggregates [316]. Due

to the presence of sulphonic groups in LS structure (just like in NSF), LS can bind to the positively charged cement particles, causing electrostatic repulsions, which hinder the agglomeration of the fresh cement mixture, *i.e.*, prevent flocculation of cement particles resulting in an increase of its fluidity [317]. Considering the fact that the fluidity of the cement paste was not significantly enhanced when using LS modified via laccase-oxidative polymerization (with increased $M_w$ of 36 800 Da [293] but mostly unaltered zeta potential) suggests that the number of ionizable groups did not change much, as proposed by Areskogh and co-workers [293]. Indeed the increase of the number of sulphonic groups is required to chelate calcium ions hence, modifying the adsorption of LS on the surface of cement particles, by altering the electrostatic repulsion and improving fluidity [150,317,334]. Therefore, this outcome suggests that the sole increase of molecular weight of LS is not crucial or even relevant to enhance the dispersing properties of LS.

The modification of LS with PEGDE or PPGDE yielded products that displayed completely distinct dispersant behaviour when tested in cement pastes (Figure 32). PEG-modified LS gave rise to spreading values (152 mm at 8 min and 142 mm at 60 min) quite below those obtained for unmodified LS and SSL (185 mm at 8 min and 161 mm at 60 min). This could be explained by the fact that the product is most probably composed of a mixture of PEG homopolymer and unmodified, or only slightly modified LS, therefore not comprising structural features that could enhance its dispersant properties. In contrast, PPG-modified LS clearly afforded a cement paste with remarkably enhanced fluidity (229 mm at 8 min and 200 mm at 60 min) compared to the cement paste formulated with unmodified LS/SSL (185 mm at 8 min and 161 mm at 60 min). According to the FTIR and $^{13}C$ NMR chemical and structural analyses of this product, PPG chains were grafted to the phenolic moieties in LS as illustrated in Figure 31a. Even with the possible presence of PPG homopolymer, the dispersant properties of this product were undoubtedly improved compared to unmodified LS/SSL probably due to the presence of polyether chains (just like in PCEs) that are responsible for the steric hindrance effect. Consequently, it is possible that the dispersant efficiency of PPG-modified LS is due to electrostatic repulsion (caused by the ionizable groups such as sulfonic groups) combined with steric hindrance (due to the grafted PPG chains). These results show that PPG-modified LS (with a LS:PPGDE ratio of 1:2) could be a promising dispersant for concrete formulations.

Based on these promising results, new formulations of PPG-modified LS were prepared with higher PPG content (LS-PPGDE ratios of 1:3 and 1:4). The fluidity of cement pastes containing these products was similar to the fluidity of cement pastes comprising unmodified LS/SSL. Therefore, it is plausible that the reaction conditions as well as the higher load of PPGDE were favourable to the formation of PPG homopolymer. Even with the modification of LS, the presence of more PPG homopolymer may reverse the dispersant effects of the product, due to the higher concentration of PPG homopolymer in solution, which would probably interfere with the adsorption of PPG-modified LS onto the surface of the cement particles.

### 5.5. CONCLUSIONS

Laccase-catalyzed oxidative polymerization of eucalyptus lignosulphonate (LS) under optimized conditions allowed a significant increase in LS molecular weight up to 11-fold from 3240 Da to a maximum of 36800 Da without the use of mediators in a considerable short reaction time (90 min). The mechanism of the oxidative polymerization process includes radical coupling of laccase catalyzed one-electron oxidized phenolic units, leading to the formation of new aryl ether and biphenyl bonds, the former being the most frequent. Although the total amounts of carbonyl and carboxyl groups increased it still remained moderate. At the same time part of syringyl structures were degraded leading to some decrease in S/G ratio after the oxidation of LS in the presence of laccase. Noteworthy, part of the newly formed bonds of unknown origin formed via oxidative polymerization are temperature labile and cleaved during concentration of modified LS at pH 4 and 80 °C during evaporation under vacuum, which led to noticeable reduction of the molecular weight of the modified lignin.

Other chemical modification strategies were used to improve LS dispersion efficiency for concrete formulations. The increase of the molecular weight of LS through POM-mediated laccase modification of LS did not significantly change the LS structure. Subsequently, other approach-es to LS modification were examined, albeit unsuccessfully in relation to LS glyoxalation and RAFT polymerization grafting. Finally, the synthesis of LS-based non-ionic polymeric dispersants using two different epoxidized oligomer derivatives of PEG and PPG, PEGDE and PPGDE, respectively, resulted in two distinct outcomes. The structural analysis by FTIR and quantitative $^{13}C$ NMR suggested that PEGDE did not react with LS.

In contrast, PPGDE reacted with phenolic LS structures. Approximately half of the phenolic LS units were involved in the reaction, while no evidence of reaction with aliphatic hydroxyls was confirmed. Finally, the PPG-modified LS revealed promising plasticizer properties for the workability/fluidity of cement pastes used in concrete formulations due to their enhanced dispersant efficiency probably related not only to electrostatic repulsion (caused by the sulfonic ionizable groups in LS) but also to steric hindrance phenomena (due to the grafted bulky PPG chains).

# 6. LS-based conducting membranes for sensing applications

This chapter was published as:

Sandra Magina, Alisa Rudnitskaya, Sílvia Soreto, Luís Cadillon Costa, Ana Barros-Timmons, Dmitry V. Evtuguin. Lignosulfonate-Based Conducting Flexible Polymeric Membranes for Liquid Sensing Applications, *Materials*, **2021**, *14*, 5331. DOI: 10.3390/ma14185331

## 6.1 ABSTRACT

In this study, lignosulphonate (LS) from the acid sulphite pulping of eucalypt wood was used to synthesize LS-based polyurethanes (PUs) doped with multiwalled carbon nanotubes (MWCNTs) within the range of 0.1–1.4 % w/w, yielding a unique conducting copolymer composite, which was employed as a sensitive material for all-solid-state potentiometric chemical sensors. LS-based PUs doped with 1.0 % w/w MWCNTs exhibited relevant electrical conductivity suitable for sensor applications. The LS-based potentiometric sensor displayed a near-Nernstian or super-Nernstian response to a wide range of transition metals, including Cu(II), Zn(II), Cd(II), Cr(III), Cr(VI), Hg(II), and Ag(I) at pH 7 and Cr(VI) at pH 2. It also exhibited a redox response to the Fe(II)/(III) redox pair at pH 2. Unlike other lignin-based potentiometric sensors in similar composite materials, this LS-based flexible polymeric membrane did not show irreversible complexation with Hg(II). Only a weak response toward ionic liquids, [$C_2$mim]Cl and ChCl, was registered. Unlike LS-based composites comprising MWCNTs, those doped with graphene oxide (GO), reduced GO (rGO), and graphite (Gr) did not reveal the same electrical conductivity, even with loads up to 10 % (w/w), in the polymer composite. This fact is associated, at least partially, with the different filler dispersion abilities within the polymeric matrix.

## 6.2 INTRODUCTION

Due to an increase in industrial and human activities, the presence of heavy metal salts such as lead (Pb), mercury (Hg), cadmium (Cd), chromium (Cr), zinc (Zn), and copper (Cu), among others, in wastewater has led to an increasing accumulation of these chemicals in the environment. Heavy metal ions are non-degradable, toxic, and harmful to aquatic life and can cause many health problems as they accumulate in the human body through the food chain. Considering environmental and health concerns, their removal from wastewaters is imperative [335]. Therefore, their detection in aqueous systems is crucial. Electrochemical sensors, such as potentiometric, amperometric, and conductometric sensors, are particularly interesting for environmental water monitoring as they are suitable for the determination of chemical species such as heavy metals, among others. They are user-friendly, well-suited for miniaturization, have short response times, a wide dynamic range, low energy

consumption, low cost, ease of preparation, good sensitivity, and high selectivity [336–338]. However, some problems still need to be addressed, such as poor reproducibility and stability and difficulties in analysing complex matrices and real samples, and some ions may act as ligands and poison the electrode (for instance, mercury) [239,338]. All-solid-state potentiometric sensors are promising sensors for in situ water analysis [339]. They have been employed in numerous studies for the determination of metal ions in water and biological samples (such as sweat) [337,338,340] and drug molecules in various biological samples (such as blood serum and urine) [341]. Furthermore, the risk of toxic and other harmful effects related to the use of other chemical species, such as, for instance, ionic liquids (ILs) and their contribution to environmental pollution through release via wastewater effluents [342], enhances the need for the development of sensors suitable for the detection of a wider range of chemicals.

Conducting polymers (CPs) are an important class of organic multifunctional materials that exhibit specific physical and electrical properties. The possibility of fi-ne-tuning their optical and conducting properties makes them promising candidates for a wide range of applications, including the fields of energy [343–345], electronics [346,347], catalysis [348], electromagnetic interference shielding [349–351], biomedicine [340,341], and sensors [265,266,337,340,341,345,352,353]. CPs usually exhibit relatively low conductivity (~$10^{-8}$–$10^{-3}$ $S \cdot m^{-1}$) in their pure state; nonetheless, this property can be effectively enhanced to ~100–$10^{6}$ $S \cdot m^{-1}$ either by chemical or electrochemical doping in the case of intrinsic CPs or by physical mixing with other electro-conducting species such as metal or metal oxide nanoparticles, metal-organic frameworks (MOFs), and carbon-based nanomaterials, among others [265–267]. According to previous results, both phenomena have been observed in lignin-based polyurethanes mixed with MWCNTs [238].

Carbon-based materials, such as carbon nanotubes (CNTs), graphene, carbon dots, and porous carbon, have attracted scientific interest worldwide since these nanofillers exhibit enhanced conductivity, high chemical stability, mechanical strength, and large surface areas. Therefore, numerous studies have focused on the preparation of CP composites using these carbon-based materials as nanofillers in order to improve their electrical and mechanical properties but also to allow the production of small, light-weight, and cost-effective composites for a variety of application fields, including electronics, energy, automotive, and aerospace industries and sensors [265,267–269].

Graphite is one of the three naturally occurring allotropes of carbon and is a crystalline material consisting of 2D-layered sp2-bonded carbon atoms arranged in a planar hexagonal structure. Graphene consists of one atomic layer of graphite and exhibits extremely high mechanical properties (1.1 TPa modulus), electrical conductivity (108 $S \cdot m^{-1}$), thermal conductivity (5000 $W \cdot mK^{-1}$), and optical properties (98% transmittance) [269]. GO derives from the oxidation of pristine graphene and, hence, is a 2D atomically thin layer of hexagonal sp2-bonded carbon atoms that comprises oxygen-based functional groups such as hydroxyl (-OH), alkoxy (C-O-C), and carboxylic (-COOH) acids, among others. These oxygen functionalities disrupt the sp2-conjugated backbone, causing a reduction of its electrical conductivity. To restore its electrical conductivity, some oxygen functional groups in GO can be partially reduced, yielding rGO [354]. CNTs are 1D conductive fillers due to their high length-to-diameter ratio, consisting of a hexagonal arrangement of sp2-hybridized carbon atoms, which may be shaped by rolling up a single sheet of graphene (single-walled carbon nanotubes, SWCNTs) or by rolling up multiple sheets of graphene (multiwalled carbon nanotubes, MWCNTs). CNTs present impressive electrical conductivities ($10^7$–$10^8$ $S \cdot m^{-1}$) and mechanical properties (1 TPa modulus, 100 GPa strength) [269].

Due to the continued depletion of finite fossil resources and the necessity to reduce the dependence on this type of resource and their environmental impacts, alternative and sustainable resources have been assessed as feedstock replacements, namely, biomass. Biorefinery and circular economy concepts have become imperative in the industrial sector, *e.g.*, the pulp and paper industry. Thus, in order to improve the economic sustainability of pulp mills, the valorisation of the ensuing by-products has been directed towards new added-value products to expand their economic profits. In particular, industrial (technical) lignin has attracted worldwide attention as it is an abundant biodegradable and renewable resource for the production of biofuels, chemicals, and polymeric materials, with the advantage that it does not compete with food stocks. Lignins have potential as adsorbents for removing metals from water due to their acid sites, namely, carboxylic and phenolic groups [355–357], though the phenolic groups exhibit a higher affinity for metal ions than the carboxylic ones [355]. In addition, other functional groups, such as nitrogen- and sulphur-containing groups that may be present in the lignin structure, can also bind heavy metal ions [356,357]. In fact, lignin modification with nitrogen- and sulphur-containing functional groups has been used in the design and development of advanced adsorbents [356–359]. Among different tech-

nical lignins, lignosulphonate (LS) is the only abundant lignin source on the market that can be considered potentially interesting for the production of conducting composites. Being soluble in water and containing ionogenic (sulphonic) groups, LS is an attractive candidate for use in conductive polymer matrices for sensor applications. In previous studies, novel lignin-based sensing polymeric membranes have been developed through covalent immobilization of the lignin inside a polymer matrix [91,237–239]. Furthermore, the production of lignin-based PU membranes through co-polymerization of different technical lignins, such as kraft lignin, LS, and organosolv lignin, with toluene diisocyanate-terminated poly(propylene glycol) has been reported [91]. Moreover, lignin-based PUs doped with MWCNTs allowed the increase of composite electrical conductivity with a prospective application as ion-selective membranes for potentiometric chemical sensors [237,239]. However, the ensuing lignin-based sensors displayed very low or no sensitivity to all alkali, alkali-earth, and most transition metal cations ions. At the same time, the sensor properties were strongly dependent on the lignin origin. Thus, some concomitants of polyphenolic origin in kraft lignin imparted to this mate-rial sensitivity and selectivity to Cu(II) [239]. Potentiometric sensors highly sensitive to Cr (VI) at pH 2 were obtained with LS and organosolv lignin [237]. However, with regards to LS, no systematic studies have been carried out on the effect of different types and loads of carbon-based fillers on the conducting performance of CPs.

In this work, we prepared LS-based PU composite membranes sensors doped with MWCNTs using the same synthesis methodology as in previous studies [91,237–239]. The main goal is to assess the viability of using LS from the spent liquor of the acidic sulfite pulping of eucalypt wood for potentiometric sensor applications. The conductive and sensory properties of the CP based on LS are compared with those of the CP based on eucalyptus kraft and kraft LignoBoost® lignin, organosolv lignin, and lignosulphonate obtained under different cooking conditions [237,239]. In addition, various carbon nanofillers such as graphene oxide (GO), reduced graphene oxide (rGO), and graphite (Gr) are used to dope LS-based PU composite for comparison.

## 6.3 RESULTS AND DISCUSSION

LS-based flexible copolymers were obtained by the reaction of LS ($M_w$ = 4130 Da) as a macromonomer bearing hydroxyl groups with PPDGI ($M_n$ = 2300 g·mol$^{-1}$) as a co-macromonomer comprising isocyanate groups and also acting as the solvent for LS, maintaining the recommended NCO/OH ratio of 1.5 [91,237–239]. The conducting car-bon nanofillers, in particular MWCNTs, were introduced jointly with lignin before the synthesis, taking into account the excellent dispersant capability of the former [91,237]. The obtained materials were characterized and analysed for their electrical conductivity and sensor properties.

### 6.3.1. Characterization of LS-based PUs

The reaction of LS and PPDGI with the formation of PU was confirmed by FTIR spectroscopy. Figure 33 shows the FTIR spectra of purified LS and LS-based PU without (LS-PU) or with 1% w/w MWCNTs (LS-PU-CNT) taken as an example. The formation of PU is confirmed by the absence of the band at ca. 2270 cm$^{-1}$, assigned to the isocyanate group (-NCO) in PPDGI, and the appearance of signals characteristic for urethane (-O-(C=O)-NH-) moieties at 1722, 1370 and 1220 cm$^{-1}$, assigned to C=O, O-CO, and C-N stretching, respectively [91,306,360]. Furthermore, the significant decrease in the relative intensity of the OH band around 3350 cm$^{-1}$ in the spectra of both LS-based PUs indicates that a relevant amount of LS hydroxyl groups was consumed during the polymerization reaction with the isocyanate groups. The characteristic aromatic bands of LS at 1598, 1510, and 1425 cm$^{-1}$ [51,301–305,307,308] decreased substantially in the LS-based PU due to the relatively low LS content (*ca*. 20 % w/w). The most abundant signals in the LS-based PU spectrum, at 1086 and 2860 cm$^{-1}$, belong to C–O and $CH_2$ vibrations, respectively, in polyether bridges connecting lignin macromolecules (Table 16). Although no significant spectral differences were found between LS-PU and LS-PU-CNT, the slightly greater abundance of free hydroxyl moieties at *ca*. 3350 cm$^{-1}$ in LS-PU-CNT can be explained by the strong interaction of MWCNTs and lignin [91,237], thus hindering, to a certain degree, their reaction with PPDGI.

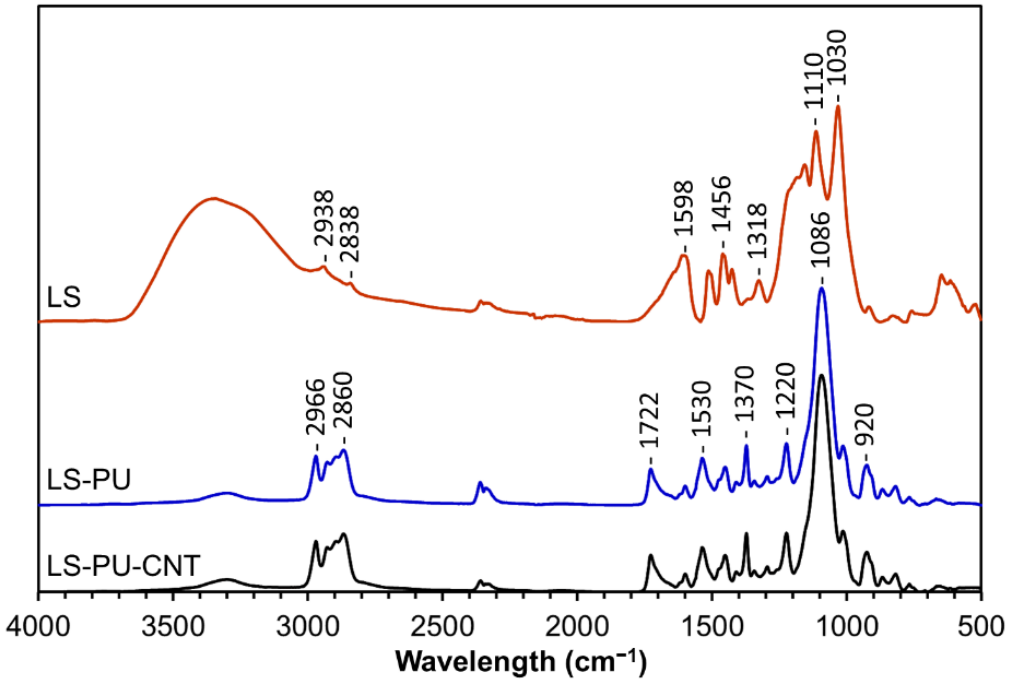


**Figure 33.** FTIR-ATR spectra of LS, LS-based PU (LS-PU), and LS-based PU doped with 1% w/w MWCNTs (LS-PU-CNT).

The glass transition temperature ($T_g$) of LS-based PUs was assessed by DMA. Both LS-based PUs, undoped and doped with 1% w/w MWCNTs, exhibited similar low $T_g$ values, −33 ± 1 °C and −32 ± 1 °C, respectively, as depicted in Figure 34. This relaxation peak relates to the soft domains of the polymeric composites [360]. The addition of MWCNTs (1% w/w) did not affect the viscoelastic properties of the polymer. The negative values of $T_g$ indicate that these materials can be used for the fabrication of self-plasticizing membranes for potentiometric chemical sensors.

Typical TGA curves of LS and LS-based PUs, undoped and doped with 1% w/w of MWCNTs, are depicted in Figure 35. LS revealed less thermal stability than the corresponding PU. The weight loss, with a maximum loss at around 120 °C, is related to moisture release followed by the degradation of functional groups and the release of low molecular mass products at temperatures as high as 200 °C (*e.g.*, $SO_2$ from sulphonic groups) [312,314]. Char formation begins at ca. 400 °C. Both LS-based PU polymers (undoped and doped with MWCNTs) exhibited improved thermal stability compared to LS since the degradation starts at *ca*. 275 °C (Figure 35). Additionally, LS-based PU samples exhibited a

**Table 16.** Assignment of bands in FTIR-ATR spectra of purified LS from eucalypt thick sulphite pulping liquor and LS-based PU undoped (LS-PU) and doped with 1% w/w MWCNTs (LS-PU-CNT) [51,91,301–308,360].

| **LS** ($cm^{-1}$) | **LS-PU/ LS-PU-CNT** ($cm^{-1}$) | **Assignment** |
|---|---|---|
| 3356 | 3298 | O-H stretching, H-bonded |
| 2940/2848 | 2966/2916/ 2860 | C-H stretching in methyl, methylene and O-$CH_3$ groups |
| – | 1722 | C=O stretching (urethane group) |
| 1604 | – | Aryl ring stretching, symmetric |
| – | 1530 | N-H bending (secondary amine in urethane group) |
| 1510 | – | Aryl ring stretching, asymmetric |
| 1460 | – | C-H bending in O-$CH_3$ groups, asymmetric |
| 1426 | – | Aromatic skeletal vibration combined with C-H bending in O-$CH_3$ groups, asymmetric in-plane |
| 1330 | | $C_{aryl}$-O vibrations, $SO_3H$ groups (S=O stretching vibration) |
| – | 1220 | C-N stretching (urethane group) |
| 1210 | – | $C_{aryl}$-O vibrations, C-C, C-O, C=O stretching, metallic salt of $SO_3H$ groups (S=O stretching vibration) |
| 1154 | – | Aromatic C-H in-plane deformation, $SO_3H$ groups |
| 1112 | – | Aromatic C-H in-plane deformation, C-O-C groups, metallic salt of $SO_3H$ groups |
| – | 1086 | C-O-C vibration (polyether bridges) |
| 1034 | – | Aromatic C-H in-plane deformation related with C-O, C-C stretching and C-OH stretching, $SO_3H$ groups, $C_{alkyl}$-O ether vibrations (O-$CH_3$ and β–O-4) |
| 914/818 | – | C-H deformation out-of-plane, aromatic ring |
| 650/630 | – | $SO_3H$ groups (S-O stretching vibration/C-S stretching vibration) |
| 630 | – | $SO_3H$ groups (C-S stretching vibration) |

two-stage degradation process, which corresponds to the thermal decomposition of the hard and soft segments, respectively [360,361]. Hard segments include the thermally weaker urethane moieties, where the maximum rate of weight loss occurred at 298 °C. Soft segments are essentially associated with the poly-ether moieties from the PPGDI co-macromonomer, where the maximum rate of weight loss occurred at 380 °C. The thermal degradation profile of both LS-based PU polymers (undoped and doped with MWCNTs) is similar since the

amount of MWCNTs (1% w/w) is too low to cause a significant change in the thermal behavior of the doped LS-based PU, at least under an inert gas atmosphere.

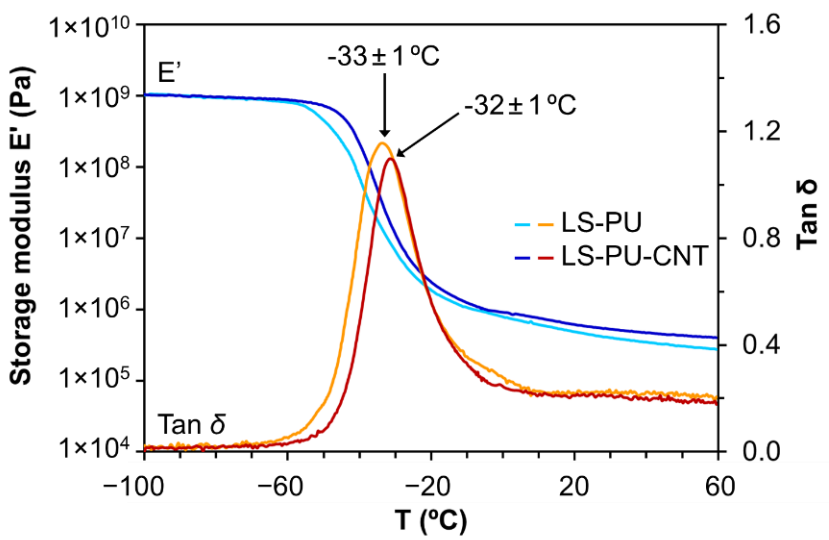


**Figure 34.** DMA profiles of LS, LS-based PU (LS-PU), and LS-based PU doped with 1% *w/w* MWCNTs (LS-PU-CNT).

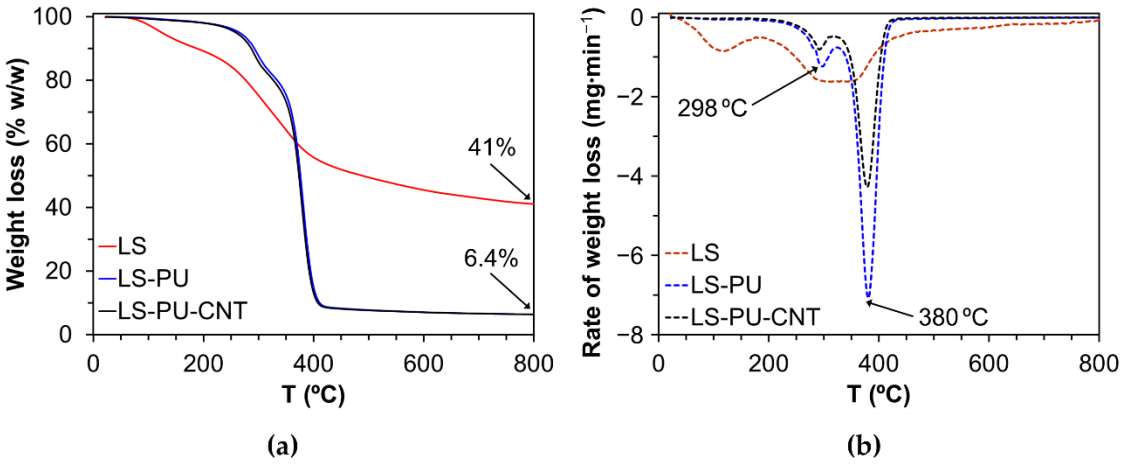


**Figure 35.** TGA curves of LS, LS-based PU (LS-PU), and LS-based PU doped with 1% w/w MWCNTs (LS-PU-CNT): (a) weight loss under inert N2 gas flow and (b) derivative of the weight loss.

### 6.3.2. DC and AC electrical conductivity of LS-based PU polymer doped with MWCNTs

The DC electrical conductivity of undoped LS-based PU polymer and the various LS-based PU polymer composites doped with variable amounts of MWCNTs was measured at room temperature, as depicted in Figure 36. Noteworthy is the fact that neat LS-based PU polymer is not a completely insulating material, exhibiting low electrical conductivity mostly due to the presence of LS in the polymeric matrix. This might be due to the mixed type electrical conductivity associated with the presence of π-conjugated aromatic moieties and of ionogenic functional groups such as carboxyl and sulphonic groups in lignosulphonates [362]. The incorporation of MWCNTs resulted in an increase in the electrical conductivity of PU-based LS composites in the order of magnitude $10^6$, from $7.2\times10^{-12}$ in undoped polymer to $7.1\times10^{-6}$ $S\cdot m^{-1}$ in polymer doped with 1.4% w/w MWCNTs (Figure 36). However, the observed conductivity curve as a function of MWCNT content in the composite did not fit the percolation theory model generally applied to composites doped with carbon nanotubes [268,363,364].

Unlike other PU-based composites produced from kraft or organosolv lignins [237], which show a sharp percolation threshold at low concentrations of MWCNTs (0.2–0.7 w/w), the LS-based PU did not reveal that feature, and the increase in conductivity with the addition of MWCNTs was not exponential (Figure 36). The plausible explanation for this conductivity behaviour could be the greater aggregation of polar LS in the PPDGI copolymer in comparison with the non-polar kraft and organosolv lignins. LS also has a molecular weight 2–3 times greater than kraft lignin, which makes it difficult to dissolve.

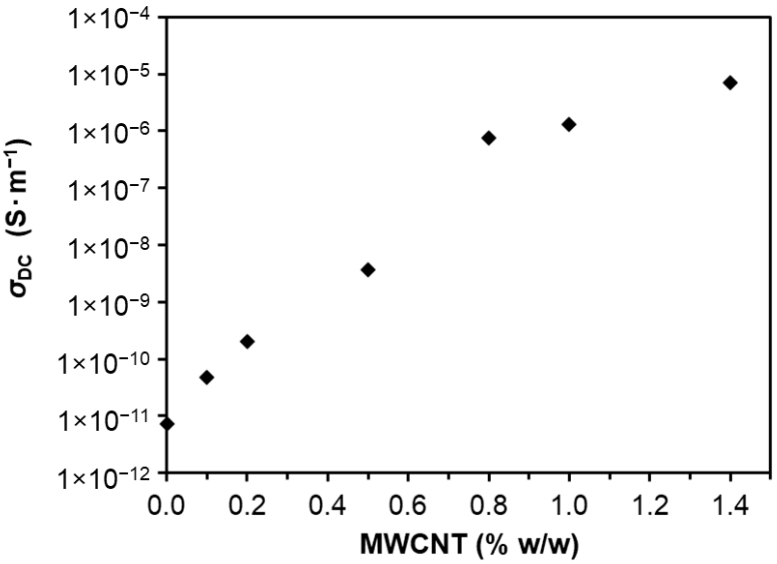


**Figure 36.** DC electrical conductivity, $\sigma_{DC}$, at room temperature as a function of MWCNT concentration (0%, 0.1 %, 0.2 %, 0.5 %, 0.8 %, 1 % and 1.4 % w/w) in LS-based PU.

Since lignin, including LS, is a dispersant of MWCNTs, its dissolution in co-macromonomer (PPDGI) is a crucial factor affecting the percolation phenomena that could compromise the formation of a continuous conductive network within the composite matrix. In fact, MWCNTs bind readily to LS, as can be seen from SEM im-ages of the LS powder mixed with 1% w/w MWCNTs (before adding the co-macromonomer PPGDI), thus forming bundles with a highly entangled structure (Figure 37). The inhomogeneous distribution of LS in the copolymer (final composite after curing) could negatively affect the long-range connectivity between the bound conductive elements within the LS-based polymeric network structure, thus reducing the electrical conductivity of the ensuing composite. In addition, the composite doped with MWCNTs revealed a more porous structure due to the more intensive bubble formation during the synthesis, which also negatively affected percolation conductivity (Figure 38). These bubbles are trapped within the composite matrix, disrupting the conductivity path, *i.e.*, the long-range connectivity between the conductive elements, hindering and even interrupting conductivity, which may also contribute to explaining why the composites do not display a common percolation behaviour.

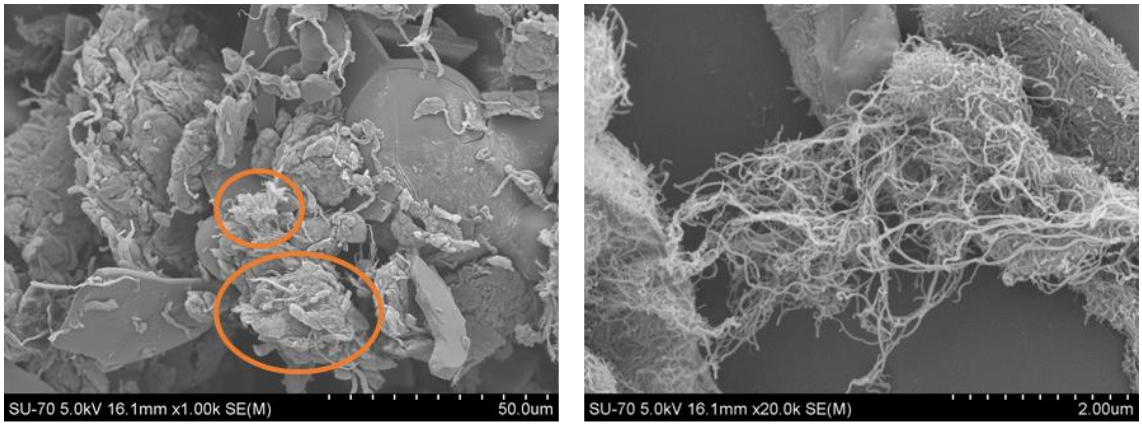


**Figure 37.** SEM image of a mixture of LS with 1% w/w MWCNTs (a) with an expanded image of MWCNT bundles bound to lignin particles (b). Examples of large MWCNT agglomerates are depicted by circles.

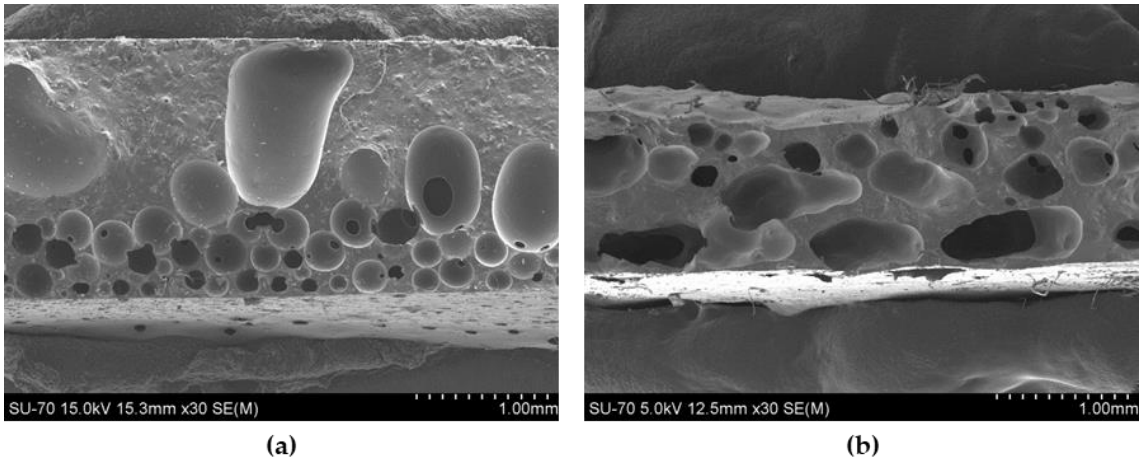


**Figure 38.** SEM images of the cross-section of LS-based PU films (a) undoped and (b) doped with 1% w/w of MWCNTs.

Alternating current conductivity, $\sigma_{AC}$, of LS-based PU polymers undoped and doped with different amounts of MWCNTs and the temperature effect on $\sigma_{AC}$ variation as a function of frequency for LS-based PU polymer composites doped with 1% w/w MWCNTs are shown in Figure 39. At first glance, the frequency dependence of AC conductivity can be divided into two discrete domains. At low frequencies (<1 kHz), AC conductivity is nearly constant and independent of the frequency, and its value comes close to the value of DC conductivity. However, in some cases, a very small slope is noticeable, especially for undoped LS-based PUs and LS-based PUs doped with 0.1 % w/w MWCNTs. The frequency region of constant conductivity extends to higher frequencies with increasing concentrations of MWCNTs.

Above a certain frequency, AC conductivity increases with increasing frequency. Hence, at higher frequencies, total AC conductivity, $\sigma_{AC}$ ($\omega$), is frequency-dependent, and its increase obeys a power law (known as the Jonscher universal power law [365]) given by Equation (3):

$$\sigma_{AC}(\omega) = \sigma_{DC} + A\omega^{s} \quad (3)$$

where ω is the angular frequency ($\omega = 2\pi f$, where $f$ is the frequency), $\sigma_{DC}$ is the independent frequency (DC) conductivity at $\omega \rightarrow 0$, $A$ is a constant dependent on temperature $T$, and s is an exponent dependent on both frequency and temperature, with values in the range 0–1. This power law is characteristic of disordered materials in which the conductivity is due to the hopping of charge carriers between localized states [366]. It is also presumed that $A$ and $s$ values are interrelated and have a mechanistic origin in terms of underlying disordered microscopic structures [367]. In fact, within the range of −13 to 107 °C, corresponding to the viscoelasticity interval, the straight-line correlation between Log $A$ and s has been observed (Figure 40). Within the same temperature range, almost constant log $A/s$ values (nearly 20) were registered while analysing the log $A/s$ vs. $T$ dependency from the universal Jonscher equation ($\sigma_{AC} = A\omega^{s}$). Similar behaviour was observed previously with epoxy polymeric formulations doped with MWCNTs and assigned to the unchanged composite morphology of the polymer-MWCNT network when charge carriers migration was affected exclusively by conformational rearrangements of disordered microscopic structures [367]. Additionally, at lower frequencies, AC conductivity is temperature-dependent, evidencing that the conductivity is a thermally activated process. The activation energy was assessed from the known Arrhenius equation while analysing the plot ln $\sigma_{AC}$ vs. $1/T$ in the temperature range of −13 to 107 °C [239]. The relatively low activation energy for $\sigma_{AC}$ at $\omega \rightarrow 0$ of the PU composite containing 1% MWCNTs (0.13 eV), when compared with that of the undoped PU composite (0.59 eV), clearly indicated the significant interaction between MWCNT and LS. This feature was similar to those observed previously with PUs doped with MWCNTs using kraft and organosolv lignins synthesized under the same conditions [237,239]. This fact supports the idea about similar conductivity mechanisms in all these lignin-based PUs doped with MWCNTs [237,239] despite no clear percolation threshold being observed with LS (Figure 36).

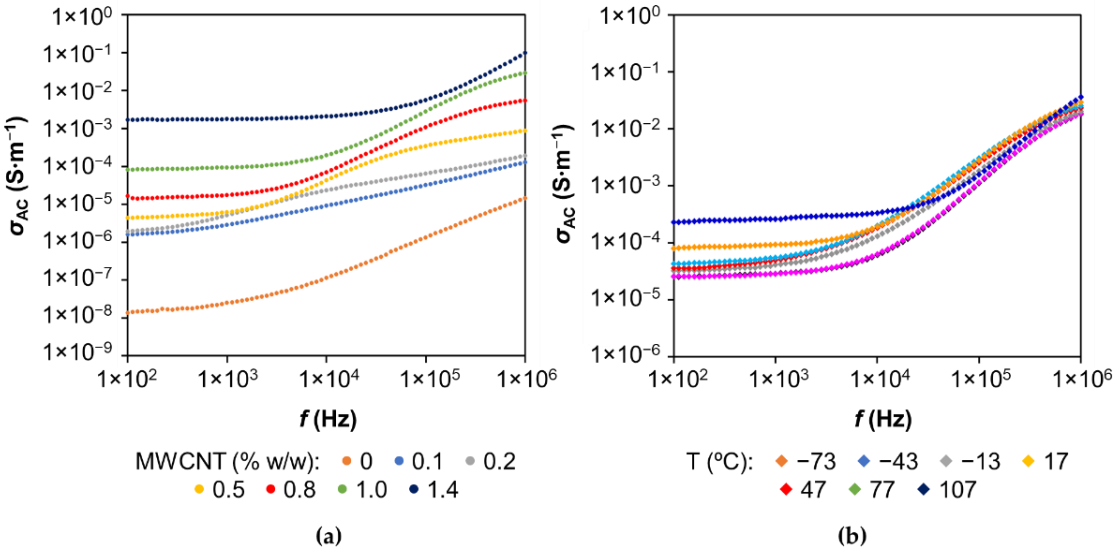


**Figure 39.** Frequency dependence of AC electrical conductivity, $\sigma_{AC}$, for LS-based PU polymer doped with different amounts of MWCNT at 77 °C (a) and with 1% (w/w) MWCNT at different temperatures (b).

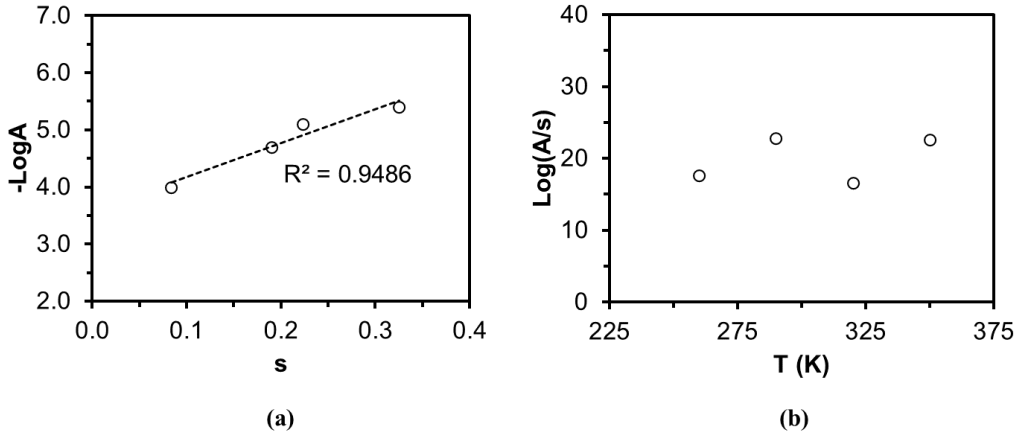


**Figure 40.** -Log*A* versus *s* (a) and Log*A*/*s* versus *T* (b) plots of LS-based PU film doped with 1% w/w of MWCNTs

The real and imaginary parts of the dielectric permittivity, $\varepsilon'$ and $\varepsilon''$, respectively, of LS-based PUs undoped and doped with different amounts of MWCNTs are presented in Figure 41 in the frequency range of 100 Hz to 1 MHz. Both real and imaginary parts of dielectric permittivity decrease with increasing frequency, especially the imaginary part, which is highly frequency-dependent. This behaviour is probably due to the interfacial polarization effect on the polymeric composites, attributed to the accumulation of polarized charges from

the difference in conductivities and permittivities of the constituents of the LS-based PU polymer composite (*i.e.*, the polymer matrix and the CNTs) [368]. Additionally, at the same frequency, both $\varepsilon'$ and $\varepsilon''$ increase with the increase in the amount of MWCNTs, which is attributed to an increase in the density of the MWCNT network [368]. Another remark from the $\varepsilon''$ plot (Figure 41b) is that a relaxation process (in the shape of a broad peak) appears at higher frequencies and higher MWCNT contents (though a slight peak for the composite with 0.2 % w/w MWCNTs is also observed). This relaxation process moves towards higher frequencies in accordance with an increase in MWCNT content in the composite. The peak of the highest concentration (1.4 % w/w MWCNTs) is not visible since it falls outside the frequency window range. Further experiments are still necessary to fully understand the dielectric relaxation mechanisms of these composites.

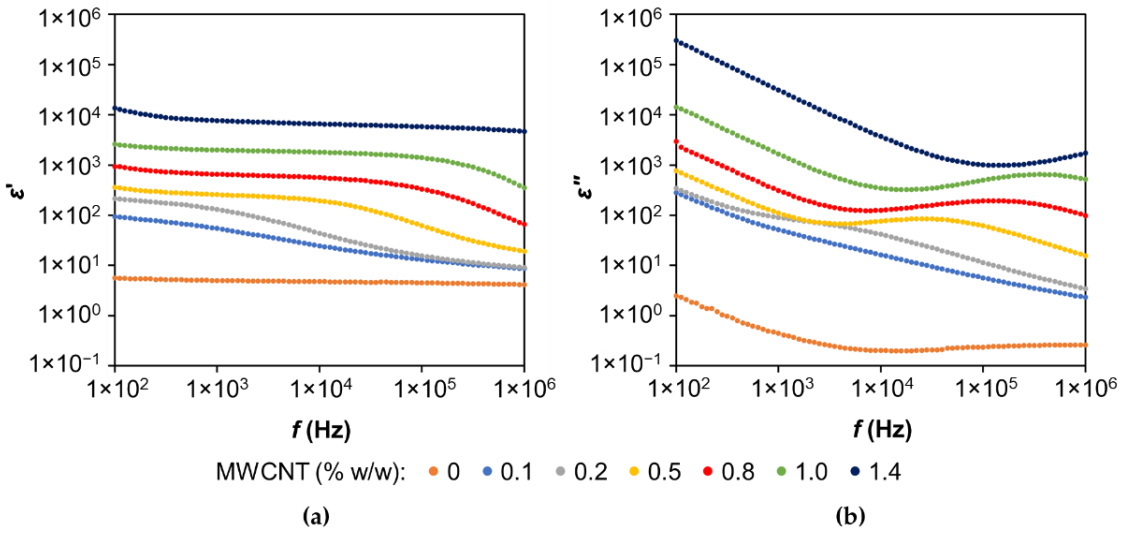


**Figure 41.** Real $\varepsilon'$ (a) and imaginary $\varepsilon''$ (b) parts of complex permittivity, $\varepsilon^*(f) = \varepsilon'(f) - i\varepsilon''(f)$ as a function of frequency, at T = 77 °C for LS-based polymer undoped and doped with different amounts of MWCNTs.

Carbon nanotubes are considered to be the most promising reinforcement fillers used to improve the mechanical, electrical, and thermal properties of polymers [268]. In this particular study, when only small amounts of MWCNTs were used in the polymer matrix, electrical conductivity improvement was achieved, thus making these composites suitable for sensor applications. The synthesis of an LS-based PU composite doped with 1.4 % w/w MWCNTs was a challenge since the mixture was very viscous, and it was very difficult to

prepare the films by moulding, which led to composites with highly irregular surfaces. Therefore, and considering the conductivity results, the LS-based PU composite containing 1% w/w MWCNTs was the formulation chosen for potential application as a potentiometric sensor.

### 6.3.3. Sensor properties of the LS-based PU polymer membrane composite doped with 1% w/w MWCNTs

Potentiometric measurements for a sensitivity assessment of an LS-based PU composite membrane sensor doped with 1% w/w MWCNTs were carried out using 1 mM Tris buffer solution at pH 7. The measurements revealed no response to $Na^+$, $NH_4^+$, and Pb(II) but had a response to Cu(II), Cd(II), Zn(II), Cr(VI), Cr(III), and Ag(I) (Figure 8). Response slopes towards studied ions were calculated based on the Nernst equation (Equation (4)) at a working temperature of 25 °C:

$$E = E^0 \pm \frac{RT}{z_i F} log a_i \quad (4)$$

where $E$ is measured potential (EMF of the electrochemical cell), $E_0$ is standard potential, $R$ is the gas constant, $T$ is the temperature in K, $F$ is the Faraday constant, $a_i$ is the activity of the studied cation, and $z_i$ is the charge of the ion. A concentration variation by a factor of 10 should give rise to a potential variation of *ca*. 59 mV for single-charged ions, but, for double-charged ions, it should be around 30 mV, and, in the case of triple charged ions, the slope value should be around 20 mV. Response slopes of the LS-based PU doped with a 1% w/w MWCNT electrode towards different ions at pH 7 and 2 are depicted in Figure 42 and Figure 43, respectively, and the detection limits and linear ranges at pH 7 are presented in Table 17. The detection limit of the sensor was determined from the intersection of two extrapolated segments of the calibration plots according to IUPAC recommendations [369].

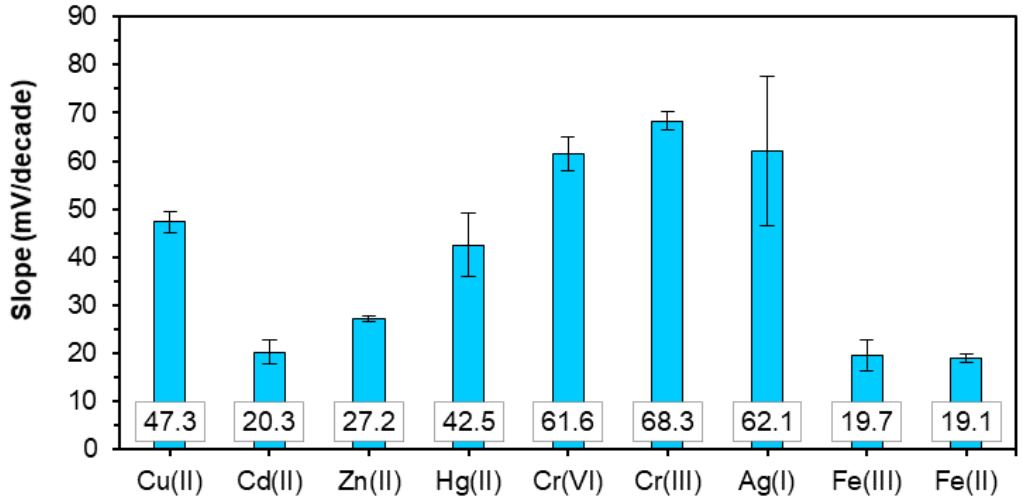


**Figure 42.** Slopes of the electrode function of the LS-based PU sensor doped with 1% w/w MWCNTs at pH 7 (mean values of at least three calibrations with their respective standard deviations).

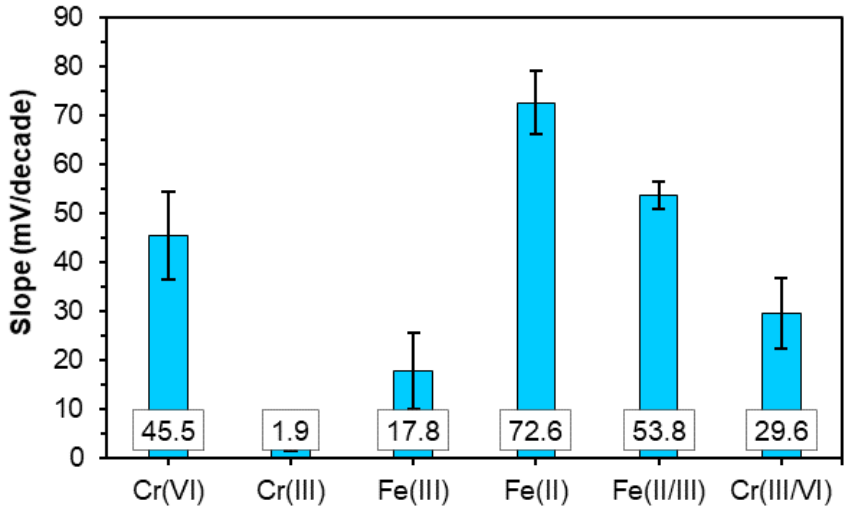


**Figure 43.** Slopes of the electrode function of the LS-based PU sensor doped with 1% w/w MWCNTs at pH 2 (mean values of at least three calibrations with their respective standard deviations).

**Table 17.** Sensitivity characteristics of LS-based PU membrane sensor doped with 1% w/w MWCNTs at pH 7.

| Cation | Slope (mV/decade) | Detection limit (M) | Linear range (M) |
|---|---|---|---|
| Cu(II) | 47.3 ± 2.1 | $4.6\times10^{-5}$ | $5.0\times10^{-5} – 1\times10^{-2}$ |
| Cd(II) | 20.3 ± 2.5 | $4.2\times10^{-6}$ | $5.0\times10^{-6} – 1\times10^{-2}$ |
| Zn(II) | 27.2 ± 0.7 | $1.2\times10^{-5}$ | $1.5\times10^{-5} – 1\times10^{-2}$ |
| Hg(II) | 40.9 ± 5.7 | $3.3\times10^{-5}$ | $5.0\times10^{-5} – 1\times10^{-2}$ |
| Cr(VI) | 61.6 ± 3.6 | $6.1\times10^{-5}$ | $1.0\times10^{-4} – 1\times10^{-2}$ |
| Cr(III) | 68.3 ± 1.8 | $6.2\times10^{-5}$ | $1.0\times10^{-4} – 1\times10^{-2}$ |
| Ag(I) | 62.1 ± 15.5 | $4.9\times10^{-6}$ | $1.0\times10^{-5} – 2.2\times10^{-3}$ |

The sensor exhibits a low response to Cd(II) (with a slope of 20.3 ± 2.5 mV) and a near-Nernstian response towards Zn(II) (with a slope of 27.2 ± 0.7 mV) and Ag(I) (with a slope of 62.1 ± 15.5 mV). For other cations such as Cu(II) and Hg(II), the super-Nernstian responses were obtained at pH 7 (Figure 44). Responses to mercury and silver ions are associated with high standard deviations, as after the first calibration measurement in the solutions of these ions, the slopes of the electrode decreased. Furthermore, some decrease of the sensor response slopes was observed in the solutions of copper and zinc after sensor exposure to mercury and silver, indicating an eventual partially irreversible interaction of the polymer membrane with these ions. At the same time, no drastic, irreversible complexation with Hg(II) ions was detected, compared with other lignin-based sensor membranes of the same polymer composite [91,237,239].

Considering that at pH 7, the predominant species of Cr(III) is $Cr(OH)^{2+}$, the sensor response to this ion is slightly above the theoretical one, *i.e.*, 68 mV/pX instead of the expected 59 mV/pX. No response to Cr(III) was observed at pH 2, which is in agreement with the literature data of Cr(III) adsorption by different sorbents and is attributed to sorbent surface protonation at acidic pH, resulting in the electrostatic repulsion of the positively charged Cr(III) species [370].

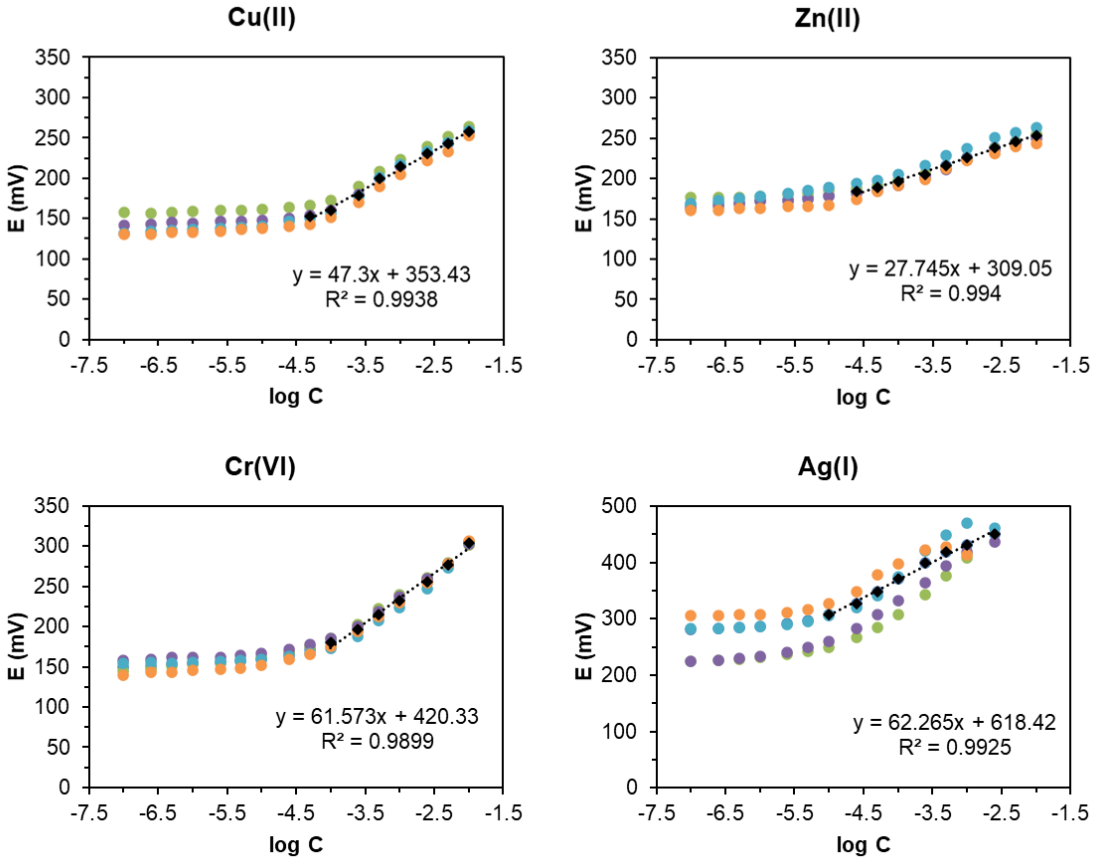


**Figure 44.** Calibration curves LS-based PU composite membrane sensor doped with 1% w/w MWCNTs towards four selected cations (four calibration curves – coloured dots – for each cation and the respective average response slope with linear trendline – black)

Response of the LS-based sensor to Cr(VI) at pH 7 corresponds to the theoretical response to a single-charged cation, although Cr(VI) is present at this pH as two anionic species, $HCrO_4^-$ and $CrO_4^{2-}$ [371]. At pH 2, the dominant Cr(VI) species are $Cr_2O_7^{2-}$ and $HCrO_4^-$, with their ratio depending on the total Cr(VI) concentration [370]. The LS-based sensor response to Cr(VI) at pH 2 is about 45 mV/pX. A similar cationic response to Cr(VI) was observed for lignin-based sensors in the previous study [237] as well as for the chromate-selective sensor with a different type of membrane material – chalcogenide glass [372]. The sensitivity of both chalcogenide- and lignin-based sensors is pH-dependent, and, in the case of the previously studied lignin-based sensors, it was observed only at pH 2, while the LS-based sensor responded at both pH 7 and 2. It was hypothesized that the response mechanism of both chalcogenide glass and lignin-based electrodes is based on the combination of ion

exchange and charge transfer, although no detailed mechanistic studies of the Cr(VI)-selective sensors' response mechanism have been done.

Based on these findings, the LS-based sensor was expected to possess redox sensitivity, and the response of the sensor was evaluated in the solutions of two redox couples, ferro-ferricyanide $Fe(CN)_6^{3-/4-}$ and Cr(III)/Cr(VI), at pH 7 and pH 2. Response slopes were calculated by Equation (5):

$$E = E^0 - \frac{RT}{zF}\log\left({}^{a}/_{b}\right) \quad (5)$$

where *a* and *b* are the activities of the reduced and oxidized ions, respectively.

No redox response was obtained at pH 7; however, at pH 2, the sensor displayed response to both pairs (Figure 43). The sensor exhibited a near-theoretical response to the pair $Fe(CN)_6^{3-/4-}$, with a slope of −53.8 ± 3.2 mV, and a super-Nernstian response to the pair Cr(III)/Cr(VI), with a slope of −29.6 ± 8.3 mV.

Sensor responses in the individual solutions of ferrum and ferrocyanide at pH 7 and 2 are depicted in Figure 42 and Figure 43, respectively. The sensor response to $Fe(CN)_6^{3-}$ did not depend on pH and was *ca*. 19 mV/pX. The sensor displayed a similarly low response of *ca*. 17 mV/pX to $Fe(CN)_6^{4-}$ at pH 7, while at pH 2, a super-Nernstian anionic response of −72 mV/pX was observed. This response may be attributed to the combination of ion exchange and charge transfer processes involving the complexation of ferricyanide, with the functional groups of LS protonated at acidic pH and their subsequent oxidation.

With the aim to expand the applicability of lignin-based potentiometric sensors, the response of the LS-based PU sensor doped with 1% w/w MWCNTs towards ionic liquids (IL), 1-ethyl-3-methylimidazolium chloride ($[C_2mim]Cl$) and choline chloride (ChCl), was examined (Figure 45). These substances are widely used for different "green" syntheses and biomass fractionation purposes, whose presence in aquatic environments could be hazardous [342]. The measurements were carried out in Tris solution at pH 7. Although the sensor did detect both ILs, the sensitivity was relatively low, giving rise to response slopes of 12.0 ± 3.8 and 7.3 ± 0.4 mV for $[C_2mim]Cl$ and ChCl, respectively. The low response of the sensor may probably be due to steric hindrance from the structure of the ILs. However, further studies are required to evaluate the response mechanism of these potentiometric sensors to such types of compounds.

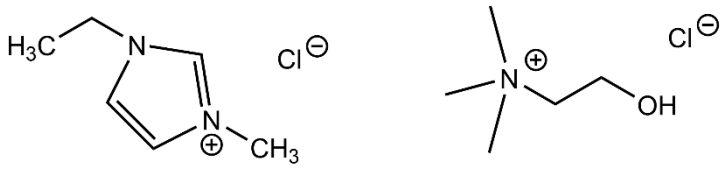


(**a**) (**b**)

**Figure 45.** Chemical structure of the ILs studied: (a) 1-ethyl-3-methylimidazolium chloride and (b) choline chloride.

Since the LS-based sensor displayed a theoretical or even super-Nernstian response to several of the studied ions, the choice of the target ion, known as the primary ion, was not an obvious one for the determination of potentiometric selectivity. Taking into account the high and reproducible response to Cr(VI) and to facilitate a comparison with the previously obtained results for other types of lignin, this ion was considered the primary ion for the selectivity study. The matched potential method (MPM) was used for selectivity determination. Accordingly, the selectivity coefficient ($K_{A,B}^{pot}$) is defined as the activity (concentration) ratio of the primary ion A ($a_A' - a_A$) and the interfering ion B ($a_B$), which give the same potential change in a reference solution (this one containing a fixed activity of primary ions $a_A$) [369,373], and is expressed by Equation (6):

$$K_{A,B}^{pot} = (a_A^{'} - a_A)/a_B \quad (6)$$

where $K_{A,B}^{pot}$ is the selectivity coefficient, $a_A$ and $a_B$ are the activities of the primary ion A and the interfering ion B, respectively. The selectivity coefficient represents a numerical measure of the electrode membrane's ability to discriminate the primary ion A (target ion) in the presence of the interfering ion B. A solution of $1.0\times10^{-4}$ M of Cr (VI) in Tris 1 mM at pH 7 was used as the background. For the calculation of selectivity coefficients, $\Delta E$ = 20.0 mV was applied. The calculated values of selectivity coefficients are summarized in Table 18. The LS-based sensor displays low selectivity to Cr(VI) in the presence of most of the studied ions and is more selective to Cd(II) and especially to Ag(I) than to Cr(VI). However, in practice, selectivity to Ag(I) ions might not be necessary as they are rarely present in the analysed samples.

**Table 18.** Selectivity coefficients, $K_{A,B}^{pot}$, of the LS-based sensor towards Cr(VI), determined using the matched potential method (mean values of at least three values).

| Interferent ion | $K_{A,B}^{pot}$ |
|---|---|
| Zn(II) | 0.29 ± 0.08 |
| Cd(II) | 1.49 ± 0.41 |
| Cu(II) | 0.40 ± 0.15 |
| Cr(III) | 0.53 ± 0.28 |
| Hg(II) | 0.54 ± 0.11 |
| Ag(I) | 2.66 ± 0.62 |
| Fe(III) | 0.50 ± 0.26 |
| Fe(II) | 0.65 ± 0.14 |

These results show that this LS-based sensor displays sensitivity and low selectivity to several transition metal cations as well as a redox response. This behaviour differs remarkably from the one observed for the other lignin-based sensors [91,237,239]. Sensors based on LignoBoost® kraft lignin displayed a Nernstian response and high selectivity to Cu(II) and quite low or even no response to other cations except Hg(II), with which it interacted irreversibly, resulting in the loss of the electrode function [239]. Sensors based on kraft, organosolv, and lignosulphonate displayed sensitivity and selectivity to Cr(VI), redox sensitivity to the Cr(VI)/Cr(III) redox couple, and low sensitivity to transition metal cations such as Cu(II) and Pb(II), with higher responses observed for the LS-based sensor [237]. Furthermore, the three aforementioned sensors neither responded to nor were affected by the exposure to Hg(II). The reason for such disparity of the sensing properties can be attributed to the difference in chemical structure and composition between lignins obtained from different cooking processes, *i.e.*, kraft lignin and LS, or isolation procedures, such as conventional kraft and LignoBoost® kraft, and LS used previously and in this study [239,374]. LS contains phenolic groups with lower pKa than those in kraft lignin due to the strong electron-withdrawing moieties on the side chain (sulphonic groups at the benzylic carbon and conjugated double bonds) [49]. In addition to the sulphonic groups, the LS structures with phenolic hydroxyls have a high capacity for chelation of metal cations, thus acting as ionophores. This induces the formation of stable coordination complexes with a wide range of transition metal cations, influencing the sensing mechanism

Other metal-sensitive sensors based on different polymeric membrane ion-selective electrodes incorporating ionophores, sensitive to different cations, have been widely

reported in the literature [375–399]. Most of these sensors exhibit a near-Nernstian or Nernstian response to the different cations studied. The super-Nernstian behaviour displayed by the LS-based PU membrane is probably due to the presence of strong anionic sites in the composite [400], *e.g.*, inherent for the LS sulfonic acid groups. Hence, this work puts in evidence the decisive role of the lignin's nature in the response of the corresponding potentiometric sensors.

The sensitivity of the LS-based polymeric sensor to redox potential and Cr(VI) was explained previously by the substructures with free phenolic hydroxyl groups involved in the eventual reversible hydroquinone/quinone type redox couples, favouring the complexation of Cr(VI) and its subsequent reduction to Cr(III) [237]. However, the high sensitivity of the LS-based sensor to several transition metals such as Zn, Cd, and Cu, found in the present work, was not registered in our previous study with another LS sample [237]. This behaviour could be explained by the structural differences in LS samples induced by variations in eucalypt wood cooking conditions [297]. The LS sample used in this study was isolated from spent liquor after a more severe cooking process to produce dissolving pulp. The resulting LS was more condensed and richer in tannins (e.g., catechin, gallic and ellagic acids) than that used in the previous work [237]. Apparently, concomitant substructures, with two or three vicinal hydroxyl groups belonging to these polyphenolic concomitants, chelate easily with transition metal cations [401]. The effect of the presence of tannins on sensing properties can be corroborated by comparing the sensing performance of polymers based on eucalyptus kraft lignins isolated by the conventional procedure and the LignoBoost® process [239]. The latter had a higher content of total hydroxyl groups and a higher relative content of phenolic hydroxyl groups and concomitant tannins, which imparted to this material metal chelating properties; thus, the resulting sensor displayed high sensitivity to Cu(II) and no redox response. Indeed, the nature of the lignin used in the polymeric formulation of composites is decisive for the potentiometric sensor response, which is defined by the interplay between different functional groups and their concentrations.

### 6.3.4. DC electrical conductivity of LS-based PU polymer embrane composite doped with other carbon nanofillers

Considering the interesting sensing results obtained with MWCNTs as nanofillers in the composite with LS, the impact of other carbon nanofillers was evaluated, namely, graphene oxide (GO), reduced GO (rGO) and graphite (Gr), using similar LS-based PU formulations. The electrical conductivity of a composite occurs mostly as a result of the formation of a consistent network of nanofillers. SEM images of the LS mixture with 1% w/w GO, rGO, and Gr show different distribution patterns of nanofillers, as depicted in Figure 37 and Figure 46. As already mentioned, MWCNTs are highly entangled in a bundle structure with LS (Figure 37). In contrast, both GO and rGO are disoriented and mostly wrinkled and folded into a fuzzy structure (Figure 46). Finally, the graphite sheets are scattered randomly among LS particles (Figure 46). The entanglement and wrinkling of the nanofillers among LS particles may indicate that during the processing conditions, under mechanical stirring, these were not able to completely orient within the powder mixture [402]. This could explain the inappropriate distribution of nanofillers, failing to yield a conductive network within the composite matrix and affecting the electrical conductivity of the ensuing composites.

The impact of different carbon nanofillers with various concentrations on the DC electrical conductivity of LS-based PU polymer composites was examined, and the results are depicted in Figure 47. The highest MWCNT concentration of 1.4 % w/w gave rise to almost $10^6$-fold higher electrical conductivity than the other nanofillers with the same concentration in the PU composite. Therefore, much larger amounts of GO, rGO, and Gr were required (up to 10 % w/w) to achieve a visible increase in the conductivity of an LS-based PU composite material. The reason for this behaviour is most probably due to the much higher aspect ratio of the MWCNT rods, which is more favourable to the creation of a continuous conductive network within the polymer matrix. Therefore, significantly improved electrical conductivity was obtained for smaller MWCNT loadings compared to the GO, rGO, and graphite samples at the same concentrations. In the case of the graphene sheets, the lack of conductivity improvement is probably due to the limited possibility of having GO, rGO, or graphite contact points and, thus, limited conduction [402].

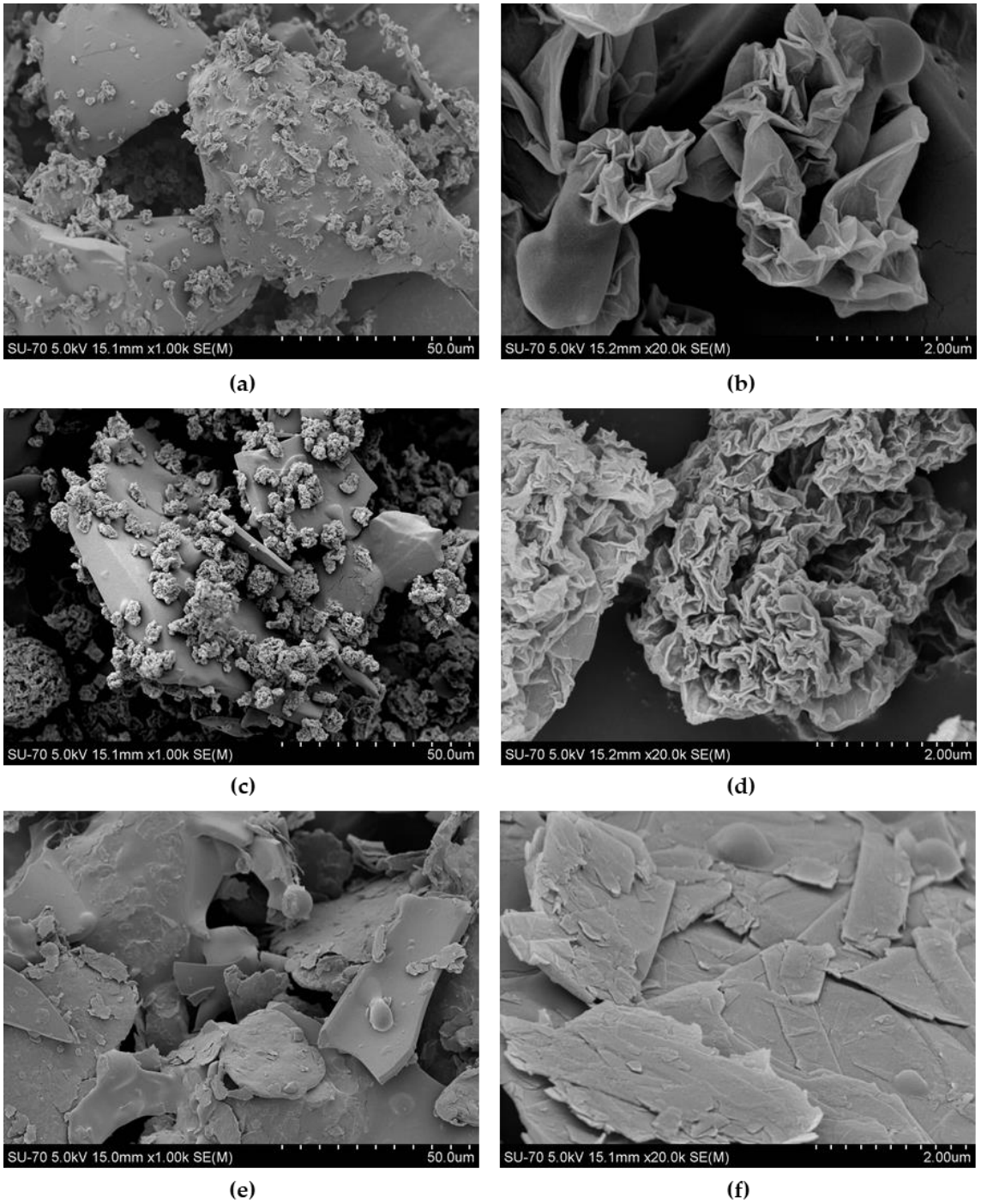


**Figure 46.** SEM images of the LS mixture with 1% w/w of GO (a) and (b), rGO (c) and (d), and Gr (e) and (f).

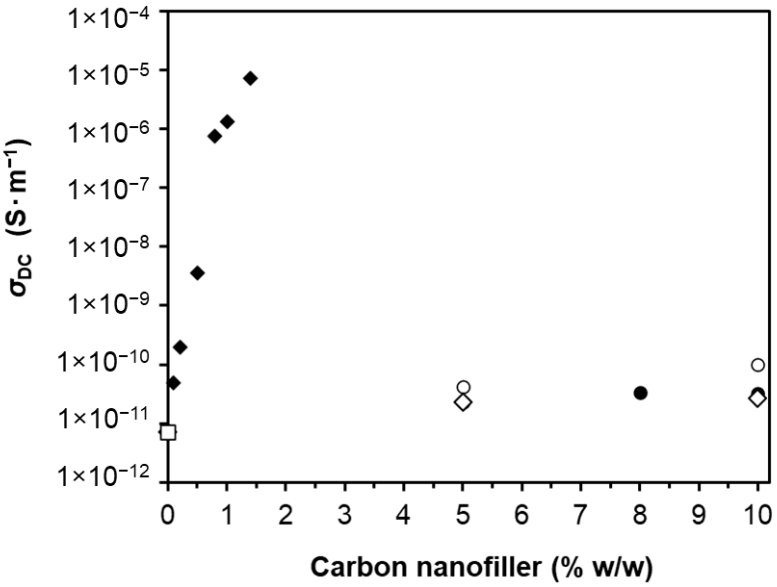


**Figure 47.** DC electrical conductivity, $\sigma_{DC}$, at room temperature as a function of carbon nanofiller concentration (υ—MWCNT; ○—GO; ●—rGO; ◇—Gr; □—undoped) in the LS-based PU composite.

## 6.4 CONCLUSIONS

Unlike PU composites based on kraft or organosolv lignins, MWCNT-doped LS-based PUs did not display a common percolation behaviour due to the specificity of LS dissolution in the co-macromonomer used for the synthesis (PPGDI). Nevertheless, LS-based PUs doped with ≥ 1% w/w multiwall carbon nanotubes (MWCNTs) displayed relevant electrical conductivity suitable for sensor applications. Among examined carbon nanofillers within the range of 0–10% w/w (multiwall nanotubes, graphene oxides, and graphite), only MWCNTs provided significantly improved electrical conductivity to LS-based PU films suitable for sensing applications. Applied as a potentiometric sensor, MWCNT-doped LS-based PUs showed sensitivity to Cu(II), Zn(II), Cd(II), Cr(III), Cr(VI), Hg(II), and Ag(I) at pH 7 and exhibited a response to the Cr(VI)/Cr(III) redox pair at pH 2. The highest selectivity in solution at pH 7 was observed for Cd(II) and especially for Ag(I) ions. It is suggested that LS obtained from the same wood but under different cooking conditions and containing polyphenolic concomitants can exhibit distinct sensing performance due to the presence of corresponding structural units with chelating vicinal phenolic hydroxyls. The LS-based conducting polymer revealed a weak but not negligible response toward ionic liquids, [$C_2$mim]Cl and ChCl. An additional study is necessary to find the sensitivity of the obtained

sensor membranes to different classes of potentially hazardous compounds for their reliable detection in solutions.

# 7. LS-based polyurethane adhesives

This chapter was published as:

Sandra Magina, Nuno Gama, Luísa Carvalho, Ana Barros-Timmons, Dmitry V. Evtuguin. Lignosulfonate-based polyurethane adhesives, *Materials*, **2021**, *14*(22), 7072. DOI: 10.3390/ma14227072

## 7.1 ABSTRACT

The feasibility of using lignosulphonate (LS) from acid sulphite pulping of eucalyptus wood as an unmodified polyol in the formulation of polyurethane (PU) adhesives was evaluated. Purified LS was dissolved in water to simulate its concentration in sulphite spent liquor and then reacted with 4,4'-diphenylmethane diisocyanate (pMDI) in the presence or absence of poly(ethylene glycol) with $M_w$ 200 ($PEG_{200}$) as soft crosslinking segment. The ensuing LS-based PU adhesives were characterized by infrared spectroscopy and thermal analysis techniques. The adhesion strength of new adhesives was assessed using Automated Bonding Evaluation System (ABES) employing wood strips as a testing material. The results showed that the addition of $PEG_{200}$ contributed positively both to the homogenization of the reaction mixture and better crosslinking of the polymeric network, as well as to the interface interactions and adhesive strength. The latter was comparable to the adhesive strength recorded for a commercial white glue with shear stress values of almost 3 MPa. The optimized LS-based PU adhesive formulation was examined for the curing kinetics using the Kissinger and Ozawa methods by non-isothermal differential scanning calorimetry. It was concluded that the curing process follows a similar trend to that observed with other PU formulations and that the activation energy is within the range of 60-70 $kJ \cdot mol^{-1}$ depending on the applied method.

## 7.2 INTRODUCTION

Wood-based composites cover a variety of products, from fibreboards to laminated beams, and are used for numerous non-structural and structural applications such as panels for interior, furniture, support structures in buildings, among others. Wood raw-materials used in the production of wood-based composites include fibres, particles, flakes, veneers, laminates, or lumber [157,158]. In most conventional wood-based composites, adhesive bonding is achieved by non-renewable petroleum-derived thermosetting synthetic resins including phenol-formaldehyde (PF), urea-formaldehyde (UF), melamine-formaldehyde (MF), polyurethanes (PUs) and polymeric diphenylmethane diisocyanate (pMDI). Several auxiliary chemicals are also added to plasticize adhesive polymers, enhance tackiness, improve heat resistance, or lower costs [158–160]. Due to the waning of the petrochemicals

supplies but also due to the public awareness related to the environment and its protection, as well as governmental regulations, the use of bio-based adhesives in wood and fiber composites has attracted scientific and economic interest for several decades [160–163].

Within the diverse synthetic resins aforementioned, PUs are versatile designer polymers that display varied properties being adjustable to a wide range of applications namely foams (rigid and flexible), elastomers, paints and coatings, adhesives, and even for medical applications [194–197]. The global PU market size was valued at USD 70.67 billion in 2020 and is expected to grow at a compound annual growth rate (CAGR) of 3.8 % from 2021 to 2028 [403].Typically, PUs are prepared through the addition of isocyanates (comprising more than one reactive isocyanate group per molecule) and polyols (containing two or more reactive OH groups per molecule) yielding polyurethane linkages in the polymer backbone [194–197]. Whilst, isocyanates are very harmful and, at the end of their life cycle, PUs may release toxic compounds such as amines leading to health and environmental concerns, so far it has been very difficult to replace them. Furthermore, the implementation of regulations by some governments have motivated both academia and industry to develop safer and "greener" alternative routes to produce more environmentally friendly PUs. To reduce the environmental impact of PUs, efforts have focused on the replacement of fossil derived polyols by bio based ones, such as castor oil [218,220–223,404,405] and other vegetable oils [406–408], crude glycerol [220,409], lignin [205,220,410], among others.

Technical lignins can act as macropolyols in PU synthesis due to high amount of phenolic and aliphatic hydroxyl moieties in their structure [78,204–208,410]. The direct exploitation of technical lignins, as polyols or blending with industrial polyols, is energetically and environmentally advantageous [75] and the ensuing biomass-based PUs are more biodegradable than those derived from petroleum-based polyols [209]. Hence, lignins can be used as such, or after chemical modification to get a more reactive lignin, alone or in combination with other polyols [204–208,210–212]. It is well known that lignins (in general) act both as a network former (due to its relatively high functionality, *i.e*., functionality higher than 2) and as a reinforcing component in PU formulations. The latter is mainly due to the high content of condensed aromatic rings in lignin contributing to its generally stiff structure. Therefore, to counterbalance the stiff character of the lignin macromolecules, other polyols can be used as soft segments, such as poly(ethylene glycol) (PEG) and poly(propylene glycol) (PPG) [207,217–219], or bio-based polyols, such as castor oil [218,220–223], crude

glycerol [220] and poly(ε-caprolactone) (PCL) [224] yielding grafted and cross-linked PUs with the possibility of controlling their flexibility and/or rigidity. Both aliphatic and phenolic OH groups in lignin are potentially reactive and samples with high OH content, for instance, organosolv lignins, can be used as macromonomers without further chemical modification [211,212]. However, considering that the structure of technical lignins is extremely dependent on the plant source from which it is obtained, the final properties of the lignin-based PUs highly depend on the lignin's plant source [213]. The low reactivity of the lignin macromonomer towards isocyanates is usually related to the fact that only a certain proportion of the total OH groups can react (due to steric hindrance from the highly branched three-dimensional structure of lignin and intramolecular hydrogen bonding) yielding products without desirable performance [213–215]. Therefore, to obtain polymeric formulations displaying acceptable performance, the content of the unmodified lignin in the ensuing PU is generally quite low (below 15–30 wt. %) [206].

Another important issue for the adhesive industry is the control of the curing process since it affects the final properties of the material. This requires knowledge about the kinetics of the curing process. In a previous work, Gama and co-workers [404] studied the curing process of castor oil-based PU adhesives by differential scanning calorimetry (DSC) using the two most known approaches, the Kissinger [411] and the Ozawa [412] methods. Both methods are rapid, easy to use and depend on a series of experiments based on heating samples at several different heating rate [413]. Kinetic parameters, such as the activation energy ($E_a$) of the cure and the degree of cure (or conversion, α), were determined from non-isothermal measurements using different heating rates ($\beta$). α varies from 0 to 1, *i.e.*, from completely uncured to fully cured, and can be determined by Equation (7).

$$\alpha = H_{(t)}/H_T \quad (7)$$

where $H_{(t)}$ is the enthalpy of the reaction up to time $t$ and $H_T$ is the total enthalpy of the reaction. Additionally, the rate of cure ($d\alpha \cdot dt^{-1}$) is proportional to the rate of the heat generated and can be determined by Equation (8).

$$d\alpha/dt = 1/H_T \times dH_{(t)}/dt \quad (8)$$

when the curing rate ($\beta$) is increased, the peak temperature ($T_p$) shifts to a higher temperature range, which can be used to calculate $E_a$, using methods such as the Kissinger method or Ozawa method [413], according to Equation (9) and Equation (10), respectively.

$$\ln(\beta/T_p^2) = C - E_a/(RT_p) \quad (9)$$

$$ln(\beta) = C - E_a/(RT_p) \quad (10)$$

where $C$ is a constant derived from $E_a$, the kinetic constant ($k_0$) and the universal gas constant ($R$). By plotting $\ln(\beta/T_p^2)$ vs $1/T_p$ and $\ln(\beta)$ vs $1/T_p$, the value of $E_a$ can be determined.

The ultimate goal of this work is to use industrial sulphite spent liquor (SSL) as a bio-based polyol to substitute petroleum-based polyols in the formulation of bio-based PU adhesives and also to reduce costs associated with LS purification. SSL from acid sulphite pulping of hardwoods, such as eucalypt, is mainly composed of LS, xylo-oligosaccharides and contains high amounts of pentose sugars, extractives of polyphenolic origin and inorganic salts [51,58,59]. In order to avoid the eventual participation of other components from SSL in the PU synthesis, LS was purified by dialysis and contained minimal organic/inorganic impurities. Therefore, in the adhesive preparation unmodified purified eucalyptus LS was used as bio-based polyol, water as LS solvent, $PEG_{200}$ as a soft segment co-polyol and pMDI as a basic crosslinker. Since lignins generally contribute to PU stiffness, the addition of PEG with $M_w$ 200 ($PEG_{200}$) allows tuning the viscoelastic properties of PUs. Therefore, the variation in $PEG_{200}$ content was studied and the final adhesion properties of the resulting adhesives were evaluated. Structural and thermal characterization was performed on the most relevant adhesive formulations. Finally, the kinetic parameters of the curing process were assessed for the most promising adhesive formulations.

## 7.3 RESULTS AND DISCUSSION

The polycondensation of unmodified lignins with isocyanates with large molecular structures like pMDI is unlikely to occur without the addition of catalysts due to the lack of reactivity, which is related to the steric hinderance of OH groups in lignin and of NCO groups in pMDI as well as low diffusion due to the high viscosity of the reaction medium [211]. Accordingly, DBDTL was used as a catalyst. It is assumed that in LS, as in other technical lignins, the primary OH groups are the most reactive with isocyanate moieties [211]. This assumption is reflected in the reaction scheme proposed in Figure 48, where the most reactive OH groups in the γ position of the lignin structural unit react with pMDI. It is noteworthy that steric hindrance of phenolic OH groups is much more pronounced in

hardwood than in softwood lignin, because the former possesses quite high ratio of syringyl (S) over guaiacyl (G) structural units [18,19]. In fact, the eucalyptus LS used in this work had the particularly high S:G ratio of 78:22 [297]. Furthermore, in the presence of water, the reactivity of pMDI with lignin is hampered by isocyanate competition reactions with the formation of the corresponding amines [161,196,405]. Therefore, it can be expected that a polymeric network of low crosslinking will result from the reaction of pMDI and LS alone. However, the addition of highly reactive water-soluble polyol to the reaction system can increase crosslinking between polymer chains and, if a polyol is polar enough to improve segmental movement of the resulting network, it can positively contribute to the adhesive properties of the final synthetic glue. Based on these considerations, a series of formulations were synthesized (Table 5) using, in addition to pMDI and LS, low molecular weight polyethylene glycol diol ($M_w$ 200). The produced LS-based adhesives were structurally and thermally characterized and the adhesion strength have been evaluated.

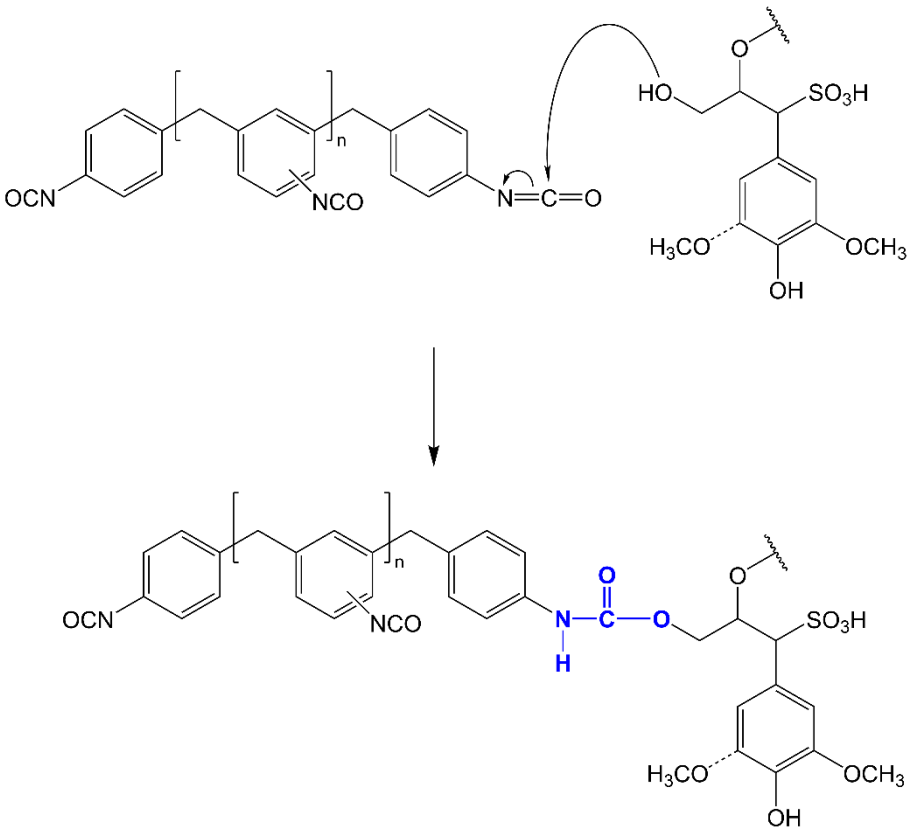


**Figure 48.** Schematic representation of the reaction between NCO group in pMDI and apliphatic OH in the γ–position of eucalypt LS.

### 7.3.1. Chemical and thermal characterization of LS-based PU adhesives

The parent LS and typical adhesive formulations involving LS and pMDI (LS-MDI) and LS, pMDI and $PEG_{200}$ were structurally characterized by FTIR. The corresponding normalized spectra of LS, LS-based adhesive without (LS-MDI) and with $PEG_{200}$ (LS-MDI-PEG) are presented in Figure 49 and the bands assignment are listed in Table 2. The reaction of OH groups in LS with pMDI in the PU samples produced was confirmed by the decrease in the intensity of the bands at 3430 (δ O-H) and 1036 $cm^{-1}$ (δ C-OH) [51,303,308]. Simultaneously, the newly formed bands in the PU samples were observed at 1766 (very slight), 1504 (the most evident), 1406 (also significant) and 1216 $cm^{-1}$ and assigned to the stretching vibration in urethane groups [414]. Meanwhile, the characteristic bands at 2262 (C-N stretching), 1644 (C=O stretching) and 1590 $cm^{-1}$ (N-H deformations) [414] are assigned to unreacted isocyanate groups from pMDI still present in the PU product suggesting that the PU curing process was not complete. This is in agreement with the formulation´s composition (Table 19) as NCO groups were used in excess amount. It is noteworthy that the intensity of the isocyanate band at 2262 $cm^{-1}$ was lower for LS-MDI-PEG than for LS-MDI (Figure 49), thus confirming the importance of adding $PEG_{200}$ to obtain more extensive crosslinking of the molecular network.

The thermal behaviour of LS, LS-PU (formulation 5 in Table 5) and LS-PU-PEG (formulation 8 in Table 5) are different from each other (Figure 50a). Under inert atmosphere ($N_2$ flow), LS undergoes a first weight loss with a maximum loss at around 120 °C (Figure 50b), related to the release of moisture followed by the degradation of basic functional groups (around 330 °C, Figure 50b), such as sulphonic groups, and the release of low molecular mass products [312,314] giving rise to a quite high char content (41 %). LS- PU and LS-PEG-PU also undergo a first weight loss around 60–100 °C (Figure 50b) related mostly to the release of moisture. The degradation of PUs can usually be divided into two major stages. The first stage is dominated by the degradation of the hard segments, while the second stage is controlled by the soft segments (polyol) [360,404]. Regarding LS-PU, the first stage with a maximum weight loss at 335 °C is likely related to the decomposition of urethane moieties in the PU and other functional groups from LS, the second slow weight loss stage with a maximum weight loss at 550 °C was attributed to further structural rearrangements of pMDI and LS counterparts during char formation [410].

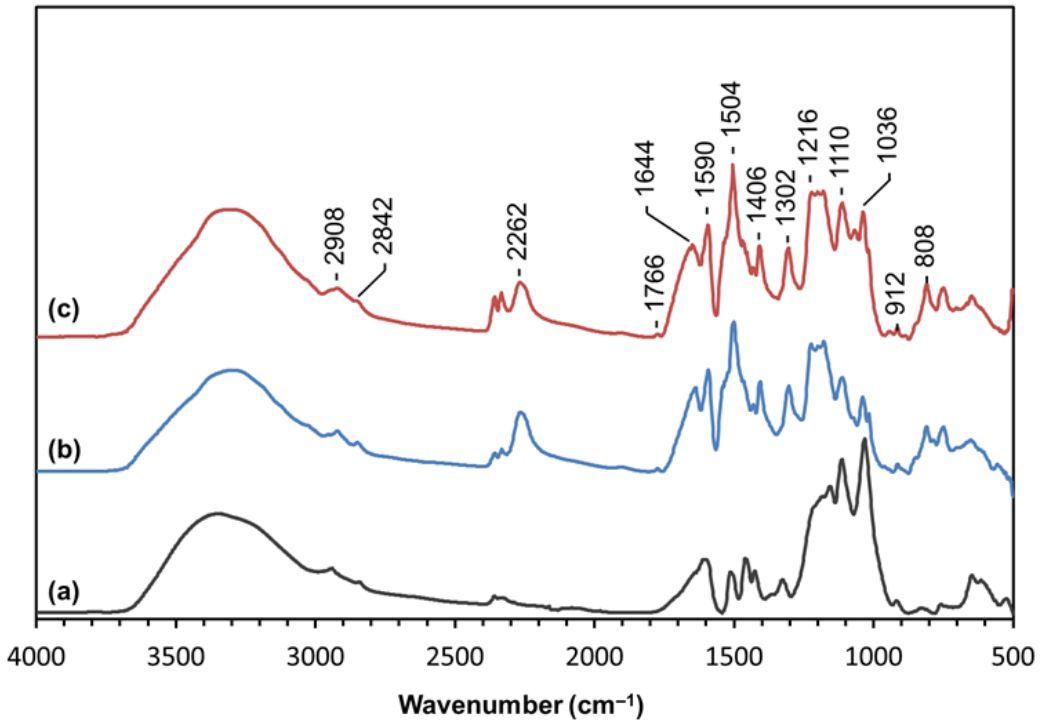


**Figure 49.** FTIR-ATR spectra of (a) LS, (b) LS-based PU adhesive (formulation 5 in Table 5), and (c) LS-based PU adhesive with $PEG_{200}$ (formulation 8 in Table 5).

**Table 19.** Assignments of the FTIR bands in the spectra of LS, LS-MDI and LS-MDI-PEG [51,303,306,308,414].

| Band ($cm^{-1}$) | Assignment |
|---|---|
| 3600-3200 | O-H stretching; N-H stretching (urethane group) |
| 2908/2842 | C-H stretching in $-CH_2-$, $-CH_3$ and $O-CH_3$ groups |
| 2262 | C-N stretching (isocyanate group) |
| 1766 | C=O stretching (urethane group) |
| 1644 | C=O stretching (isocyanate group) |
| 1590 | N-H deformation (isocyanate group), lignin aromatic groups |
| 1504 | N-H bending (urethane group), lignin aromatic groups |
| 1406 | C-N stretching in amide (urethane group) |
| 1302 | C-N stretching (urethane group) |
| 1216 | C-N stretching (urethane group) |
| 1036 | C-O stretching in aliphatic OH |
| 808 | C-H deformation out-of-plane, aromatic ring |

Regarding LS-PEG-PU, the first stage with a maximum weight loss at 330 °C is related to the decomposition of urethane groups and LS (similarly to LS-PU) but, in this case, the second stage appears as a shoulder around 450 °C in Figure 50b and is most probably

associated to the degradation of PEG [360]. Significantly higher residual char content in the thermal degradation of LS-PEG-PU than LS-PU (Figure 50a) is indicative of the much denser molecular structure of the former. This is in tune with FTIR analysis results that showed the eventual intensification of molecular crosslinking in LS-pMDI adhesive with addition of $PEG_{200}$ in the reaction system.

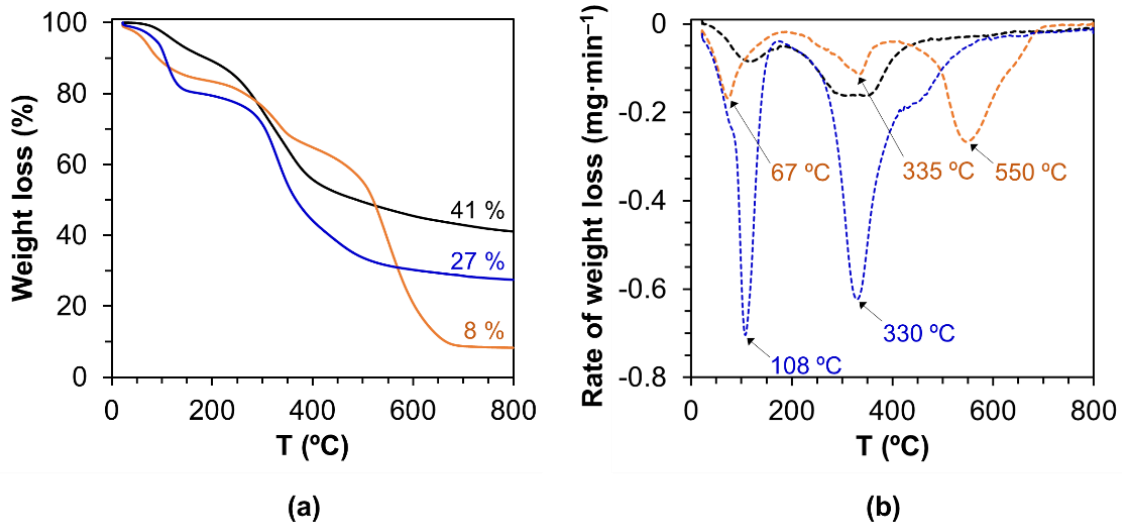


**Figure 50.** TGA curves of LS (— ---), LS-based PU without $PEG_{200}$ (formulation 5; — --- LS-PU), and LS-based PU containing $PEG_{200}$ (formulation 8; — --- LS-PEG-PU): (a) weight loss under inert $N_2$ gas flow and (b) derivative of the weight loss.

The curing of LS-based PU formulation with and without the addition of $PEG_{200}$ was studied by DMA analysis under non-isothermal conditions, as depicted in Figure 51-1a and Figure 51-1b. A post curing heating scan was carried out to assess the $T_g$ of both LS-based PU adhesives (Figure 51-2a and Figure 51-2b). For each PU formulation, a replica was prepared and analysed. It should be noted that the curves of the storage and loss modulus, *E*' and *E*'' respectively, are not shown due to the influence of the material pocket.

Concerning the curing process, in the tan $\delta$ profile the transition assigned to the PU curing starts around 60 °C for both types of LS-based PU formulations with and without $PEG_{200}$, *i.e.*, formulations 5 and 8 (Table 5), respectively. To study curing processes using DMA analysis, two points should be determined, the point of gelation (when the material changes from a viscous liquid to a viscoelastic solid, which is the *E*'–*E*'' crossover or where tan $\delta$ is equal to one) and the point of vitrification (when the curing system reaches such high

viscosity that limits further curing and the bulk reaction stops, commonly taken as the onset plateau of the storage modulus) [296]. However, in this case, this type of study could not be carried out since the *E*' and *E*'' curves couldn't be considered due to the use of the material pocket accessory. Still, some observations can be pointed out when comparing the DMA profile of each formulation with its respective replica. Taking into account that each formulation was replicated using exactly the same procedure, it is clear that the curing behaviour of two equal PU formulations does not match (the profile has some similarities but is still different). The only possible explanation for this occurrence is the mixing process after the addition of crosslinker pMDI and consequently the reagents diffusion. In the formulation without $PEG_{200}$, isocyanate groups react with water and OH groups in LS (most likely aliphatic OH groups in the $\gamma$–position [211]), while in the formulation with $PEG_{200}$, isocyanate groups react with water, OH groups in LS and OH groups from $PEG_{200}$. Reactions between the isocyanate groups with available OH groups depend mostly on the accessibility/reactivity of different OH groups and also on the efficiency of the mixing process and consequently diffusion. Therefore, due to the high apparent viscosity of the reaction mixture, it is possible that the mixing was not perfect enough and that crosslinking was different for the same formulation affecting the curing process. Furthermore, the addition of $PEG_{200}$ to the formulation also changed the curing profile compared to the one from the LS-based PU without $PEG_{200}$, increasing the temperature at which the curing process appears to be completed around 135–140 °C. Moreover, the broadening of tan $\delta$ peak for the system containing $PEG_{200}$ seems to be less pronounced indicating a more uniform crosslinked network.

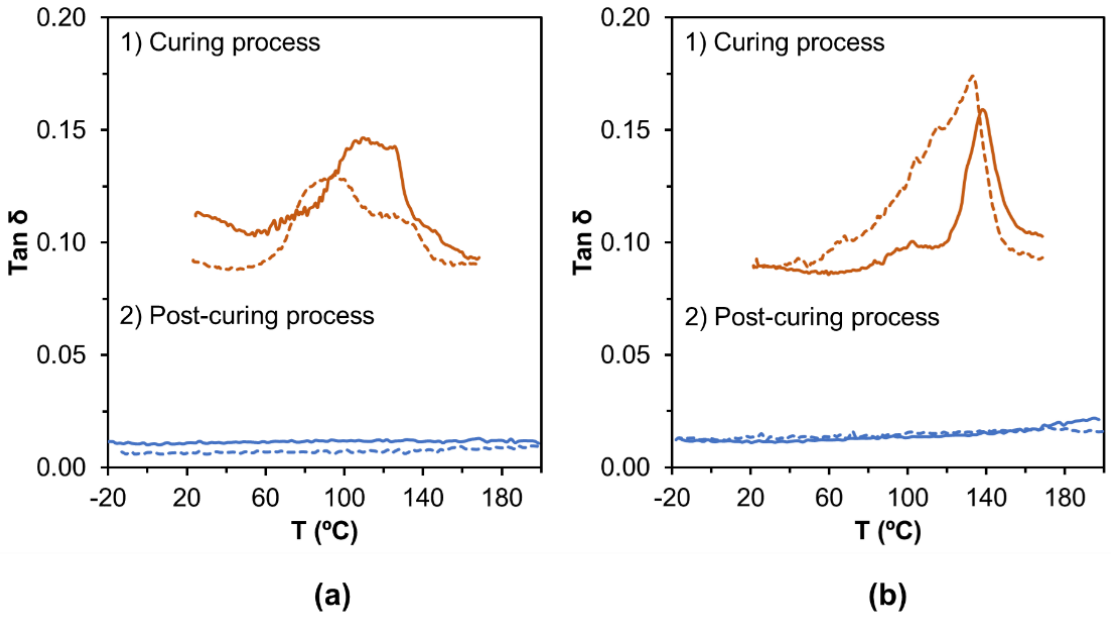


**Figure 51.** DMA profiles of (a) LS-based PU without $PEG_{200}$ (LS-PU) and (b) LS-based PU with $PEG_{200}$ (LS-PEG-PU).

Since DMA is much more sensitive to detect $T_g$ than other techniques, such as DSC, and can easily measure transitions that may not be apparent in other thermal methods [296], after the curing process, each material pocket containing the cured PU adhesive was cooled back to –20 °C and was used to perform a second DMA run to determine the $T_g$. Based on TGA analysis (Figure 50), this run was carried out only up to 200 °C to avoid potential thermal degradation of the products. Surprisingly, no $T_g$ was observed in any post-curing tan $\delta$ profile, which means that LS-based PU adhesives do not display clear softening behaviour in the temperature range between –20 and 200 °C. The values of $T_g$ are dependent on the lignin and PEG contents and usually increase with increasing weight fraction of lignin (stiff component) and decrease with increasing weight fraction of PEG (soft segment) [211,415]. Though most values reported in the literature (ranging from –40 to 105 °C [211,415]) were determined by DSC and values determined from DMA analysis can be higher than DSC's by 25 °C [296], some softening behaviour would be expected.

### 7.3.2. Evaluation of the adhesion strength of LS-based PU adhesives

It is known that an efficient wood adhesive must spread across the wood surface but also wet said surface to increase the contact area, *i.e.*, the interface. The goal is to develop

molecular interactions between the adhesive and wood. Therefore, a good adhesive wetting can produce an effective wood bonding. Yet, other parameters are also important such as efficient solidification of the adhesive to provide strength (in this case, through chemical curing) and sufficient deformability (related to the flexibility of the resulting adhesive due to the addition of $PEG_{200}$) of the cured adhesive to reduce stress [416]. ABES testing was performed to evaluate the strength of adhesion of the LS-based PU adhesives and to assess the effect of the $PEG_{200}$ amount on the adhesion results. Additionally, results were compared from those obtained when using commercial white glue (Figure 52). ABES testing measures the force under tension needed to break the adhesive bond and shear strength gives an indication of the strength of an adhesive. Therefore, the higher is the force needed to break the bond, the higher is the shear strength value. At first glance, all LS-based PU adhesives showed adhesion strengths somewhat lower or similar to those obtained using commercial white glue. This means that LS-based PUs displayed variable adhesive properties depending on the formulation composition, but still comparable to the commercial adhesive. Another fact is that the errors associated to each strength value are quite high. This was especially noticeable for the commercial white glue. Considering that one replica of each formulation was prepared, the results suggest that there are significant differences between replicas of the same formulation, as observed when performing DMA analysis (Figure 51), affecting crosslinking and thus the curing process and eventually the adhesion strength. Furthermore, for each formulation, a minimum of three sets of bonded strips were prepared and even within the same formulation, different strength values were obtained (yet, only concordant values were chosen and individual data are not shown). This indicates that, for the same formulation, the samples applied on the wood strip are different from one another, possibly due to poor reagents mixing. Furthermore, only 10 mg of adhesive was applied to the strip, which may not be fully representative of the entire product. It could be also suggested that comparing formulations containing 900 mg of pMDI with those containing 1000 mg of pMDI, strength values are quite similar. However, it appears that the strength values of formulations containing 1000 mg showed less variability than those of formulations containing 900 mg of pMDI. These results suggest that when the system comprise higher amounts of pMDI it is under kinetic control (higher reactivity, hence more reticulation) as opposed to diffusion control (which leads to higher heterogeneity, hence less reticulation) when lower amounts of pMDI are used. As expected, the best adhesion results were obtained

with the addition of 100 μL of $PEG_{200}$ as this polyol provides flexibility and promotes further crosslinking extension as discussed above.

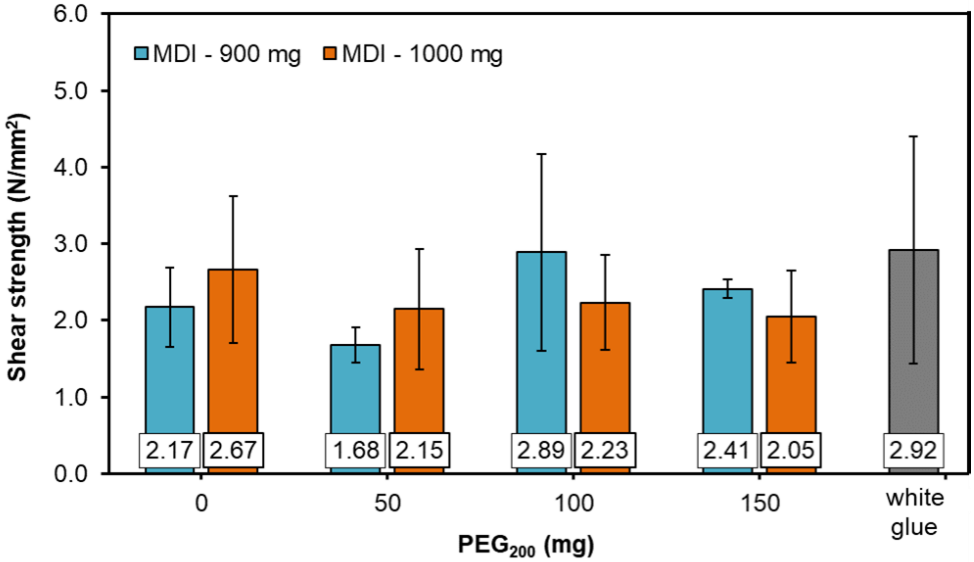


**Figure 52.** Shear strength values for each LS-based PU formulation as a function of the content of $PEG_{200}$ against the shear strength of commercial white glue (each value correspond to the average of a minimum of three values.

Indeed, in practice, when adhesives were prepared, formulations containing higher amount of pMDI and also containing $PEG_{200}$ were easier to homogenize. Overall, adhesion strength results showed significant effect of the variation in pMDI content and the amount of added $PEG_{200}$. This is not particularly surprising since, as suggested by Thring and co-workers [417], the chain length of $PEG_{200}$ may be too short to bridge in the network due to steric hindrance from the chemical structure of lignin. Therefore, a balance must be found between the lignin content and $PEG_{200}$ since lignin-derived PU materials produced using $PEG_{200}$ are either too weak at low lignin content, or too brittle at higher amounts of lignin. In this case, it is possible that PEG with higher molecular weight could have provided different adhesion behaviour.

It is noteworthy that when performing ABES testing, the way adhesive bonding breaks is extremely important. Figure 53 depicts some photographs of the bonding areas of some wood strips after ABES testing. Since the main objective of ABES testing is to determine the adhesive strength, the adhesive failure must occur within the adhesive (as it is shown by

green circles when adhesive remained in both strips), but not adhesive failure with adhesion to the substrate (as it is shown by yellow circles when the adhesive was transferred to one of the strips due to adhesion failure between adhesive and substrate). Additionally, substrate failure (red circles) should not occur neither though, when it does, it means that the strength of the adhesive is too high [418]. Based on the results obtained, the occurrence of adhesion failure to the substrate suggests that the LS-based PU adhesive did not sufficiently wet the strip surface. Adhesives must flow to the surface of the wood and penetrate the entire tissue of the wood so that intermolecular interactions (strong covalent bonds and/or mechanical locking) between the adhesive and the wood can occur [416]. In fact, all adhesives lacked sufficient fluidity and low viscosity to be sufficiently absorbed by the wood strip. In addition, the bonding failure of the adhesives was very irregular confirming the lack of homogeneity in the composition of each LS-based PU formulation. In practice, optimization of the adhesive composition in relation to the bonded substrate is still required.

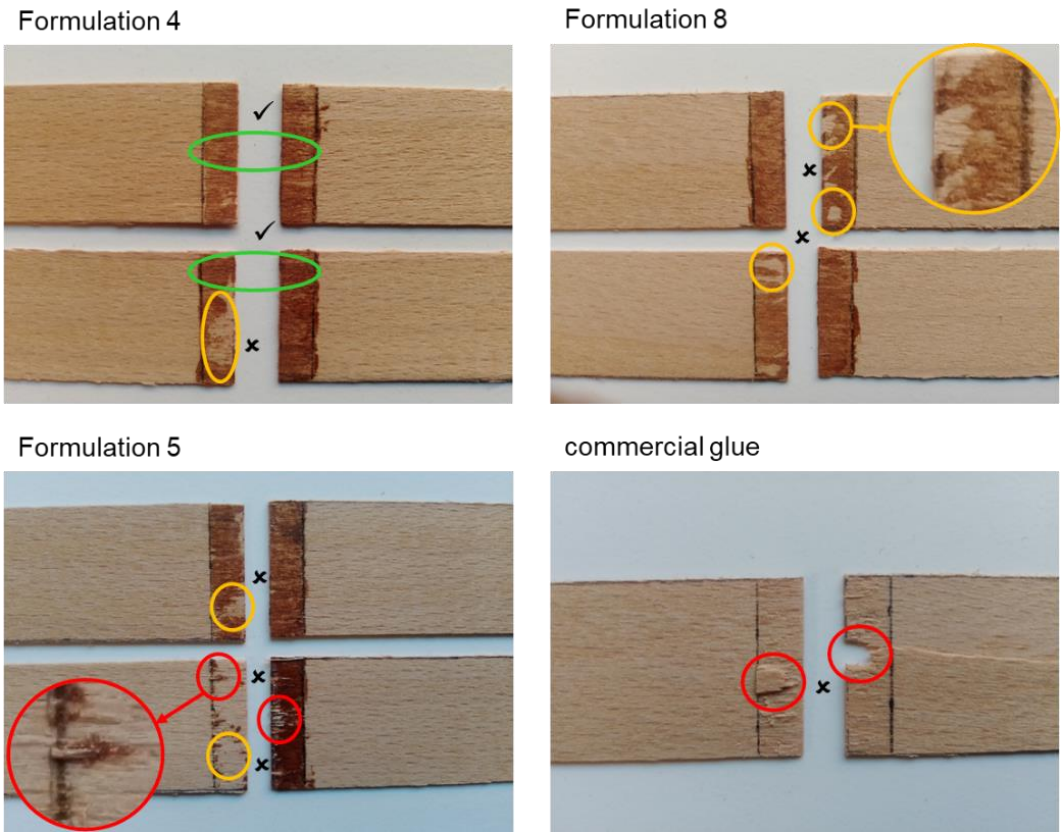


**Figure 53.** Photographs of selected veneer strips after ABES testing showing different types of failure (O Adhesion failure within the adhesive – good result ✓; O Adhesion failure to the substrate – failed result ×; and O substrate failure – failed result ×).

### 7.3.3. Kinetic study of the curing process of LS-based PU adhesive containing soft segment $PEG_{200}$

The study of the curing process is highly important in the industry as it is a complementary analysis tool that provides additional understanding on the mechanism of curing reaction, in order to control and optimize the curing process. Therefore, the cure of LS-$PEG_{200}$(150)-PU (formulation 8 in Table 5), which is the most promising and flexible adhesive, was studied using non-isothermal DSC. The plots of the degree of cure (conversion, $\alpha$) and the rate of heat generated ($d\alpha \cdot dT^{-1}$) at different heating rates ($\beta$) as a function of the temperature ($T$) are depicted in Figure 54. As expected [404,419], the conversion rate increased up to a maximum value and then decreased indicating that the free volume between the macromolecules allows molecular movement during the curing process up to 70 to 80 % of conversion but beyond crosslinks start to break down. Furthermore, peaks shifted towards higher temperatures as $\beta$ increased. As the temperature increased, α also increased up to 1 (maximum degree of conversion) slowly at the initial curing stage and then more abruptly at the end. The S-shaped curves confirmed that the reaction only starts after a certain temperature is achieved and this occurrence is in agreement with the literature [404,420].

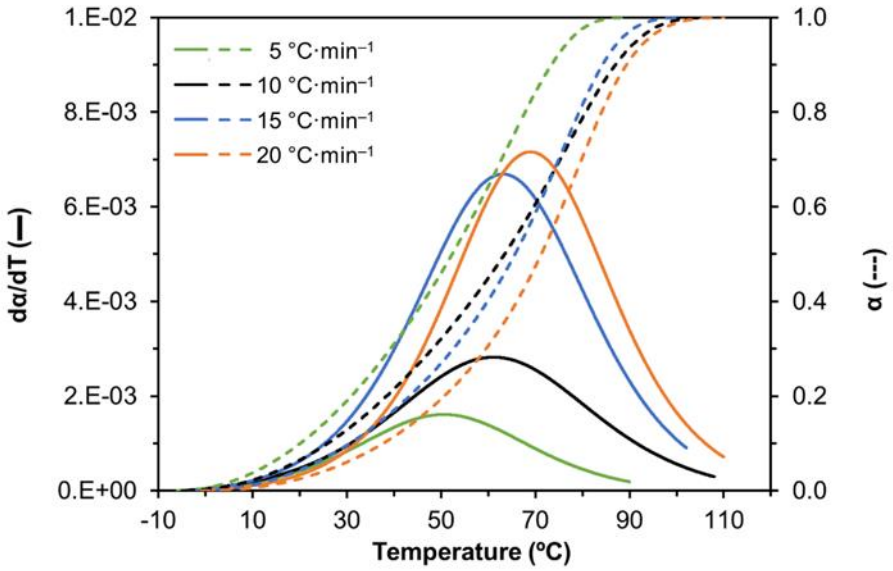


**Figure 54.** Effect of heating rate on the cure of LS-based PU containing 150 µL $PEG_{200}$ (formulation 8, Table 5).

Next, the $E_a$ of the curing process of LS-based PU containing $PEG_{200}$ (150 µL) was determined using the Kissinger and the Ozawa methods, and the corresponding plots are depicted in Figure 55. From the slopes of each linear plot, $E_a$ was 65.2 and 70.7 $kJ \cdot mol^{-1}$, for the Kissinger and Ozawa methods, respectively. The value of $E_a$ for the Ozawa method is higher than the one for the Kissinger method due to approximations performed in the Ozawa method, which is in agreement with the literature data [404,421].

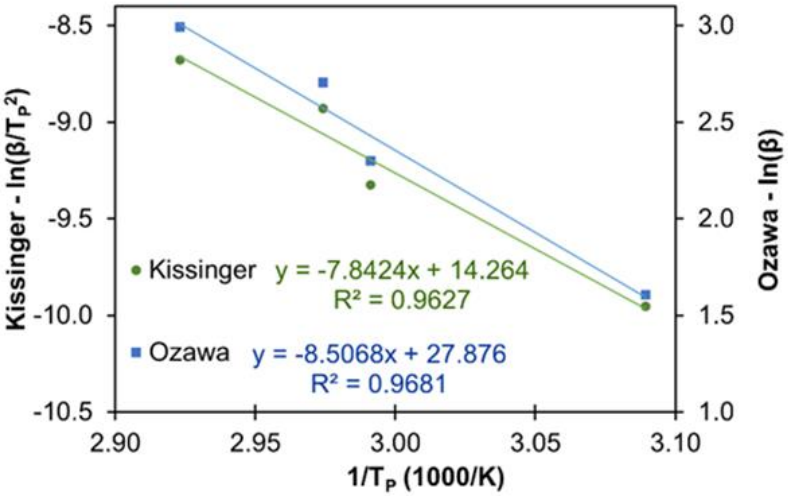


**Figure 55.** Kissinger and Ozawa plots for the determination of the $E_a$ for the curing process of LS-based PU containing 150 µL $PEG_{200}$ (formulation 8, Table 5).

Since $E_a$ is not constant and varies with α, the Kissinger and the Ozawa methods can be used to determine the $E_a$ throughout the entire cure reaction [404,419–421]. Therefore, the resulting Kissinger and Ozawa plots are presented in Figure 56 including the respective equations for the different α, which are listed in Table 20. The $E_a$ calculated for different extends of reaction using the Kissinger and the Ozawa methods are shown in Figure 57. The trend observed is in agreement with that registered in a previous study regarding the variation of $E_a$ throughout the curing process of a castor oil based PU [404]. As suggested in that study, the increase in $E_a$ at lower α values (from α = 0.1 to 0.7) can be attributed to the crosslinking within the PU network while the slight decrease in $E_a$ at higher α values can be attributed to the breaking of crosslinks resulting in increasing chain flexibility. This type of behaviour was also observed for epoxy resins [421].

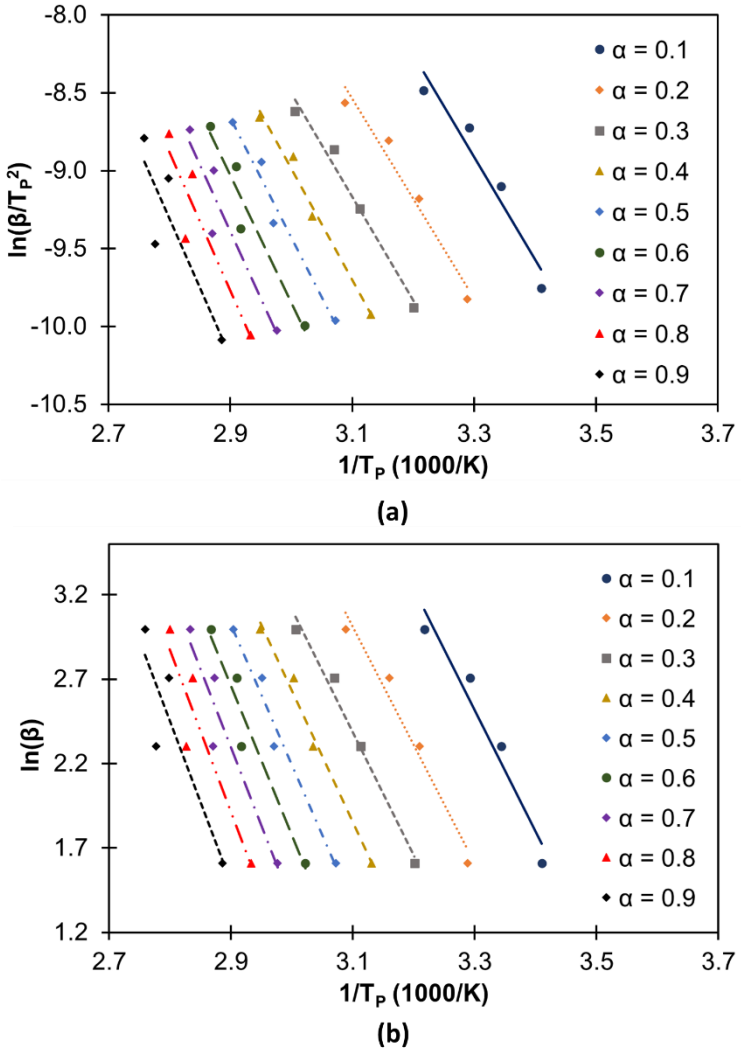


**Figure 56.** Determination of Ea using (a) the Kissinger and (b) the Ozawa methods for the curing process of LS-based PU containing $PEG_{200}$ (150 μL).

**Table 20.** Kissinger and Ozawa equations from plots in **Figure 56**.

| α | Kissinger | | Ozawa | |
|---|---|---|---|---|
| | Equation | $R^2$ | Equation | $R^2$ |
| 0.1 | y = –6.582x + 12.811 | 0.940 | y = –7.186x + 26.232 | 0.950 |
| 0.2 | y = –6.395x + 11.283 | 0.962 | y = –7.022x + 24.780 | 0.969 |
| 0.3 | y = –6.643x + 11.424 | 0.980 | y = –7.287x + 24.974 | 0.983 |
| 0.4 | y = –7.122x + 12.378 | 0.983 | y = –7.779x + 25.968 | 0.986 |
| 0.5 | y = –7.677x + 13.604 | 0.967 | y = –8.346x + 27.228 | 0.972 |
| 0.6 | y = –8.186x + 14.712 | 0.934 | y = –8.864x + 28.365 | 0.943 |
| 0.7 | y = –8.599x + 15.545 | 0.889 | y = –9.286x + 29.224 | 0.903 |
| 0.8 | y = –8.879x + 15.979 | 0.839 | y = –9.576x + 29.686 | 0.858 |
| 0.9 | y = –8.845x + 15.459 | 0.773 | y = –9.552x + 29.197 | 0.799 |

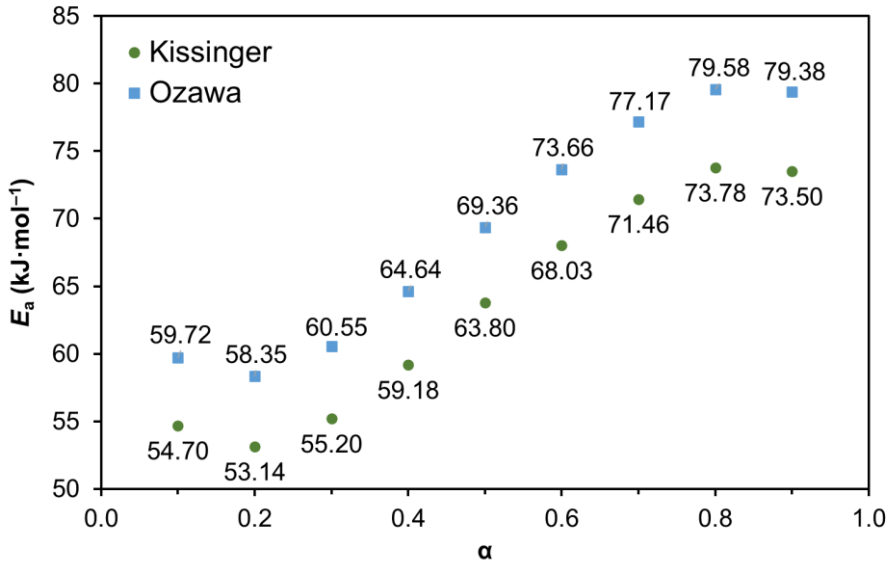


**Figure 57.** Plots representing the dependence of $E_a$ with α using the Kissinger and the Ozawa methods.

## 7.4 CONCLUSIONS

The results of this study demonstrate the possibility of using hardwood lignosulphonates as macropolyols in polyurethane formulations suitable for adhesive purposes. Due to some limitations in the accessibility/reactivity of hydroxyl groups in lignosulphonate (LS) in the reaction with 4'-methylene diphenyl diisocyanate (pMDI) and difficulties in effective homogenization of the reaction mixture, the addition of polyethylene glycol diol of low molecular weight ($M_w$ 200, $PEG_{200}$) seems to be advantageous to overcome, at least partially, these drawbacks. The important role of $PEG_{200}$ in the consolidation of LS-based PU network via crosslinking reactions with pMDI has been demonstrated. It was also suggested that the addition of $PEG_{200}$ in the LS-pMDI reaction mixture favoured the interfacial interaction between the LS-based PU adhesive and the glued material (wood strips). The adhesion strength of LS-based PU was comparable to the commercial white glue. The curing kinetics of LS-based PU adhesive with addition of $PEG_{200}$ showed similar trend to those observed previously with other PU formulations. The activation energy determined is within the range of 60-70 kJ·mol$^{-1}$ depending the applied methodology. The next step would be to study the use of unrefined spent liquor for the same purpose.

# 8. Conclusions and future perspectives

## 8.1 FINAL REMARKS

The rising awareness of climate change and scarcity of fossil resources has drawn attention to the relevance of the biorefinery concept worldwide and as a result of this to the potential of renewable materials. It is known that technical lignins can be functionalized and directed to various applications as dispersants, adhesives, plastics, resins, conducting polymeric composites, among many others. Since most of the current industrial applications depend on the good water-solubility of technical lignins, world lignin market is largely restricted to lignosulphonates (LS), therefore their marketing and consequent profit is guaranteed. Still, the possibility of increasing the company profits with the valorization of LS, through the production of value-added products for different market applications is highly motivating.

Due to the re-profiling of the acidic sulphite process at CAIMA company in the last years, the primary study was required to evaluate the chemical composition of thin (SSL) and thick (THSL) sulphite spent liquors from the production of dissolving pulp and the structural features of dissolved lignosulphonates (LS). The results suggest that the current SSL and THSL maintained similar features to those from the production of paper-grade pulp and that the harsher conditions of the modified cooking process for dissolving pulp production affected moderately the main structural features of the ensuing LS. In particular, the molecular weight of LS was increased by about 50% and almost doubled the amount of phenolic and sulfonic acid groups, although the degree of condensation of LS has also increased by almost 25%. In general, considering the possible applications of LS, the changes detected in its composition and structure due to the modification of cooking are not critical and can be potentially advantageous for the production of polymeric formulations based on LS.

Another goal of this study was to improve LS dispersion efficiency for concrete formulations with the ultimate aim of substituting (partially or even fully) commercial petroleum-based superplasticizers, such as polycarboxylates. Therefore, different chemical modification strategies were used to achieve this purpose. The first approach consisted of increasing the molecular weight of LS through laccase-catalyzed oxidative polymerization, which yielded a modified LS with increased $M_w$ (11-fold from initial $M_w$ of LS) and some structural changes (such as decreased of the S/G ratio compared to unmodified LS). Other

strategies were also employed, such as POM-mediated laccase modification of LS, which did not significantly change the LS structure, and glyoxalation and RAFT polymerization, both of which turned out to be unsuccessful. Finally, the synthesis of LS-based non-ionic polymeric dispersants, when using epoxidized oligomer derivatives of PPG yielded the targeted enhanced dispersant properties. Although the molecular weight of this product increased only slightly, it was the only product exhibiting relevant enhanced dispersant efficiency compared to unmodified LS and the other modified LS. This behaviour was not as relevant as the dispersion efficiency of the commercial petroleum-based superplasticizers used for comparison. Yet, the results suggest that this study is well on the way to obtaining improved dispersants from LS. While the dispersion mechanism of LS is related with electrostatic repulsion, it is possible that the dispersion mechanism of PPG-modified LS might involve electrostatic repulsions along with steric hindrance (just like for polycarboxylates).

The development of conducting polymeric formulations resulted in the preparation of all-solid-state potentiometric chemical sensors for the detection of transition metals in aqueous solutions. For this purpose, LS-based polyurethane (PU) flexible membranes doped with different amounts of MWCNTs were synthesised. The LS-based composite containing 1 % w/w MWCNTs displayed relevant electrical conductivity being suitable for sensing applications. These sensors showed sensitivity to a series of transition metals, such as Cu(II), Zn(II), Cd(II), Cr(III), Cr(VI), Hg(II), and Ag(I) at pH 7, exhibited a response to the Cr(VI)/Cr(III) redox pair at pH 2 and a weak but not negligible response toward ionic liquids, [$C_2$mim]Cl and ChCl. The results suggested that the response is highly dependent on the type of lignin used (including the wood source and pulping conditions). Other carbon nanofillers, such as graphene oxide, reduced graphene oxide and graphite, were also studied. However, none of the ensuing composites displayed electrical conductivity probably due to the lack of a continuous conductive network within the polymer matrix.

Finally, the unmodified LS was used as macropolyol in PU formulations for adhesive purposes. Due to some limitations in the accessibility/reactivity of hydroxyl groups in LS in the reaction with pMDI and difficulties in effective homogenization of the reaction mixture, the addition of PEG with low molecular weight ($M_w$ 200, $PEG_{200}$) seems to be advantageous to overcome, at least partially, these drawbacks. The results suggested that the addition of $PEG_{200}$ in the LS-pMDI reaction mixture favoured the interfacial interaction between the

LS-based PU adhesive and the glued material (wood strips). The adhesion strength of LS-based PU was comparable to a commercial white glue. Since the final properties of an adhesive material are highly dependent on the control of the curing process, the kinetic parameters of the curing process were assessed for the most promising adhesive formulation using the Kissinger and the Ozawa methods by non-isothermal differential scanning calorimetry. It was concluded that the curing process follows a similar trend to that observed with other PU formulations and that the activation energy is within the range of 60-70 $kJ \cdot mol^{-1}$ depending on the applied method.

In conclusion, this thesis demonstrated the potential of using eucalypt LS, an abundant biodegradable renewable resource for the production of value-added products such as polymeric formulations for different applications.

## 8.2 FUTURE PERSPECTIVES

As previously mentioned, the main goal of this thesis was the valorization of eucalypt LS towards new added-value products to expand the economic profits of the pulp industry within the scope of biorefinery and circular economy concepts. Considering the studies presented above, further work can still be performed to complement the results:

1) Considering the enhanced dispersion efficiency of the obtained PPG-modified LS materials for concrete formulations, it would be interesting to study other types of functionalised oligomers of different molecular weight reactive with LS in aqueous solutions, such as PEG/PPG monoglycidyl ether derivatives or water-soluble polysiloxane derivatives. The further study on the dispersion mechanisms of cement particles using promising LS-based dispersants would be desirable.
2) Regarding the preparation of potentiometric sensors, it would be interesting to investigate the sensitivity of LS-based conducting composites to different classes of potentially hazardous compounds for their reliable detection in solutions. The evaluation of conducting polymeric membranes in fuel cell assembles would be another interesting topic.
3) Concerning the synthesis of LS-based PU adhesives, it would be worth to investigate the effect of using other polyols as soft segments, such as PEGs with molecular weight

higher than 200 and other bio-based polyols (*e.g.*, castor oil). Also, to reduce costs associated with LS purification, industrial sulphite spent liquor should be tested as macropolyols (instead of purified LS) to prepare the most promising adhesive formulations and their adhesion strength determined. Other types of PU adhesives can also be prepared such as non-isocyanate PUs as well as completely different adhesives, namely formaldehyde-free phenolic resins using LS as a replacement of phenol (with and without modification).

In brief, the results obtained from this thesis have opened new avenues to be followed towards the production of high-added value materials within the circular economy concept. Nevertheless, life cycle and cost analyses will be crucial for further progress.

# 9. References

# 9. References


1. FAO. *FAO Yearbook of Forest Products 2019*; Rome, 2021; ISBN 9789251341186.
2. Bajwa, D.S.; Pourhashem, G.; Ullah, A.H.; Bajwa, S.G. A concise review of current lignin production, applications, products and their environment impact. *Ind. Crops Prod.* **2019**, *139*, 111526, doi:10.1016/j.indcrop.2019.111526.
3. Kalogiannis, K.G.; Matsakas, L.; Lappas, A.A.; Rova, U.; Christakopoulos, P. Aromatics from beechwood organosolv lignin through thermal and catalytic pyrolysis. *Energies* **2019**, *12*, 1606, doi:10.3390/en12091606.
4. Caima Indústria de Celulose. Negócio - Pasta Solúvel. http://www.caima.pt/pt/negocio/pasta-soluvel (accessed on 26/05/2021).
5. Sjöström, E. *Wood chemistry. Fundamentals and applications*; 2nd ed.; Academic Press Inc.: London, 1993; ISBN 0126474818.
6. Sjöström, E.; Westermark, U. Chemical Composition of Wood and Pulps: Basic Constituents and Their Distribution. In *Analytical methods in wood chemistry, pulping, and papermaking*; Sjöström, E., Alén, R., Eds.; Springer-Verlag: Berlin Heidelberg, 1999; pp. 1–19 ISBN 3-540-63102-X.
7. Neiva, D.; Fernandes, L.; Araújo, S.; Lourenço, A.; Gominho, J.; Simões, R.; Pereira, H. Chemical composition and kraft pulping potential of 12 eucalypt species. *Ind. Crops Prod.* **2015**, *66*, 389–95, doi:10.1016/j.indcrop.2014.12.016.
8. Pinto, P.C.O.R. PhD Thesis. Influência da estrutura química dos componentes da madeira no seu desempenho nos processos de produção de pastas celulósicas. Estudo comparativo entre Eucalyptus globulus e outras folhosas, University of Aveiro, 2005.
9. Miranda, I.; Pereira, H. Variation of pulpwood quality with provenances and site in Eucalyptus globulus. *Ann. For. Sci.* **2002**, *59*, 283–291, doi:10.1051/forest.
10. Pereira, H. Variability in the chemical composition of plantation eucalyptus (Eucalyptus globuls Labill.). *Wood fiber Sci.* **1988**, *20*, 82–90.
11. Crowther, T.W.; Glick, H.B.; Covey, K.R.; Bettigole, C.; Maynard, D.S.; Thomas, S.M.; Smith, J.R.; Hintler, G.; Duguid, M.C.; Amatulli, G.; et al. Mapping tree density at a global scale. *Nature* **2015**, *525*, 201–205, doi:10.1038/nature14967.
12. Budnyak, T.M.; Slabon, A.; Sipponen, M.H. Lignin–Inorganic Interfaces: Chemistry and Applications from Adsorbents to Catalysts and Energy Storage Materials. *ChemSusChem* **2020**, doi:10.1002/cssc.202000216.
13. Grand View Research Inc. Lignin Market - Forecasts from 2020 to 2027 - Sample report. https://www.grandviewresearch.com/press-release/global-lignin-market (accessed on 25/05/2021).
14. Aro, T.; Fatehi, P. Production and Application of Lignosulfonates and Sulfonated Lignin. *ChemSusChem* **2017**, *10*, 1861–1877, doi:10.1002/cssc.201700082.
15. Buranov, A.U.; Mazza, G. Lignin in straw of herbaceous crops. *Ind. Crops Prod.* **2008**, *28*, 237–259, doi:10.1016/j.indcrop.2008.03.008.
16. Guragain, Y.N.; Herrera, A.I.; Vadlani, P. V.; Prakash, O. Lignins of bioenergy crops: A review. *Nat. Prod. Commun.* **2015**, *10*, 201–208, doi:10.1177/1934578x1501000141.
17. Ragauskas, A.J.; Beckham, G.T.; Biddy, M.J.; Chandra, R.; Chen, F.; Davis, M.F.; Davison, B.H.; Dixon, R.A.; Gilna, P.; Keller, M.; et al. Lignin valorization: Improving lignin processing in the biorefinery. *Science (80-. ).* **2014**, *344*, 1246843-(1-10), doi:10.1126/science.1246843.
18. Calvo-Flores, F.G. Lignin: A Renewable Raw Material. *Encycl. Renew. Sustain. Mater.* **2020**,

1–20, doi:10.1016/b978-0-12-803581-8.11517-6.

19. Boerjan, W.; Ralph, J.; Baucher, M. Lignin Biosynthesis. *Annu. Rev. Plant Biol.* **2003**, *54*, 519–546, doi:10.1146/annurev.arplant.54.031902.134938.

20. Gellerstedt, G.; Henriksson, G. Lignins: major sources, structure and properties. In *Monomers, Polymers and Composites from Renewable Resources*; Belgacem, M.N., Gandini, A., Eds.; Elsevier: Amsterdem, 2008; pp. 201–224 ISBN 9780080453163.

21. Lawoko, M.; Henriksson, G.; Gellerstedt, G. Characterisation of lignin-carbohydrate complexes (LCCs) of spruce wood (Picea abies L.) isolated with two methods. *Holzforschung* **2006**, *60*, 156–161, doi:10.1515/HF.2006.025.

22. Zikeli, F.; Ters, T.; Fackler, K.; Srebotnik, E.; Li, J. Wheat straw lignin fractionation and characterization as lignin-carbohydrate complexes. *Ind. Crops Prod.* **2016**, *85*, 309–317, doi:10.1016/j.indcrop.2016.03.012.

23. Kubo, S.; Kadla, J.F. Hydrogen bonding in lignin: A fourier transform infrared model compound study. *Biomacromolecules* **2005**, *6*, 2815–2821, doi:10.1021/bm050288q.

24. Marques, A.P.; Evtuguin, D. V.; Magina, S.; Amado, F.M.L.; Prates, A. Structure of Lignosulphonates from Acidic Magnesium-Based Sulphite Pulping of Eucalyptus globulus. *J. Wood Chem. Technol.* **2009**, *29*, 337–357, doi:10.1080/02773810903207762.

25. Constant, S.; Wienk, H.L.J.; Frissen, A.E.; Peinder, P. de; Boelens, R.; van Es, D.S.; Grisel, R.J.H.; Weckhuysen, B.M.; Huijgen, W.J.J.; Gosselink, R.J.A.; et al. New insights into the structure and composition of technical lignins: a comparative characterisation study. *Green Chem.* **2016**, *18*, 2651–2665, doi:10.1039/C5GC03043A.

26. Gandini, A.; Belgacem, M.N. Lignins as Components of Macromolecular Materials. In *Monomers, Polymers and Composites from Renewable Resources*; Belgacem, M.N., Gandini, A., Eds.; Elsevier Ltd., 2008; pp. 243–271 ISBN 9780080453163.

27. Lora, J. Industrial Commercial Lignins: Sources, Properties and Applications. In *Monomers, Polymers and Composites from Renewable Resources*; Belgacem, M.N., Gandini, A., Eds.; Elsevier: Oxford, 2008 ISBN 9780080453163.

28. Gabbott, P. A Practical Introduction to Differential Scanning Calorimetry. In *Principles and Applications of Thermal Analysis*; Gabbott, P., Ed.; Blackwell Publishing, 2008; pp. 1–50 ISBN 9781405131711.

29. Dimmel, D. Overview. In *Lignin and lignans: advances in chemistry*; Heitner, C., Dimmel, D., Schmidt, J.A., Eds.; CRC Press Taylor and Francis Group, LLC: Boca Raton, FL, 2010; pp. 1–10 ISBN 9781574444865.

30. Balakshin, M.; Capanema, E. On the quantification of lignin hydroxyl groups with 31P and 13C NMR spectroscopy. *J. Wood Chem. Technol.* **2015**, *35*, 220–237, doi:10.1080/02773813.2014.928328.

31. Melro, E.; Filipe, A.; Sousa, D.; Medronho, B.; Romano, A. Revisiting lignin: A tour through its structural features, characterization methods and applications. *New J. Chem.* **2021**, *45*, 6986–7013, doi:10.1039/d0nj06234k.

32. Ralph, J.; Landucci, L.L. NMR of Lignins. In *Lignin and lignans : advances in chemistry*; Heitner, C., Dimmel, D.R., Schmidt, J.A., Eds.; CRC Press Taylor and Francis Group, LLC: Boca Raton, FL, 2010; pp. 137–243 ISBN 9781574444865.

33. Zakis, G.F. *Functional Analysis of Lignins and Their Derivatives*; Tappi Press: Atlanta, 1991;

34. *Methods in lignin chemistry*; Lin, S.Y., Dence, C.W., Eds.; Springer-Verlag: Berlin Heidelberg, 1992; ISBN 9783540261230.

35. Evtuguin, D. V; Amado, F.M.L. Application of Electrospray Ionization Mass Spectrometry to the Elucidation of the Primary Structure of Lignin. *Macromol. Biosci.* **2003**, *3*, 339–343, doi:10.1002/mabi.200350006.

36. Brunow, G.; Lundquist, K.; Gellerstedt, G. Lignin. In *Analytical Methods in Wood Chemistry, Pulping and Papermaking*; Sjöström, E., Alén, R., Eds.; Springer-Verlag: Berlin Heidelberg, 1999; pp. 77–124 ISBN 3-540-63102-X.

37. Sun, R.C. Lignin Source and Structural Characterization. *ChemSusChem* **2020**, *13*, 4385–4393, doi:10.1002/cssc.202001324.

38. Hänninen, T.; Tukiainen, P.; Svedström, K.; Serimaa, R.; Saranpää, P.; Kontturi, E.; Hughes, M.; Vuorinen, T. Ultrastructural evaluation of compression wood-like properties of common juniper (Juniperus communis L.). *Holzforschung* **2012**, *66*, 389–395, doi:10.1515/hf.2011.166.

39. Olsson, A.-M.; Salmén, L. The effect of lignin composition on the viscoelastic properties of wood. *Nord. Pulp Pap. Resour. J.* **1997**, *12*, 140–144, doi:10.3183/NPPRJ-1997-12-03-p140-144.

40. Ucar, M.B. A comparative study on the chemical composition of the oriental spruce woods Picea orientalis from planted and natural forests. *Chem. Nat. Compd.* **2005**, *41*, 494–498, doi:10.1007/s10600-005-0191-y.

41. Hafizoğlu, H.; Usta, M. Chemical composition of coniferous wood species occurring in Turkey. *Holz als Roh - und Werkst.* **2005**, *63*, 83–85, doi:10.1007/s00107-004-0539-1.

42. Smelstorius, J.A. Chemical Composition of Wood of Australian-Grown Pinus radiata D. Don. I. Extraneous Substances, Lignin and the Summative Analysis. *Holzforschung* **1971**, *25*, 33–39.

43. Pettersen, R.C. The Chemical Composition of Wood. In *The Chemistry of Solid Wood*; Rowell, R., Ed.; ACS Advances in Chemistry Series; American Chemical Society: Washington, DC, 1984; pp. 57–126 ISBN 0-8412-0796-8.

44. Pinto, P.C.; Evtuguin, D. V.; Neto, C.P. Chemical composition and structural features of the macromolecular components of plantation Acacia mangium wood. *J. Agric. Food Chem.* **2005**, *53*, 7856–7862, doi:10.1021/jf058081b.

45. Nguyen, Q.N.; Cloutier, A.; Achim, A.; Stevanovic, T. Fuel properties of sugar maple and yellow birch wood in relation with tree vigor. *BioResources* **2016**, *11*, 3275–3288, doi:10.15376/biores.11.2.3275-3288.

46. del Río, J.C.; Rodríguez, I.M.; Gutiérrez, A. Chemical characterization of fibers from herbaceous plants commonly used for manufacturing of high quality paper pulps. In Proceedings of the 9th European Workshop on Lignocellulosics and Pulp (EWLP); Vienna, Austria, 2006; pp. 109–112.

47. Li, T.; Takkellapati, S. The current and emerging sources of technical lignins and their applications. *Biofuels, Bioprod. Biorefining* **2018**, *12*, 756–787, doi:10.1002/bbb.1913.

48. Ekielski, A.; Mishra, P.K. Lignin for bioeconomy: The present and future role of technical lignin. *Int. J. Mol. Sci.* **2021**, *22*, 1–24, doi:10.3390/ijms22010063.

49. Evtuguin, D. V. Sulphite Pulping. In *Lignocellulosic Fibers and Wood Handbook: Renewable Materials for Today's Environment*; Belgacem, N., Pizzi, A., Eds.; Scrivener Publishing LLC: Hoboken, NJ, USA, 2016; pp. 225–244 ISBN 9781118773727.

50. Sixta, H.; Potthast, A.; Krotschek, A.W. Chemical Pulping Processes. In *Handbook of Pulp*; Sixta, H., Ed.; WILEY-VCH Verlag GmbH & Co.: Weinheim, 2006; pp. 109–509 ISBN

9783527309993.

51. Marques, A.P.; Evtuguin, D. V.; Magina, S.; Amado, F.M.L.; Prates, A. Chemical Composition of Spent Liquors from Acidic Magnesium–Based Sulphite Pulping of Eucalyptus globulus. *J. Wood Chem. Technol.* **2009**, *29*, 322–336, doi:10.1080/02773810903207754.

52. Gellerstedt, G.; Gierer, J. The reactions of lignin during acidic sulphite pulping. *Sven. Papperstidning* **1971**, *74*, 117–127.

53. Gellerstedt, G. The reactions of lignin during sulfite pulping. *Sven. Papperstidning* **1976**, *79*, 537–543.

54. Gierer, J. The Chemistry of Delignification. A General Concept. *Holzforschung* **1982**, *36*, 43–51, doi:10.1515/hfsg.1982.36.1.43.

55. Glennie, D.W. Reactions in sufite pulping. In *Lignins Occurrence, Formation, Structure and Reactions*; Sarkanen, K.V., Ludwig, C.H., Eds.; Wiley Interscience: New York, 1971; pp. 597–637.

56. Ekeberg, D.; Gretland, K.S.; Gustafsson, J.; Bråten, S.M.; Fredheim, G.E. Characterisation of lignosulphonates and kraft lignin by hydrophobic interaction chromatography. *Anal. Chim. Acta* **2006**, *565*, 121–128, doi:10.1016/j.aca.2006.02.008.

57. Xavier, A.M.R.B.; Correia, M.F.; Pereira, S.R.; Evtuguin, D. V. Second-generation bioethanol from eucalypt sulphite spent liquor. *Bioresour. Technol.* **2010**, *101*, 2755–2761, doi:10.1016/j.biortech.2009.11.092.

58. Pereira, S.R.; Portugal-Nunes, D.J.; Evtuguin, D. V.; Serafim, L.S.; Xavier, A.M.R.B. Advances in ethanol production from hardwood spent sulphite liquors. *Process Biochem.* **2013**, *48*, 272–282, doi:10.1016/j.procbio.2012.12.004.

59. Fatehi, P.; Ni, Y. Integrated forest biorefinery - Sulfite process. In *Sustainable Production of Fuels, Chemicals, and Fibers from Forest Biomass (ACS Symposium Series)*; Zhu, J., Zhang, X., Pan, X., Eds.; American Chemical Society: Washington, DC, 2011; Vol. 1067, pp. 409–441 ISBN 9780841226432.

60. Restolho, J.A.; Prates, A.; de Pinho, M.N.; Afonso, M.D. Sugars and lignosulphonates recovery from eucalyptus spent sulphite liquor by membrane processes. *Biomass and Bioenergy* **2009**, *33*, 1558–1566, doi:10.1016/j.biombioe.2009.07.022.

61. Fernandes, D.L.A.; Silva, C.M.; Xavier, A.M.R.B.; Evtuguin, D. V. Fractionation of sulphite spent liquor for biochemical processing using ion exchange resins. *J. Biotechnol.* **2012**, *162*, 415–421, doi:10.1016/j.jbiotec.2012.03.013.

62. Holladay, J.E.; White, J.F.; Bozell, J.J.; Johnson, D. *Report PNNL-16983. Top Value-Added Chemicals from Biomass Volume II - Results of Screening for Potential Candidates from Biorefinery Lignin*; Richland WA, 2007;

63. Gosselink, R.J.A. PhD Thesis. Lignin as a renewable aromatic resource for the chemical industry, Wageningen University, 2011.

64. Verified Market Research. Lignosulfonates Market Size And Forecast - Sample report. https://www.verifiedmarketresearch.com/product/lignosulfonates-market/ (accessed on 24/05/2021).

65. Transparency Market Research. Lignosulfonates Market - Sample report (https://www.transparencymarketresearch.com/global-lignosulfonates-market.html; accessed on 24/05/2021).

66. Myrvold, B.O. A new model for the structure of lignosulphonates. Part 1. Behaviour in dilute

solutions. *Ind. Crops Prod.* **2008**, *27*, 214–219, doi:10.1016/j.indcrop.2007.07.010.

67. Myrvold, B.O. The polyelectrolyte behavior of randomly branched lignosulfonates. *Tappi J.* **2007**, *6*, 10–15.

68. Myrvold, B.O. Evidence for a very slow disaggregation of lignosulfonates. *Holzforschung* **2015**, *69*, 9–16, doi:10.1515/hf-2013-0242.

69. Qian, Y.; Deng, Y.; Qiu, X.; Huang, J.; Yang, D. Aggregation of sodium lignosulfonate above a critical temperature. *Holzforschung* **2014**, *68*, 641–647, doi:10.1515/hf-2013-0167.

70. Ruwoldt, J. A Critical Review of the Physicochemical Properties of Lignosulfonates: Chemical Structure and Behavior in Aqueous Solution, at Surfaces and Interfaces. *Surfaces* **2020**, *3*, 622–648, doi:10.3390/surfaces3040042.

71. Yu, O.; Kim, K.H. Lignin to materials: A focused review on recent novel lignin applications. *Appl. Sci.* **2020**, *10*, 4626, doi:10.3390/app10134626.

72. Chung, H.; Washburn, N.R. Improved lignin polyurethane properties with lewis acid treatment. *ACS Appl. Mater. Interfaces* **2012**, *4*, 2840–2846, doi:10.1021/am300425x.

73. Yan, M.; Yang, D.; Deng, Y.; Chen, P.; Zhou, H.; Qiu, X. Influence of pH on the behavior of lignosulfonate macromolecules in aqueous solution. *Colloids Surfaces A Physicochem. Eng. Asp.* **2010**, *371*, 50–58, doi:10.1016/j.colsurfa.2010.08.062.

74. Upton, B.M.; Kasko, A.M. Strategies for the conversion of lignin to high-value polymeric materials: Review and perspective. *Chem. Rev.* **2016**, *116*, 2275–2306, doi:10.1021/acs.chemrev.5b00345.

75. Eraghi Kazzaz, A.; Hosseinpour Feizi, Z.; Fatehi, P. Grafting strategies for hydroxy groups of lignin for producing materials. *Green Chem.* **2019**, *21*, 5714–5752, doi:10.1039/c9gc02598g.

76. Laurichesse, S.; Avérous, L. Chemical modification of lignins: Towards biobased polymers. *Prog. Polym. Sci.* **2014**, *39*, 1266–1290, doi:10.1016/j.progpolymsci.2013.11.004.

77. Che, C.; Vagin, M.; Ail, U.; Gueskine, V.; Phopase, J.; Brooke, R.; Gabrielsson, R.; Jonsson, M.P.; Mak, W.C.; Berggren, M.; et al. Twinning Lignosulfonate with a Conducting Polymer via Counter-Ion Exchange for Large-Scale Electrical Storage. *Adv. Sustain. Syst.* **2019**, *3*, 1–9, doi:10.1002/adsu.201900039.

78. Gouveia, J.R.; da Costa, C.L.; Tavares, L.B.; dos Santos, D.J. Synthesis of Lignin-Based Polyurethanes: A Mini-Review. *Mini. Rev. Org. Chem.* **2018**, *16*, 345–352, doi:10.2174/1570193x15666180514125817.

79. Luo, H.; Abu-Omar, M.M. Chemicals From Lignin. In *Encyclopedia of Sustainable Technologies*; Abraham, M.A., Strezov, V., Zoeller, J., Eds.; Elsevier Inc., 2017; Vol. 3, pp. 573–585 ISBN 9780128046777.

80. Chen, J.; Kazzaz, A.E.; AlipoorMazandarani, N.; Feizi, Z.H.; Fatehi, P. Production of flocculants, adsorbents, and dispersants from lignin. *Molecules* **2018**, *23*, 1–25, doi:10.3390/molecules23040868.

81. Moreno, A.; Sipponen, M.H. Lignin-based smart materials: A roadmap to processing and synthesis for current and future applications. *Mater. Horizons* **2020**, *7*, 2237–2257, doi:10.1039/d0mh00798f.

82. Gargulak, J.D.; Lebo, S.E. Commercial use of lignin-based material. In *Lignin: Historical, Biological, and Materials Perspectives*; Glasser, W.G., Northey, R.A., Schultz, T.P., Eds.; ACS Symposium Series; American Chemical Society: Washington, DC, 2000; pp. 304–320 ISBN 0-8412-3611-9.

83. Rueda, C.; Calvo, P.A.; Moncalián, G.; Ruiz, G.; Coz, A. Biorefinery options to valorize the spent liquor from sulfite pulping. *J. Chem. Technol. Biotechnol.* **2015**, *90*, 2218–2226, doi:10.1002/jctb.4536.

84. Bjørsvik, H.-R.; Minisci, F. Fine Chemicals from Lignosulfonates. 1. Synthesis of Vanillin by Oxidation of Lignosulfonates. *Org. Process Res. Dev.* **1999**, *3*, 330–340, doi:10.1021/op9900028.

85. Santos, S.G.; Marques, A.P.; Lima, D.L.D.; Evtuguin, D. V.; Esteves, V.I. Kinetics of eucalypt lignosulfonate oxidation to aromatic aldehydes by oxygen in alkaline medium. *Ind. Eng. Chem. Res.* **2011**, *50*, 291–298, doi:10.1021/ie101402t.

86. Bjørsvik, H.R.; Liguori, L. Organic processes to pharmaceutical chemicals based on fine chemicals from lignosulfonates. *Org. Process Res. Dev.* **2002**, *6*, 279–290, doi:10.1021/op010087o.

87. Kim, S.; Silva, C.; Zille, A.; Lopez, C.; Evtuguin, D. V.; Cavaco-Paulo, A. Characterisation of enzymatically oxidised lignosulfonates and their application on lignocellulosic fabrics. *Polym. Int.* **2009**, *58*, 863–868, doi:10.1002/pi.2600.

88. Sazanov, Y.N.; Podeshvo, I. V.; Mikhailov, G.M.; Fedorova, G.N.; Goikhman, M.Y.; Lebedeva, M.F.; Kudryavtsev, V. V. Polymeric materials derived from vanillic acid. *Russ. J. Appl. Chem.* **2002**, *75*, 777–780, doi:10.1023/A:1020362613234.

89. Sellers, T.; McGinnis, G.; Ruffin, T.; Janiga, E. Lignin-modified phenol-formaldehyde resin development for fiberboard. *For. Prod. J.* **2004**, *54*, 45–51.

90. El Mansouri, N.E.; Farriol, X.; Salvadó, J. Structural modification and characterization of lignosulfonate by a reaction in an alkaline medium for its incorporation into phenolic resins. *J. Appl. Polym. Sci.* **2006**, *102*, 3286–3292, doi:10.1002/app.24744.

91. Faria, F.A.C.; Evtuguin, D. V.; Rudnitskaya, A.; Gomes, M.T.S.R.; Oliveira, J.A.B.P.; Graça, M.P.F.; Costa, L.C. Lignin-based polyurethane doped with carbon nanotubes for sensor applications. *Polym. Int.* **2012**, *61*, 788–794, doi:10.1002/pi.4140.

92. Chen, Z.; Zhou, Q.; Guan, W.; Wang, J.; Li, Y.; Yu, N.; Wei, J. Effects of imidazolium-based ionic liquids with different anions on wheat seedlings. *Chemosphere* **2018**, *194*, 20–27, doi:10.1016/j.chemosphere.2017.11.145.

93. Avelino, F.; Almeida, S.L.; Duarte, E.B. Thermal and mechanical properties of coconut shell lignin-based polyurethanes synthesized by solvent-free polymerization. *J. Mater. Sci.* **2017**, *53*, 1470–1486, doi:10.1007/s10853-017-1562-z.

94. Pandey, M.P.; Kim, C.S. Lignin Depolymerization and Conversion: A Review of Thermochemical Methods. *Chem. Eng. Technol.* **2011**, *34*, 29–41, doi:10.1002/ceat.201000270.

95. Mahmood, N.; Yuan, Z.; Schmidt, J.; Xu, C. Depolymerization of lignins and their applications for the preparation of polyols and rigid polyurethane foams: A review. *Renew. Sustain. Energy Rev.* **2016**, *60*, 317–329, doi:10.1016/j.rser.2016.01.037.

96. Jing, Y.; Dong, L.; Guo, Y.; Liu, X.; Wang, Y. Chemicals from Lignin: A Review of Catalytic Conversion Involving Hydrogen. *ChemSusChem* **2020**, *13*, 4181–4198, doi:10.1002/cssc.201903174.

97. Silva, E.A.B. da; Zabkova, M.; Araújo, J.D.; Cateto, C.A.; Barreiro, M.F.; Belgacem, M.N.; Rodrigues, A.E. An integrated process to produce vanillin and lignin-based polyurethanes from Kraft lignin. *Chem. Eng. Res. Des.* **2009**, *87*, 1276–1292, doi:10.1016/j.cherd.2009.05.008.

98. Fache, M.; Boutevin, B.; Caillol, S. Vanillin, a key-intermediate of biobased polymers. *Eur. Polym. J.* **2015**, *68*, 488–502, doi:10.1016/j.eurpolymj.2015.03.050.

99. Fache, M.; Darroman, E.; Besse, V.; Auvergne, R.; Caillol, S.; Boutevin, B. Vanillin, a promising biobased building-block for monomer synthesis. *Green Chem.* **2014**, *16*, 1987–1998, doi:10.1039/C3GC42613K.

100. Llevot, A.; Grau, E.; Carlotti, S.; Grelier, S.; Cramail, H. From Lignin-derived Aromatic Compounds to Novel Biobased Polymers. *Macromol. Rapid Commun.* **2016**, *37*, 9–28, doi:10.1002/marc.201500474.

101. Kristufek, S.L.; Wacker, K.T.; Tsao, Y.Y.T.; Su, L.; Wooley, K.L. Monomer design strategies to create natural product-based polymer materials. *Nat. Prod. Rep.* **2017**, *34*, 433–459, doi:10.1039/c6np00112b.

102. Ganewatta, M.S.; Lokupitiya, H.N.; Tang, C. Lignin biopolymers in the age of controlled polymerization. *Polymers (Basel).* **2019**, *11*, 1176, doi:10.3390/polym11071176.

103. Feghali, E.; Torr, K.M.; van de Pas, D.J.; Ortiz, P.; Vanbroekhoven, K.; Eevers, W.; Vendamme, R. Thermosetting Polymers from Lignin Model Compounds and Depolymerized Lignins. *Top. Curr. Chem.* **2018**, *376*, 1–25, doi:10.1007/s41061-018-0211-6.

104. Matsushita, Y. Conversion of technical lignins to functional materials with retained polymeric properties. *J. Wood Sci.* **2015**, *61*, 230–250, doi:10.1007/s10086-015-1470-2.

105. Duval, A.; Lawoko, M. A review on lignin-based polymeric, micro- and nano-structured materials. *React. Funct. Polym.* **2014**, *85*, 78–96, doi:10.1016/j.reactfunctpolym.2014.09.017.

106. BS EN 206-1. Concrete - Part 1: Specification, performance, production and conformity, 2000, 1–74.

107. Wiliński, D.; Łukowski, P.; Rokicki, G. Polymeric superplasticizers based on polycarboxylates for ready-mixed concrete: current state of the art. *Polimery* **2016**, *61*, 474–481, doi:10.14314/polimery.2016.474.

108. ASTM C494. Standard Specification for Chemical Admixtures for Concrete, 2004, 1–10.

109. Gelardi, G.; Mantellato, S.; Marchon, D.; Palacios, M.; Eberhardt, A.B.; Flatt, R.J. Chemistry of chemical admixtures. In *Science and Technology of Concrete Admixtures*; Aïtcin, P.-C., Flatt, R.J., Eds.; Elsevier Ltd, 2016; pp. 149–218 ISBN 9780081006962.

110. Flatt, R.; Schober, I. Superplasticizers and the rheology of concrete. In *Understanding the Rheology of Concrete*; Roussel, N., Ed.; Woodhead Publishing Limited, 2012; pp. 144–208.

111. Yoshioka, K.; Tazawa, E.I.; Kawai, K.; Enohata, T. Adsorption characteristics of superplasticizers on cement component minerals. *Cem. Concr. Res.* **2002**, *32*, 1507–1513, doi:10.1016/S0008-8846(02)00782-2.

112. Qian, Y.; De Schutter, G. Different effects of NSF and PCE superplasticizer on adsorption, dynamic yield stress and thixotropy of cement pastes. *Materials (Basel).* **2018**, *11*, doi:10.3390/ma11050695.

113. Zhang, Y.; Kong, X. Correlations of the dispersing capability of NSF and PCE types of superplasticizer and their impacts on cement hydration with the adsorption in fresh cement pastes. *Cem. Concr. Res.* **2015**, *69*, 1–9, doi:10.1016/j.cemconres.2014.11.009.

114. Singh, N.B.; Singh, V.D.; Rai, S.; Chaturvedi, S. Effect of lignosulfonate, calcium chloride and their mixture on the hydration of RHA-blended portland cement. *Cem. Concr. Res.* **2002**, *32*, 387–392, doi:10.1016/S0008-8846(01)00688-3.

115. Grierson, L.H.; Knight, J.C.; Maharaj, R. The role of calcium ions and lignosulphonate

plasticiser in the hydration of cement. *Cem. Concr. Res.* **2005**, *35*, 631–636, doi:10.1016/j.cemconres.2004.05.048.

116. Yang, D.; Qiu, X.; Zhou, M.; Lou, H. Properties of sodium lignosulfonate as dispersant of coal water slurry. *Energy Convers. Manag.* **2007**, *48*, 2433–2438, doi:10.1016/j.enconman.2007.04.007.

117. Zhou, M.; Qiu, X.; Yang, D.; Lou, H.; Ouyang, X. High-performance dispersant of coal-water slurry synthesized from wheat straw alkali lignin. *Fuel Process. Technol.* **2007**, *88*, 375–382, doi:10.1016/j.fuproc.2006.11.004.

118. Grigg, R.B.; Bai, B. Calcium lignosulfonate adsorption and desorption on Berea sandstone. *J. Colloid Interface Sci.* **2004**, *279*, 36–45, doi:10.1016/j.jcis.2004.06.035.

119. Li, Z.; Ge, Y. Extraction of lignin from sugar cane bagasse and its modification into a high performance dispersant for pesticide formulations. *J. Braz. Chem. Soc.* **2011**, *22*, 1866–1871, doi:10.1590/S0103-50532011001000006.

120. Scripture, E.W. Indurating composition for concrete. *US Pat. 2081643 A* 1937, *54*, 1–4.

121. Miyake, N.; Ando, T.; Sakai, E. Superplasticized concrete using refined lignosulfonate and its action mechanism. *Cem. Concr. Res.* **1985**, *15*, 295–302, doi:10.1016/0008-8846(85)90041-9.

122. Plank, J. Applications of biopolymers and other biotechnological products in building materials. *Appl. Microbiol. Biotechnol.* **2004**, *66*, 1–9, doi:10.1007/s00253-004-1714-3.

123. Stern, T.; Schwarzbauer, P. Wood-based lignosulfonate versus synthetic polycarboxylate in concrete admixture systems: The perspective of a traditional pulping by-product competing with an oil-based substitute in a business to business market in central Europe. *For. Prod. J.* **2008**, *58*, 81–86.

124. Recalde Lummer, N.; Plank, J. Combination of lignosulfonate and AMPS-co-NNDMA water retention agent-An example for dual synergistic interaction between admixtures in cement. *Cem. Concr. Res.* **2012**, *42*, 728–735, doi:10.1016/j.cemconres.2012.02.009.

125. Areskogh, D.; Li, J.; Gellerstedt, G.; Henriksson, G. Investigation of the molecular weight increase of commercial lignosulfonates by laccase catalysis. *Biomacromolecules* **2010**, *11*, 904–910, doi:10.1021/bm901258v.

126. Areskogh, D.; Henriksson, G. Immobilisation of laccase for polymerisation of commercial lignosulphonates. *Process Biochem.* **2011**, *46*, 1071–1075, doi:10.1016/j.procbio.2011.01.024.

127. Leonowicz, A.; Edgehill, R.U.; Bollag, J.M. The effect of pH on the transformation of syringic and vanillic acids by the laccases of Rhizoctonia praticola and Trametes versicolor. *Arch. Microbiol.* **1984**, *137*, 89–96, doi:10.1007/BF00414446.

128. Areskogh, D.; Li, J.; Gellerstedt, G.; Henriksson, G. Structural modification of commercial lignosulphonates through laccase catalysis and ozonolysis. *Ind. Crops Prod.* **2010**, *32*, 458–466, doi:10.1016/j.indcrop.2010.06.016.

129. Mattinen, M.L.; Suortti, T.; Gosselink, R.; Argyropoulos, D.S.; Evtuguin, D.; Suurnäkki, A.; De Jong, E.; Tamminen, T. Polymerization of different lignins by laccase. *BioResources* **2008**, *3*, 549–565, doi:10.15376/biores.3.2.549-565.

130. Riva, S. Laccases: blue enzymes for green chemistry. *Trends Biotechnol.* **2006**, *24*, 219–226, doi:10.1016/j.tibtech.2006.03.006.

131. Chauhan, P.S.; Goradia, B.; Saxena, A. Bacterial laccase: recent update on production, properties and industrial applications. *3 Biotech* **2017**, *7*, 1–20, doi:10.1007/s13205-017-

0955-7.

132. Brijwani, K.; Rigdon, A.; Vadlani, P. V. Fungal laccases: Production, function, and applications in food processing. *Enzyme Res.* **2010**, *2010*, 149748, doi:10.4061/2010/149748.

133. Mate, D.M.; Alcalde, M. Laccase: a multi-purpose biocatalyst at the forefront of biotechnology. *Microb. Biotechnol.* **2017**, *10*, 1457–1467, doi:10.1111/1751-7915.12422.

134. Mojsov, K. Biotechnological applications of laccases in the textile industry. *Adv. Technol.* **2014**, *3*, 76–79, doi:10.5937/savteh1401076m.

135. Singh, G.; Capalash, N.; Kaur, S.; Puri, S.; Sharma, P. Enzymes: Applications in Pulp and Paper Industry. In *Agro-Industrial Wastes as Feedstock for Enzyme Production*; Singh, G., Kaur, S., Eds.; Elsevier, 2016; pp. 157–172 ISBN 9780128023921.

136. Singh, G.; Arya, S.K. Utility of laccase in pulp and paper industry: A progressive step towards the green technology. *Int. J. Biol. Macromol.* **2019**, *134*, 1070–1084, doi:10.1016/j.ijbiomac.2019.05.168.

137. Kawai, S.; Umezawa, T.; Higuchi, T. Degradation Mechanisms of Phenolic Beta-1 Lignin Substructure Model Compounds by Lactase of Coriolus versicolor. *Arch. Biochem. Biophys.* **1988**, *262*, 99–110, doi:10.1016/0003-9861(88)90172-5.

138. Hilgers, R.; Vincken, J.P.; Gruppen, H.; Kabel, M.A. Laccase/Mediator Systems: Their Reactivity toward Phenolic Lignin Structures. *ACS Sustain. Chem. Eng.* **2018**, *6*, 2037–2046, doi:10.1021/acssuschemeng.7b03451.

139. Huber, D.; Ortner, A.; Daxbacher, A.; Nyanhongo, G.S.; Bauer, W.; Guebitz, G.M. Influence of Oxygen and Mediators on Laccase-Catalyzed Polymerization of Lignosulfonate. *ACS Sustain. Chem. Eng.* **2016**, *4*, 5303–5310, doi:10.1021/acssuschemeng.6b00692.

140. Ortner, A.; Huber, D.; Haske-Cornelius, O.; Weber, H.K.; Hofer, K.; Bauer, W.; Nyanhongo, G.S.; Guebitz, G.M. Laccase mediated oxidation of industrial lignins: Is oxygen limiting? *Process Biochem.* **2015**, *50*, 1277–1283, doi:10.1016/j.procbio.2015.05.003.

141. Bourbonnais, R.; Paice, M.G. Oxidation of non-phenolic substrates. *FEBS Lett.* **1990**, *267*, 99–102, doi:10.1016/0014-5793(90)80298-W.

142. Morozova, O. V.; Shumakovich, G.P.; Shleev, S. V.; Yaropolov, Y.I. Laccase-mediator systems and their applications: A review. *Appl. Biochem. Microbiol.* **2007**, *43*, 523–535, doi:10.1134/S0003683807050055.

143. Cañas, A.I.; Camarero, S. Laccases and their natural mediators: Biotechnological tools for sustainable eco-friendly processes. *Biotechnol. Adv.* **2010**, *28*, 694–705, doi:10.1016/j.biotechadv.2010.05.002.

144. Bourbonnais, R.; Paice, M.G.; Reid, I.D.; Lanthier, P.; Yaguchi, M. Lignin oxidation by laccase isozymes from Trametes versicolor and role of the mediator 2,2'-azinobis(3-ethylbenzthiazoline- 6-sulfonate) in kraft lignin depolymerization. *Appl. Environ. Microbiol.* **1995**, *61*, 1876–1880.

145. Bourbonnais, R.; Paice, M.G.; Freiermuth, B.; Bodie, E. Reactivities of various mediators and laccases with kraft pulp and lignin model compounds . Reactivities of Various Mediators and Laccases with Kraft Pulp and Lignin Model Compounds. *Appl. Environ. Microbiol.* **1997**, *63*, 4627–4632.

146. Balakshin, M.Y.; Evtuguin, D. V.; Pascoal Neto, C.; Cavaco-Paulo, A. Polyoxometalates as mediators in the laccase catalyzed delignification. *J. Mol. Catal. - B Enzym.* **2001**, *16*, 131–140, doi:10.1016/S1381-1177(01)00054-6.

147. Gamelas, J.A.F.; Tavares, A.P.M.; Evtuguin, D. V.; Xavier, A.M.B. Oxygen bleaching of

kraft pulp with polyoxometalates and laccase applying a novel multi-stage process. *J. Mol. Catal. B Enzym.* **2005**, *33*, 57–64, doi:10.1016/j.molcatb.2005.03.001.

148. Gamelas, J.A.F.; Gaspar, A.R.; Evtuguin, D. V.; Pascoal Neto, C. Transition metal substituted polyoxotungstates for the oxygen delignification of kraft pulp. *Appl. Catal. A Gen.* **2005**, *295*, 134–141, doi:10.1016/j.apcata.2005.07.047.

149. Gamelas, J.A.F.; Pontes, A.S.N.; Evtuguin, D. V.; Xavier, A.M.R.B.; Esculcas, A.P. New polyoxometalate-laccase integrated system for kraft pulp delignification. *Biochem. Eng. J.* **2007**, *33*, 141–147, doi:10.1016/j.bej.2006.10.014.

150. Yu, G.; Li, B.; Wang, H.; Liu, C.; Mu, X. Preparation of concrete superplasticizer by oxidation- sulfomethylation of sodium lignosulfonate. *BioResources* **2013**, *8*, 1055–1063, doi:10.15376/biores.8.1.1055-1063.

151. Aso, T.; Koda, K.; Kubo, S.; Yamada, T.; Nakajima, I.; Uraki, Y. Preparation of novel lignin-based cement dispersants from isolated lignins. *J. Wood Chem. Technol.* **2013**, *33*, 286–298, doi:10.1080/02773813.2013.794841.

152. Homma, H.; Kubo, S.; Yamada, T.; Matsushita, Y.; Uraki, Y. Preparation and characterization of amphiphilic lignin derivatives as surfactants. *J. Wood Chem. Technol.* **2008**, *28*, 270–282, doi:10.1080/02773810802510688.

153. Homma, H.; Kubo, S.; Yamada, T.; Koda, K.; Matsushita, Y.; Uraki, Y. Conversion of technical lignins to amphiphilic derivatives with high surface activity. *J. Wood Chem. Technol.* **2010**, *30*, 164–174, doi:10.1080/02773810903349713.

154. Cortés-Triviño, E.; Valencia, C.; Delgado, M.A.; Franco, J.M. Modification of alkali lignin with poly(ethylene glycol) diglycidyl ether to be used as a thickener in bio-lubricant formulations. *Polymers (Basel).* **2018**, *10*, doi:10.3390/polym10060670.

155. Perkins, K.M.; Gupta, C.; Charleson, E.N.; Washburn, N.R. Surfactant properties of PEGylated lignins: Anomalous interfacial activities at low grafting density. *Colloids Surfaces A Physicochem. Eng. Asp.* **2017**, *530*, 200–208, doi:10.1016/j.colsurfa.2017.07.061.

156. Childs, C.M.; Perkins, K.M.; Menon, A.; Washburn, N.R. Interplay of Anionic Functionality in Polymer-Grafted Lignin Superplasticizers for Portland Cement. *Ind. Eng. Chem. Res.* **2019**, *58*, 19760–19766, doi:10.1021/acs.iecr.9b03973.

157. Stark, N.M.; Ai, Z.; Carll, C. Wood-Based Composite Materials. In *Wood handbook: wood as an engineering material. General Technical Report FPL-GTR-190*; Ross, R.J., Ed.; U.S. Dept. of Agriculture, Forest Service, Forest Products Laboratory: Madison, WI, USA, 2010; pp. 11.1-11.28.

158. Lehmann, W.F. Wood-based composites and laminates. In *Kirk-Othmer Encyclopedia of Chemical Technology*; John Wiley & Sons Inc.: New York, USA, 2011; pp. 1–47.

159. Frihart, C.R.; Hunt, C.G. Adhesives with Wood Materials. In *Wood Handbook: Wood as an Engineering Material. General Technical Report FPL- GTR-190*; Ross, R.J., Ed.; U.S. Dept. of Agriculture, Forest Service, Forest Products Laboratory: Madison, WI, USA, 2010; pp. 10.1-10.24.

160. Ormondroyd, G.A. Adhesives for wood composites. In *Wood Composites (Woodhead Publishing Series in Composites Science and Engineering)*; Elsevier Ltd., 2015; pp. 47–66 ISBN 9781782424772.

161. Pizzi, A. Natural Adhesives, Binders and Matrices for Wood and Fiber Composites: Chemistry and Technology. In *Lignocellulosic Fibers and Wood Handbook: Renewable Materials for Today's Environment*; Belgacem, N., Pizzi, A., Eds.; Scrivener Publishing LLC: Hoboken, New Jersey, 2016; pp. 277–303.

162. Roffael, E. Volatile organic compounds and formaldehyde in nature, wood and wood based panels. *Holz als Roh - und Werkst.* **2006**, *64*, 144–149, doi:10.1007/s00107-005-0061-0.

163. Lithner, D.; Larsson, A.; Dave, G. Environmental and health hazard ranking and assessment of plastic polymers based on chemical composition. *Sci. Total Environ.* **2011**, *409*, 3309–3324, doi:10.1016/j.scitotenv.2011.04.038.

164. Hemmilä, V.; Adamopoulos, S.; Karlsson, O.; Kumar, A. Development of sustainable bio-adhesives for engineered wood panels - A Review. *RSC Adv.* **2017**, *7*, 38604–38630, doi:10.1039/c7ra06598a.

165. Ang, A.F.; Ashaari, Z.; Lee, S.H.; Md Tahir, P.; Halis, R. Lignin-based copolymer adhesives for composite wood panels – A review. *Int. J. Adhes. Adhes.* **2019**, *95*, 102408, doi:10.1016/j.ijadhadh.2019.102408.

166. Ferdosian, F.; Pan, Z.; Gao, G.; Zhao, B. Bio-based adhesives and evaluation for wood composites application. *Polymers (Basel).* **2017**, *9*, 70, doi:10.3390/polym9020070.

167. Gadhave, R. V.; Srivastava, S.; Mahanwar, P.A.; Gadekar, P.T. Lignin: Renewable Raw Material for Adhesive. *Open J. Polym. Chem.* **2019**, *9*, 27–38, doi:10.4236/ojpchem.2019.92003.

168. Lewis, N.; Lantzy, T.; Branhm, S. Lignin in adhesives: Introduction and historical perspective. In *Adhesives from Renewable Resources*; Hemigway, R.W., Conner, A.H., Branham, S.J., Eds.; ACS Symposium Series; American Chemical Society: Washington, DC, 1989; pp. 13–26 ISBN 0841215626.

169. Xu, C.; Ferdosian, F. Lignin-Based Phenol–Formaldehyde (LPF) Resins/Adhesives. In *Conversion of Lignin into Bio-Based Chemicals and Materials*; Springer-Verlag: Berlin, Heidelberg, 2017; pp. 91–109 ISBN 9783662549599.

170. Ghorbani, M.; Konnerth, J.; van Herwijnen, H.W.G.; Zinovyev, G.; Budjav, E.; Requejo Silva, A.; Liebner, F. Commercial lignosulfonates from different sulfite processes as partial phenol replacement in PF resole resins. *J. Appl. Polym. Sci.* **2018**, *135*, 1–11, doi:10.1002/app.45893.

171. Akhtar, T.; Lutfullah, G.; Zahoorullah Ligonsulfonate-phenolformaldehyrde adhesive: A potenstial binder for wood panel industries. *J. Chem. Soc. Pakistan* **2011**, *33*, 535–538.

172. Hu, L.; Pan, H.; Zhou, Y.; Zhang, M. Methods to improve lignin's reactivity as a phenol substitute and as replacement for other phenolic compounds: A brief review. *BioResources* **2011**, *6*, 3515–3525, doi:10.15376/biores.6.3.3515-3525.

173. Cook, P.M.; Sellers, T. Organosolv Lignin-Modified Phenolic Resins. In *Lignin Properties and Materials*; Glasser, W.G., Sarkanen, S., Eds.; ACS Symposium Series; American Chemical Society: Washington, DC, 1989; pp. 324–333.

174. Taverna, M.E.; Felissia, F.; Area, M.C.; Estenoz, D.A.; Nicolau, V.V. Hydroxymethylation of technical lignins from South American sources with potential use in phenolic resins. *J. Appl. Polym. Sci.* **2019**, *136*, 1–12, doi:10.1002/app.47712.

175. Malutan, T.; Nicu, R.; Popa, V.I. Contribution to the study of hydroxymetylation reaction of alkali lignin. *BioResources* **2008**, *3*, 13–20, doi:10.15376/biores.3.1.13-20.

176. Alonso, M. V.; Rodrguez, J.J.; Oliet, M.; Rodrguez, F.; Garca, J.; Gilarranz, M.A. Characterization and structural modification of ammonic lignosulfonate by methylolation. *J. Appl. Polym. Sci.* **2001**, *82*, 2661–2668, doi:10.1002/app.2119.

177. Domínguez, J.C.; Oliet, M.; Alonso, M. V.; Rojo, E.; Rodríguez, F. Structural, thermal and rheological behavior of a bio-based phenolic resin in relation to a commercial resol resin. *Ind.*

*Crops Prod.* **2013**, *42*, 308–314, doi:10.1016/j.indcrop.2012.06.004.

178. Alonso, M. V.; Oliet, M.; Rodríguez, F.; Astarloa, G.; Echeverría, J.M. Use of a methylolated softwood ammonium lignosulfonate as partial substitute of phenol in resol resins manufacture. *J. Appl. Polym. Sci.* **2004**, *94*, 643–650, doi:10.1002/app.20887.

179. Alonso, M. V.; Oliet, M.; Rodríguez, F.; García, J.; Gilarranz, M.A.; Rodríguez, J.J. Modification of ammonium lignosulfonate by phenolation for use in phenolic resins. *Bioresour. Technol.* **2005**, *96*, 1013–1018, doi:10.1016/j.biortech.2004.09.009.

180. European Chemicals Agency. Substance Infocard − Formaldehyde. https://echa.europa.eu/substance-information/-/substanceinfo/100.000.002 (accessed on 21/07/2021).

181. Franz, A.W.; Kronemayer, H.; Pfeiffer, D.; Pilz, R.D.; Reuss, G.; Disteldorf, W.; Gamer, A.O.; Hilt, A. Formaldehyde. In *Ullmann's Encyclopedia of Industrial Chemistry*; WILEY-VCH Verlag GmbH & Co.: Weinheim, 2016; pp. 1–34.

182. Mattioda, G.; Blanc, A. Glyoxal. In *Ullmann's Encyclopedia of Industrial Chemistry*; WILEY-VCH: Weinheim, 2012; pp. 83–87.

183. El Mansouri, N.E.; Pizzi, A.; Salvadó, J. Lignin-based wood panel adhesives without formaldehyde. *Holz als Roh - und Werkst.* **2007**, *65*, 65–70, doi:10.1007/s00107-006-0130-z.

184. El Mansouri, N.E.; Pizzi, A.; Salvadó, J. Lignin-Based Polycondensation Resins for Wood Adhesives. *J. Appl. Polym. Sci.* **2007**, *103*, 1690–1699, doi:10.1002/app.25098.

185. El Mansouri, N.-E.; Yuan, Q.L.; Huang, F. Study of Chemical Modification of Alkaline Lignin By the Glyoxalation Reaction. *Mater. Sci.* **2011**, *6*, 4523–4536.

186. Aziz, N.A.; Latip, A.F.A.; Peng, L.C.; Latif, N.H.A.; Brosse, N.; Hashim, R.; Hussin, M.H. Reinforced lignin-phenol-glyoxal (LPG) wood adhesives from coconut husk. *Int. J. Biol. Macromol.* **2019**, *141*, 185–196, doi:10.1016/j.ijbiomac.2019.08.255.

187. Younesi-Kordkheili, H. Ionic liquid modified lignin-phenol-glyoxal resin: a green alternative resin for production of particleboards. *J. Adhes.* **2019**, *95*, 1075–1087, doi:10.1080/00218464.2018.1471994.

188. Tupa Esfandiyari, M.R.; Pour, M.T.; Khademieslam, H.; Mir Shokraei, S.A.; Bazyar, B. Investigating the Possibility of Making Lignin-glyoxal Resins as Adhesives in the Production of Plywood. *BioResources* **2020**, *14*, 7122–7133, doi:10.15376/biores.14.3.7122-7133.

189. Hazwan Hussin, M.; Aziz, A.A.; Iqbal, A.; Ibrahim, M.N.M.; Latif, N.H.A. Development and characterization novel bio-adhesive for wood using kenaf core (Hibiscus cannabinus) lignin and glyoxal. *Int. J. Biol. Macromol.* **2019**, *122*, 713–722, doi:10.1016/j.ijbiomac.2018.11.009.

190. Ramires, E.C.; Megiatto, J.D.; Gardrat, C.; Castellan, A.; Frollini, E. Biobased composites from glyoxal-phenolic resins and sisal fibers. *Bioresour. Technol.* **2010**, *101*, 1998–2006, doi:10.1016/j.biortech.2009.10.005.

191. Van Nieuwenhove, I.; Renders, T.; Lauwaert, J.; De Roo, T.; De Clercq, J.; Verberckmoes, A. Biobased Resins Using Lignin and Glyoxal. *ACS Sustain. Chem. Eng.* **2020**, *8*, 18789–18809, doi:10.1021/acssuschemeng.0c07227.

192. Navarrete, P.; Pizzi, A.; Pasch, H.; Delmotte, L. Study on lignin-glyoxal reaction by MALDI-TOF and CP-MAS 13C-NMR. *J. Adhes. Sci. Technol.* **2012**, *26*, 1069–1082, doi:10.1163/016942410X550030.

193. Navarrete, P.; Pizzi, A.; Rode, K.; Vignali, M.; Pasch, H. MALDI-TOF study of oligomers distribution in spray-dried glyoxalated lignin for wood adhesives. *J. Adhes. Sci. Technol.*

**2013**, *27*, 586–597, doi:10.1080/01694243.2012.690618.

194. Engels, H.W.; Pirkl, H.G.; Albers, R.; Albach, R.W.; Krause, J.; Hoffmann, A.; Casselmann, H.; Dormish, J. Polyurethanes: Versatile materials and sustainable problem solvers for today's challenges. *Angew. Chemie - Int. Ed.* **2013**, *52*, 9422–9441, doi:10.1002/anie.201302766.

195. Fink, J.K. Poly(urethane)s. In *Reactive Polymers: Fundamentals and Applications: A Concise Guide to Industrial Polymers*; Elsevier Inc., 2018; pp. 71–138 ISBN 9780128145098.

196. Janik, H.; Sienkiewicz, M.; Kucinska-lipka, J. Polyurethanes. In *Handbook of Thermoset Plastics*; Dodiuk, H., Goodman, S.H., Eds.; Elsevier Inc., 2014; pp. 253–295 ISBN 9781455731077.

197. Gama, N. V.; Ferreira, A.; Barros-Timmons, A. Polyurethane foams: Past, present, and future. *Materials (Basel).* **2018**, *11*, 1841, doi:10.3390/ma11101841.

198. Six, Ch.; Richter, F. Isocyanates, Organic. In *Ullmann's Encyclopedia of Industrial Chemistry*; WILEY-VCH Verlag GmbH & Co.: Weinheim, 2003; pp. 63–82.

199. Collins, M.A. Toxicology of toluene diisocyanate. *Appl. Occup. Environ. Hyg.* **2002**, *17*, 846–855, doi:10.1080/10473220290107048.

200. Rokicki, G.; Parzuchowski, P.G.; Mazurek, M. Non-isocyanate polyurethanes: Synthesis, properties, and applications. *Polym. Adv. Technol.* **2015**, *26*, 707–761, doi:10.1002/pat.3522.

201. Suryawanshi, Y.; Sanap, P.; Wani, V. Advances in the synthesis of non-isocyanate polyurethanes. *Polym. Bull.* **2019**, *76*, 3233–3246, doi:10.1007/s00289-018-2531-7.

202. Cornille, A.; Auvergne, R.; Figovsky, O.; Boutevin, B.; Caillol, S. A perspective approach to sustainable routes for non-isocyanate polyurethanes. *Eur. Polym. J.* **2017**, *87*, 535–552, doi:10.1016/j.eurpolymj.2016.11.027.

203. Błażek, K.; Datta, J. Renewable natural resources as green alternative substrates to obtain bio-based non-isocyanate polyurethanes-review. *Crit. Rev. Environ. Sci. Technol.* **2019**, *49*, 173–211, doi:10.1080/10643389.2018.1537741.

204. Zhang, Q.; Zhang, G.; Xu, J.; Gao, C.; Wu, Y. Recent advances on lignin-derived polyurethane polymers. *Rev. Adv. Mater. Sci.* **2015**, *40*, 146–154.

205. Alinejad, M.; Henry, C.; Nikafshar, S.; Gondaliya, A.; Bagheri, S.; Chen, N.; Singh, S.K.; Hodge, D.B.; Nejad, M. Lignin-Based Polyurethanes: Opportunities for Bio-Based Foams, Elastomers, Coatings and Adhesives. *Polymers (Basel).* **2019**, *11*, 1202.

206. Xu, C.; Ferdosian, F. Lignin-Based Polyurethane (PU) Resins and Foams. In *Conversion of Lignin into Bio-Based Chemicals and Materials*; Springer-Verlag: Berlin, Heidelberg, 2017; pp. 133–156 ISBN 9783662549599.

207. Li, H.; Liang, Y.; Li, P.; He, C. Conversion of biomass lignin to high-value polyurethane: A review. *J. Bioresour. Bioprod.* **2020**, *5*, 163–179, doi:10.1016/j.jobab.2020.07.002.

208. de Oliveira, F.; Ramires, E.C.; Frollini, E.; Belgacem, M.N. Lignopolyurethanic materials based on oxypropylated sodium lignosulfonate and castor oil blends. *Ind. Crops Prod.* **2015**, *72*, 77–86, doi:10.1016/j.indcrop.2015.01.023.

209. Cateto, C.A.; Barreiro, M.F.; Ottati, C.; Lopretti, M. Lignin-based rigid polyurethane foams with improved biodegradation. *J. Cell. Plast.* **2014**, *50*, 81–95, doi:10.1177/0021955X13504774.

210. Cateto, C.A.; Barreiro, M.F.; Rodrigues, A.E. Monitoring of lignin-based polyurethane synthesis by FTIR-ATR. *Ind. Crops Prod.* **2008**, *7*, 168–174, doi:10.1016/j.indcrop.2007.07.018.

211. Evtuguin, D.V.; Andreolety, J.P.; Gandini, A. Polyurethanes based on oxygen-organosolv lignin. *Eur. Polym. J.* **1998**, *34*, 1163–1169, doi:10.1016/S0014-3057(97)00245-0.

212. Gandini, A.; Belgacem, Mohamed Naceur Guo, Z.-X.; Montanari, S. Lignins as macromonomers for polyesters and polyurethanes. In *Chemical modification, properties, and usage of lignin*; Hu, T.Q., Ed.; Springer Science + Business Media: New York, 2002; pp. 57–80 ISBN 9781461351733.

213. Lang, J.M.; Shrestha, U.M.; Dadmun, M. The effect of plant source on the properties of lignin-based polyurethanes. *Front. Energy Res.* **2018**, *6*, 4, doi:10.3389/fenrg.2018.00004.

214. Griffini, G.; Passoni, V.; Suriano, R.; Levi, M.; Turri, S. Polyurethane Coatings Based on Chemically Unmodified Fractionated Lignin. *ACS Sustain. Chem. Eng.* **2015**, *3*, 1145–1154, doi:10.1021/acssuschemeng.5b00073.

215. Nacas, A.M.; Ito, N.M.; De Sousa JR, R.R.; Spinacé, M.A.; Dos Santos, D.J. Effects of NCO:OH ratio on the mechanical properties and chemical structure of Kraft lignin – based polyurethane adhesive. *J. Adhes.* **2017**, *93*, 18–29, doi:10.1080/00218464.2016.1177793.

216. Hatakeyama, H.; Hatakeyama, T. Lignin Structure, Properties, and Applications. In *Biopolymers. Lignin, Proteins, Bioactive Nanocomposites*; Abe, A., Karel, D., Kobayashi, S., Eds.; Springer-Verlag Berlin Heidelberg, 2009; pp. 1–63.

217. Hatakeyama, H. Polyurethanes containing lignin. In *Chemical modification, properties, and usage of lignin*; Hu, T.Q., Ed.; Springer Science + Business Media: New York, 2002; pp. 41–56 ISBN 978-1-4613-5173-3.

218. Cinelli, P.; Anguillesi, I.; Lazzeri, A. Green synthesis of flexible polyurethane foams from liquefied lignin. *Eur. Polym. J.* **2013**, *49*, 1174–1184, doi:10.1016/j.eurpolymj.2013.04.005.

219. Llovera, L.; Benjelloun-Mlayah, B.; Delmas, M. Organic acid lignin-based polyurethane films: Synthesis parameter optimization. *BioResources* **2016**, *11*, 6320–6334, doi:10.15376/biores.11.3.6320-6334.

220. Carriço, C.S.; Fraga, T.; Pasa, V.M.D. Production and characterization of polyurethane foams from a simple mixture of castor oil, crude glycerol and untreated lignin as bio-based polyols. *Eur. Polym. J.* **2016**, *85*, 53–61, doi:10.1016/j.eurpolymj.2016.10.012.

221. Tavares, L.B.; Boas, C. V; Schleder, G.R.; Nacas, A.M.; Rosa, D.S.; Santos, D.J. Bio-based polyurethane prepared from Kraft lignin and modified castor oil. *eXPRESS Polym. Lett.* **2016**, *10*, 927–940, doi:10.3144/expresspolymlett.2016.86.

222. Cassales, A.; Antônio, L.; Frollini, E. Synthesis of bio-based polyurethanes from Kraft lignin and castor oil with simultaneous film formation. *Int. J. Biol. Macromol.* **2020**, *145*, 28–41, doi:10.1016/j.ijbiomac.2019.12.173.

223. Zhang, W.; Zhang, Y.; Liang, H.; Liang, D.; Cao, H.; Liu, C.; Qian, Y.; Lu, Q.; Zhang, C. High bio-content castor oil based waterborne polyurethane/sodium lignosulfonate composites for environmental friendly UV absorption application. *Ind. Crops Prod.* **2019**, *142*, 111836, doi:10.1016/j.indcrop.2019.111836.

224. Zhang, Y.; Liao, J.; Fang, X.; Bai, F.; Qiao, K.; Wang, L. Renewable High-Performance Polyurethane Bioplastics Derived from Lignin-Poly(ε-caprolactone). *ACS Sustain. Chem. Eng.* **2017**, *5*, 4276–4284, doi:10.1021/acssuschemeng.7b00288.

225. Bernardini, J.; Cinelli, P.; Anguillesi, I.; Coltelli, M.B.; Lazzeri, A. Flexible polyurethane foams green production employing lignin or oxypropylated lignin. *Eur. Polym. J.* **2015**, *64*, 147–156, doi:10.1016/j.eurpolymj.2014.11.039.

226. Glasser, W.G.; Barnett, C.A.; Rials, T.G.; Saraf, V.P. Engineering plastics from lignin II.

Characterization of hydroxyalkyl lignin derivatives. *J. Appl. Polym. Sci.* **1984**, *29*, 1815–1830, doi:10.1002/app.1984.070290533.

227. Nadji, H.; Bruzzèse, C.; Belgacem, M.N.; Benaboura, A.; Gandini, A. Oxypropylation of lignins and preparation of rigid polyurethane foams from the ensuing polyols. *Macromol. Mater. Eng.* **2005**, *290*, 1009–1016, doi:10.1002/mame.200500200.

228. de Oliveira, W.; Glasser, W.G. Engineering plastics from lignin. XVI. Starlike macromers with propylene oxide. *J. Appl. Polym. Sci.* **1989**, *37*, 3119–3135, doi:10.1002/app.1989.070371105.

229. Li, Y.; Ragauskas, A.J. Kraft lignin-based rigid polyurethane foam. *J. Wood Chem. Technol.* **2012**, *32*, 210–224, doi:10.1080/02773813.2011.652795.

230. Berrima, B.; Mortha, G.; Boufi, S.; Aloui, E. El; Naceur Belgacem, M. Oxypropylation of Soda Lignin: Characterization and Application in Polyurethane Foams Production. *Cellul. Chem. Technol.* **2016**, *50*, 941–950.

231. Cateto, C.A.; Barreiro, M.F.; Rodrigues, A.E.; Belgacem, M.N. Optimization study of lignin oxypropylation in view of the preparation of polyurethane rigid foams. *Ind. Eng. Chem. Res.* **2009**, *48*, 2583–2589, doi:10.1021/ie801251r.

232. Baer, H.; Bergamo, M.; Forlin, A.; Pottenger, L.H.; Lindner, J. Propylene Oxide. In *Ullmann's Encyclopedia of Industrial Chemistry*; WILEY-VCH Verlag GmbH & Co.: Weinheim, 2012; pp. 1–29.

233. Clements, J.H. Reactive applications of cyclic alkylene carbonates. *Ind. Eng. Chem. Res.* **2003**, *42*, 663–674, doi:10.1021/ie020678i.

234. Schäffner, B.; Schäffner, F.; Verevkin, S.P.; Börner, A. Organic carbonates as solvents in synthesis and catalysis. *Chem. Rev.* **2010**, *110*, 4554–4581, doi:10.1021/cr900393d.

235. Mimini, V.; Amer, H.; Hettegger, H.; Bacher, M.; Gebauer, I.; Bischof, R.; Fackler, K.; Potthast, A.; Rosenau, T. Lignosulfonate-based polyurethane materials via cyclic carbonates: Preparation and characterization. *Holzforschung* **2020**, *74*, 203–211, doi:10.1515/hf-2018-0298.

236. Hemmilä, V.; Adamopoulos, S.; Hosseinpourpia, R.; Ahmed, S.A. Ammonium lignosulfonate adhesives for particleboards with pMDI and furfuryl alcohol as crosslinkers. *Polymers (Basel).* **2019**, *11*, 1633, doi:10.3390/polym11101633.

237. Rudnitskaya, A.; Evtuguin, D. V.; Costa, L.C.; Graça, M.P.F.; Fernandes, A.J.S.; Correia, M.R.P.; Gomes, M.T.S.R.; Oliveira, J.A.B.P. Potentiometric chemical sensors from lignin-poly(propylene oxide) copolymers doped by carbon nanotubes. *Analyst* **2013**, *138*, 501–508, doi:10.1039/c2an36390a.

238. Graça, M.P.F.; Rudnitskaya, A.; Faria, F.A.; Evtuguin, D. V.; Gomes, M.T.S.R.; Oliveira, J.A.B.P.; Costa, L.C. Electrochemical impedance study of the lignin-derived conducting polymer. *Electrochim. Acta* **2012**, *76*, 69–76, doi:10.1016/j.electacta.2012.04.155.

239. Gonçalves, S.S.L.; Rudnitskaya, A.; Sales, A.J.M.; Costa, L.M.C.; Evtuguin, D. V. Nanocomposite polymeric materials based on eucalyptus lignoboost® kraft lignin for liquid sensing applications. *Materials (Basel).* **2020**, *13*, 1637, doi:10.3390/ma13071637.

240. Wysocka, K.; Szymona, K.; McDonald, A.G.; Maminski, M. Characterization of thermal and mechanical properties of lignosulfonate- and hydrolyzed lignosulfonate-based polyurethane foams. *BioResources* **2016**, *11*, 7355–7364, doi:10.15376/biores.11.3.7355-7364.

241. Muller, L.C.; Marx, S.; Vosloo, H.C.M.; Fosso-Kankeu, E.; Chiyanzu, I. Rigid polyurethane foams from unrefined crude glycerol and technical lignins. *Polym. from Renew. Resour.* **2018**,

*9*, 111–132, doi:10.1177/2041247918803187.

242. Muller, L.C.; Marx, S.; Vosloo, H.C.M. Polyol preparation by liquefaction of technical lignins in crude glycerol. *J. Renew. Mater.* **2017**, *5*, 67–80, doi:10.7569/JRM.2016.634130.

243. Hatakeyama, T.; Matsumoto, Y.; Asano, Y.; Hatakeyama, H. Glass transition of rigid polyurethane foams derived from sodium lignosulfonate mixed with diethylene, triethylene and polyethylene glycols. *Thermochim. Acta* **2004**, *416*, 29–33, doi:10.1016/j.tca.2002.12.002.

244. Lu, W.; Li, Q.; Zhang, Y.; Yu, H.; Hirose, S.; Hatakeyama, H.; Matsumoto, Y.; Jin, Z. Lignosulfonate/APP IFR and its flame retardancy in lignosulfonate-based rigid polyurethane foams. *J. Wood Sci.* **2018**, *64*, 287–293, doi:10.1007/s10086-018-1701-4.

245. Lu, W.; Ye, J.; Zhu, L.; Jin, Z.; Matsumoto, Y. Intumescent flame retardant mechanism of lignosulfonate as a char forming agent in rigid polyurethane foam. *Polymers (Basel).* **2021**, *13*, 1–13, doi:10.3390/polym13101585.

246. Wang, F.; Yang, X.; Zou, Y. Effect of the maleation of lignosulfonate on the mechanical and thermal properties of lignosulfonate/poly(ε-caprolactone) blends. *J. Appl. Polym. Sci.* **2016**, *133*, 1–7, doi:10.1002/app.42925.

247. Wang, F.; Yang, X.; Zou, Y. The Esterification of Sodium Lignosulfonate with Maleic Anhydride in Water Solution. *Int. J. Polym. Anal. Charact.* **2015**, *20*, 69–81, doi:10.1080/1023666X.2014.961117.

248. Xu, Y.; Adekunle, K.; Ramamoorthy, S.K.; Skrifvars, M.; Hakkarainen, M. Methacrylated lignosulfonate as compatibilizer for flax fiber reinforced biocomposites with soybean-derived polyester matrix. *Compos. Commun.* **2020**, *22*, 100536, doi:10.1016/j.coco.2020.100536.

249. Petrie, E.M. *Epoxy Adhesive Formulations (Chemical Engineering)*; McGraw-Hill, 2006; ISBN 0071589082.

250. Ellis, B. The kinetics of cure and network formation. In *Chemistry and Technology of Epoxy Resins*; Ellis, B., Ed.; Springer Science+Business Media: Dordrecht, 1993; pp. 72–116 ISBN 9789401053020.

251. Xu, C.; Ferdosian, F. Lignin-Based Epoxy Resins. In *Conversion of Lignin into Bio-Based Chemicals and Materials*; Springer Verlag: Berlin, Heidelberg, 2017; pp. 111–131 ISBN 9783662549599.

252. Raquez, J.M.; Deléglise, M.; Lacrampe, M.F.; Krawczak, P. Thermosetting (bio)materials derived from renewable resources: A critical review. *Prog. Polym. Sci.* **2010**, *35*, 487–509, doi:10.1016/j.progpolymsci.2010.01.001.

253. Flint, S.; Markle, T.; Thompson, S.; Wallace, E. Bisphenol A exposure, effects, and policy: A wildlife perspective. *J. Environ. Manage.* **2012**, *104*, 19–34, doi:10.1016/j.jenvman.2012.03.021.

254. Ma, Y.; Liu, H.; Wu, J.; Yuan, L.; Wang, Y.; Du, X.; Wang, R.; Marwa, P.W.; Petlulu, P.; Chen, X.; et al. The adverse health effects of bisphenol A and related toxicity mechanisms. *Environ. Res.* **2019**, *176*, doi:10.1016/j.envres.2019.108575.

255. Nikafshar, S.; Wang, J.; Dunne, K.; Sangthonganotai, P.; Nejad, M. Choosing the Right Lignin to Fully Replace Bisphenol A in Epoxy Resin Formulation. *ChemSusChem* **2021**, *14*, 1184–1195, doi:10.1002/cssc.202002729.

256. Ismail, T.N.M.T.; Hassan, H.A.; Hirose, S.; Taguchi, Y.; Hatakeyama, T.; Hatakeyama, H. Synthesis and thermal properties of ester-type crosslinked epoxy resins derived from lignosulfonate and glycerol. *Polym. Int.* **2010**, *59*, 181–186, doi:10.1002/pi.2705.

257. Yamini, G.; Shakeri, A.; Zohuriaan-Mehr, M.J.; Kabiri, K. Cyclocarbonated lignosulfonate as a bio-resourced reactive reinforcing agent for epoxy biocomposite: From natural waste to value-added bio-additive. *J. CO2 Util.* **2018**, *24*, 50–58, doi:10.1016/j.jcou.2017.12.007.

258. Yamini, G.; Shakeri, A.; Vafayan, M.; Zohuriaan-Mehr, M.J.; Kabiri, K.; Zolghadr, M. Cure kinetics of modified lignosulfonate/epoxy blends. *Thermochim. Acta* **2019**, *675*, 18–28, doi:10.1016/j.tca.2019.03.003.

259. Matyjaszewski, K.; Xia, J. Atom transfer radical polymerization. *Chem. Rev.* **2001**, *101*, 2921–2990, doi:10.1021/cr940534g.

260. Matyjaszewski, K.; Tsarevsky, N. V. Nanostructured functional materials prepared by atom transfer radical polymerization. *Nat. Chem.* **2009**, *1*, 276–288, doi:10.1038/nchem.257.

261. Chernikova, E. V.; Sivtsov, E. V. Reversible addition-fragmentation chain-transfer polymerization: Fundamentals and use in practice. *Polym. Sci. - Ser. B* **2017**, *59*, 117–146, doi:10.1134/S1560090417020038.

262. Liu, H.; Chung, H. Lignin-based polymers via graft copolymerization. *J. Polym. Sci. Part A Polym. Chem.* **2017**, *55*, 3515–3528, doi:10.1002/pola.28744.

263. Matyjaszewski, K.; Spanswick, J. Controlled/living radical polymerization. *Mater. Today* **2005**, *8*, 26–33.

264. Ngo, T.-D. Introduction to Composite Materials. In *Composite and Nanocomposite Materials - From Knowledge to Industrial Applications*; Ngo, T.-D., Ed.; IntechOpen, 2020; pp. 1–27.

265. Naveen, M.H.; Gurudatt, N.G.; Shim, Y.B. Applications of conducting polymer composites to electrochemical sensors: A review. *Appl. Mater. Today* **2017**, *9*, 419–433, doi:10.1016/j.apmt.2017.09.001.

266. Chauhan, M.; Bhardwaj, S.K.; Bhanjana, G.; Kumar, R.; Dilbaghi, N.; Kumar, S.; Chaudhary, G.R. Conducting Polymers and Metal-Organic Frameworks as Advanced Materials for Development of Nanosensors. In *Advances in Nanosensors for Biological and Environmental Analysis*; Deep, A., Kumar, S., Eds.; Elsevier Inc.: St. Louis, Missouri, 2019; pp. 43–62 ISBN 9780128174562.

267. Nehra, M.; Dilbaghi, N.; Hassan, A.A.; Kumar, S. Carbon-Based Nanomaterials for the Development of Sensitive Nanosensor Platforms. In *Advances in Nanosensors for Biological and Environmental Analysis*; Deep, A., Kumar, S., Eds.; Elsevier Inc.: St. Louis, Missouri, 2019; Vol. 60, pp. 1–25 ISBN 9780128174562.

268. Loos, M. Fundamentals of Polymer Matrix Composites Containing CNTs. In *Carbon Nanotube Reinforced Composites*; Elsevier Inc., 2015; pp. 125–170 ISBN 9781455731961.

269. Li, Y.; Huang, X.; Zeng, L.; Li, R.; Tian, H.; Fu, X.; Wang, Y.; Zhong, W.H. A review of the electrical and mechanical properties of carbon nanofiller-reinforced polymer composites. *J. Mater. Sci.* **2019**, *54*, 1036–1076, doi:10.1007/s10853-018-3006-9.

270. Chen, C.; Wang, X.; Li, M.; Fan, Y.; Sun, R. Humidity sensor based on reduced graphene oxide/lignosulfonate composite thin-film. *Sensors Actuators B Chem.* **2018**, *255*, 1569–1576, doi:10.1016/j.snb.2017.08.168.

271. Sharma, S.; Jain, K.K.; Sharma, A. Solar Cells: In Research and Applications—A Review. *Mater. Sci. Appl.* **2015**, *6*, 1145–1155, doi:10.4236/msa.2015.612113.

272. Bagher, A.M.; Vahid, M.M.A.; Mohsen, M. Types of Solar Cells and Application. *Am. J. Opt. Photonics* **2015**, *3*, 94–113, doi:10.11648/j.ajop.20150305.17.

273. Espinoza-Acosta, J.L.; Torres-Chávez, P.I.; Olmedo-Martínez, J.L.; Vega-Rios, A.; Flores-Gallardo, S.; Zaragoza-Contreras, E.A. Lignin in storage and renewable energy applications:

A review. *J. Energy Chem.* **2018**, *27*, 1422–1438, doi:10.1016/j.jechem.2018.02.015.

274. Wu, X.; Jiang, J.; Wang, C.; Liu, J.; Pu, Y.; Ragauskas, A.; Li, S.; Yang, B. Lignin-derived electrochemical energy materials and systems. *Biofuels, Bioprod. Biorefining* **2020**, 1–23, doi:10.1002/bbb.2083.

275. ISO 14040 Environmental management - Life cycle assessment - Principles and framework 2006.

276. ISO 14044 Environmental management - Life cycle assessment - Requirements and guidelines 2009.

277. Lettner, M.; Solt, P.; Rößiger, B.; Pufky-Heinrich, D.; Jääskeläinen, A.S.; Schwarzbauer, P.; Hesser, F. From wood to resin-identifying sustainability levers through hotspotting lignin valorisation pathways. *Sustain.* **2018**, *10*, doi:10.3390/su10082745.

278. Hildebrandt, J.; Budzinski, M.; Nitzsche, R.; Weber, A.; Krombholz, A.; Thrän, D.; Bezama, A. Assessing the technical and environmental performance of wood-based fiber laminates with lignin based phenolic resin systems. *Resour. Conserv. Recycl.* **2019**, *141*, 455–464, doi:10.1016/j.resconrec.2018.10.029.

279. Yuan, Y.; Guo, M. Do green wooden composites using lignin-based binder have environmentally benign alternatives? A preliminary LCA case study in China. *Int. J. Life Cycle Assess.* **2017**, *22*, 1318–1326, doi:10.1007/s11367-016-1235-1.

280. Arias, A.; González-García, S.; González-Rodríguez, S.; Feijoo, G.; Moreira, M.T. Cradle-to-gate Life Cycle Assessment of bio-adhesives for the wood panel industry. A comparison with petrochemical alternatives. *Sci. Total Environ.* **2020**, *738*, 140357, doi:10.1016/j.scitotenv.2020.140357.

281. Isola, C.; Sieverding, H.L.; Numan-Al-Mobin, A.M.; Rajappagowda, R.; Boakye, E.A.; Raynie, D.E.; Smirnova, A.L.; Stone, J.J. Vanillin derived from lignin liquefaction: a sustainability evaluation. *Int. J. Life Cycle Assess.* **2018**, *23*, 1761–1772, doi:10.1007/s11367-017-1401-0.

282. Corona, A.; Biddy, M.J.; Vardon, D.R.; Birkved, M.; Hauschild, M.Z.; Beckham, G.T. Life cycle assessment of adipic acid production from lignin. *Green Chem.* **2018**, *20*, 3857–3866, doi:10.1039/c8gc00868j.

283. Montazeri, M.; Eckelman, M.J. Life Cycle Assessment of Catechols from Lignin Depolymerization. *ACS Sustain. Chem. Eng.* **2016**, *4*, 708–718, doi:10.1021/acssuschemeng.5b00550.

284. Manzardo, A.; Marson, A.; Roso, M.; Boaretti, C.; Modesti, M.; Scipioni, A.; Lorenzetti, A. Life Cycle Assessment Framework to Support the Design of Biobased Rigid Polyurethane Foams. *ACS Omega* **2019**, *4*, 14114–14123, doi:10.1021/acsomega.9b02025.

285. Moretti, C.; Corona, B.; Hoefnagels, R.; Vural-Gürsel, I.; Gosselink, R.; Junginger, M. Review of life cycle assessments of lignin and derived products: Lessons learned. *Sci. Total Environ.* **2021**, *770*, 144656, doi:10.1016/j.scitotenv.2020.144656.

286. Lettner, M.; Hesser, F.; Hedeler, B.; Schwarzbauer, P.; Stern, T. Barriers and incentives for the use of lignin-based resins: Results of a comparative importance performance analysis. *J. Clean. Prod.* **2020**, *256*, 120520, doi:10.1016/j.jclepro.2020.120520.

287. Tourné, C.M.; Tourné, G.F.; Malik, S.A.; Weakley, T.J.R. Triheteropolyanions containing copper(II), manganese(II), or manganese(III). *J. Inorg. Nucl. Chem.* **1970**, *32*, 3875–3890, doi:10.1016/0022-1902(70)80566-8.

288. NP EN 197-1. Cimento Parte 1: Composição, específicações e critérios de conformidade para

cimentos correntes, 2001, 1–19.

289. CIMPOR Technical data sheet of Portland limestone cement CEM II/A-L 42,5R (accessed on 30/08/2021), 2019, 1–2.

290. Selvendran, R.R.; March, J.F.; Ring, S.G. Determination of Aldoses and Uranic of Vegetable Fiber Acid Content. *Anal. Biochem.* **1979**, *292*, 282–292, doi:10.1016/0003-2697(79)90583-9.

291. Gautam, R.; Vanga, S.; Ariese, F.; Umapathy, S. Review of multidimensional data processing approaches for Raman and infrared spectroscopy. *EPJ Tech. Instrum.* **2015**, *2*, 8, doi:10.1140/epjti/s40485-015-0018-6.

292. Evtuguin, D. V.; Pascoal Neto, C.; Rocha, J.; Pedrosa De Jesus, J.D. Oxidative delignification in the presence of molybdovanadophosphate heteropolyanions: Mechanism and kinetic studies. *Appl. Catal. A Gen.* **1998**, *167*, 123–139, doi:10.1016/S0926-860X(97)00306-2.

293. Magina, S.; Barros-Timmons, A.; Evtuguin, D. V. Laccase-catalyzed oxidative modification of lignosulfonates from acidic sulfite pulping of eucalyptus wood. *Holzforschung* **2020**, *74*, 589–596, doi:10.1515/hf-2019-0272.

294. BS EN 12350-5. Testing fresh concrete - Part 5: Flow table test,. *Br. Stand.* 2009, 1–14.

295. Duncan, J. Principles and Applications of Mechanical Thermal Analysis. In *Principles and Applications of Thermal Analysis*; Gabbott, P., Ed.; Blackwell Publishing Ltd, 2008; pp. 1–263 ISBN 9781405131711.

296. Menard, K. *Dynamic mechanical analysis: a practical introduction*; 2nd ed.; CRC Press, Taylor & Francis Group, LLC: Boca Raton, FL, 2008; ISBN 978-1-4200-5312-8.

297. Magina, S.; Barros-Timmons, A.; Evtuguin, D. V. Changes in potentialities of acidic sulphite pulping spent liquors while re-profiling mill from paper-grade to dissolving pulps. In Proceedings of the 15th European Workshop on Lignocellulosics and Pulp (EWLP2018) - Posters Presentations; Aveiro, Portugal, 2018; pp. 303–306.

298. Royall, P.G.; Huang, C.Y.; Tang, S.W.J.; Duncan, J.; Van-De-Velde, G.; Brown, M.B. The development of DMA for the detection of amorphous content in pharmaceutical powdered materials. *Int. J. Pharm.* **2005**, *301*, 181–191, doi:10.1016/j.ijpharm.2005.05.015.

299. Gmelin, E.; Sarge, S.M. Calibration of differential scanning calorimeters. *Pure Appl. Chem.* **1995**, *67*, 1789–1800, doi:10.1351/pac199567111789.

300. Martins, J.A.; Cruz-Pinto, J.J.C. The temperature calibration on cooling of differential scanning calorimeters. *Thermochim. Acta* **1999**, *332*, 179–188, doi:10.1016/0040-6031(90)80235-Q.

301. Collier, W.; Kalasinsky, V.F.; Schultz, T.P. Infrared study of lignin: Assignment of methoxyl C-H bending and stretching bands. *Holzforschung* **1997**, *51*, 167–168, doi:10.1515/hfsg.1997.51.2.167.

302. Dawy, M.; Shabaka, A.A.; Nada, A.M.A. Molecular structure and dielectric properties of some treated lignins. *Polym. Degrad. Stab.* **1998**, *62*, 455–462, doi:10.1016/S0141-3910(98)00026-3.

303. Agarwal, U.P.; Atalla, R.H. Vibrational Spectroscopy. In *Lignin and lignans: advances in chemistry*; Heitner, C., Dimmel, D., Schmidt, J.A., Eds.; Taylor and Francis Group, LLC: Boca Raton, FL, 2010; pp. 103–136 ISBN 9781574444865.

304. Boeriu, C.G.; Bravo, D.; Gosselink, R.J.A.; van Dam, J.E.G. Characterisation of structure-dependent functional properties of lignin with infrared spectroscopy. *Ind. Crops Prod.* **2004**, *20*, 205–218, doi:10.1016/j.indcrop.2004.04.022.

305. Detoni, S.; Hadzi, D. Infra-red spectra of some organic sulphur-oxygen compounds. *Spectrochim. Acta* **1956**, *11*, 601–608, doi:10.1016/S0371-1951(56)80102-1.

306. Bellamy, L.J. *The Infrared Spectra of Complex Molecules. Volume 2. Advances in Infrared group frequencies*; 2nd Ed.; Chapmanand Hall: London and New York, 1980; ISBN 978-94-011-6522-8.

307. Collier, W.E.; Schultz, T.P.; Kalasinsky, V.F. Infrared study of lignin: reexamination of acryl-alkyl ether C-O stretching. *Holzforschung* **1992**, *46*, 523–528, doi:10.1515/hfsg.1992.46.6.523.

308. Hergert, H.L. Infrared spectra. In *Lignins: Occurrence, formation, structure and reactions*; Sarkanen, K. V., Ludwig, C.H., Eds.; John Wiley & Sons, Inc.: New York, 1971; pp. 267–297 ISBN 978-0471754220.

309. Evtuguin, D. V.; Neto, C.P.; Silva, A.M.S.; Domingues, P.M.; Amado, F.M.L.; Robert, D.; Faix, O. Comprehensive study on the chemical structure of dioxane lignin from plantation Eucalyptus globulus wood. *J. Agric. Food Chem.* **2001**, *49*, 4252–4261, doi:10.1021/jf010315d.

310. Magina, S.; Marques, A.P.; Evtuguin, D. V. Study on the residual lignin in Eucalyptus globulus sulphite pulp. *Holzforschung* **2015**, *69*, 513–522, doi:10.1515/hf-2014-0218.

311. Lutnaes, B.F.; Myrvold, B.O.; Lauten, A.; Endeshaw, M.M. 1H and 13C NMR data of benzylsulfonic acids – model compounds for lignosulfonate. *Magn. Reson. Chem.* **2008**, *46*, 299–305, doi:10.1002/mrc.2184.

312. Jakab, B.E.; Faix, O.; Till, F.; Szekely, T. Thermogravimetry/Mass Spectrometry of Various Lignosulfonates as well as of a Kraft and Acetosolv Lignin. *Holzforschung* **1991**, *45*, 355–360, doi:10.1515/hfsg.1991.45.5.355.

313. Yang, H.; Yan, R.; Chen, H.; Lee, D.H.; Zheng, C. Characteristics of hemicellulose, cellulose and lignin pyrolysis. *Fuel* **2007**, *86*, 1781–1788, doi:10.1016/j.fuel.2006.12.013.

314. Brebu, M.; Vasile, C. Thermal degradation of lignin - a review. *Cellul. Chem. Technol.* **2010**, *44*, 353–363.

315. Scripture, E.W. US Patent 2081642. Indurating Composition for Concrete, 1937.

316. Li, R.; Yang, D.; Guo, W.; Qiu, X. The adsorption and dispersing mechanisms of sodium lignosulfonate on Al2O3 particles in aqueous solution. *Holzforschung* **2013**, *67*, 387–394, doi:10.1515/hf-2012-0108.

317. Ouyang, X.; Qiu, X.; Chen, P. Physicochemical characterization of calcium lignosulfonate-A potentially useful water reducer. *Colloids Surfaces A Physicochem. Eng. Asp.* **2006**, *282–283*, 489–497, doi:10.1016/j.colsurfa.2005.12.020.

318. Kim, S.; Silva, C.; Evtuguin, D. V.; Gamelas, J.A.F.; Cavaco-Paulo, A. Polyoxometalate/laccase-mediated oxidative polymerization of catechol for textile dyeing. *Appl. Microbiol. Biotechnol.* **2011**, *89*, 981–987, doi:10.1007/s00253-010-2932-5.

319. Plank, J.; Winter, C. Competitive adsorption between superplasticizer and retarder molecules on mineral binder surface. *Cem. Concr. Res.* **2008**, *38*, 599–605, doi:10.1016/j.cemconres.2007.12.003.

320. Magina, S.; Barros-Timmons, A.; Evtuguin, D. V. Oxidative polymerization of magnesium-based lignosulphonates from acidic Eucalyptus globulus sulfite pulping by laccase: preliminary results. In Proceedings of the Book of Extended Abstracts of the 13th International Chemical and Biological Engineering Conference (CHEMPOR 2018); Aveiro, Portugal, 2018; pp. 359–360.

321. Gärtner, A.; Gellerstedt, G.; Tamminen, T. Determination of phenolic hydroxyl groups in residual lignin using a modified UV-method. *Nord. Pulp Pap. Res. J.* **1999**, *14*, 163–170, doi:10.3183/npprj-1999-14-02-p163-170.

322. Areskogh, D.; Li, J.; Nousiainen, P.; Gellerstedt, G.; Sipilä, J.; Henriksson, G. Oxidative polymerisation of models for phenolic lignin end-groups by laccase. *Holzforschung* **2010**, *64*, 21–34, doi:10.1515/HF.2010.001.

323. Ralph, S.; Ralph, J. NMR Database of Lignin and Cell Wall Model Compounds Available online: http://ars.usda.gov/Services/docs.htm?docid=10491.

324. Areskogh, D.; Nousiainen, P.; Li, J.; Gellerstedt, G.; Sipilä, J.; Henriksson, G. Sulfonation of phenolic end groups in lignin directs laccase-initiated reactions towards cross-linking. *Ind. Biotechnol.* **2010**, *6*, 50–59, doi:10.1089/ind.2010.6.050.

325. Bujanovic, B.; Ralph, S.; Reiner, R.; Hirth, K.; Atalla, R. Polyoxometalates in oxidative delignification of chemical pulps: Effect on lignin. *Materials (Basel).* **2010**, *3*, 1888–1903, doi:10.3390/ma3031888.

326. Lai, J.T.; Filla, D.; Shea, R. Functional polymers from novel carboxyl-terminated trithiocarbonates as highly efficient RAFT agents. *Macromolecules* **2002**, *35*, 6754–6756.

327. Silmore, K.S.; Gupta, C.; Washburn, N.R. Tunable Pickering emulsions with polymer-grafted lignin nanoparticles (PGLNs). *J. Colloid Interface Sci.* **2016**, *466*, 91–100, doi:10.1016/j.jcis.2015.11.042.

328. Gupta, C.; Washburn, N.R. Polymer-grafted lignin surfactants prepared via reversible addition-fragmentation chain-transfer polymerization. *Langmuir* **2014**, *30*, 9303–9312, doi:10.1021/la501696y.

329. Chung, H.; Al-Khouja, A.; Washburn, N.R. Lignin-Based Graft Copolymers via ATRP and Click Chemistry. In *Green Polymer Chemistry: Biocatalysis and Materials II*; Cheng, H.N., Gross, R.A., Smith, P.B., Eds.; ACS Symposium Series; American Chemical Society: Washington, DC, 2013; pp. 373–391.

330. Passauer, L. Highly Swellable Lignin Hydrogels : Novel Materials with Interesting Properties. In *Functional Materials from Renewable Sources (ACS Symposium Series)*; Liebner, F., Rosenau, T., Eds.; American Chemical Society: Washington, DC, 2012; pp. 211–228.

331. Ilg, M.; Plank, J. Synthesis and Properties of a Polycarboxylate Superplasticizer with a Jellyfish-Like Structure Comprising Hyperbranched Polyglycerols. *Ind. Eng. Chem. Res.* **2019**, *58*, 12913–12926, doi:10.1021/acs.iecr.9b02077.

332. Uchikawa, H.; Hanehara, S.; Sawaki, D. The role of steric repulsive force in the dispersion of cement particles in fresh paste prepared with organic admixture. *Cem. Concr. Res.* **1997**, *27*, 37–50, doi:10.1016/S0008-8846(96)00207-4.

333. Gelardi, G.; Flatt, R.J. Working mechanisms of water reducers and superplasticizers. In *Science and Technology of Concrete Admixtures*; Aïtcin, P.-C., Flatt, R.J.., Eds.; Elsevier Ltd., 2016; pp. 257–278 ISBN 9780081006931.

334. Wu, X.; Zhang, H. Preparation of cement water reducer of modified lignosulfonate. *Adv. Mater. Res.* **2011**, *168–170*, 541–544, doi:10.4028/www.scientific.net/AMR.168-170.541.

335. Qasem, N.A.A.; Mohammed, R.H.; Lawal, D.U. Removal of heavy metal ions from wastewater: a comprehensive and critical review. *npj Clean Water* **2021**, *4*, 36, doi:10.1038/s41545-021-00127-0.

336. Bansod, B.; Kumar, T.; Thakur, R.; Rana, S.; Singh, I. A review on various electrochemical

techniques for heavy metal ions detection with different sensing platforms. *Biosens. Bioelectron.* **2017**, *94*, 443–455, doi:10.1016/j.bios.2017.03.031.

337. Isildak, Ö.; Özbek, O. Application of Potentiometric Sensors in Real Samples. *Crit. Rev. Anal. Chem.* **2021**, *51*, 218–231, doi:10.1080/10408347.2019.1711013.

338. Jin Mei, C.; Ahmad, S.A.A. A review on the determination heavy metals ions using calixarene-based electrochemical sensors. *Arab. J. Chem.* **2021**, *14*, 103303, doi:10.1016/j.arabjc.2021.103303.

339. Cuartero, M.; Crespo, G.A. All-solid-state potentiometric sensors: A new wave for in situ aquatic research. *Curr. Opin. Electrochem.* **2018**, *10*, 98–106, doi:10.1016/j.coelec.2018.04.004.

340. Parrilla, M.; Cuartero, M.; Crespo, G.A. Wearable potentiometric ion sensors. *TrAC - Trends Anal. Chem.* **2019**, *110*, 303–320, doi:10.1016/j.trac.2018.11.024.

341. Özbek, O.; Berkel, C.; Isildak, Ö. Applications of Potentiometric Sensors for the Determination of Drug Molecules in Biological Samples. *Crit. Rev. Anal. Chem.* **2020**, doi:10.1080/10408347.2020.1825065.

342. Magina, S.; Barros-Timmons, A.; Ventura, S.P.M.; Evtuguin, D. V. Evaluating the hazardous impact of ionic liquids – Challenges and opportunities. *J. Hazard. Mater.* **2021**, *412*, 125215, doi:10.1016/j.jhazmat.2021.125215.

343. Yang, J.; Liu, Y.; Liu, S.; Li, L.; Zhang, C.; Liu, T. Conducting polymer composites: Material synthesis and applications in electrochemical capacitive energy storage. *Mater. Chem. Front.* **2017**, *1*, 251–268, doi:10.1039/c6qm00150e.

344. Bach-Toledo, L.; Hryniewicz, B.M.; Marchesi, L.F.; Dall'Antonia, L.H.; Vidotti, M.; Wolfart, F. Conducting polymers and composites nanowires for energy devices: A brief review. *Mater. Sci. Energy Technol.* **2020**, *3*, 78–90, doi:10.1016/j.mset.2019.09.006.

345. Tajik, S.; Beitollahi, H.; Nejad, F.G.; Shoaie, I.S.; Khalilzadeh, M.A.; Asl, M.S.; Van Le, Q.; Zhang, K.; Jang, H.W.; Shokouhimehr, M. Recent developments in conducting polymers: Applications for electrochemistry. *RSC Adv.* **2020**, *10*, 37834–37856, doi:10.1039/d0ra06160c.

346. Kitto, T.; Bodart-Le Guen, C.; Rossetti, N.; Cicoira, F. Processing and patterning of conducting polymers for flexible, stretchable, and biomedical electronics. In *Handbook of Organic Materials for Electronic and Photonic Devices*; Ostroverkhova, O., Ed.; Elsevier Ltd., 2019; pp. 817–842 ISBN 9780081022849.

347. Khalifeh, S. Optimized Electronic Polymers, Small Molecules, Complexes, and Elastomers for Organic Electronic Systems. In *Polymers in Organic Electronics*; ChemTec Publishing, 2020; pp. 49–184 ISBN 978-1-927885-68-0.

348. Zhou, Q.; Shi, G. Conducting Polymer-Based Catalysts. *J. Am. Chem. Soc.* **2016**, *138*, 2868–2876, doi:10.1021/jacs.5b12474.

349. Iqbal, S.; Ahmad, S. Conducting polymer composites: An efficient EMI shielding material. In *Materials for Potential EMI Shielding Applications*; Kuruvilla, J., Runcy, W., Gejo, G., Eds.; Elsevier Inc., 2020; pp. 257–266 ISBN 9780128175903.

350. Maruthi, N.; Faisal, M.; Raghavendra, N. Conducting polymer based composites as efficient EMI shielding materials: A comprehensive review and future prospects. *Synth. Met.* **2021**, *272*, 116664, doi:10.1016/j.synthmet.2020.116664.

351. Teixeira, S.S.; Gama, N.; Cordeiro, T.; Barros-Timmons, A.; Dionísio, M.; Graça, M.P.F.; Costa, L.C. Poly (L-lactic acid)/lithium ferrite composites: Electrical properties. *Polymer*

*(Guildf).* **2021**, doi:10.1016/j.polymer.2021.124100.

352. Wang, Y.; Liu, A.; Han, Y.; Li, T. Sensors based on conductive polymers and their composites: a review. *Polym. Int.* **2020**, *69*, 7–17, doi:10.1002/pi.5907.

353. Chen, J.; Zhu, Y.; Huang, J.; Zhang, J.; Pan, D.; Zhou, J.; Ryu, J.E.; Umar, A.; Guo, Z. Advances in Responsively Conductive Polymer Composites and Sensing Applications. *Polym. Rev.* **2021**, *61*, 157–193, doi:10.1080/15583724.2020.1734818.

354. Aradhana, R.; Mohanty, S.; Nayak, S.K. Comparison of mechanical, electrical and thermal properties in graphene oxide and reduced graphene oxide filled epoxy nanocomposite adhesives. *Polymer (Guildf).* **2018**, *141*, 109–123, doi:10.1016/j.polymer.2018.03.005.

355. Guo, X.; Zhang, S.; Shan, X.Q. Adsorption of metal ions on lignin. *J. Hazard. Mater.* **2008**, *151*, 134–142, doi:10.1016/j.jhazmat.2007.05.065.

356. Li, Z.; Ge, Y. Application of Lignin and Its Derivatives in Adsorption of Heavy Metal Ions in Water: A Review. *ACS Sustain. Chem. Eng.* **2018**, *6*, 7181–7192, doi:10.1021/acssuschemeng.8b01345.

357. Santander, P.; Butter, B.; Oyarce, E.; Yáñez, M.; Xiao, L.P.; Sánchez, J. Lignin-based adsorbent materials for metal ion removal from wastewater: A review. *Ind. Crops Prod.* **2021**, *167*, 113510, doi:10.1016/j.indcrop.2021.113510.

358. Ge, Y.; Xiao, D.; Li, Z.; Cui, X. Dithiocarbamate functionalized lignin for efficient removal of metallic ions and the usage of the metal-loaded bio-sorbents as potential free radical scavengers. *J. Mater. Chem. A* **2014**, *2*, 2136–2145, doi:10.1039/c3ta14333c.

359. Jin, C.; Zhang, X.; Xin, J.; Liu, G.; Wu, G.; Kong, Z.; Zhang, J. Clickable Synthesis of 1,2,4-Triazole Modified Lignin-Based Adsorbent for the Selective Removal of Cd(II). *ACS Sustain. Chem. Eng.* **2017**, *5*, 4086–4093, doi:10.1021/acssuschemeng.7b00072.

360. Zou, J.; Chen, Y.; Liang, M.; Zou, H. Effect of hard segments on the thermal and mechanical properties of water blown semi-rigid polyurethane foams. *J. Polym. Res.* **2015**, *22*, 120, doi:10.1007/s10965-015-0770-y.

361. Chattopadhyay, D.K.; Webster, D.C. Thermal stability and flame retardancy of polyurethanes. *Prog. Polym. Sci.* **2009**, *34*, 1068–1133, doi:10.1016/j.progpolymsci.2009.06.002.

362. Chupka, E.I.; Rykova, T.M. Electrical properties of lignin. *Chem. Nat. Compd.* **1983**, *19*, 78–80, doi:10.1007/BF00579968.

363. Mansor, M.R.; Fadzullah, S.H.S.M.; Masripan, N.A.B.; Omar, G.; Akop, M.Z. Comparison Between Functionalized Graphene and Carbon Nanotubes: Effect of Morphology and Surface Group on Mechanical, Electrical, and Thermal Properties of Nanocomposites. In *Functionalized Graphene Nanocomposites and Their Derivatives: Synthesis, Processing and Applications*; Jawaid, M., Bouhfid, R., Qaiss, A. el K., Eds.; Elsevier Inc., 2019; pp. 177–204 ISBN 9780128145531.

364. Min, C.; Shen, X.; Shi, Z.; Chen, L.; Xu, Z. The electrical properties and conducting mechanisms of carbon nanotube/polymer nanocomposites: A review. *Polym. - Plast. Technol. Eng.* **2010**, *49*, 1172–1181, doi:10.1080/03602559.2010.496405.

365. Jonscher, A.K. The "universal" dielectric response. *Nature* **1977**, *267*, 673–679, doi:10.1038/267673a0.

366. Jonscher, A.K. A new understanding of the dielectric relaxation of solids. *J. Mater. Sci.* **1981**, *16*, 2037–2060, doi:10.1007/BF00542364.

367. Greenhoe, B.M.; Hassan, M.K.; Wiggins, J.S.; Mauritz, K.A. Universal power law behavior

of the AC conductivity versus frequency of agglomerate morphologies in conductive carbon nanotube-reinforced epoxy networks. *J. Polym. Sci. Part B Polym. Phys.* **2016**, *54*, 1918–1923, doi:10.1002/polb.24121.

368. Sun, H.; Zhang, H.; Liu, S.; Ning, N.; Zhang, L.; Tian, M.; Wang, Y. Interfacial polarization and dielectric properties of aligned carbon nanotubes/polymer composites: The role of molecular polarity. *Compos. Sci. Technol.* **2018**, *154*, 145–153, doi:10.1016/j.compscitech.2017.11.008.

369. Buck, R.P.; Lindner, E. Recomendations for nomenclature of ion-selective electrodes (IUPAC recommendations 1994). *Pure Appl. Chem.* **1994**, *66*, 2527–2536, doi:10.1351/pac199466122527.

370. Bedemo, A.; Chandravanshi, B.S.; Zewge, F. Removal of trivalent chromium from aqueous solution using aluminum oxide hydroxide. *Springerplus* **2016**, *5*, 1288, doi:10.1186/s40064-016-2983-x.

371. Shen-Yang, T.; Ke-An, L. The distribution of chromium(VI) species in solution as a function of pH and concentration. *Talanta* **1986**, *33*, 775–777, doi:10.1016/0039-9140(86)80187-4.

372. Vlasov, Y.G.; Bychkov, E.A.; Legin, A. V. Chalcogenide glass chemical sensors: Research and analytical applications. *Talanta* **1994**, *41*, 1059–1063, doi:10.1016/0039-9140(94)00124-3.

373. Umezawa, Y.; Bühlmann, P.; Umezawa, K.; Tohda, K.; Amemiya, S. Potentiometric selectivity coefficients of ion-selective electrodes part I. Inorganic cations (technical report). *Pure Appl. Chem.* **2000**, *72*, 1851–2082, doi:10.1351/pac200072101851.

374. Rudnitskaya, A.; Evtuguin, D. V. Lignin Applications in Chemical Sensing. In *Multisensor Systems For Chemical Analysis*; Lvova, L., Kirsanov, D., Di Natale, C., Legin, A., Eds.; CRC Press, Taylor & Francis Group, LLC, 2013; pp. 181–210 ISBN 9780120149018.

375. Faridbod, F.; Davarkhah, N.; Beikzadeh, M.; Yekefallah, M.; Rezapour, M. Cu2+-selective sensors based on a new ion-carrier and their application for the analysis of copper content of water samples. *Int. J. Electrochem. Sci.* **2017**, *12*, 876–889, doi:10.20964/2017.02.11.

376. Amr, A.E.G.E.; Al-Omar, M.A.; Kamel, A.H.; Elsayed, E.A. Single-piece solid contact Cu2+-Selective Electrodes Based on a synthesized macrocyclic calix[4]arene derivative as a neutral carrier ionophore. *Molecules* **2019**, *24*, 1–12, doi:10.3390/molecules24050920.

377. Seo, H.; Jeong, E.; Ahmed, M.S.; Lee, H.K.; Jeon, S. Polymeric membrane silver-ion selective electrodes based on schiff base N,N'-bis(pyridin-2-ylmethylene)benzene-1,2-diamine. *Bull. Korean Chem. Soc.* **2010**, *31*, 1699–1703, doi:10.5012/bkcs.2010.31.6.1699.

378. Mazloum Ardakani, M.; Safaei - Ghomi, J.; Mehdipoor, M. Highly selective copper membrane electrode using C-p-nitrophenyl-N-phenylnitrone. *New J. Chem.* **2003**, *27*, 1140–1143, doi:10.1039/b302819b.

379. Singh, G.; Yadav, K.C. A Zinc Selective Polymeric Membrane Electrode Based on N,N'-benzene-1,2-diylbis[1-(pyridin-2-yl)ethanimine] as an Ionophore. *Sch. Acad. J. Pharm.* **2014**, *3*, 438–443.

380. Chandra, S.; Tomar, P.K.; Kumar, A.; Malik, A.; Singh, A. Fabrication of copper-selective PVC membrane electrode based on newly synthesized copper complex of Schiff base as carrier. *J. Saudi Chem. Soc.* **2016**, *20*, S293–S299, doi:10.1016/j.jscs.2012.11.010.

381. Gupta, V.K.; Jain, A.K.; Maheshwari, G.; Lang, H.; Ishtaiwi, Z. Copper(II)-selective potentiometric sensors based on porphyrins in PVC matrix. *Sensors Actuators, B Chem.* **2006**, *117*, 99–106, doi:10.1016/j.snb.2005.11.003.

382. Kamel, A.H.; Mahmoud, W.H.; Mostafa, M.S. Response characteristics of copper-selective polymer membrane electrodes based on a newly synthesized macrocyclic calix[4]arene derivative as a neutral carrier ionophore. *Electroanalysis* **2010**, *22*, 2453–2459, doi:10.1002/elan.201000187.

383. Kopylovich, M.N.; Mahmudov, K.T.; Pombeiro, A.J.L. Poly(vinyl) chloride membrane copper-selective electrode based on 1-phenyl-2-(2-hydroxyphenylhydrazo)butane-1,3-dione. *J. Hazard. Mater.* **2011**, *186*, 1154–1162, doi:10.1016/j.jhazmat.2010.11.119.

384. Isa, I.M.; Noor, S.M.; Juahir, Y.; Hashim, N.; Ahmad, M.; Kamari, A.; Mohamed, A.; Ghani, S.A.; Wardani, N.I. Zinc(II) Selective Electrode based on Polymeric Membrane of 2,6-Diacetylpyridinebis(benzenesulfonylhydrazide) Ligand. *Int. J. Electrochem. Sci.* **2014**, *9*, 4812–4522.

385. Rezvani Ivari, S.A.; Darroudi, A.; Arbab Zavar, M.H.; Zohuri, G.; Ashraf, N. Ion imprinted polymer based potentiometric sensor for the trace determination of Cadmium (II) ions. *Arab. J. Chem.* **2017**, *10*, S864–S869, doi:10.1016/j.arabjc.2012.12.021.

386. Kaushal, S.; Badru, R.; Singh, P.; Kumar, S.; Mittal, S.K. Estimation of Trace Level Cadmium(II) by Polyaniline-zirconium Phosphoborate Nanocomposite-based Membrane Electrode. *J. Anal. Chem.* **2019**, *74*, 800–808, doi:10.1134/S1061934819080148.

387. Ansari, R.; Delavar, A.F.; Mohammad-Khah, A. Solid-state ion selective electrode based on polypyrrole conducting polymer nanofilm as a new potentiometric sensor for Zn 2+ ion. *J. Solid State Electrochem.* **2012**, *16*, 3315–3322, doi:10.1007/s10008-012-1759-7.

388. Gupta, V.K.; Singh, A.K.; Gupta, B. Schiff bases as cadmium(II) selective ionophores in polymeric membrane electrodes. *Anal. Chim. Acta* **2007**, *583*, 340–348, doi:10.1016/j.aca.2006.10.039.

389. Gupta, V.K.; Singh, A.K.; Al Khayat, M.; Gupta, B. Neutral carriers based polymeric membrane electrodes for selective determination of mercury (II). *Anal. Chim. Acta* **2007**, *590*, 81–90, doi:10.1016/j.aca.2007.03.014.

390. Puri, R.K.; Kumar, V.; Mahajan, M.P.; Mahajan, R.K. Mercury(II) ion recognition by newly synthesized oxadiazaphosphepine based receptors: Coated graphite and polymeric membrane electrodes. *J. Incl. Phenom. Macrocycl. Chem.* **2011**, *69*, 263–271, doi:10.1007/s10847-010-9837-x.

391. Hassan, A.K. Chemical Sensor for Determination of Mercury in Contaminated Water. *Mod. Chem. Appl.* **2013**, *01*, 1–4, doi:10.4172/2329-6798.1000111.

392. Ansari, R.; Delavar, A.F.; Mohammad-khah, A. A solid state Cr(VI) ion-selective electrode based on polypyrrole. *Microchim. Acta* **2012**, *178*, 71–79, doi:10.1007/s00604-012-0802-9.

393. Benvidi, A.; Elahizadeh, M.; Zare, H.R.; Vafazadeh, R. Highly sensitive membrane electrode based on a copper(II)-bis(n-4-Methylphenyl-salicyldenaminato) complex for the determination of chromate. *Anal. Lett.* **2011**, *44*, 595–606, doi:10.1080/00032711003783028.

394. Andac, M.; Coldur, F.; Bilir, S.; Birinci, A.; Demir, S.; Uzun, H. Solid-contact polyvinyl chloride membrane electrode based on the bis[(2-(hydroxyethylimino)phenolato]copper(II) complex for trace level determination of copper ions in wastewater. *Can. J. Chem.* **2014**, *92*, 324–328, doi:10.1139/cjc-2013-0530.

395. Kumar, P.; Sharma, H.K. Development of all solid state chromium(III) selective sensor by using newly synthesized triazole derivative as an ionophore in PVC matrix. *Electrochim. Acta* **2013**, *87*, 925–929, doi:10.1016/j.electacta.2012.09.027.

396. Yan, Z.; Zhang, S.; Wang, H.; Kang, Y. Preparation and analytical application of new Cr3+-selective membrane electrodes based on acylhydrazone-containing benzimidazole

derivatives. *J. Iran. Chem. Soc.* **2016**, *13*, 411–420, doi:10.1007/s13738-015-0749-y.

397. Chen, L.; Zeng, X.; He, X.; Zhengzhi; Zhang Selective electrodes for silver based on polymeric membranes containing calix[4]arene derivatives. *Fresenius. J. Anal. Chem.* **2000**, *367*, 535–538, doi:10.1007/s002160000397.

398. Mahajan, R.K.; Kaur, I.; Sharma, V.; Kumar, M. Sensor for silver(I) ion based on schiff-base-p-tert-butylcalix[4]arene. *Sensors* **2002**, *2*, 417–423, doi:10.3390/s21000417.

399. Masrournia, M.; Zamani, H.A.; Mohamadzadeh, H.; Seyedi, S.M.; Ganjali, M.R.; Eshghi, H. A Silver(I) PVC-Membrane Sensor Based on Synthesized Dilaktam Crown Ether. *J. Chil. Chem. Soc.* **2009**, *53*, 63–67, doi:10.4067/S0717-97072009000100015.

400. Amemiya, S.; Bühlmann, P.; Umezawa, Y. A Phase Boundary Potential Model for Apparently "Twice-Nernstian" Responses of Liquid Membrane Ion-Selective Electrodes. *Anal. Chem.* **1998**, *70*, 445–454, doi:10.1021/ac9710184.

401. Karamać, M. Chelation of Cu(II), Zn(II), and Fe(II) by tannin constituents of selected edible nuts. *Int. J. Mol. Sci.* **2009**, *10*, 5485–5497, doi:10.3390/ijms10125485.

402. Ghislandi, M.; Tkalya, E.; Marinho, B.; Koning, C.E.; De With, G. Electrical conductivities of carbon powder nanofillers and their latex-based polymer composites. *Compos. Part A Appl. Sci. Manuf.* **2013**, *53*, 145–151, doi:10.1016/j.compositesa.2013.06.008.

403. Grand View Research. Polyurethane Market Size, Share & Trends Analysis Report - Sample report (accessed on 7/10/2021) Available online: https://www.grandviewresearch.com/industry-analysis/polyurethane-pu-market#.

404. Gama, N.; Ferreira, A.; Barros-Timmons, A. Cure and performance of castor oil polyurethane adhesive. *Int. J. Adhes. Adhes.* **2019**, *95*, 102413, doi:10.1016/j.ijadhadh.2019.102413.

405. Bresolin, D.; Valério, A.; de Oliveira, D.; Lenzi, M.K.; Sayer, C.; de Araújo, P.H.H. Polyurethane Foams Based on Biopolyols from Castor Oil and Glycerol. *J. Polym. Environ.* **2018**, *26*, 2467–2475, doi:10.1007/s10924-017-1138-7.

406. Ekkaphan, P.; Sooksai, S.; Chantarasiri, N.; Petsom, A. Bio-Based Polyols from Seed Oils for Water-Blown Rigid Polyurethane Foam Preparation. *Int. J. Polym. Sci.* **2016**, *2016*, 4909857, doi:10.1155/2016/4909857.

407. Stirna, U.; Fridrihsone, A.; Lazdiņa, B.; Misāne, M.; Vilsone, D. Biobased Polyurethanes from Rapeseed Oil Polyols: Structure, Mechanical and Thermal Properties. *J. Polym. Environ.* **2013**, *21*, 952–962, doi:10.1007/s10924-012-0560-0.

408. Mizera, K.; Ryszkowska, J. Thermal properties of polyurethane elastomers from soybean oil-based polyol with a different isocyanate index. *J. Elastomers Plast.* **2019**, *51*, 157–174, doi:10.1177/0095244318772323.

409. Gama, N. V.; Soares, B.; Freire, C.S.R.; Silva, R.; Ferreira, A.; Barros-Timmons, A. Effect of unrefined crude glycerol composition on the properties of polyurethane foams. *J. Cell. Plast.* **2018**, *54*, 633–649, doi:10.1177/0021955X17732304.

410. Luo, S.; Gao, L.; Guo, W. Effect of incorporation of lignin as bio-polyol on the performance of rigid lightweight wood–polyurethane composite foams. *J. Wood Sci.* **2020**, *66*, 23, doi:10.1186/s10086-020-01872-5.

411. Kissinger, H.E. Reaction Kinetics in Differential Thermal Analysis. *Anal. Chem.* **1957**, *29*, 1702–1706, doi:10.1021/ac60131a045.

412. Ozawa, T. A New Method of Analyzing Thermogravimetric Data. *Bull. Chem. Soc. Jpn.* **1965**, *38*, 1881–1886, doi:10.1246/bcsj.38.1881.

413. Zhang, X. Applications of kinetic methods in thermal analysis: A review. *Eng. Sci.* **2021**, *14*,

1–13, doi:10.30919/es8d1132.

414. Tejado, A.; Kortaberria, G.; Peña, C.; Labidi, J.; Echeverria, J.M.; Mondragon, I. Isocyanate curing of novolac-type ligno-phenol-formaldehyde resins. *Ind. Crops Prod.* **2008**, *27*, 208–213, doi:10.1016/j.indcrop.2007.07.009.

415. Yoshida, H.; Mörck, R.; Kringstad, K.P.; Hatakeyama, H. Kraft lignin in polyurethanes. II. Effects of the molecular weight of kraft lignin on the properties of polyurethanes from a kraft lignin–polyether triol–polymeric MDI system. *J. Appl. Polym. Sci.* **1990**, *40*, 1819–1832, doi:10.1002/app.1990.070401102.

416. Hunt, C.G.; Frihart, C.R.; Dunky, M.; Rohumaa, A. Understanding wood bonds-going beyond what meets the eye: A critical review. *Rev. Adhes. Adhes.* **2018**, *6*, 369–463, doi:10.7569/RAA.2018.097312.

417. Thring, R.W.; Ni, P.; Aharoni, S.M. Molecular weight effects of the soft segment on the ultimate properties of lignin-derived polyurethanes. *Int. J. Polym. Mater. Polym. Biomater.* **2004**, *53*, 507–524, doi:10.1080/00914030490267627.

418. Frihart, C.R.; Lorenz, L. Standard test method ASTM D 7998-19 for the cohesive strength development of wood adhesives. *J. Vis. Exp.* **2020**, *159*, e61184, doi:10.3791/61184.

419. Sahoo, S.; Kalita, H.; Mohanty, S.; Nayak, S.K. Meticulous study on curing kinetics of green polyurethane-clay nanocomposite adhesive derived from plant oil: Evaluation of decomposition activation energy using TGA analysis. *J. Macromol. Sci. Part A Pure Appl. Chem.* **2017**, *54*, 819–826, doi:10.1080/10601325.2017.1336727.

420. Singh, A.K.; Panda, B.P.; Mohanty, S.; Nayak, S.K.; Gupta, M.K. Thermokinetics behavior of epoxy adhesive reinforced with low viscous aliphatic reactive diluent and nano-fillers. *Korean J. Chem. Eng.* **2017**, *34*, 3028–3040, doi:10.1007/s11814-017-0221-z.

421. Thanki, J.D.; Parsania, P.H. Dynamic DSC curing kinetics and thermogravimetric study of epoxy resin of 9,90-bis(4-hydroxyphenyl)anthrone-10. *J. Therm. Anal. Calorim.* **2017**, *127*, 239–246.